

**SEMICARBAZIDE-SENSITIVE AMINE  
OXIDASE (SSAO) AND ITS  
INTERACTION WITH LYSYL  
OXIDASE (LOX) IN RAT AORTIC  
VASCULAR SMOOTH MUSCLE  
CELLS**

**By  
Vesna Manasieva**

**October 2021**

Submitted to the University of Hertfordshire in partial  
fulfilment of the requirement of the degree of PhD

## TABLE OF CONTENTS

|  |       |
|--|-------|
| <b>LIST OF FIGURES</b> .....   | 7-11  |
| <b>LIST OF TABLES</b> .....  | 12    |
| <b>ABSTRACT</b> .....  | 13-14 |
| <b>ABBREVIATIONS</b> .....   | 15-18 |
| <b>CHAPTER I: INTRODUCTION</b> .....   | 19    |
| <b>SECTION 1.0: AMINE OXIDASES</b> .....   | 19    |
| 1.1: Amine oxidase family of enzymes.....  | 19-20 |
| <b>SECTION 2.0: COPPER AMINE OXIDASES - SEMICARBAZIDE SENSITIVE AMINE OXIDASE (SSAO)</b> ..... | 21-26 |
| 2.1: Semicarbazide sensitive amine oxidase (SSAO).....   | 21-23 |
| 2.2: Molecular structure of SSAO.....  | 23-25 |
| 2.3: Soluble and membrane bound SSAO.....  | 25-26 |
| <b>SECTION 3.0: PHYSIOLOGICAL AND PATHOPHYSIOLOGICAL FUNCTIONS OF SSAO/VAP-1</b> .....         | 27-31 |
| 3.1: Leukocyte-endothelial cell interaction.....   | 27-29 |
| 3.2: Adipocyte's differentiation and obesity.....  | 29    |
| 3.3: Glucose transport.....  | 30-31 |
| 3.4: Structural organisation of vascular smooth muscle cells.....                              | 31    |
| <b>SECTION 4.0: SSAO SUBSTRATES AND THEIR CORRESPONDING ALDEHYDES PRODUCTS</b> .....           | 32-39 |
| 4.1: Methylamine and formaldehyde.....   | 34-36 |
| 4.2: Aminoacetone and methylglyoxal.....   | 36-37 |
| 4.3: Allylamine and acrolein.....  | 37-38 |
| 4.4: Benzylamine and benzaldehyde.....   | 38-39 |

|  |       |
|--|-------|
| <b>SECTION 5.0: COPPER AMINE OXIDASES – LYSYL OXIDASE</b> .....                | 40-44 |
| 5.1: Lysyl Oxidase family.....   | 40-41 |
| 5.2: Lysyl Oxidase isoform.....  | 41-42 |
| 5.3: Substrate specificity for LOX.....  | 42-43 |
| 5.4: Biological activities of LOX.....   | 43-44 |
| <b>SECTION 6.0: SSAO AND LOX IN CARDIOVASCULAR DISEASE</b> .....               | 45-52 |
| 6.1: Development of atherosclerosis.....                                       | 45-46 |
| 6.2: SSAO and CVD.....   | 47-48 |
| 6.3: SSAO in atherosclerosis.....  | 49    |
| 6.4: LOX in CVD.....   | 50-52 |
| <b>SECTION 7.0: SSAO AND LOX IN INFLAMMATION</b> .....                         | 52-55 |
| 7.1: SSAO in inflammation.....   | 53-54 |
| 7.2: LOX in inflammation.....  | 54-55 |
| <b>SECTION 8.0: REACTION PRODUCTS OF SSAO AND LOX ENZYMATIC ACTIVITY</b> ..... | 55-62 |
| 8.1: Hydrogen peroxide.....  | 55-56 |
| 8.2: Hydrogen peroxide in VSMCs.....   | 56    |
| 8.3: Physiological roles of H <sub>2</sub> O <sub>2</sub> in VSMCs.....        | 57    |
| 8.4: Pathological effects of H <sub>2</sub> O <sub>2</sub> in VSMCs.....       | 57-58 |
| 8.5: Aldehydes and biological consequences of aldehydes exposure.....          | 59-60 |
| 8.6: Oxidative stress and aldehydes.....                                       | 61-62 |
| <b>SECTION 9.0: SSAO AND LOX INHIBITORS</b> .....                              | 63-74 |
| 9.1: SSAO inhibitors.....  | 63    |
| 9.2: Hydrazine based derivative inhibitors of SSAO.....                        | 70-71 |
| 9.3: Suicide (mechanism-based) inhibitors of SSAO.....                         | 72    |
| 9.4: Function blocking antibodies for SSAO.....                                | 73    |
| 9.5: LOX inhibitors.....   | 73    |
| 9.6: β-Aminopropionitrile (βAPN).....  | 74    |

|   |         |
|---|---------|
| <b>SECTION 10: AIMS AND OBJECTIVES</b> .....  | 75-76   |
| <b>CHAPTER II: METHODOLOGY</b> .....  | 77      |
| <b>SECTION 2.1: MATERIALS</b> .....   | 77-79   |
| <b>SECTION 2.2: METHODS – CELL CULTURE</b> .....  | 80      |
| 2.2.1: Animals.....   | 80      |
| 2.2.2: Cells.....   | 81      |
| 2.2.3: Preparation of cell culture reagents.....  | 82      |
| 2.2.4: Isolation of rat aortic smooth muscle cells.....   | 82-83   |
| 2.2.5: Sub-culture of rat aortic smooth muscle cells.....   | 83-84   |
| 2.2.6: Cell Counting Using a Haemocytometer.....  | 84      |
| 2.2.7: Cryopreservation of rat aortic VSMCs.....  | 84      |
| 2.2.8: Resuscitation of rat aortic VSMCs.....   | 85      |
| 2.2.9: Phenotypic characterisation of rat aortic VSMCs.....   | 85-86   |
| 2.2.10: Protein quantification using BCA assay.....   | 87-89   |
| 2.2.11: Protein quantification using Bradford assay.....  | 89-90   |
| 2.2.12: Measurement of SSAO activity in rat aortic VSMCs.....   | 91-92   |
| 2.2.13: Western blot analysis.....  | 92-93   |
| 2.2.14: Protein quantification with Image J.....  | 93      |
| <b>SECTION 2.3: STATISTICS</b> .....  | 94      |
| <b>CHAPTER III: RESULTS</b> .....   | 95      |
| <b>SECTION 3.1: DEVELOPMENT OF <i>IN VITRO</i> MODEL TO CHARACTERISE SSAO<br/>ACTIVITY IN RAT AORTIC VASCULAR SMOOTH MUSCLE CELLS</b> ..... | 95      |
| 3.1.1: Introduction.....  | 95-97   |
| 3.1.2: Methods.....   | 97-99   |
| 3.1.3: Results.....   | 100-104 |
| 3.1.4: Discussion.....  | 105-107 |
| 3.1.5: Conclusion.....  | 107     |

|   |            |
|---|------------|
| <b>SECTION 3.2: FURTHER EVALUATION OF THE MODEL USING REVERSIBLE AND IRREVERSIBLE SSAO INHIBITORS AND METHYLAMINE AND AMINOACETONE AS SUBSTRATES.....</b> | <b>108</b> |
| 3.2.1: Introduction.....  | 108-110    |
| 3.2.2: Methods.....   | 110-113    |
| 3.2.3: Results.....   | 113-121    |
| 3.2.4: Discussion.....  | 122-125    |
| 3.2.5: Conclusion.....  | 125        |
| <br>  |            |
| <b>SECTION 3.3: SSAO AND LOX ACTIVITY DURING RAT AORTIC VASCULAR SMOOTH MUSCLE CELLS AGING .....</b>  | <b>126</b> |
| 3.3.1: Introduction.....  | 126-129    |
| 3.3.2: Methods.....   | 130-132    |
| 3.3.3: Results.....   | 132-151    |
| 3.3.4: Discussion.....  | 152-157    |
| 3.3.5: Conclusion.....  | 157        |
| <br>  |            |
| <b>SECTION 3.4: MOLECULAR STUDIES ON THE INTERACTION BETWEEN SSAO AND LOX IN RAT AORTIC VASCULAR SMOOTH MUSCLE CELLS.....</b>                             | <b>158</b> |
| 3.4.1: Introduction.....  | 158-160    |
| 3.4.2: Methods.....   | 161-169    |
| 3.4.3: Results.....   | 169-173    |
| 3.4.4: Discussion.....  | 173-177    |
| 3.4.5: Conclusion.....  | 177        |
| <br>  |            |
| <b>SECTION 3.5: SSAO AND LOX IN ROS FORMATION.....</b>  | <b>178</b> |
| 3.5.1: Introduction.....  | 178-182    |
| 3.5.2: Methods.....   | 182-185    |
| 3.5.3: Results.....   | 186-194    |
| 3.5.4: Discussion.....  | 194-199    |
| 3.5.5: Conclusion.....  | 200        |

|   |                |
|---|----------------|
| <b>CHAPTER IV: MAIN DISCUSSION.....</b>   | <b>201-214</b> |
| <b>SECTION 4.1: CONCLUSION.....</b>       | <b>215-216</b> |
| <b>SECTION 4.2: FUTURE DIRECTION.....</b> | <b>217</b>     |
| <br>                                      |                |
| <b>LITERATURE CITED.....</b>              | <b>218-236</b> |
| <br>                                      |                |
| <b>APPENDIX.....</b>                      | <b>237</b>     |
| <b>APPENDIX 1.....</b>                    | <b>237-238</b> |
| <b>APPENDIX 2.....</b>                    | <b>239-242</b> |
| <b>APPENDIX 3.....</b>                    | <b>242-243</b> |
| <b>APPENDIX 4.....</b>                    | <b>243-244</b> |

## LIST OF FIGURES

|   |    |
|---|----|
| <b>Figure 1:</b> The reaction catalysed by copper-containing amine oxidases.....  | 21 |
| <b>Figure 2:</b> SSAO oxidase primary amines into aldehydes, ammonia, and hydrogen peroxide .....                                 | 22 |
| <b>Figure 3:</b> Chromosome location of AOC3 gene in a human.....   | 23 |
| <b>Figure 4:</b> Chromosome location of AOC3 gene in a rat.....   | 23 |
| <b>Figure 5:</b> Structure of SSAO.....   | 24 |
| <b>Figure 6:</b> Conserved regions of SSAO.....   | 25 |
| <b>Figure 7:</b> Leukocyte extravasation mediated by a multistep adhesion cascade.....  | 27 |
| <b>Figure 8:</b> SSAO induces leukocyte adhesion <i>via</i> its adhesive and enzymatic function.....                              | 28 |
| <b>Figure 9:</b> The role of SSAO in regulation of glucose uptake in adipocytes.....  | 30 |
| <b>Figure 10:</b> Formation and degradation of methylamine.....   | 34 |
| <b>Figure 11:</b> Methylamine (MeNH <sub>2</sub> ) stimulates glucose uptake through a hydrogen peroxide dependent mechanism..... | 35 |
| <b>Figure 12:</b> SSAO produced formaldehyde induces apoptosis through release of pro-apoptotic protein P53 and caspases.....     | 36 |
| <b>Figure 13:</b> Reaction pathways surrounding aminoacetone and methylglyoxal.....   | 37 |
| <b>Figure 14:</b> Conversion of allylamine to acrolein.....   | 37 |
| <b>Figure 15:</b> Hypothetical model of allylamine induction of coronary artery vasospasm and vasomotion.....                     | 38 |
| <b>Figure 16:</b> The role of SSAO in glucose homeostasis.....  | 39 |
| <b>Figure 17:</b> The mechanism of action of lysyl oxidase-catalysed reaction.....  | 41 |
| <b>Figure 18:</b> Reaction catalysed by lysyl oxidase.....  | 42 |
| <b>Figure 19:</b> Pathophysiology of atherosclerosis.....   | 45 |

|   |     |
|---|-----|
| <b>Figure 20:</b> Early, developing, and mature stages of atherosclerosis.....  | 46  |
| <b>Figure 21:</b> Involvement of lysyl oxidase in atherosclerosis and restenosis.....   | 52  |
| <b>Figure 22:</b> the role of hydrogen peroxide in VSMCs physiology and pathology.....  | 58  |
| <b>Figure 23:</b> Exogenous and endogenous sources of human exposure to aldehydes.....  | 59  |
| <b>Figure 24:</b> Structure of common aldehydes.....  | 60  |
| <b>Figure 25:</b> Cellular fates of $\alpha$ , $\beta$ – unsaturated aldehydes and carbonylated proteins.....   | 62  |
| <b>Figure 26:</b> Small molecule inhibitors of LOX family enzymes.....  | 73  |
| <b>Figure 27:</b> The oxidation mechanism by LOX and its inhibition by $\beta$ APN.....   | 74  |
| <b>Figure 28:</b> <i>In vitro</i> culture of rat VSMCs from aortic explants viewed at 160X magnification (10X E-PL, 4X objective lens, 40X image magnification) under an inverted Olympus light microscope..... | 83  |
| <b>Figure 29:</b> Immuno-stained microscopic image of rat aortic smooth muscle cells depicting the presence of SM22 $\alpha$ actin fibres (scale bar 400 $\mu$ m).....  | 86  |
| <b>Figure 30:</b> Schematic drawing to display the chemical species in a solution during the BCA protein assay.....   | 87  |
| <b>Figure 31:</b> A linear regression of a protein standard curve.....  | 89  |
| <b>Figure 32:</b> A liner regression of protein standard curve with Bradford.....   | 90  |
| <b>Figure 33:</b> Amplex <sup>®</sup> Red, a non-fluorescent substrate, produces a highly fluorescent product resorufin, in response to H <sub>2</sub> O <sub>2</sub> upon the oxidation by HRP .....           | 91  |
| <b>Figure 34:</b> Principle of the assay.....   | 92  |
| <b>Figure 35:</b> A linear regression of resorufin standard curve .....   | 99  |
| <b>Figure 36:</b> 24h SSAO fluorescence measurements with three different gain percentages .....  | 100 |
| <b>Figure 37:</b> SSAO activity (nmolH <sub>2</sub> O <sub>2</sub> /h/mg protein) over different time intervals (0h, 0.5h, 1h, 2h, 4h, 6h, 8h) in rat aortic VSMCs.....   | 101 |
| <b>Figure 38:</b> SSAO activity (nmolH <sub>2</sub> O <sub>2</sub> /h/mg protein) over different time intervals (0h, 0.5h, 1h, 2h, 4h, 6h, 8h, 24h) in rat aortic VSMCs.....                                    | 102 |

|  |         |
|--|---------|
| <b>Figure 39:</b> The highest activity ( $V_{max}$ ) of SSAO and its affinity ( $K_m$ ) for the substrate benzylamine (0, 0.5, 2, 10, and 20mM) in rat aortic VSMCs determined with Michaelis-Menten kinetics ( $n = 1$ ).....         | 103     |
| <b>Figure 40:</b> The highest activity ( $V_{max}$ ) of SSAO and its affinity ( $K_m$ ) for the substrate benzylamine (0, 0.02, 0.05, 0.1, 0.5, 1, 5mM) in rat aortic VSMCs determined with Michaelis-Menten kinetics ( $n = 5$ )..... | 104     |
| <b>Figure 41:</b> Structure of MTT and coloured product formazan.....  | 110     |
| <b>Figure 42:</b> Viability of rat aortic VSMCs after 1h treatment with semicarbazide, methylhydrazine and MDL72527.....   | 113-114 |
| <b>Figure 43:</b> SSAO inhibition with (A) semicarbazide, (B) methylhydrazine, and (C) MDL72527 after 15 min incubation ( $n = 5$ ).....   | 116-117 |
| <b>Figure 44:</b> Viability of rat aortic VSMCs treated with aminoacetone and methylamine ( $n = 5$ ).....   | 118     |
| <b>Figure 45:</b> Viability of rat aortic VSMCs treated with methylglyoxal and formaldehyde ( $n = 5$ ).....   | 120     |
| <b>Figure 46:</b> SSAO kinetic parameters in the presence of aminoacetone and methylamine ( $n = 5$ ).....   | 121     |
| <b>Figure 47:</b> PDGF-PDGFR interactions.....   | 128     |
| <b>Figure 48:</b> SSAO activity expressed as $H_2O_2$ production in rat aortic VSMCs from passage 3, 4, 5, 6, 7 & 8 ( $n = 5$ ).....   | 133     |
| <b>Figure 49:</b> SSAO activity expressed as $H_2O_2$ production in rat aortic VSMCs from passage 3, 5, & 8 ( $n = 5$ ).....   | 134-135 |
| <b>Figure 50:</b> LOX activity expressed as $H_2O_2$ production in rat aortic VSMCs from passage 3, 5, & 8 ( $n = 5$ ).....  | 136     |
| <b>Figure 51:</b> SSAO kinetic parameters in the presence of 200 $\mu$ M $\beta$ APN.....  | 137     |
| <b>Figure 52:</b> LOX kinetic parameters in rat aortic VSMCs.....  | 138     |
| <b>Figure 53:</b> Western blot analysis of VAP-1 and Pro-LOX in non-treated and $\beta$ APN treated rat aortic VSMCs from passage 3, 5 & 8 ( $n = 3$ ).....  | 139     |
| <b>Figure 54:</b> VAP-1 and Pro-LOX protein expression in non-treated and $\beta$ APN treated rat aortic VSMCs from passage 3, 5 & 8 ( $n = 3$ ).....  | 139-140 |
| <b>Figure 55:</b> Western blot analysis of ACTA2 and SM22 $\alpha$ in non-treated and $\beta$ APN treated rat aortic VSMCs from passage 3, 5 & 8 ( $n = 3$ ).....  | 140     |

|  |         |
|--|---------|
| <b>Figure 56:</b> ACTA2 and SM22 $\alpha$ protein expression in non-treated and $\beta$ APN treated rat aortic VSMCs from passage 3, 5 & 8 (n = 3).....      | 141     |
| <b>Figure 57:</b> Western blot analysis of PDGFR $\beta$ in non-treated and $\beta$ APN treated rat aortic VSMCs from passage 3, 5 & 8 (n = 3).....          | 141     |
| <b>Figure 58:</b> PDGFR $\beta$ protein expression in non-treated and $\beta$ APN treated rat aortic VSMCs from passage 3, 5 & 8 (n = 3).....                | 142     |
| <b>Figure 59:</b> Western blot analysis of VAP-1 and Pro-LOX in non-treated and MDL72527 treated rat aortic VSMCs from passage 3, 5 & 8 (n = 3).....         | 142     |
| <b>Figure 60:</b> VAP-1 and Pro-LOX protein expression in non-treated and MDL72527 treated rat aortic VSMCs from passage 3, 5 & 8 (n = 3).....               | 143     |
| <b>Figure 61:</b> Western blot analysis of ACTA2 and SM22 $\alpha$ in non-treated and MDL72527 treated rat aortic VSMCs from passage 3, 5 & 8 (n = 3).....   | 144     |
| <b>Figure 62:</b> ACTA2 and SM22 $\alpha$ protein expression in non-treated and MDL72527 treated rat aortic VSMCs from passage 3, 5 & 8 (n = 3).....         | 144     |
| <b>Figure 63:</b> Western blot analysis of PDGFR $\beta$ in non-treated and MDL72527 treated rat aortic VSMCs from passage 3, 5 & 8 (n = 3).....             | 145     |
| <b>Figure 64:</b> PDGFR $\beta$ protein expression in non-treated and MDL72527 treated rat aortic VSMCs from passage 3, 5 & 8 (n = 3).....                   | 145     |
| <b>Figure 65:</b> Western blot analysis of VAP-1 and Pro-LOX in benzylamine and cadaverine treated rat aortic VSMCs from passage 3, 5 & 8 (n = 3).....       | 146     |
| <b>Figure 66:</b> VAP-1 protein expression in benzylamine and cadaverine treated rat aortic VSMCs from passage 3, 5 & 8 (n = 3).....                         | 146-147 |
| <b>Figure 67:</b> Pro-LOX protein expression in benzylamine and cadaverine treated rat aortic VSMCs from passage 3, 5 & 8 (n = 3).....                       | 147     |
| <b>Figure 68:</b> Western blot analysis of ACTA2 and SM22 $\alpha$ in benzylamine and cadaverine treated rat aortic VSMCs from passage 3, 5 & 8 (n = 3)..... | 148     |
| <b>Figure 69:</b> ACTA2 protein expression in benzylamine treated rat aortic VSMCs from passage 3, 5 & 8 (n = 3).....  | 148-149 |
| <b>Figure 70:</b> SM22 $\alpha$ protein expression in benzylamine treated rat aortic VSMCs from passage 3, 5 & 8 (n = 3).....                                | 149-150 |
| <b>Figure 71:</b> Western blot analysis of PDGFR $\beta$ in benzylamine and cadaverine treated rat aortic VSMCs from passage 3, 5 & 8 (n = 3).....           | 150     |
| <b>Figure 72:</b> PDGFR $\beta$ protein expression in benzylamine and cadaverine treated rat aortic VSMCs from passage 3, 5 & 8 (n = 3).....                 | 151     |

|  |         |
|--|---------|
| <b>Figure 73:</b> AOC3 and LOX gene expression in non-treated, MDL72527 and $\beta$ APN treated rat aortic VSMCs from passage 3, 5 and 8.....  | 170     |
| <b>Figure 74:</b> LOX gene expression after treatment with Si control, SiRNA5, SiRNA6 and SiRNA8 48h and 72h post transfection (n = 1) .....   | 171     |
| <b>Figure 75:</b> LOX and AOC3 gene expression in early passage (2 & 3) VSMCs treated with Si control, SiRNA6, SiRNA8 (n = 4).....   | 172     |
| <b>Figure 76:</b> Western blot analysis of Pro-LOX and VAP-1 in rat aortic VSMCs 72h post transfection with Si control, SiRNA6 and SiRNA8 (n =4).....                                  | 172     |
| <b>Figure 77:</b> Pro-LOX and VAP-1 protein expression in early passage (2 & 3) VSMCs treated with Si control, SiRNA6, SiRNA8 (n = 4).....   | 173     |
| <b>Figure 78:</b> Balance between GSH and GSSG.....  | 180     |
| <b>Figure 79:</b> DMNQ chemical structure.....   | 182     |
| <b>Figure 80:</b> The enzymatic recycling of GSH from GSSG by glutathione reductase (GR) in the presence of NADPH.....   | 183     |
| <b>Figure 81:</b> A linear regression of glutathione standard curve.....   | 185     |
| <b>Figure 82:</b> ROS production after treatment with benzylamine, cadaverine, methylamine and aminoacetone (n = 5).....   | 186-187 |
| <b>Figure 83:</b> ROS production after treatment with SSAO and LOX amines and inhibitors (n = 5).....  | 188     |
| <b>Figure 84:</b> Fluorescent images depicting ROS production.....   | 189-193 |
| <b>Figure 85:</b> GSH production in VSMCs treated with SSAO and LOX amines and inhibitors (n = 4).....   | 193-194 |
| <b>Figure 86:</b> Progress curves of SSAO activity (nmolH <sub>2</sub> O <sub>2</sub> /h/mg protein vs time) in the presence of different substrate concentrations.....                | 237-238 |
| <b>Figure 87:</b> Substrate-velocity curves for each SSAO inhibitor after 5, 15 and 30 minutes incubation.....   | 239-242 |
| <b>Figure 88:</b> Immuno-stained microscopic image of rat aortic VSMCs depicting the presence of clustered SM22 $\alpha$ actin fibres (passage 3, 5 & 8) (scale bar 1000 $\mu$ m)..... | 241-243 |
| <b>Figure 89:</b> SiRNA5, SiRNA6 and SiRNA8 targeted to LOX gene.....  | 243-244 |

## LIST OF TABLES

|  |       |
|--|-------|
| <b>Table 1:</b> Classification of amine oxidases.....  | 20    |
| <b>Table 2:</b> Compounds known as SSAO substrates.....  | 33    |
| <b>Table 3:</b> SSAO inhibitors.....   | 63-70 |
| <b>Table 4:</b> Materials used in this thesis .....  | 77-79 |
| <b>Table 5:</b> Standards for BCA protein assay.....   | 88    |
| <b>Table 6:</b> Standards for Bradford protein assay.....  | 90    |
| <b>Table 7:</b> Standards for resorufin.....   | 98    |
| <b>Table 8:</b> SSAO kinetic parameters after 5, 15 and 30 minutes incubation with semicarbazide, methylhydrazine and MDL72527.....                    | 115   |
| <b>Table 9:</b> Primers sequences.....   | 162   |
| <b>Table 10:</b> An illustration of the qPCR experimental design.....  | 163   |
| <b>Table 11:</b> qPCR thermal cycling protocol.....  | 163   |
| <b>Table 12:</b> LOX SiRNAs and their target sequences.....  | 165   |
| <b>Table 13:</b> Standards for GSH assay.....  | 185   |
| <b>Table 14:</b> SSAO activity in rat aortic VSMCs from passage 3, over different times and in the presence of different substrate concentrations..... | 237   |
| <b>Table 15:</b> SSAO reaction velocity (V) in rat aortic VSMCs from passage 3 (n = 5).....  | 238   |

## ABSTRACT

**Introduction:** Semicarbazide-sensitive amine oxidase (SSAO) is both a soluble and membrane bound transmembrane protein expressed in the vasculature. In endothelial cells, SSAO is involved in leukocyte rolling, adhesion, and transmigration into inflammatory sites which may imply a pathological role in the development of atherosclerosis. In vascular smooth muscle cells (VSMCs - the main stromal cells located in the middle layer of the arteries), SSAO has been highlighted as important factor in the oxidation of low-density cholesterol (LDL) and inducer of cell death. Lysyl oxidase (LOX) is another vascular enzyme which contributes to VSMCs extra cellular matrix (ECM) formation and stability. In these cells LOX has been associated with chemotaxis, which may imply a pathological role in the development of atherosclerosis. There is insufficient evidence regarding the interaction of these enzymes in VSMCs, their toxicological consequence, and the mechanism through which they contribute to LDL oxidation and the induction of chemotaxis. This thesis aims to investigate SSAO and LOX catalytic activity in rat aortic VSMCs, and their contributory role in oxidative stress and chemotaxis (important hallmarks in atherosclerosis), through ROS formation and vascular remodelling.

**Methods:** To address this, an *in vitro* assay was developed and optimised for assessing SSAO and LOX activity in rat cultured aortic VSMCs through H<sub>2</sub>O<sub>2</sub> generation. Toxicity of SSAO substrates and inhibitors was assessed colourimetrically. Cells at passage 3, 5 & 8 and confluency of ~80-90% were treated with the substrates benzylamine and cadaverine, and with LOX and SSAO irreversible suicide inhibitors  $\beta$ APN and MDL72527. Western blot analysis was utilised to assess the membrane bound forms of the enzymes, vascular adhesion protein 1 (VAP-1) and Pro-LOX, the contractile markers smooth muscle 22 $\alpha$  (SM22 $\alpha$ ) and alpha actin 2 (ACTA2) which indicate VSMCs physiological – contractile phenotype, and the expression of platelet derived growth factor receptor  $\beta$  (PDGFR $\beta$ ), a receptor implicated in the mechanism of VSMCs chemotaxis. A quantitative polymerase chain reaction (qPCR) was applied to study mRNA levels of the gene that encodes for SSAO, amine oxidase copper containing 3 (AOC3) and LOX (LOX) in the presence of their respective irreversible inhibitors, and after silencing LOX gene. ROS and total glutathione (GSH) content were evaluated with ROS and the recycling GSH assay.

**Results:** SSAO activity was maximal at 6h from addition of reaction mixture. There was a passage dependent increase in SSAO affinity for its substrate benzylamine (\*\*p < 0.01) as shown by a 3-fold reduction in the Km as passage increased from 3 (Km = 0.2084) to 8 (Km = 0.07267). Methylhydrazine was identified as the most potent reversible, and MDL72527 as the most potent irreversible inhibitor.

Aminoacetone and methylamine induced VSMCs death at concentrations of 50 & 1000 $\mu$ M, and higher SSAO affinity was detected for aminoacetone comparing to methylamine ( $K_m = 12\mu\text{M}$  vs  $65\mu\text{M}$ ). The cytotoxicity was reversed with MDL72527 which completely abolished cell death. Enhanced cytotoxicity was detected after simultaneous addition of aldehydes and  $\text{H}_2\text{O}_2$ . VAP-1, Pro-LOX and PDGFR $\beta$  were expressed in cultured VSMCs under control conditions with levels maintained between passages. At basal level, LOX activity decreased with passage and its affinity and protein expression were maintained between passages.  $\beta$ APN abolished LOX activity (\*\* $p < 0.01$  for 3 vs 8 and \* $p < 0.05$  for 5 vs 8) and had no effect on Pro-LOX expression and LOX mRNA levels; and MDL72527 had no effect on LOX activity, protein, and mRNA expression. At basal level, SSAO activity also decreased with passage and its protein expression was maintained between passages. MDL72527 abolished SSAO activity (\*\*\*\* $p < 0.0001$  for 3 vs 8 and \* $p < 0.05$  for 5 vs 8), VAP-1 expression at passage 5 (\*\* $p < 0.01$ ) and passage 8 (\*\*\*\* $p < 0.0001$ ), and AOC3 mRNA levels at passage 8 (\* $p < 0.05$ ).  $\beta$ APN inhibited SSAO activity (\*\*\*\* $p < 0.0001$  for 3 vs 5 and 3 vs 8 and \* $p < 0.05$  for 5 vs 8), VAP-1 expression at passage 3 (\* $p < 0.05$ ), and AOC3 mRNA levels at passage 3 (\* $p < 0.05$ ). Benzylamine did not alter VAP-1 and LOX expression and cadaverine reduced VAP-1 at passage 3 (\*\* $p < 0.01$ ), passage 5 (\* $p < 0.05$ ), and passage 8 (\*\* $p < 0.01$ ). Loss of contractile markers was observed in non-treated cells and after treatment with MDL72527, cadaverine and benzylamine. PDGFR $\beta$  expression was reduced at passage 8 after LOX (\* $p < 0.05$ ) and passage 3 (\* $p < 0.05$ ), 5 (\* $p < 0.05$ ), and 8 (\*\* $p < 0.01$ ) after SSAO inhibition. PDGFR $\beta$  expression was also reduced at passage 3 (\* $p < 0.05$ ) after benzylamine and cadaverine treatment. Silencing LOX gene at passage 3 reduced AOC3 mRNA (#### $p < 0.0001$  for SiRNA6 and ### $p < 0.001$  for SiRNA8) and VAP-1 protein (# $p < 0.05$  for SiRNA8). Highest ROS production was detected with aminoacetone and benzylamine treatment. MDL72527 abolished ROS in benzylamine (\*\*\*\* $p < 0.0001$ ), methylamine (\*\*\*\* $p < 0.0001$ ), and aminoacetone (\*\*\*\* $p < 0.0001$ ), and  $\beta$ APN in benzylamine (\* $p < 0.05$ ) treated cells. Total GSH levels were reduced after benzylamine, methylamine and aminoacetone treatment (\*\*\*\* $p < 0.0001$ ); however, failed to be restored after addition of MDL72527 and  $\beta$ APN.

**Conclusion:** A robust method was optimised and validated to effectively characterise SSAO and LOX activity *in vitro*. A cytotoxic consequence of SSAO catalytic activity was observed in cultured VSMCs and a contributory role of SSAO and LOX was detected in VSMCs chemotaxis, through changes in PDGFR $\beta$  expression. A synergistic relationship between SSAO and LOX was identified in early passage VSMCs. In late passage VSMCs, SSAO expressed predominant activity over LOX, and was demonstrated as the leading enzyme in ROS formation. Overall, these novel findings suggest a passage dependent interplay between SSAO and LOX in rat aortic primary VSMCs and associate their activity with VSMCs phenotyping modulation and ROS formation.

## **ABBREVIATIONS**

AA = Allylamine

ACTA2 = Actin alpha 2

ADH5 = Alcohol dehydrogenase

AGEs = Advanced glycation end products

AKR = Aldo-keto reductase

ALDH2 = Aldehyde dehydrogenase

AMD = Age -related macular degeneration

AOC3 = Amine oxidase copper containing 3

$\beta$ APN –  $\beta$ -aminopropionitrile

BCA = Bicinchoninic acid assay

BLM - Bleomycin

BMP-1 = Bone morphogenic protein -1

BSA = Bovine serum albumin

CD62P = Type I transmembrane glycoprotein

CRAO = Clorgyline-resistant amine oxidase

CuAO = Copper-containing amine oxidase

CVD = Cardiovascular disease

DAO's = Diamine oxidases

DMEM = Dulbecco's modified eagle medium

DMNQ = 2,3 – dimethoxy – 1,4 naphthquinone

DMSO = Dimethyl Sulfoxide

DNA = Deoxyribonucleic Acid

DsRNA = Double-stranded RNA

ECM – Extracellular matrix

EDTA = Disodium ethylenediaminetetraacetic acid

eNOS = Endothelial nitric oxide synthase

FAD = Flavin adenine dinucleotide

FBS = Foetal Bovine Serum

FGH = S-formyl glutathione hydrolase

FGSH = S-formylglutathione

GLOX = Glyoxalase

GLUT-1 = Glucose transporter type 1

GLUT-4 = Glucose transporter type 4

GM-CSF = Granulocyte macrophage colony-stimulating factor

GPX = Glutathione peroxidase

GSH = Glutathione

GSH = Reduced sulfhydryl form

GSSG = Glutathione disulphide

HASMC = Human aortic smooth muscle cells

HC = Homocysteine

HCTL = Homocysteine thiolactone

HMGSH = S-hydroxy methyl glutathione

HRPO = Horseradish peroxidase

IFN-c = Interferon

IL-1 = Interleukin 1

IL-1 = Interleukin 1 $\beta$

IL-6 = Interleukin 6

IRS-1 = Insulin receptor substrate protein 1

IRS-3 = Insulin receptor substrate protein 3

LDL = Low density lipoprotein

LO's = Lysis oxidases

LOX = Lysyl oxidase

LOXL1 = Lysyl oxidase like-1

LOXL2 = Lysyl oxidase like-2

LOXL3 = Lysyl oxidase like-3

LOXL4 = Lysyl oxidase like-4

LOX-PP = pro-peptide domain of LOX

LPS = Lipopolysaccharide

LTQ = Lysine tyrosylquinone

MAO's = Monoamine oxidases

MCP-1 = Monocyte chemoattractant protein-1

MDA = Malondialdehyde

MDL72527 = N1, N4-bis(2,3-butadienyl)-1,4-butanediamine

MMP = Matrix metalloproteinase

mRNA = Messenger ribonucleic acid

NADPH = Nicotinamide adenine dinucleotide phosphate

NF- $\kappa$ B = nuclear factor kappa-light-chain-enhancer of activated  $\beta$  cells

NOX = NADPH oxidase proteins

PAO's = Polyamine oxidases

PARP = Poly (ADP-ribose) polymerase

PBS = Phosphate Buffer Saline

PDGF $\beta$  = Platelet derived growth factor  $\beta$

PDGFR $\beta$  = Platelet derived growth factor receptor  $\beta$

PI 3-kinase = Phosphatidylinositol 3-kinase

PRX = Peroxiredoxin

PUFA = Polyunsaturated fatty acids

qPCR = Quantitative polymerase chain reaction

RAGEs = Receptors of advanced glycation end products

RANKL = Receptor activator of nuclear factor kappa B ligand

RFU = Relative fluorescence units

RISC = RNA induced silencing complex

RLIP76 = Ral-interacting protein

RNS = Reactive nitrogen species

ROS = Reactive oxygen species

SiRNAs = Short interfering RNAs

SMMHC = Smooth muscle myosin heavy chain

SSAO = Semicarbazide-sensitive amine oxidase

TGF $\beta$  = Transforming growth factor  $\beta$

TLL1 = Tolloid-like protein 1

TLL2 = Tolloid-like protein 2

TNF $\alpha$  = Tumour necrosis factor  $\alpha$

TPQ = Topaquinone

VAP-1 = Vascular adhesion protein-1

VCAM-1 = Vascular cell adhesion protein 1

VSMCs = Vascular smooth muscle cells

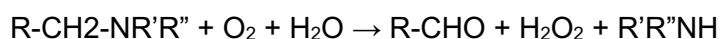
WHO = World health organisation

# CHAPTER I: INTRODUCTION

## SECTION 1.0 AMINE OXIDASES

### *1.1 Amine oxidase family of enzymes*

Amine oxidases are heterogenous family of enzymes that metabolise aliphatic and aromatic amines such as: polyamines (produced endogenously or absorbed as dietary substances), diamines and monoamines. These enzymes catalyse the oxidative deamination of substrates with amine moiety (- NR'R'') connected *via* an unsubstituted methylene group to another group, as described with the following equation:



In the case of primary amines, the amino function is released as ammonia together with hydrogen peroxide and an aldehyde metabolite. The amine oxidases are usually classified based on their substrates as well as chemical structure of their cofactors (Lyles, 1996). In relation to their substrates, they are subdivided into monoamine oxidases (MAO's), diamine oxidases (DAO's), polyamine oxidases (PAO's) and lysis oxidases (LO's) (Table 1). In terms of their cofactor differences MAO's and PAO's contain flavin adenine dinucleotide (FAD) as their cofactor, whereas DAO's and LO's contain a cofactor with one or more carbonyl groups such as topa-quinone (TPQ) which contribute for their high sensitivity to carbonyl reagents like semicarbazide (Sullivan *et al.*, 2004).

MAO are intracellular enzymes located on the outer mitochondrial membrane within most cell types and are mainly involved in the metabolism of physiological primary amines such as dopamine, noradrenaline and 5-hydroxytryptamine, but also biogenic amines such as tyramine and tryptamine. PAO's metabolise polyamines implicated in cell growth regulation such as spermine and spermidine. DAO's metabolize diamines and are sometimes called histaminases because of their deaminating function on histamine (Sullivan *et al.*, 2004). LO's are known to contribute to the formation of the extracellular matrix of connective tissue due to producing aldehyde moieties which participate in peptide cross linking. LO's do that by deaminating side chain amino groups of lysine residues located inside collagen and elastin (Sullivan *et al.*, 2004).

**Table 1. Classification of amine oxidases (Jalkanen *et al.*, 2001).**

|                          | Amine oxidases (AOs)   |                          |  |  |   |  |                                |
|--------------------------|--|--------------------------|--|--|---|--|--------------------------------|
|                          | FAD-containing AOs   |                          |  | CAOs                                   |   |  |                                |
|                          | MAO  | PAO                      | renalase                                 | DAO                                    | SSAO  | RAO  | LO                             |
| <b>Cofactor</b>          | FAD  | FAD                      | FAD                                      | TPQ                                    | TPQ   | TPQ  | LTQ                            |
| <b>Coding human gene</b> | MAO-A, MAO-B, chromosome X   |                          |  | AOC1, chromosome 17                    | AOC3, chromosome 17                                       | AOC2, chromosome 17                                    | LOX1-4, chromosome 10          |
| <b>Presence</b>          | mitochondria   | intracell.               | soluble                                  | intracell.                             | extracell., soluble                                       | extracell.   | extracell.                     |
| <b>Substrates</b>        | noradrenaline<br>dopamine<br>adrenaline<br>$\beta$ -phenylethyl-amine<br>tyramine<br>tryptamine<br>BzA<br>octopamine | spermine<br>spermidine   | nor-adrenaline<br>dopamine<br>adrenaline | putrescine,<br>cadaverine<br>histamine | BzA,<br>methylamine<br>aminoacetone                       | $\beta$ -phenylethyl-amine<br>tryptamine<br>p-tyramine | lysine                         |
| <b>Inhibitors</b>        | pargyline<br>clorgyline<br>selegiline  | carbonyl reactive agents | not known                                | semi-carbazide,<br>hydroxylamine       | semicarbazide,<br>hydroxylamine                           | semi-carbazide   | semicarbazide<br>hydroxylamine |
| <b>Effect</b>            | neuro-transmission   | cell growth              | cardiac function,<br>blood pressure      | Histamine-degradation<br>cell division | amine oxidation,<br>glucose uptake,<br>leucocyte-adhesion | not known  | forming of ECM                 |

**Abbreviations:** AOC1 – amine oxidase copper containing 1, AOC2 – amine oxidase copper containing 2, AOC3 – amine oxidase copper containing 3, BzA – benzylamine, CAOs – copper amine oxidases, DAO – diamine oxidase, ECM – extra cellular matrix, FAD - flavin adenine dinucleotide, LO – lysyl oxidase, LOX1-4 – lyzyl oxidase 1, 2, 3 & 4, LTQ – lysine tyrozyloquinone, MAO – monoamine oxidase, MAO-A – monoamine oxidase A, MAO-B – monoamine oxidase B, PAO – polyamine oxidase, RAO – retina specific amine oxidase, SSAO – semicarbazide sensitive amine oxidase, TPQ – topaquinone.

## SECTION 2.0 COPPER AMINE OXIDASES – SEMICARBAZIDE SENSITIVE AMINE OXIDASE (SSAO)

Copper amine oxidases (CuAOs) can be found in many different organisms ranging from bacteria to mammals (Brazeau *et al.*, 2004). In bacteria, the CuAOs support bacterial growth through their involvement in the metabolism of primary amines, as alternate sources of carbon and nitrogen. In contrast, the role of CuAOs in higher organisms has not been clearly established, although they have been implicated as key components in complex processes such as leukocyte trafficking, endothelial dysfunction, cell differentiation etc (Obata *et al.*, 2006; Gimbrone & Garcia-Cardena, 2016; Wang *et al.*, 2018). In their chemical structure CuAOs are dimers, have subunit masses ranging from 70 to 95 kDa, and share fundamentally identical chemistry. In terms of their enzymatic activity CuAOs catalyse three different reactions: (i) the biogenesis of TPQ, (ii) the oxidation of amine substrates to generate reduced TPQ (termed the reductive half-reaction), and (iii) the reduction of molecular oxygen by reduced TPQ (termed the oxidative half-reaction) (Figure 1) (Brazeau *et al.*, 2004).

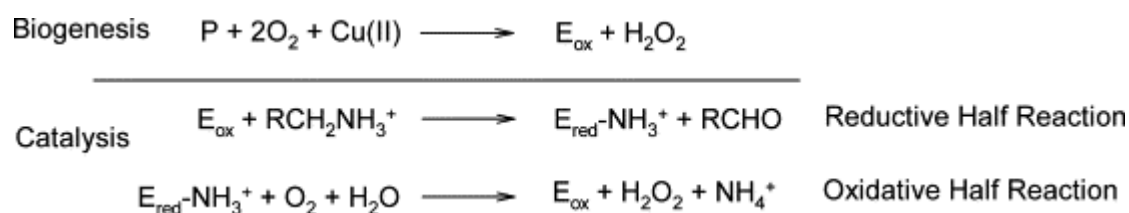


**Figure 1. The reactions catalysed by copper-containing amine oxidases (CuAOs): Biogenesis, the catalytic reductive half-reaction, and the catalytic oxidative half-reaction.  $E_{\text{apo}}$  is the apo-enzyme, containing the precursor tyrosine to the cofactor 2,4,5-trihydroxyphenylalanine quinone (TPQ) and no bound copper.  $E_{\text{ox}}$  is the mature native holo-enzyme, containing TPQ and Cu (II).  $E_{\text{red}}$  is the substrate reduced form of the enzyme, principally containing the aminoquinol form of cofactor and Cu(II), which in some CuAOs is in equilibrium with a Cu(I)-semiquinone form of cofactor (Brazeau *et al.*, 2004).**

### 2.1 Semicarbazide sensitive amine oxidase (SSAO)

Semicarbazide-sensitive amine oxidase (SSAO) is a copper amine oxidase with a carbonyl cofactor topa-quinone (TPQ) which makes SSAO highly sensitive to carbonyl reagents like semicarbazide. SSAO catalyse oxidative deamination and converts primary amines into their corresponding aldehydes, while generating hydrogen peroxide and ammonia.

According to Salmi & Jalkanen (2017), this catalytic reaction is a two-step reaction consisting of a reductive half-reaction, subsequent hydrolysis step, and oxidative half-reaction. In the reductive half-reaction, a protonated primary amine first interacts with the oxidised form of topa-quinone (a posttranslational modification of a specific tyrosine residue in SSAO). This causes the active site base to catalyse proton abstraction leading to the formation of a product Schiff base and reduced topa-quinone (Figure 2, 1-4). In the subsequent hydrolysis step, a product aldehyde is released; and in the oxidative half-reaction, molecular oxygen re-oxidises topa-quinone with concomitant production of ammonia and hydrogen peroxide (Figure 2, 5-6).

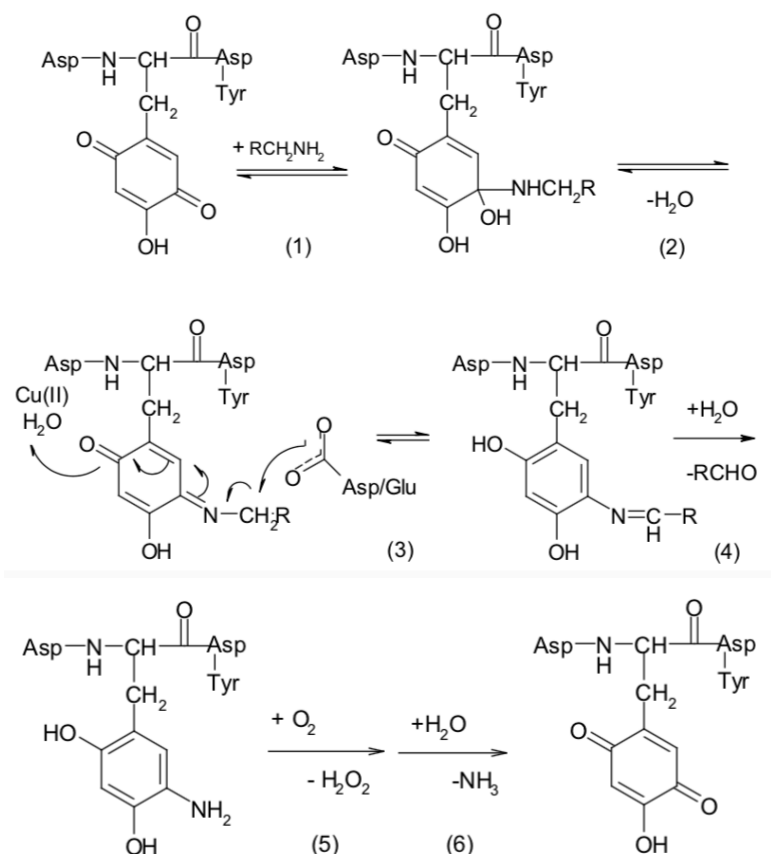


**Figure 2. SSAO oxidase primary amines into aldehydes, ammonia, and hydrogen peroxide in a two-step reaction (Salmi & Jalkanen, 2017).**

SSAO is defined as a multi-functional enzyme with diverse biological role that differ significantly between tissues and species (Salmi & Jalkanen, 2017). It is present in both, eukaryotes, and prokaryotes, including microorganisms, plants, animals, and humans. In microorganisms, SSAO is found in some bacterial species such as *Acinetobacter*, *Klebsiella*, *Shigella*, and *Escherichia coli* where it has been identified as important factor in supporting bacterial growth (Brazeau *et al.*, 2004).

Furthermore, recent studies have proposed that the hydrogen peroxide-generating enzymatic activity of SSAO may provide a growth advantage to *E. coli* over other bacteria, which are not able to handle hydrogen peroxide in their living environment (Salmi & Jalkanen, 2017). The other name for SSAO is clorgyline-resistant amine oxidase (CRAO) because of its insensitivity to inhibition by the acetylenic monoamine oxidase inhibitors such as clorgyline, l-deprenyl and pargyline. Being a copper amine oxidase, SSAO has rich copper content, as much as 1 mole of copper per subunit (Sullivan *et al.*, 2004). The gene that encodes for SSAO is the amine oxidase copper containing 3 (AOC3), which in humans is located on chromosome 17, at region 17q21 (Figure 3); and in rats is located on chromosome 10, at region q31 (Figure 4).

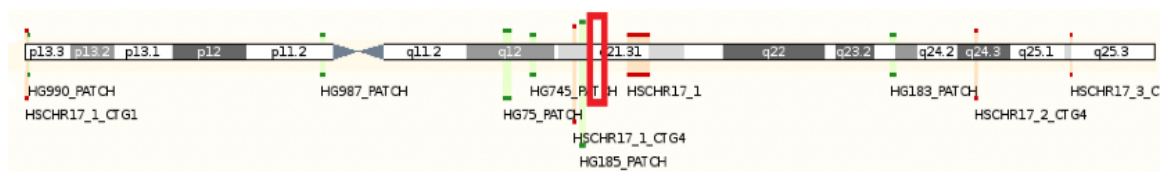


**Figure 3. Chromosome location of AOC3 gene in a human (<http://www.ensembl.org>)**



**Figure 4. Chromosome location of AOC3 gene in a rat (<http://www.ensembl.org>)**

## 2.2 Molecular structure of SSAO

The molecular structure of SSAO is sometimes described as mushroom-like, with an N-terminal “stalk”, binding the protein to the plasma membrane, and a large C-terminal “cap”. SSAO is a heavily sialylated homodimeric glycoprotein with a molecular weight of 170–180 kDa, depending on the degree of glycosylation (Figure 5). The dimers consist of two identical subunits with a short N-terminal anchor. As co-factors, each subunit contains one copper ion Cu (II) and an oxidised tyrosine residue which interacts directly with the substrate.

The tyrosine residue is part of the protein backbone, and a lot of interest has been focused upon its conversion to topa-quinone (TPQ) cofactor, which has been previously established to be a self-processing reaction mediated by the enzyme-bound copper (Jacobsson *et al.*, 2005). Pannecoeck *et al.* (2015) have identified that His520, His522 and His684 (three conserved histidines) coordinate the copper ion involved in TPQ biogenesis. The TPQ cofactor, together with an aspartic acid residue (Asp386), acts as a highly conserved active site involved in the catalytic reaction (Jacobsson *et al.*, 2005).

During the catalytic reaction TPQ oxidatively deaminates primary monoamines *via* Schiff base formation, with the TPQ, before base-assisted cleavage and release of the corresponding aldehyde (Smith & Vainio, 2007). Amines such as lysine side chains presented on peptide or protein ligands are known to access the TPQ and serve as substrates. Recent studies have demonstrated that TPQ forms a centre for adhesive interactions with amine ligands presented on the leukocyte surface (Salmi & Jalkanen, 2017; Smith & Vainio, 2007; Jalkanen & Salmi, 2001). SSAO shares a similar fold with the other CuAOs and contains three domains: D2, D3 and D4 (Figure 5). The N terminal of the protein acts as D1 domain in a form of transmembrane helix. D2 - D4 are located extracellularly. The highest degree of structural similarity with the others CuAOs is observed for the central D4  $\beta$ -sandwich domain, which contains the dimer interface. On the outside of the D4 domain there are two smaller  $\alpha/\beta$ -domains, D2 and D3 (Figure 5).

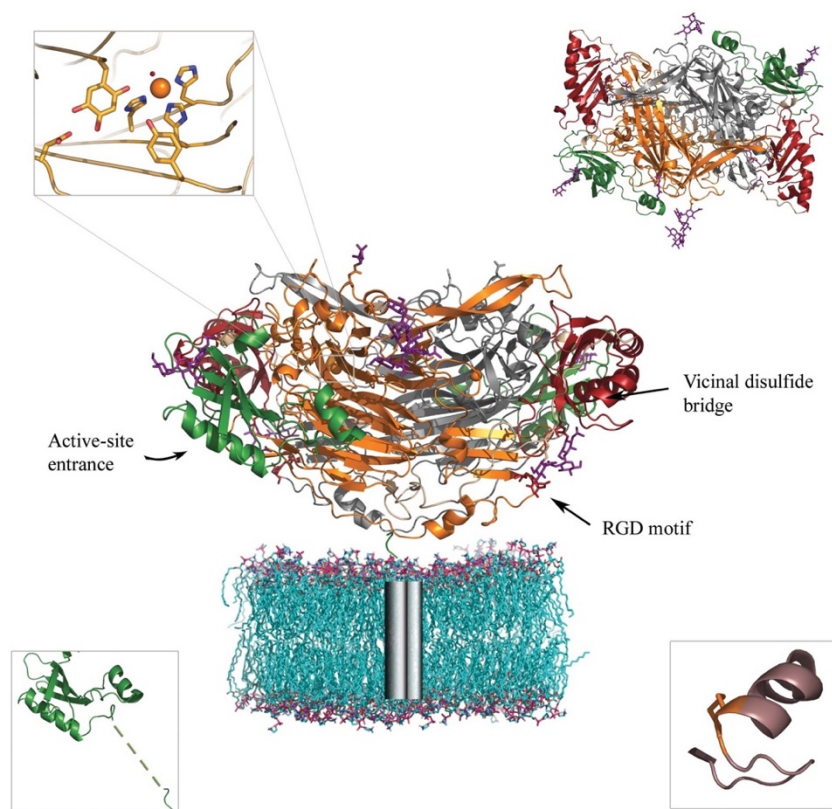


**Figure 5. Structure of SSAO. Domain D2 is shown in green, domain D3 in red and domain D4 in grey (monomer A) or orange (monomer B) and carbohydrates are shown as purple sticks. The grey cylinders represent the membrane-bound helices. The insets show, clockwise from the top left, the active site of SSAO, a view of the homodimer from the top towards the membrane, the vicinal disulphide bridge, and parts of domain D2 (Jakobsson *et al.*, 2005).**

Despite being defined as enzyme that varies between tissues and species, SSAO has conserved main characteristics that are same regardless of these factors. These include:

- 763-765 amino acids which form a homodimer.
- A transmembrane domain which forms the N terminal.
- An Asn-TPQ-Asp/Glu-Tyr sequence in the active site of the enzyme (Figure 6).
- Tyr which is situated at 470 or 471 amino acids from N terminal and is post-translationally modified to TPQ (Figure 6).
- Asp which is approximately 100 residues from TPQ, the catalytic base of the deamination in its reductive half-reaction (Figure 6).
- 6 sites of N-glycosylation (Asn).
- Arg-Gly-Asp (RGD) motif for binding with integrins.

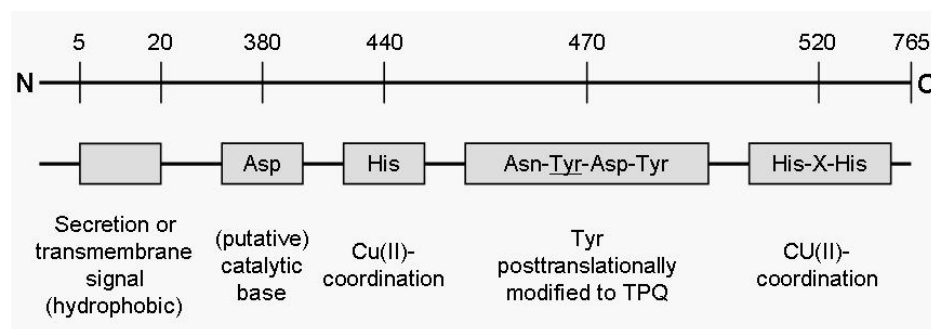


**Figure 6. Conserved regions of SSAO (Salmi & Jalkanen, 2001).**

### **2.3 Soluble and membrane bound SSAO**

In mammals, the enzyme exists both as a soluble protein, as well as a tissue bound type II transmembrane protein. The latter often referred to as vascular adhesion protein-1 (VAP-1). VAP-1 is a dual-function molecule that possesses an amine oxidase activity. The two monomers making up the VAP-1 dimer, each possess a monoamine oxidase (MAO) activity in the extracellular part of the protein (Smith & Vainio, 2007). VAP-1 is attached to the cell surface by an N - terminal helix and is involved in leukocyte trafficking in the endothelial cells, glucose uptake and metabolism in the adipocytes, and vascular elasticity (Smith & Vainio, 2007). The soluble SSAO is a result of a proteolytic cleavage of the membrane bound VAP-1. During this process, anchored SSAO molecules are released into the bloodstream by shedding from the membrane by a metalloproteinase-dependent activity (Abella *et al.*, 2004; Stolen *et al.*, 2004).

Soluble SSAO in the circulation modulates adhesive activity of the membrane bound VAP-1 and has a comparable molecular weight with the same (Pannecoeck *et al.*, 2015). Levels of soluble SSAO have been reported to increase in conditions such as diabetes, liver disease and obesity (Abella *et al.*, 2004; Stolen *et al.*, 2004). It has also been reported that soluble SSAO might be involved in the production of non-enzymatic additions of oligosaccharides to proteins during formation of advanced glycation end products (Abella *et al.*, 2004). In the endothelial cells, soluble SSAO has been reported to modulate lymphocyte adhesion by triggering positive signal on the lymphocytes (Kurkijarvi *et al.*, 1998).

From embryonic week 7, SSAO/VAP-1 is synthesized in many organs and tissues, including the vasculature and adipocytes. The most prominent cell types producing SSAO/VAP-1 are vascular endothelial cells, smooth muscle cells, and adipocytes. In the vasculature, SSAO/VAP-1 is present in all three types of endothelial cells, including continuous (most vessels), fenestrated (e.g., kidney peri-tubular capillaries), and sinusoidal (liver and bone marrow) endothelial cells (Salmi & Jalkanen, 2017). In the endothelial cells, SSAO/VAP-1 is localized in the intracellular/cytoplasmic vesicles (often more on the venous than capillary or arterial side), which are also responsible for recycling of VAP-1 (Boomsma *et al.*, 2005; Pannecoeck *et al.*, 2015). SSAO/VAP-1 is also strongly expressed in smooth muscle, but not in skeletal or cardiac muscle cells.

In smooth muscle cells, SSAO/VAP-1 is enriched in the caveolae of the plasma membrane and is also found in pericytes, occupying the outer surface of blood vessels (O'Sullivan *et al.*, 2002). In adipocytes, 25% of SSAO/VAP-1 is found in GLUT4<sup>+</sup> vesicles. It is also expressed on dendritic cells in the germinal centres (but not on other leukocyte types), and in chondrocytes (Smith & Vainio, 2007).

## SECTION 3. PHYSIOLOGICAL AND PATHOPHYSIOLOGICAL FUNCTIONS OF SSAO/VAP-1

As a result of its enzymatic nature, the function of SSAO/VAP-1 is regulated by the availability and affinity of its substrates, secondary effects of the reaction products, and natural inhibitors (Jalkanen *et al.*, 2007). In normal physiological conditions, SSAO/VAP-1 act as a scavenger for various monoamines released into the circulation. However, its catalysed reaction results in the generation of bioactive compounds (aldehydes, hydrogen peroxide and ammonium). The oxidase activity of SSAO/VAP-1 has been linked to leukocyte-endothelial cell interactions, adipocyte differentiation, glucose transport and structural organisation of vascular smooth muscle (Pannecoeck *et al.*, 2015).

### 3.1 Leukocyte-endothelial cell interaction

SSAO/VAP-1 induces and regulates leukocytes adhesion and trafficking on the endothelial wall (Figure 7). Circulating leukocytes reversibly tether and roll on the endothelial cells as a first step of a well-orchestrated cascade, which is then followed by firm adhesion of the leukocytes on the endothelial wall and transmigration into the tissue (Salmi & Jalkanen, 2001). This process is regulated by multiple adhesion and activation molecules such as selectins, sialomucins, chemokines and integrins (Figure 7).

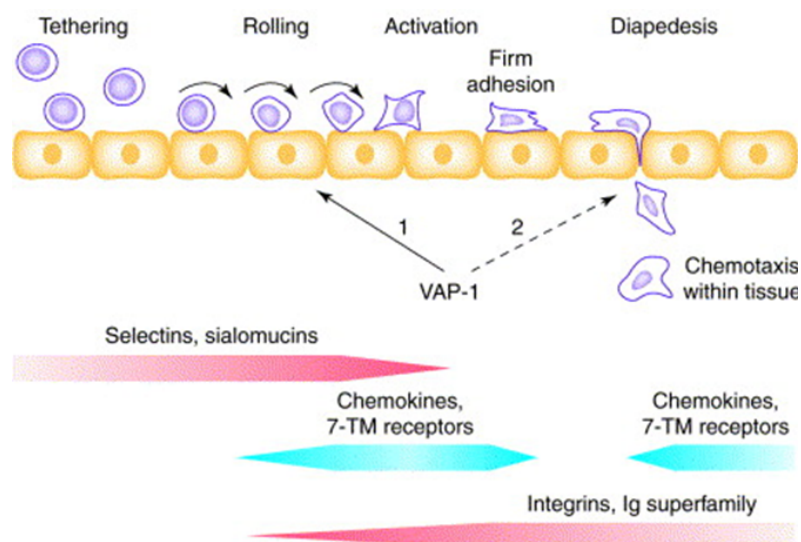


**Figure 7. Leukocyte extravasation mediated by a multistep adhesion cascade (Salmi & Jalkanen, 2001).**

SSAO/VAP-1 induces leukocyte adhesion under shear stress conditions *via* enzyme-activity–dependent and enzyme-activity–independent manner (Figure 8). The adhesive and enzymatic function of SSAO/VAP-1 usually involves two separate lymphocyte molecules. However, if the adhesive counter-receptor is the amine-containing substrate, the same molecule can be used in both events (Salmi & Jalkanen, 2001). The cell surface expression of the membrane bound VAP-1 is induced under inflammatory conditions which promote the translocation of this enzyme from the intracellular storage granules of the endothelial cells into the lumen. Inflammatory mediators, such as interleukin (IL)-1, tumour necrosis factor (TNF), interferon (IFN)- $\gamma$ , and lipopolysaccharide (LPS) have been identified to increase VAP-1 protein expression *ex vivo* (Salmi & Jalkanen, 2017). After its expression is increased, the adhesive event of leukocytes adhesion and trafficking involves reaction between VAP-1 and the surface bound primary amines presented by lymphocyte surface proteins such as amino-sugars, N-termini of proteins or NH<sub>2</sub>-containing amino acid side chains (Salmi & Jalkanen, 2017). Pannecoeck *et al.* (2015) have demonstrated that in conditions of sheer stress there is a transitional covalent bond between the membrane bound endothelial VAP-1 and a surface-expressed amine on leukocytes, which is crucial during the rolling step of the leukocyte adhesion cascade. Moreover, freely flowing leukocytes bind to the endothelium via a putative leukocyte receptor specific to the surface epitopes of VAP-1. This leads to a catalytic reaction in which there is aldehyde formation and the release of H<sub>2</sub>O<sub>2</sub> and NH<sub>3</sub>. Furthermore, the spontaneous cleavage of the Schiff base allows leukocytes to migrate through the vessel wall, which leads to a cascade of sequential events such as rolling, adhesion and transmigration.

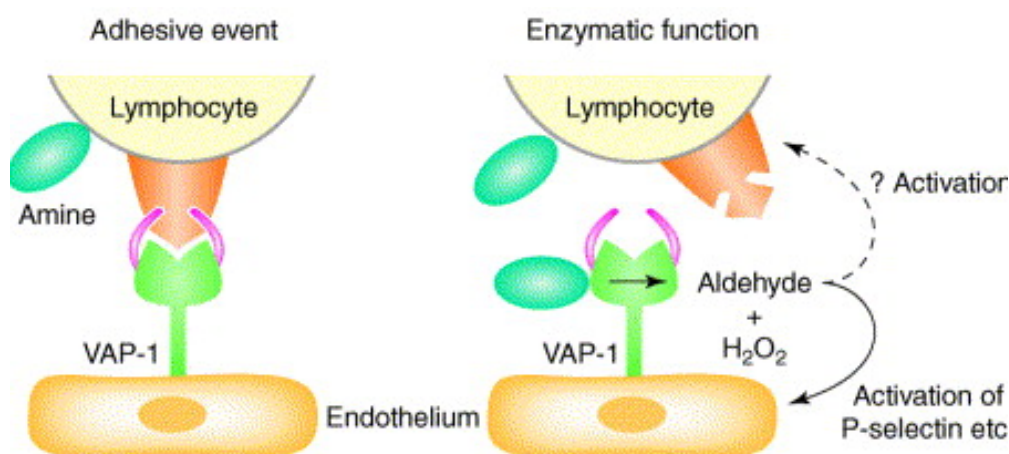


**Figure 8. SSAO induces leukocyte adhesion *via* its adhesive and enzymatic function (Salmi & Jalkanen, 2001).**

SSAO can also contribute to lymphocyte binding through enzyme-activity-dependent manner. With the enzymatic function SSAO acts as ectoenzyme and converts soluble primary amines into corresponding aldehydes and hydrogen peroxide. The hydrogen peroxide produced with this enzymatic reaction induces transcription and translation of adhesion molecules such as selectins (Figure 8). Jalkanen *et al.* (2007) have demonstrated that hydrogen peroxide alone, or in combination with other end products, contributes to crosstalk between E- and P-selectins, which after being activated can regulate leukocyte trafficking by competing with the cell-membrane-bound forms for the ligands. Johnston *et al.* (1996) have demonstrated that exogenous hydrogen peroxide has ability to elicit leukocyte rolling within a narrow response window between 10 and 500 $\mu$ M, in a P-selectin dependent manner.

### **3.2 Adipocyte's differentiation and obesity**

SSAO/VAP-1 plays an important role in the regulation of adipogenesis and the development of obesity. It has already been established that fat cells exhibit higher levels of SSAO/VAP-1 than any other cells. Zorzano *et al.* (2003) have observed  $14 \times 10^6$  copies of SSAO per cell in isolated rat adipocytes. Highly expressed levels of this enzyme have been found in various subcellular compartments of the adipocytes, such as the plasma membrane, glucose transporter-containing vesicles and micro vesicles (Enrique-Tarancon *et al.*, 2000; Souto *et al.*, 2003). Moldes *et al.* (1999) have detected a significant increase of SSAO/VAP-1 mRNA levels and activity during adipocyte differentiation in the murine cell lines 3T3-F442A and 3T3-L1.

The involvement of SSAO/VAP-1 in adipogenesis has been mentioned in other studies. Morin *et al.* (2001) and Bour *et al.* (2007) have identified that AOC3 gene significantly increases during adipogenesis of preadipocytes, which would consequently result in high levels of SSAO/VAP-1 in mature adipocytes. Mature adipocytes release leptin which acts centrally to regulate food intake and energy expenditure. The imbalance between energy intake and expenditure would lead to excessive storage of energy as fat, leading to the development of obesity. The involvement of SSAO/VAP-1 in the development of obesity is also a result of the formation of hydrogen peroxide which can mimic the effect of insulin (El Hadri *et al.*, 2001; 2002). El Hadri *et al.* (2002) have demonstrated an ability of methylamine and other SSAO substrates to induce maturation of adipocytes in a dose-dependent manner, through insulin which acts as a stimulant for adipocyte differentiation.

### 3.3 Glucose transport

SSAO/VAP-1 stimulates glucose transport in adipocytes through hydrogen peroxide dependent mechanism. By mimicking the effect of insulin, hydrogen peroxide plays an important role in enhancing glucose transport in adipocytes. It has been shown that hydrogen peroxide can activate phosphatidylinositol-3 kinase and protein kinase B, and consequently lead to translocation of GLUT4 to the plasma membrane (El Hadri *et al.*, 2001). Zorzano *et al.* (2003) have further established that the SSAO driven glucose uptake mechanism through hydrogen peroxide is due to the synergistic relationship between SSAO substrates and vanadate (Figure 9). Zorzano *et al.* (2003) incubated 3T3-L1 adipocytes for 3.5h with 1mM benzylamine and 0.1mM vanadate and demonstrated a 10-fold stimulation of glucose transport into the cells. This synergistic action between SSAO substrates and vanadate results in production of a potent insulin-like agent peroxovanadate, which can be formed extra or intracellularly (Zorzano *et al.*, 2003). Peroxovanadate acts as an active compound and can activate a protein-tyrosine kinase or inhibit a protein-tyrosine phosphatase, which in turn causes tyrosine phosphorylation of insulin receptors substrate proteins (IRS-1 and IRS-3). After being phosphorylated these proteins stimulate phosphatidylinositol 3-kinase (PI 3-kinase) by rapidly interacting with the p85 and p110 subunits of the same. Activated PI 3-kinase has an important role in insulin-signal transduction by causing GLUT4 recruitment to the cell surface and stimulation of glucose transport in adipose cells (Zorzano *et al.*, 2003).

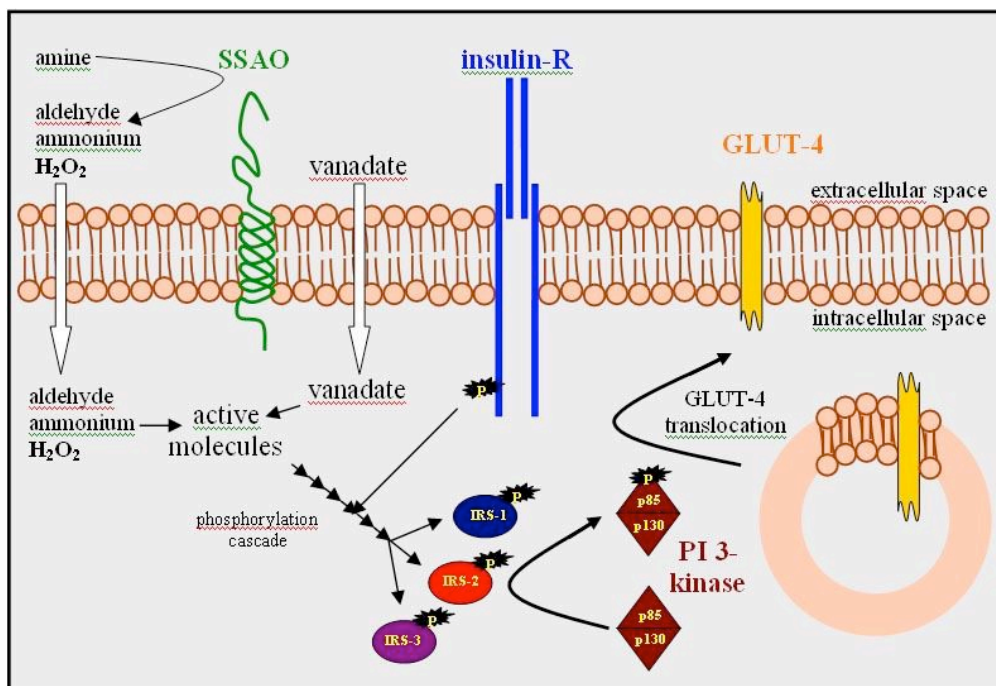


Figure 9. The role of SSAO in regulation of glucose uptake in adipocytes (Zorzano *et al.*, 2003).

GLUT4 is insulin sensitive and represents the rate-limiting step for glucose transport into adipose tissue. It mediates glucose transport and is essential for the maintenance of normal glucose homeostasis (Yu *et al.*, 2004). Apart from its ability to influence GLUT4 translocation to the cell membrane in adipocytes, SSAO might also have ability to induce translocation of glucose transporter 1 (GLUT1) receptor, which is constitutively present in the plasma membrane of vascular smooth muscle cells (VSMCs). El Hadri *et al.* (2001) have demonstrated that in VSMCs, GLUT1 accumulation on the plasma membrane can occur within one hour after methylamine exposure. The molecular mechanism behind this effect remains unknown; however, El Hadri *et al.* (2001) have postulated that in VSMCs glucose exerts pleiotropic effects and regulates growth factor synthesis and lipid peroxidation.

This mechanism was later evident in a study done by Pyla *et al.* (2013) which demonstrated that by activating certain growth factors, glucose can induce VSMCs proliferation and contribute to phenotype switching of VSMCs from contractile to synthetic. Pyla *et al.* (2013) have further demonstrated that the initiating event toward increased glucose metabolism in proliferative VSMCs is the cellular uptake of glucose *via* facilitative glucose transporters such as GLUT1 receptors.

### **3.4 Structural organisation of vascular smooth muscle**

SSAO may also play an important role in vascular tone regulation, VSMCs differentiation, and extracellular matrix organisation (El Hadri *et al.*, 2002; Langford *et al.*, 2002; Vidrio *et al.*, 2003). The vascular smooth muscle cells in blood vessels are responsible for producing collagen and elastin in arteries. The maturation and structure of these elastic fibres and collagen depends on the formation of intra and intermolecular crosslinks and can strongly influence elasticity and resistance of the arteries (Mercier, 2009). Salmi *et al.* (2001) have demonstrated that in addition to soluble primary amines, SSAO may also act on amino acids, including matrix proteins. This reaction could contribute to cross-linking of elastic and collagen fibres, thus consequently affecting structural organisation of VSMCs (Salmi *et al.*, 2001). Langford *et al.* (2002) have demonstrated that *in vitro* inhibition of SSAO could lead to elastic fibre disorganisation in heart and smooth-muscle cells. Furthermore, Gokturk *et al.* (2007) have developed a transgenic murine model over-expressing human SSAO/VAP-1 in VSMCs. The mouse model developed by Gokturk *et al.* (2007) presented abnormal elastic lamellar structure in the aorta, together with an elevated pulse pressure, suggesting increased rigidity of large arteries because of elevated SSAO activity, as well as a possible physiological role of SSAO in elastic fibre maturation.

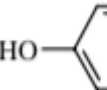
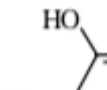
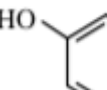
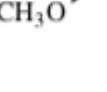
## **SECTION 4. SSAO SUBSTRATES AND THEIR CORRESPONDING ALDEHYDES PRODUCTS**

The mammalian SSAO/VAP-1 can metabolise various aromatic and aliphatic monoamines which act as substrates and are produced endogenously or absorbed as dietary or xenobiotic substances. This includes exogenous (e.g., benzylamine, tyramine) or endogenous (e.g., phenylethylamine, histamine) aromatic primary amines, but also endogenous (e.g., methylamine, aminoacetone) aliphatic primary amines (O'Sullivan *et al.*, 2004). Some of the substrates for SSAO/VAP-1 are listed in Table 2.

Certain monoamine substrates are common to both, SSAO/VAP-1 and MAO-A & MAO-B, as well as SSAO/VAP-1 and LOX's. However, some are very specific to SSAO/VAP-1 such as aminoacetone, methylamine and allylamine.

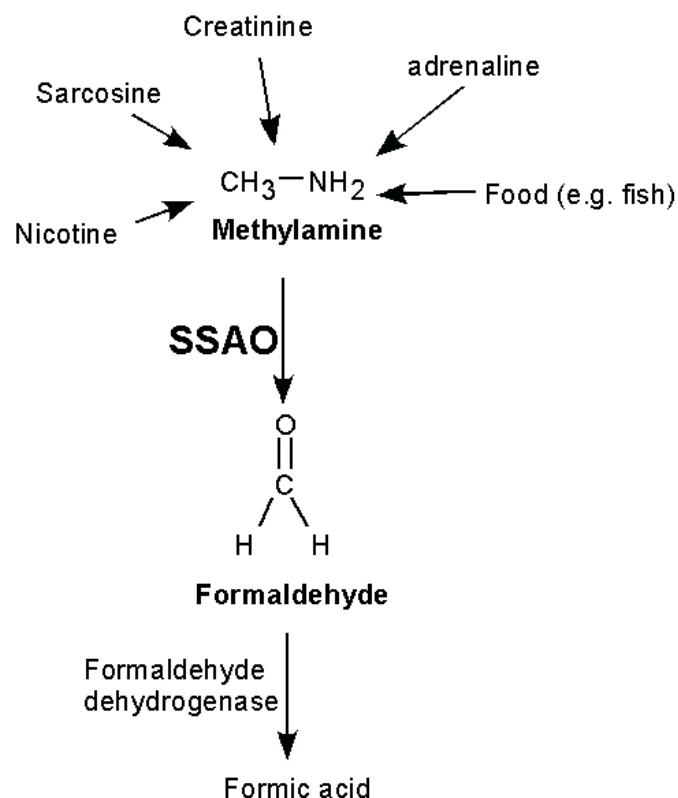
During the process of oxidative deamination catalysed by SSAO/VAP-1, the primary monoamines are converted to aldehydes. Aldehydes, together with ammonium and hydrogen peroxide, are the same as those produced in the MAO catalysed reaction. However, MAO produces its products within the cell whereas those formed by SSAO/VAP-1 are extracellular. Aldehydes can be either reduced (to alcohols) or oxidized (to acids). Also, being strong electrophiles, when produced by SSAO/VAP-1 can undergo additional reactions with thiols and amines to form toxic adducts in cellular proteins, with the most notable being genotoxic DNA–protein cross-links (Kuykendall, 2010).

Table 2. Compounds known as SSAO substrates (O'Sullivan *et al.*, 2004).

| SUBSTRATES  | COMMENTS   |
|---|--|
| CH <sub>3</sub> NH <sub>2</sub> Methylamine   | Endogenous and xenobiotic.<br>Not a substrate for MAO        |
| CH <sub>2</sub> =CHCH <sub>2</sub> NH <sub>2</sub> Allylamine   | Xenobiotic. Not a substrate for<br>MAO. Highly toxic product |
| $\text{CH}_3 - \overset{\text{O}}{\parallel}{\text{C}} - \text{H}_2\text{NH}_2$ Aminoacetone            | Endogenous.<br>Not a substrate for MAO                       |
| CH <sub>3</sub> (CH <sub>2</sub> ) <sub>3</sub> CH <sub>2</sub> NH <sub>2</sub> <i>n</i> -Pentylamine   | Xenobiotic. Also MAO-B substrate                             |
|  Benzylamine           | Xenobiotic<br>Also MAO-B substrate                           |
|  2-Phenethylamine      | Trace amine<br>Also MAO-B substrate                          |
|  Tyramine              | Endogenous & xenobiotic<br>Also MAO A & B substrate          |
|  Dopamine             | Endogenous<br>Also MAO A & B substrate                       |
|  5-Hydroxytryptamine | Substrate in dental pulp.<br>MAO-A substrate                 |
|  Mescaline           | Xenobiotic.<br>Also MAO substrate                            |
|  Primaquine          | Xenobiotic.<br>Also MAO substrate                            |

#### 4.1 Methylamine and formaldehyde

Methylamine is a dietary amine and substrate for SSAO/VAP-1. It is produced *in vivo* by cellular metabolism of creatinine, sarcosine, and adrenaline (Figure 10), and is also known as end-product of nicotine metabolism. Smoking nicotine can induce the release of adrenaline, which is in turn deaminated by monoamine oxidase, resulting with methylamine production (Yu, 1998). The breakdown of adrenaline by MAO would result with elevated levels of methylamine, which is then oxidized by SSAO/VAP-1.



**Figure 10. Formation and degradation of methylamine (Sartori *et al.*, 2008).**

SSAO oxidised methylamine can stimulate glucose uptake through hydrogen peroxide dependent mechanism (Figure 11). The hydrogen peroxide formed as a by-product of this oxidative reaction would recruit the GLUT-4 insulin receptor on the cell surface (Figure 11) and stimulate glucose uptake into adipocytes (El Hadri *et al.*, 2001; O'Sullivan *et al.*, 2004).

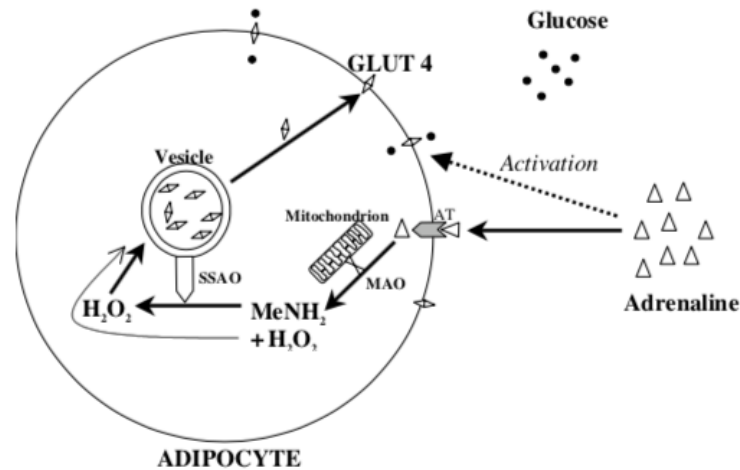


**Figure 11. Methylamine (MeNH<sub>2</sub>) stimulates glucose uptake through a hydrogen peroxide dependent mechanism. Adrenaline uptake, through its transporter (AT), is followed by intracellular metabolism by mitochondrial monoamine oxidase to form methylamine which is then oxidised by SSAO. Both the MAO and SSAO reactions form H<sub>2</sub>O<sub>2</sub> (O'Sullivan *et al.*, 2004).**

SSAO/VAP-1 converts methylamine to formaldehyde (Figure 10) which is an extremely reactive aldehyde capable of cross-linking with proteins following a pseudo-first order kinetic (Gubisne-Haberle *et al.*, 2004). It has ability to induce lipid peroxidation, formation of advanced-glycation end products (AGE), oxidative stress and vascular damage (Unzeta *et al.*, 2006). Formaldehyde has also been demonstrated as main apoptotic inducer in endothelial and smooth muscle cells. Hernandez *et al.* (2006) have observed formaldehyde induced apoptosis in A7r5 cells, detected by chromatin condensation, Caspase-3 activation, PARP cleavage and cytochrome c release to cytosol. In addition. Hernandez *et al.* (2006) have also observed almost 100% loss of VSMCs viability at only 0.5mM Formaldehyde.

Formaldehyde can induce cell death by interacting with macromolecular constituents, thus altering cellular structures. Hernandez *et al.* (2006) have demonstrated that by generating cross-linking with DNA and proteins, formaldehyde can alter mitochondrial membrane structures and induce the opening of the mitochondrial transition pore, thus promote cytochrome c release to the cytosol, caspase activation and cell death. Mercier (2009) has further demonstrated that apart from producing AGEs, when formed from methylamine, through soluble SSAO, formaldehyde can upregulate apoptosis by inducing the expression of the pro-apoptotic protein p53, member of the Bcl2 family proteins, and activation of caspases 9/3 (Figure 12). These authors have also demonstrated that the hydrogen peroxide formed through this reaction plays an important role in free radical formation and oxidation of LDL, as well as inducing expression of endothelial E and P selectins (Figure 12).

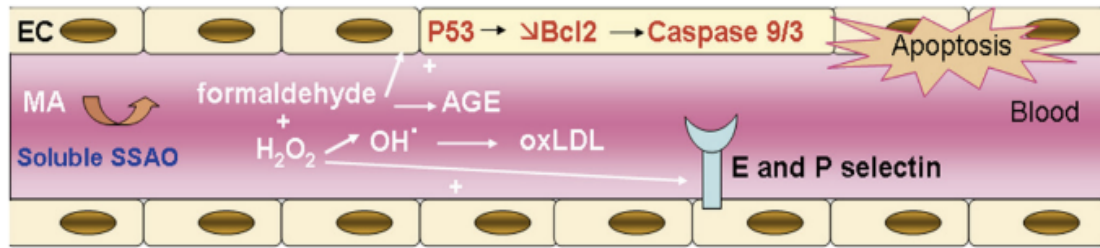


**Figure 12. SSAO produced formaldehyde induces apoptosis through release of pro-apoptotic protein P53 and caspases (Mercier, 2009).**

#### **4.2 Aminoacetone and methylglyoxal**

Aminoacetone is an aliphatic amine, and threonine and glycine catabolite produced in the mitochondrial matrix (Figure 13). It is another substrate for SSAO/VAP-1, through which it is converted to methylglyoxal, a highly reactive aldehyde, also known as a powerful modifying agent of proteins and DNA, and mediator in the synthesis of advanced glycation end products (Kenneth *et al.*, 2002). It has been previously established that by modifying proteins, as well as through formation of oxygen free radicals, methylglyoxal acts as cytotoxic agent and induces apoptosis in cells (Mathys *et al.*, 2002). Mathys *et al.* (2002) have further identified that methylglyoxal modifies cell proteins non-enzymatically through the Maillard reaction, in which aldehydes and ketones react with  $\epsilon$ -amino groups of lysine residues and guanidino groups of arginine residues. Maillard reactions contribute to the formation of stable chemical adducts in proteins known as advanced glycation end products (AGEs). AGEs can contribute to arterial stiffness and vascular complications by interacting with their receptors (RAGEs), and consequently inducing the expression of pro-inflammatory cytokines (Mercier, 2020; 2009).

Since SSAO/VAP-1 is a membrane bound protein, methylglyoxal formation from aminoacetone might occur both intra and extracellularly in smooth muscle cells. Endothelial cells lining the vascular wall are in intimate contact with smooth muscle cells; this means that the methylglyoxal produced extracellularly by smooth muscle cells might have toxic effects on the endothelium. The cytotoxic effect of methylglyoxal on the endothelial cells has been previously linked with the pathology of diabetes neuropathy, nephropathy, and retinopathy (Sartori *et al.*, 2008). In another study by Kenneth *et al.* (2002) it was demonstrated that SSAO/VAP-1 not only produces methylglyoxal from aminoacetone, but also directly mediates the synthesis of methylglyoxal AGEs.

Kenneth *et al.* (2002) were able to link the metabolism of aminoacetone to argpyrimidine formation in tissues or cells exposed to abnormally high concentrations of glucose. Argpyrimidine is a useful marker of AGE formation, and it is one of the many pathways through which methylglyoxal can modify proteins.

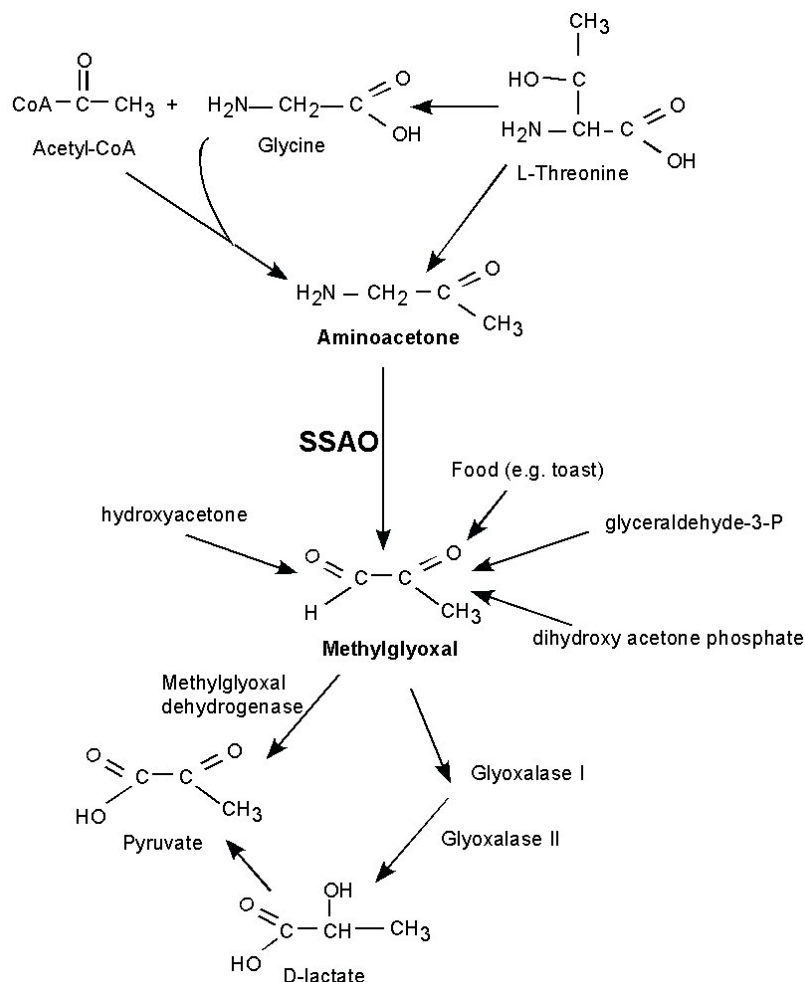


Figure 13. Reaction pathways surrounding aminoacetone and methylglyoxal (Sartori *et al.*, 2008).

### 4.3 Allylamine and acrolein

Allylamine is an industrial three-carbon amine and toxic xenobiotic that is metabolised by SSAO/VAP-1 to acrolein (Figure 14). Acrolein is a highly toxic aldehyde that is present in cigarette smoke, automobile exhaust, wood smoke and overheated cooking oils.

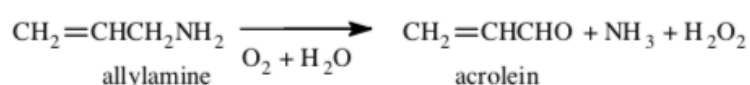
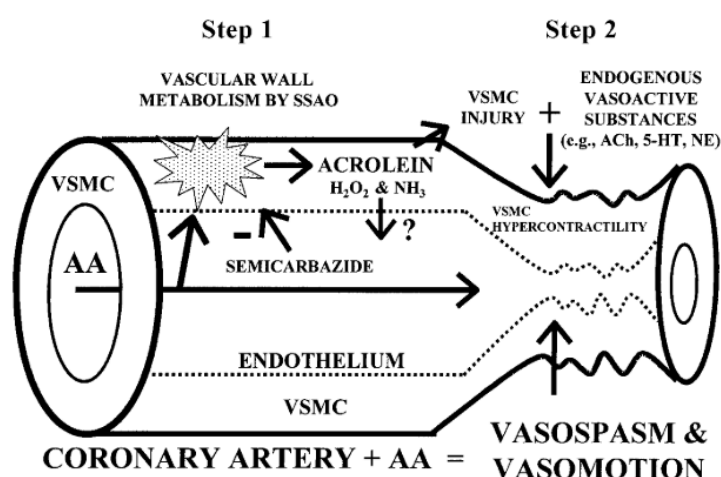


Figure 14. Conversion of allylamine to acrolein (O'Sullivan *et al.*, 2004)

Both, allylamine and acrolein have been associated with the development of hypertension and myocardial ischemic damage caused by coronary artery vasospasm, because of induced irreversible contraction of VSMCs (Conklin *et al.*, 2001; 2006; Toraason *et al.*, 2009). In their study Conklin *et al.* (2001) have proposed a two-step model explaining the mechanism behind the effect allylamine has on stimulating vasospasm, thus promoting the development of hypertension, and inducing myocardial injury (Figure 15). The first step of the model proposed by Conklin *et al.* (2001) explains the SSAO/VAP-1 facilitated metabolism of allylamine to acrolein, hydrogen peroxide and ammonia. The second step demonstrates how acrolein induces vasospasm and vasomotion of the vascular smooth muscle cells, leading to hypercontractility of the same, at the same time sparing the endothelial layer (Figure 15). Furthermore, the conversion of allylamine to acrolein has also been shown to have an important role in the development of atherosclerosis by inducing necrotic and fibrous lesions in vascular and myocardial tissue (Mercier, 2009).



**Figure 15. Hypothetical model of allylamine (AA) induction of coronary artery (CA) vasospasm and vasomotion proposed by Conklin *et al.* (2001). The role of SSAO in generating AA metabolites, including acrolein, a highly reactive aldehyde (Step 1). Acrolein, as a product of AA metabolism, acts alone or in conjunction with other AA metabolites to injure the vascular smooth muscle cells (VSMC), the presumed site of SSAO and AA metabolism, but largely spares the endothelium (Step 2) (Conklin *et al.*, 2001).**

#### **4.4 Benzylamine and benzaldehyde**

Benzylamine is an aromatic monoamine and another non-physiological, xenobiotic substrate for SSAO/VAP-1. Through oxidative deamination catalysed by SSAO, benzylamine is oxidised to an aromatic aldehyde benzaldehyde which is less cytotoxic than formaldehyde, methylglyoxal and acrolein.

Recent studies have demonstrated insulin mimicking effect of benzylamine and its involvement in the stimulation of glucose transport and inhibition of lipolysis (Iffiú-Soltés *et al.*, 2010). In a study done by Iffiú-Soltés *et al.* (2010) it was demonstrated that benzylamine administration could improve glucose tolerance and lower fasting blood glucose in high-fat diet mice. Another study done by Abella *et al.* (2003) has suggested that concomitant administration of benzylamine and vanadate could acutely stimulate insulin secretion, glucose uptake and lipogenesis, and reverse muscle insulin resistance (Figure 16). The mechanism behind this action involves the generation of hydrogen peroxide which reacts with vanadate to form peroxovanadium compounds (Figure 16). Abella *et al.* (2003) further demonstrated that the benzylamine driven glucose uptake in adipocytes is dependent on PI3-kinase and phosphorylation of the insulin receptor substrate proteins (IRS)-1 and (IRS)-3 (Abella *et al.*, 2003).

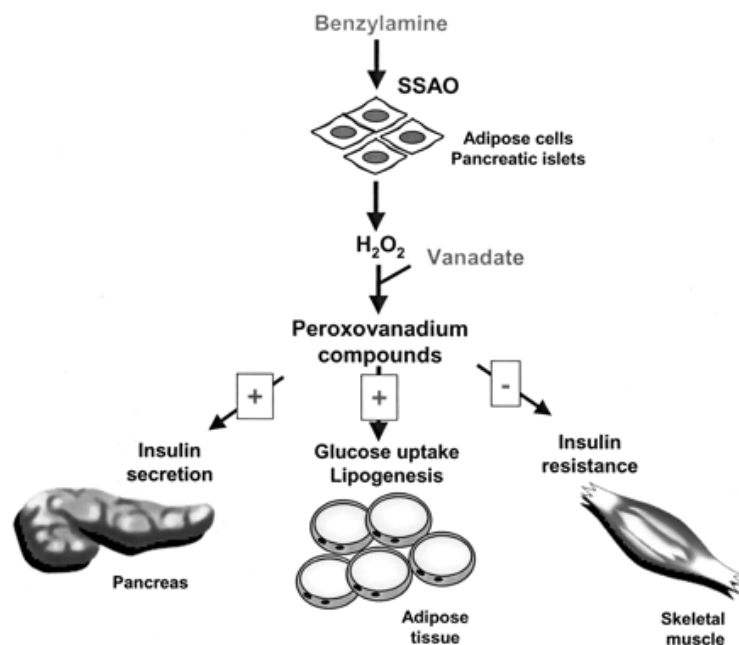


Figure 16. The role of SSAO in glucose homeostasis (Abella *et al.*, 2003)

## SECTION 5. COPPER AMINE OXIDASES – LYSYL OXIDASE

### 5.1 Lysyl Oxidase family

The lysyl oxidase family is a group of five copper containing amine oxidase enzymes. This includes: lysyl oxidase (LOX), lysyl oxidase like-1 (LOXL1), lysyl oxidase like-2 (LOXL2), lysyl oxidase like-3 (LOXL3) and lysyl oxidase like-4 (LOXL4). All five enzymes are secreted into the extracellular environment and contain a signal peptide. Furthermore, all five enzymes have conserved C-terminal domain that includes the lysine tyrosyl quinone (LTQ) cofactor, a copper-binding site, and a cytokine receptor-like domain (Trackman, 2016; Rodriguez *et al.*, 2008). LOX and LOXL1 both undergo extracellular proteolytic processing by procollagen C-proteinases; however, it is not certain whether the same applies for LOXL2 – LOXL4 (Trackman, 2016; Uzel *et al.*, 2001). LOX is firstly synthesized as a pre-pro LOX that after a series of post-translational modifications transforms into 50 kDa pro-LOX (Rodríguez *et al.*, 2008). This pro-enzyme is secreted into the extracellular environment where after being proteolytically processed by bone morphogenetic protein-1 (BMP-1) and other procollagen C-proteinases is released as mature and active 32 kDa form and its pro-peptide (Rodríguez *et al.*, 2008). LOXL2 – LOXL4 contain four scavenger receptor cysteine rich domains which are not present in LOX or LOXL1. LOXL1 assists its own trafficking and activation by procollagen C-proteinase through its own pro-region; and the pro-peptide domain of LOX, known as LOX-PP (Trackman, 2016). Like SSAO, all lysyl oxidase isoforms incorporate copper intracellularly, which is required for optimal enzymatic activity. The binding of the copper in lysyl oxidases is dependent on the conserved tyrosine and lysine residue, which in these enzymes becomes the active site carbonyl cofactor lysine tyrosyl quinone (LTQ). The LTQ cofactor is required for lysyl oxidase oxidation of its primary amine substrates: the epsilon amino group of lysine or hydroxylysine residues in collagens and lysine residues in elastin (Trackman, 2016; Tang & Klinman, 2001). In comparison to SSAO, the biogenesis of the LTQ cofactor in these enzymes requires only copper ions and does not depend on different enzyme proteins. Thus, the major function of the copper bound in LOX is the biogenesis of LTQ cofactor, which is known as spontaneous auto-catalysed post-translational modification that is crucial for ultimate acquisition of enzyme activity (Trackman, 2016). The reaction mechanism of lysyl oxidase enzymes is the same as with SSAO; it requires Schiff base formation, in this case with the lysine tyrosyl quinone (LTQ) cofactor in the first step, which then facilitates the required redox reaction (Figure 17). Moreover, here, as in the case of SSAO, the secondary and tertiary amines cannot function as lysyl oxidase substrates due to not being able to lead to Schiff base formation (Trackman, 2016).

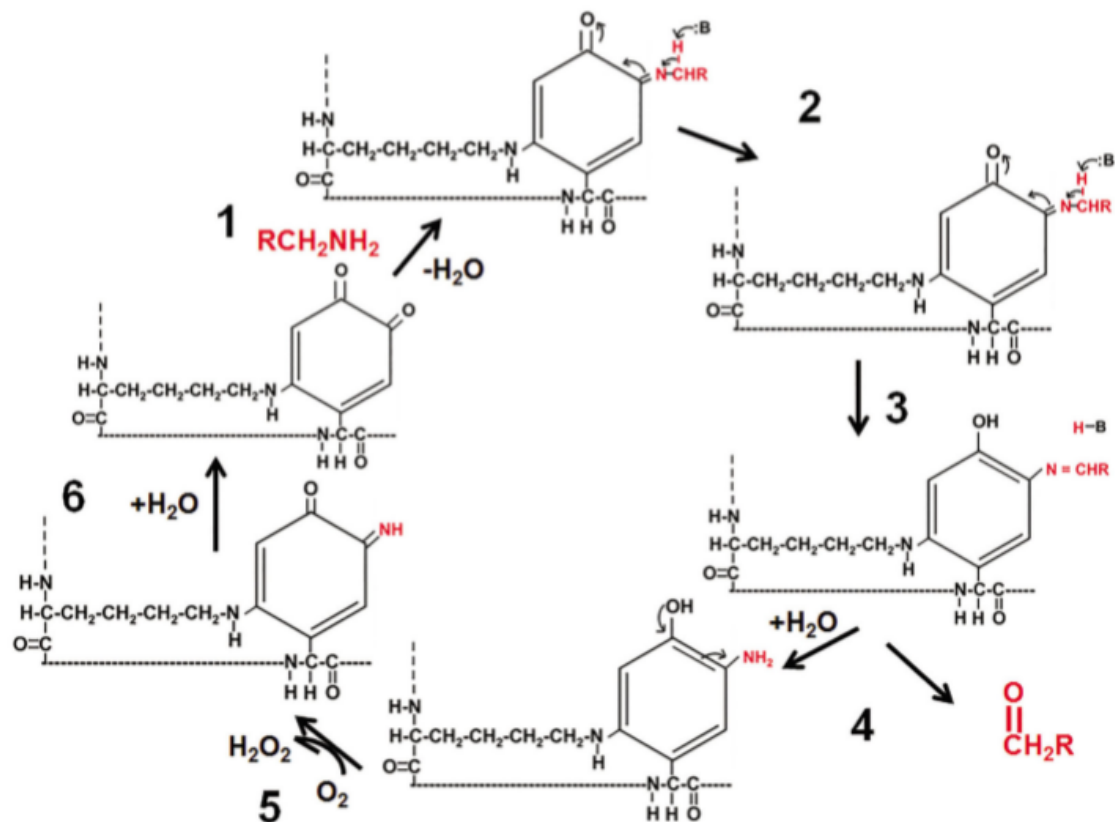
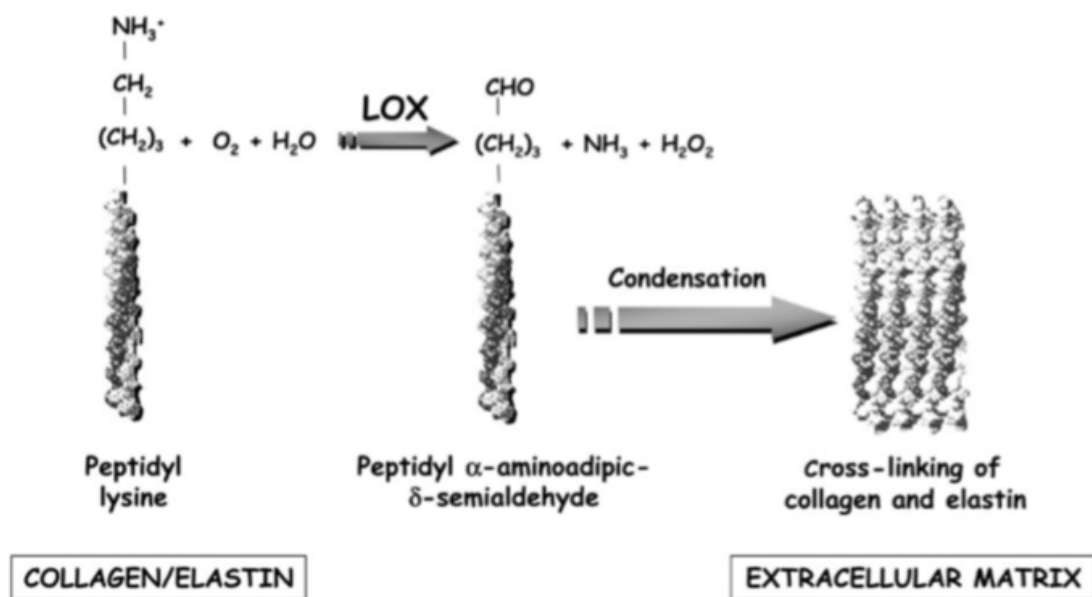


Figure 17. The mechanism of action of the lysyl oxidase-catalysed reaction. The red molecule represents the primary amine substrate or lysine side chain substrate. The numbers identify the sequence of the reaction steps (Trackman, 2016).

## 5.2 Lysyl Oxidase isoform (LOX)

LOX is first synthesized as a 50 kDa pre-proenzyme and like all five isoforms undergoes signal peptide removal and intracellular N-glycosylation in the endoplasmic reticulum. After being released into the extracellular environment as an inactive precursor, pro-LOX undergoes proteolytic processing by procollagen C-proteinases which are products of the bone morphogenetic protein-1 (BMP1), tollid-like protein 1 (TLL1) and tollid-like protein 2 (TLL2) genes (Uzel *et al.*, 2001; Trackman, 2016). This process results with release of the active enzyme (LOX) and the lysyl oxidase pro-peptide (LOX-PP). Both, active LOX and LOX-PP have independent biological activities. As an active enzyme LOX catalyses oxidative deamination of lysine and hydroxylysine residues to peptidyl  $\alpha$ -amino adipic- $\beta$ -semialdehydes (Rodriguez *et al.*, 2008). These highly reactive semi aldehydes condense to form intra- and intermolecular covalent cross-linkages that would eventually lead to extracellular matrix (ECM) stability (Figure 18). Therefore, LOX has an essential role in maintaining elastic features of connective tissues of many systems including pulmonary, cardiovascular, and skeletal system.



**Figure 18.** Reaction catalysed by lysyl oxidase (LOX). Lysyl oxidase oxidizes primary amines on collagen and elastin substrates to reactive semialdehydes that condense to form covalent cross-linkages (Rodríguez *et al.*, 2008).

### 5.3 Substrate specificity for LOX

The earliest identified biological targets of LOX are soluble precursors and immature fibrillar forms of elastin and collagen (Lucero & Kagan, 2006). However, future scientific discoveries have demonstrated that LOX can also oxidise globular and soluble cationic proteins. Furthermore, the formation of an electrostatic potential between LOX and its substrate proteins has been identified essential for the catalytic reaction (Lucero & Kagan, 2006). In the LOX driven catalytic reaction the ionic charge of the protein substrates can affect the distribution of anionic residues within LOX. This is because the sequence region where LTQ is found, as well as the region in which the lysine residue (Lys314), that becomes part of LTQ, is found, are enriched in anionic residues. Since these two regions of LOX become covalently crosslinked to each other as the LTQ cofactor is generated, both regions would cooperatively provide an abundance of negatively charged sites; and it is this arrangement that underlies the strong preference of LOX for cationic protein substrates (Kagan *et al.*, 2003).

Recently, the non-peptidyl amines such as n-butylamine and 1,5-diaminopentane (cadaverine) have been demonstrated as more suitable substrates for an *in vitro* study of LOX activity; and have been extensively used in a fluorescence-based assays for the detection of LOX-dependent H<sub>2</sub>O<sub>2</sub> production (Palamakumbura & Trackman, 2002; Lucero & Kagan, 2006; Ma *et al.*, 2017). Moreover, 1,5-d diamino pentane dihydrochloride (cadaverine) has been more frequently used as substrate to study LOX enzymatic activity in *in vitro* cell culture models (Palamakumbura & Trackman, 2002). This is because cadaverine is an alkane- $\alpha$ ,  $\omega$ -diamine comprising a straight-chain pentane core with amino substituents at positions 1 and 5, and it is synthesized through direct decarboxylation of L-lysine, which is catalysed by lysine decarboxylase in living cells (Ma *et al.*, 2017). In a study by Palamakumbura & Trackman (2002), the Amplex<sup>®</sup> Red Monoamine Oxidase was utilised to detect LOX activity using cadaverine as substrate. Palamakumbura & Trackman (2002) demonstrated that this method eliminates the interference that occurs in some biological samples and is 7.5 times more sensitive than the currently available fluorometric assays for LOX enzymatic activity by detecting 40ng of enzyme per 2ml assay at 37°C. Therefore, this study also utilised the use of cadaverine to study LOX enzymatic activity (nmolH<sub>2</sub>O<sub>2</sub>/h/mg protein) in rat aortic VSMCs.

#### **5.4 Biological activities of LOX**

As previously mentioned, LOX is crucial in maintaining elastic features through biosynthesis of collagens and elastin, and therefore its role is decisive for vascular, mineralized, and non-mineralized connective tissues. However, recent studies have reported novel biological functions of LOX. These include the control of epithelial to-mesenchymal transition, adhesion, transformation, cell migration, and gene regulation (Trackman, 2016; Sharma-Bhandari *et al.*, 2015; Higgins *et al.*, 2007). Furthermore, catalytically active LOX has also been identified in nuclear and cytosolic compartments of cells (Higgins *et al.*, 2007; Kagan *et al.*, 1991); this could point towards additional undefined roles of this enzyme in cellular homeostasis.

Elevated LOX activity has been observed in fibrotic disease where LOX affects the resistance of the extracellular matrix to proteolytic degradation, hence contributes to connective tissue accumulation and fibrosis (Iwasaki *et al.*, 2016). Additionally, upregulated LOX activity has been documented in a variety of fibrotic conditions, including liver, lung, skin, heart, and hypertension (Nave *et al.*, 2014; Gonzales-Santamaria *et al.*, 2016; Iwasaki *et al.*, 2016; Wang *et al.*, 2016). This was confirmed with a comprehensive analysis on the expression of LOX isoform after addition of  $\beta$ -aminopropionitrile ( $\beta$ APN) (Gonzales-Santamaria *et al.*, 2016; Iwasaki *et al.*, 2016).

An important and novel role for LOX enzyme activity, that extends beyond its role in collagen cross-linking, has been demonstrated in the development of myelofibrosis (Trackman, 2016). It is known that LOX exhibits high expression in the early stage of megakaryocyte differentiation and its activity and expression is required for optimal PDGF signalling and cell proliferation (Trackman, 2016). Therefore, decreased LOX expression would result with slow proliferation to permit differentiation of megakaryocytes to platelets. In the GATA-1 low mouse model of myelofibrosis it was found that high LOX expression leads to extracellular matrix accumulation and bone marrow fibrosis (Elliades *et al.*, 2011). The same study demonstrated attenuation of myelofibrosis after successful inhibition of LOX activity with  $\beta$ APN (Elliades *et al.*, 2011). This indicates that excessive LOX activity in the bone marrow could contribute to myelofibrosis.

High expression of LOX has also been documented in the development of diabetic retinopathy which is a major cause of blindness in aging subjects and diabetic individuals. A study by Roy *et al.* (2010) has linked elevated LOX expression with the progression of diabetic retinopathy, by studying its role in increasing basement membrane thickening and permeabilization. Roy *et al.* (2010) have demonstrated that an increase in basement thickening and permeabilization is a result of uneven crosslinking's of the same and distortion of its structure, which would consequently lead to increased permeability of retinal capillaries. This process in diabetic retinopathy could result with increased vascular permeability, leading to bleeding and blindness.

The role of LOX has also been investigated in the development of metastatic cancer and several ideas have emerged regarding its contribution mechanism in this disease (Levental *et al.*, 2009; Lee *et al.*, 2009). It is well known that dysplastic tissues are characterized by fibrosis and increased tissue stiffness that can enhance cell migration. Levental *et al.* (2009) have suggested that LOX-dependent collagen cross-linking can elevate stiffness, enhance fibrosis and integrin signalling, and thereby can create a suitable environment for tumour cell migration and intravasation. Furthermore, a study by Lee *et al.* (2009) has demonstrated an ability of LOX to promote formation of a metastatic niche at distant sites. In the model presented by Lee *et al.* (2009) LOX has been shown to localize at a distant site and from there play an important role in attracting tumour cells to extravasate. LOX has also been associated with the process of angiogenesis after tumour development (Payne *et al.*, 2006).

## SECTION 6. SSAO AND LOX IN CARDIOVASCULAR DISEASE

Cardiovascular disease remains a leading cause of death and morbidity in the western world (WHO, 2020). The World Health Organisation estimates 17.9 million deaths from cardiovascular disease (CVD) each year (WHO, 2020). CVD is an umbrella term used for disorders affecting the heart and the blood vessels, including coronary heart disease and cerebrovascular disease. One of the main features of coronary heart disease is atherosclerosis which is a progressive disorder characterised by fatty deposits (plaques), calcification, inflammation, and oxidative stress, and as such affects the medium and large size coronary arteries.

### 6.1 Development of atherosclerosis

Atherosclerosis is defined as progressive and complex inflammatory disease that develops because of disturbed vascular homeostasis caused by endothelial injury (Gimbrone & Garcia-Cardena, 2016). Damage to the endothelial lining is crucial starting point which sets into motion a complex pathogenic sequence. This involves recruitment of circulating monocytes from the circulation into the intimal layer, where they differentiate into macrophages and engulf modified (oxidised) lipoproteins to form foam cells (Figure 19). Multiple growth factors released by the damaged endothelium, macrophages and foam cells induce proliferation and migration of the neighbouring smooth muscles cells from the medial to the intimal layer, thus generating a fibromuscular plaque (Figure 19), the hallmark of established atherosclerosis (Gimbrone & Garcia-Cardena, 2016).

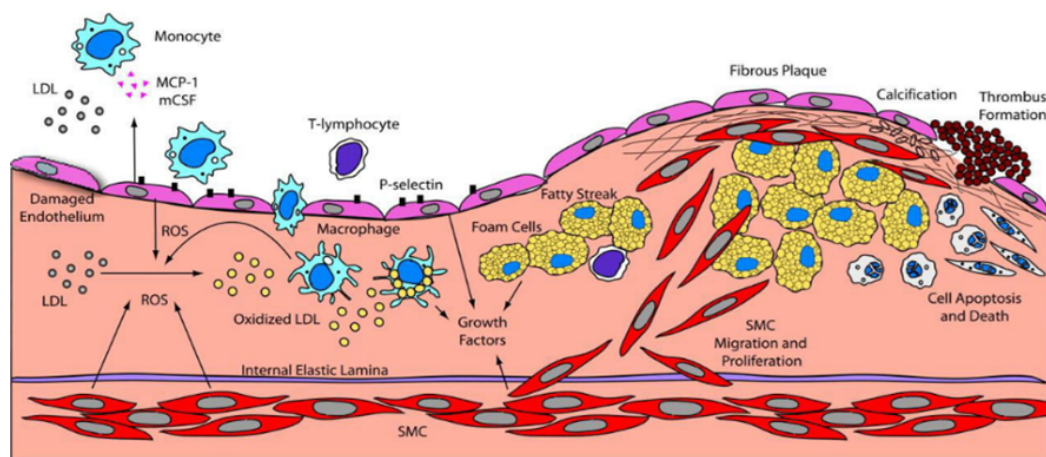
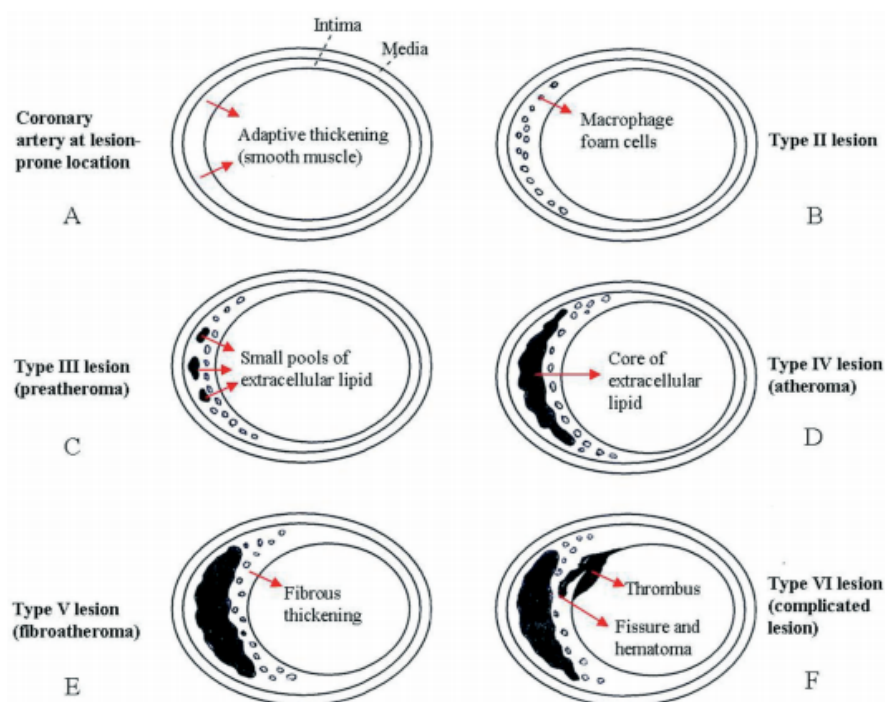


Figure 19. Pathophysiology of atherosclerosis (Gimbrone & Garcia-Cardena, 2016).

The atherosclerotic plaques, also known as arterial lesions, can be classified into 6 types based on the degree of progression of atherosclerosis. Intimal thickening is characterised in the early stage (Figure 20A), and the accumulation of macrophages and formation of foam cells are the main characteristic in the developing stages of atherosclerosis (Figure 20B, C, D, E). The fully developed atherosclerotic plaque contains lipid rich necrotic core formed from oxidised lipoproteins, cell debris and cholesterol crystals, accompanied by varying degrees of matrix remodelling and calcification (Bonomini *et al.*, 2008). The lateral edges of the plaque are rich with inflammatory cells such as activated macrophages, T cells, natural killer T cells and dendritic cells, which further modulate the endothelial proinflammatory phenotype and contribute to structural instability of the plaque (Gimbrone & Garcia-Cardena, 2016). Advanced plaques (Figure 20F) can grow large and block blood flow; when ruptured the plaque would form a thrombus or blood clot which is the major cause for stroke and myocardial infarction (Bonomini *et al.*, 2008).



**Figure 20. Early, developing, and mature stages of atherosclerosis. A – earliest stage; B, C, D, E – developing stage; F – advance stage that culminates with plaque rupture and thrombosis (Bonomini *et al.*, 2008).**

## 6.2 SSAO and cardiovascular disease (CVD)

SSAO/VAP-1 is highly implicated in the pathophysiology of various cardiovascular diseases (CVD) including stroke, myocardial infarction, and atherosclerosis, as well as health risks associated with CVD such as obesity and diabetes. High levels of active SSAO and increased turnover of its endogenous substrate methylamine have been correlated with increased atherosclerosis susceptibility in C57BL/6 mice (Yu and Deng, 1998). In humans, elevated levels of soluble SSAO have been found in patients with arterial stiffness, aortic stenosis, hypertension, chronic/ congestive heart failure, and ischemic/haemorrhagic stroke (Li *et al.*, 2021). Hernández-Guillamón *et al.* (2010) associated SSAO activity with parenchymal haemorrhages in ischemic stroke patients following tissue plasminogen activator (tPA) treatment. In a follow up study, Hernández-Guillamón *et al.* (2012) linked neurological outcomes of intracerebral haemorrhage in patients with increased plasma SSAO activity. In another study, Aalto *et al.* (2012) identified direct correlation between increased SSAO activity, intima-media thickening, and carotid plaque formation in atherosclerotic women. Furthermore, in a study done by Li *et al.* (2009) SSAO activity has been observed higher in non-diabetic subjects with increased carotid intima–media thickness comparing to those with normal thickness.

There is extensive evidence of preclinical and clinical studies done on rodents suggesting the improvement of various CVD, diabetes, and obesity after inhibition of SSAO/VAP-1. In a study by Hernández-Guillamón *et al.* (2010) SSAO inhibition with semicarbazide resulted with a reduced stroke volume in rat embolic stroke model. In another study by Zhang *et al.* (2016) SSAO inhibition with semicarbazide promoted stability of atherosclerotic lesions in LDLr<sup>-/-</sup> mice (Zhang *et al.*, 2016). In addition to this, Peng *et al.* (2016) also demonstrated enhanced stabilization of established lesions in LDLr<sup>-/-</sup> mice after treatment with semicarbazide. While studying health risks associated with atherosclerosis, Yu *et al.* (2002) suggested that active SSAO contributes to the harmful effects of hyperglycaemia on obesity and atherosclerosis. Yu *et al.* (2002) established this by preventing the development of atherosclerotic lesions and obesity in diabetic KKAY mice by two different SSAO inhibitors, MDL-72974A, and aminoguanidine. In a follow up study, Yu *et al.* (2004) demonstrated a strong inhibitory potential of another selective SSAO inhibitor, (E)-2-(4-fluorophenethyl)-3-fluoroallylamine (FPFA) in reducing atherosclerotic lesions and weight gain in obese KKAY mice fed on atherogenic diet.

In another study done on mice, 1h after induction of intracerebral haemorrhage, Ma *et al.* (2011) observed a reduction in brain inflammation and oedema, as well as neurobehavioral deficit after administrating two SSAO inhibitors, LJP-1586, and semicarbazide. Yang *et al.* (2011) studied the role of SSAO activity in rat myocardial ischemia and demonstrated a reduction in the myocardial infarct size *in vivo* after administration of semicarbazide, hydralazine, and LJP-1207. Additionally, studies done by Wang *et al.* (2018a; 2018b) on ApoE<sup>-/-</sup> mice and rabbits treated with PXS-4728A, a specific SSAO inhibitor, exhibited reduced atheroma with less oxidative stress and endothelial dysfunction, and alleviated plasma levels of lipids and glucose (Wang *et al.*, 2018a; Wang *et al.*, 2018b). Wang *et al.* (2018a; 2018b) further postulated the atheroprotective effect of PXS-4728A as being anti-inflammatory, as well as attributed this to the reduced levels of LDL-C/glucose. SSAO has previously been associated with hepatic inflammation caused by increased LDL-C/glucose, which has been regarded as important contributing factor in the development of hyperglycaemia and hyperlipidaemia (Min *et al.*, 2012; Okin and Medzhitov, 2016).

In a study by Jarolimek and Charlton (2015), PXS-4728A has been demonstrated effective in inhibiting inflammatory response in non-alcoholic fatty liver disease. In another study using non-obese diabetic (NOD) mice model, a half-year-long administration of anti-VAP-1 antibodies have postponed the development of diabetic hyperglycaemia (Merinen *et al.*, 2005). Obesity is associated with type 2 diabetes through evoking insulin resistance, which is linked to the pathology of hyperlipidaemia and atherosclerosis (Yu *et al.*, 2004). Insulin does not only promote glucose uptake in adipocytes but also enhances adipocyte triglyceride storage and adipocyte differentiation and maturation. SSAO catalysed reaction in adipocytes exerts very similar effect by producing hydrogen peroxide, which mimics the effect of insulin and contributes to the translocation of GLUT4 on the plasma membrane of adipocytes (Yu *et al.*, 2004). Therefore, inhibition of SSAO activity would prevent weight gain due to the reduction of adipose glucose uptake and subsequently reduced effect on adipocytes differentiation.

Apart from PXS-4728A, other PXS compounds have also been investigated as potential anti CVD agents due to their anti-inflammatory properties caused by SSAO inhibition. The PXS compound PXS-4681A, a selective mechanism-based SSAO inhibitor with no substrate turnover *in vitro* has been studied *in vivo* in mice for its anti-inflammatory properties (Foot *et al.*, 2013). In his study Foot *et al.* (2013) studied the atheroprotective effect of PXS-4681A and demonstrated reduced neutrophils rolling and diminished release of inflammatory cytokines, TNF- $\alpha$  and IL-6 after SSAO inhibition.

### 6.3 SSAO in atherosclerosis

Being strongly expressed in vascular endothelial and smooth muscle cells, SSAO/VAP-1 is involved in the development of atherosclerosis and atherogenesis through production of highly unstable and reactive aldehydes and H<sub>2</sub>O<sub>2</sub>. Both endogenously produced aldehydes (formaldehyde and methylglyoxal) can cross-link proteins and enhance advanced glycation. This effect would alter functional and structural proteins, and therefore initiate acute damage and cause chronic hardening of blood vessels, subsequently leading to atherosclerosis. Hydrogen peroxide on the other hand contributes to atherogenesis by increasing ROS levels in the vascular wall. Furthermore, it has already been demonstrated that the membrane bound endothelial SSAO initiates leukocyte rolling, adhesion, and transmigration into inflammatory sites by inducing transcription and translation of adhesion molecules E and P selectin (Obata, 2006). The hydrogen peroxide and ammonia produced by SSAO have already been established as being cytotoxic to vascular cells at high concentrations (Wang *et al.*, 2018). The aldehydes can induce endothelial injury through their unstable and highly reactive nature, and the cross-linking of proteins to each other (Wang *et al.*, 2018). The protein cross-linkage on the surface of the blood vessels triggered by the highly reactive aldehydes is silent and accumulative process and as such could contribute to the chronic formation of plaques (Obata, 2006).

With regards to LDL, it has been postulated that the copper content of SSAO/VAP-1 is one of the reasons leading to LDL oxidation. Previous studies have identified that copper containing enzymes such as ceruloplasmin support endothelial cell mediated LDL oxidation (Exner *et al.*, 2001; Obata, 2006). Exner *et al.* (2001) have suggested that this mechanism is dependent on the presence of copper and independent from the amine oxidase activity. In addition, recent papers have postulated that the involvement of SSAO in oxidative stress formation is a result of a concomitant production of toxic aldehyde and hydrogen peroxide (Wang *et al.*, 2018); however, Wang *et al.* (2018) have not investigated whether this effect is a consequence of synergism between SSAO derived products. Hydrogen peroxide is the most abundant nonradical oxidant in the vessel wall and is considered as generally weak oxidant. However, it is currently unknown whether when produced in large amounts can initiate oxidative stress formation and consequently LDL oxidation. As mentioned above, recent literature has already identified the involvement of SSAO in the development and progression of atherosclerosis, while also emphasising the copper content as an important component in this process. This could indicate potential interactions between SSAO and other copper rich amine oxidases such as LOX, which have not been previously explored and require further research to fully understand the role of copper rich amine oxidases in the pathophysiology of atherosclerosis.

### 6.3 LOX in CVD

In the vasculature LOX expression has been observed in endothelial cells, vascular smooth muscle cells and fibroblasts. The role of this enzyme in cardiovascular functions has been studied with gene knockout strategies (Rodriguez *et al.*, 2008; Maki *et al.*, 2002). In a study by Maki *et al.* (2002) LOX deficient mice have developed signs of aortic rupture because of extended fragmentation of elastic fibres, disruption of VSMC contact, discontinuities of internal elastic lamina and lamellae, detachment of endothelial cells from the basal lamina, and alterations on endothelial cell morphology. Furthermore, other cardiovascular diseases caused by an intense de-structuration of ECM, such as aneurysms and coronary dissections, have been associated with disturbed LOX expression levels (Huffman *et al.*, 2000; Nakashima & Sueshi, 1992).

Recent studies have also shed light on the involvement of LOX in the development of atherosclerosis; from endothelial dysfunction to plaque progression and rupture (Rodriguez *et al.*, 2008; 2002; Raposo *et al.*, 2004). In the endothelial cells LOX downregulation has been associated with endothelial dysfunction (Rodriguez *et al.*, 2008; 2004; 2002; Liu *et al.*, 1997). In a study by Rodrigues *et al.* (2002) it was demonstrated that atherogenic concentrations of LDL can reduce LOX expression and activity in endothelial cells through transcriptional mechanism. In a follow up study Rodriguez *et al.* (2008) confirmed this, while also stating that both LDL and  $\beta$ APN, an inhibitor of LOX activity, can downregulate LOX expression. When downregulated, LOX can increase the exchange of macromolecules across the endothelial monolayer and consequently alter ECM structure and impair endothelial barrier function (Rodriguez *et al.*, 2008).

Inhibition of LOX activity has also been demonstrated because of altered homocysteine levels. Studies performed using purified LOX *in vitro* have shown that pathophysiological concentrations of homocysteine (HC), homocysteine thiolactone (HCTL) and other analogues can irreversibly inhibit LOX activity and consequently impair endothelial function (Liu *et al.*, 1997; Rodriguez *et al.*, 2008). Pro-inflammatory cytokines such as TNF $\alpha$  can also play an important role in reducing LOX expression. In a study done by Rodrigues *et al.* (2004) TNF $\alpha$  administration in rats decreased vascular LOX mRNA levels about two-fold. Rodrigues *et al.* (2004) have further suggested that this effect is mediated through the activation of TNF receptor-2 and is independent of the pro-apoptotic effect elicited by this cytokine.

In the VSMCs LOX is the main isoform responsible for 80% of total LOX activity. In these cells LOX has been associated with VSMC migration, proliferation, and in solubilization of ECM components (Rodriguez *et al.*, 2008). Studies have shown that transforming growth factor  $\beta$  (TGF $\beta$ ) increases LOX expression and activity in VSMCs through enhancing the production of proteoglycans and fibronectin (Toma *et al.*, 2012; Rodriguez *et al.*, 2008; Gacheru *et al.*, 1997). Fibronectin is known to be involved in LOX proteolytic activation; hence can be said that LOX activation is affected by transforming growth factor  $\beta$  (TGF $\beta$ ) levels (Fogelgren *et al.*, 2005). Furthermore, platelet derived growth factor  $\beta$  (PDGF $\beta$ ), a key mitogen that promotes neointimal growth, and granulocyte macrophage colony-stimulating factor (GM-CSF), a cytokine implicated in vascular remodelling, have also been shown to increase LOX expression in VSMC (Weissen-Plenz *et al.*, 2008). As seen in Figure 21, increased expression of TGF $\beta$  and PDGF $\beta$  are critical in vascular remodelling associated with atherosclerosis and re-stenosis (Rodriguez *et al.*, 2008).

Studies have demonstrated downregulated LOX expression in early stage of atherosclerosis and upregulated in advance stages of this disease (Rodriguez *et al.*, 2008; Kagan *et al.*, 1991). Furthermore, LOX has been suggested to have an important role in the progression of atherosclerotic plaques (Rodriguez *et al.*, 2008; Nellaiappan *et al.*, 2000; Bode *et al.*, 1999). Enzymatically active forms of LOX have been detected in the nucleus of VSMC (Nellaiappan *et al.*, 2000). It has been suggested that the biological activity of nuclear LOX in VSMC could impact chromatin organization and modulate the expression of ECM components such as elastin and collagen III, the most abundant collagen in atherosclerotic plaques (Bode *et al.*, 1999). LOX activity has also been associated with neointimal growth (Figure 21). Studies have reported LOX dependent increase in chemotactic activity of VSMC and monocytes because of hydrogen peroxide mediated mechanism (Lazarus *et al.*, 1995; Liu *et al.*, 2000). In a study done by Gacheru *et al.* (1997) LOX has been identified as a responsive gene to proliferative stimulus in quiescent rat adult VSMC where stimulated cell proliferation has resulted with increased LOX expression in these cells. However, in neonatal VSMC, an inverse correlation between the proliferation rate of these cells and LOX expression has been described (Green *et al.*, 1995).

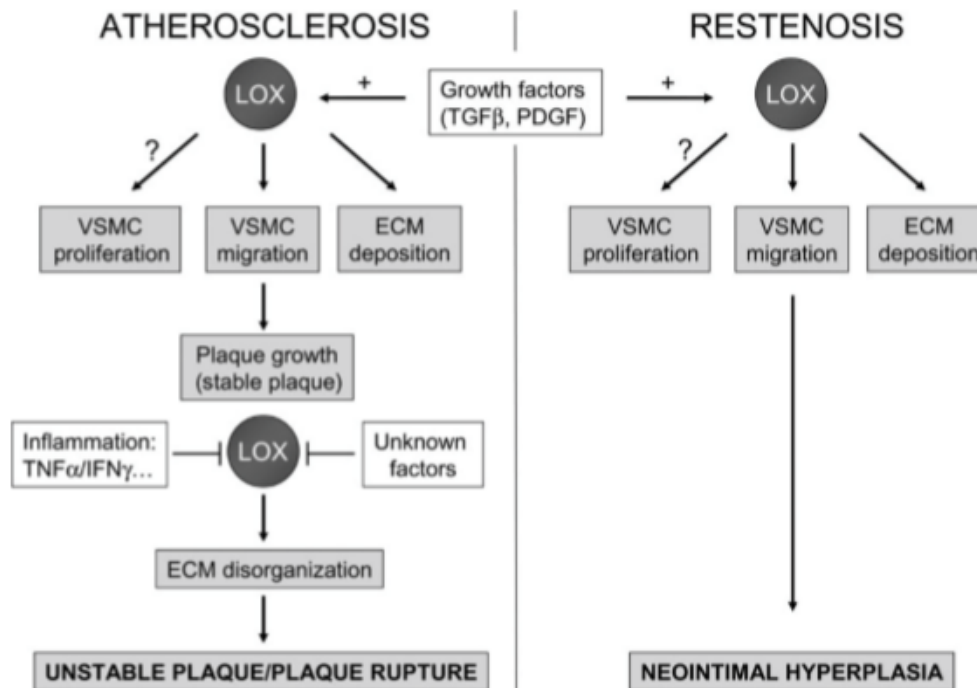


**Figure 21. Involvement of lysyl oxidase (LOX) in atherosclerosis and restenosis. Critical growth factors in both plaque progression and restenosis, such as transforming growth factor  $\beta$  (TGF $\beta$ ) and platelet-derived growth factor  $\beta$  (PDGF $\beta$ ) induce lysyl oxidase expression in vascular smooth muscle cells (VSMC). Lysyl oxidase has a chemotactic activity for vascular smooth muscle cells and monocytes and actively participates in extracellular matrix (ECM) deposition (Rodríguez *et al.*, 2008).**

## SECTION 7. SSAO AND LOX IN INFLAMMATION

Inflammation plays a key role in numerous pathologies. Chronic inflammatory conditions are known to result with impaired endogenous antioxidant capacities due to high levels of reactive oxygen species (ROS). In inflammation-associated diseases ROS are mainly produced by activated immune effector cells like macrophages, however there are other contributing factors that could lead to increased ROS levels, such as SSAO and LOX activity. As mentioned previously, SSAO and LOX driven catalytic reaction leads to generation of hydrogen peroxide, aldehydes, and ammonia. When converted to ROS in a form of hydroxyl radical (OH $\cdot$ ), hydrogen peroxide can directly injure cell membranes and nuclei (Bonomini *et al.*, 2008). In the case of atherosclerotic inflammatory response, hydrogen peroxide in a form of hydroxyl radical would also interact with endogenous vasoactive mediators formed in endothelial cells and therefore modulate vasomotion and the atherogenic process.

Furthermore, it would peroxidise lipid components, leading to the formation of oxidized lipoproteins (LDL). After being modified through oxidation LDL will be engulfed by macrophages, and as such would cause cholesterol ester accumulation in the same, leading to the formation of foam cells (Bonomini *et al.*, 2008).

### **7.1 SSAO in inflammation**

SSAO mediates two key inflammatory processes. The first process is through the highly reactive aldehydes and hydrogen peroxide, which, as mentioned above, if converted to ROS would injure cells and generate oxidative stress. The other involvement of SSAO in inflammatory processes is through its role in transmigration of intraluminal leukocytes into sites of tissue inflammation, which is initially a protective reparative process, but if persistent, could lead to chronic inflammatory cell accumulation. This is evident in the case of atherosclerotic inflammatory responses in which SSAO facilitates the recruitment of leukocytes through increased expression of adhesion molecules (Salmi & Jalkanen, 2017). Apart from atherosclerosis, the involvement of SSAO in regulating leukocyte trafficking to sites of inflammation has been recognised in many other chronic inflammatory responses such as in the case of kidney fibrosis, pulmonary fibrosis, cerebral ischemia, diabetic retinopathy and inflammatory liver disease (Wong *et al.*, 2014; Singh *et al.*, 2003; Sun *et al.*, 2015; 2018; Noda *et al.*, 2008; 2009; Hernandez *et al.*, 2010); but also, in acute inflammation responses like acute fibrosis and peritonitis (Yu *et al.*, 2004; 2006).

Wong *et al.* (2014) have demonstrated that SSAO inhibition can significantly suppress profibrotic and proinflammatory cytokine secretion, limit inflammatory cell accumulation, extra-cellular matrix expression, and oxidative stress in an acute model of renal fibrosis. Yu *et al.* (2006) have used a transgenic mice model overexpressing human VAP-1 (SSAO) to study the involvement of SSAO in a lipopolysaccharide-induced pulmonary inflammation and have reported overexpression of SSAO activity which was particularly pronounced in lung in comparison to other tissues. Moreover, Yu *et al.* (2006) have observed higher lipopolysaccharide-induced increase in inflammatory cells in the bronchoalveolar lavage (BAL) fluid in the transgenic comparing to the non-transgenic mice. Furthermore, they have demonstrated that by blocking SSAO activity with a selective inhibitor can significantly reduce the number of neutrophils as well as levels of macrophage inflammatory protein-1 $\alpha$ , granulocyte colony-stimulating factor, tumour necrosis factor  $\alpha$ , and interleukin-6 in the BAL fluid (Yu *et al.*, 2006).

Another study done by Singh *et al.* (2003) has suggested the involvement of SSAO in chronic lung inflammation. Singh *et al.* (2003) have demonstrated that SSAO expression in the pulmonary arteries and in the perivascular areas in inflamed lungs contributes to functional heterogeneity of endothelial cells within the lung and creates distinct sites for perivascular recruitment of inflammatory cells. In the case of cerebral ischemia, the dysfunction of the blood-brain barrier and the occurrence of haemorrhages after stroke have been associated with leukocyte adhesion to brain endothelium and subsequent transmigration into the injured tissue (Sun *et al.*, 2015). It has been suggested that when released, soluble SSAO can travel through the circulation and reach other brain areas, where it induces inflammation, therefore, amplifying the damage induced by the ischemic process (Sun *et al.*, 2018). Hernandez *et al.* (2010) have observed reduced infarct volume and improved neurological outcome after SSAO inhibition in stroke animal models. SSAO driven leukocyte recruitment has also been observed in inflammatory processes related to eye pathology such as diabetic retinopathy, endotoxin-induced uveitis, and macular degeneration (Noda *et al.*, 2008; 2009). Noda *et al.* (2008) have demonstrated reduced cytokine expression and macrophage recruitment after successful inhibition of SSAO activity in a laser-induced model of age-related macular degeneration (AMD).

## **7.2 LOX in inflammation**

LOX is also known as a powerful inflammatory mediator and its expression has been reported increased in various pathologies associated with inflammation such as lung fibrosis, liver cirrhosis, atherosclerosis, scleroderma, and desmoplastic tumours (Kagan, 1994; Kagan 2000; Cheng *et al.*, 2014). Cheng *et al.* (2014) have identified upregulated LOX expression in bleomycin (BLM)-induced experimental lung fibrosis and have suggested that high LOX expression enhances the inflammatory response in the fibrosis-resistant Balb/c mice. Furthermore, they have demonstrated that inhibition of LOX activity could alleviate fibrosis progression at the later, inflammatory stage of this disease due to impaired inflammatory cell infiltration and TGF- $\beta$  signalling (Cheng *et al.*, 2014). LOX expression was also studied in another inflammatory disease known as scleroderma (Chanoki *et al.*, 1995). Chanoki *et al.* (1995) have compared LOX activity and expression in sclerodermatous and in normal skin. In the sclerotic stage of systemic scleroderma Chanoki *et al.* (1995) have observed increased intracellular LOX expression in fibroblasts and increased extracellular LOX expression among collagen bundles, between the lower dermis and the subcutaneous fat tissue.

Furthermore, in the sclerotic stage of localized scleroderma Chanoki *et al.* (1995) have observed a marked increase in LOX expression in mononuclear cells and fibroblasts near blood vessels in the lower dermis, and in the subcutaneous fat tissue, in addition to the extracellular deposits between collagen bundles.

Changes in LOX activity have also been observed in the progressive inflammatory disease, atherosclerosis. Various *in vitro* and *in vivo* studies have associated endothelial dysfunction with LOX downregulation in the early stage of the atherosclerotic process (Rodriguez *et al.*, 2008; Nellaiappan *et al.*, 2000; Bode *et al.*, 1999). Conversely, upregulated LOX activity in the vascular cells has been associated with induced neointimal thickening in atherosclerosis and restenosis (Rodriguez *et al.*, 2008). Moreover, LOX has been demonstrated as being chemotactic for vascular smooth muscle cells and monocytes in the inflammatory process associated with atherosclerosis. Furthermore, Rodriguez *et al.* (2008) have demonstrated that LOX activity is mainly modulated by proliferative stimulus in these cells, and as such could control other cellular processes such as gene expression and cell transformation.

## **SECTION 8. REACTION PRODUCTS OF SSAO AND LOX ENZYMATIC ACTIVITY**

### **8.1 Hydrogen peroxide ( $H_2O_2$ )**

Bioactive  $H_2O_2$  is mainly derived from spontaneous dismutation (simultaneous oxidation and reduction process), or superoxide catalysed dismutation of a superoxide ( $O_2^-$ ) radical, through an enzyme called superoxide dismutase, which is a side product of many enzymatic reactions (Zheshuan *et al.*, 2011). These include mitochondrial electron transport chain; lipoxygenase; cyclooxygenase; cytochrome P450s; NADPH oxidases; and uncoupled eNOS (Zheshuan *et al.*, 2011). Other enzymes, like glucose oxidase, amine oxidases and xantine oxidase can produce  $H_2O_2$  directly. Deamination reactions catalysed by SSAO/VAP-1 and LOX also lead to production of  $H_2O_2$ .  $H_2O_2$  alone is not reactive; however, in the presence of transition metals it can be converted to toxic hydrogen free hydroxyl radical ( $OH^\cdot$ ) *via* the Fenton reaction (Obata, 2006).

This makes H<sub>2</sub>O<sub>2</sub> a major component of reactive oxygen species (ROS) and as such is implicated in a variety of disease states. It is produced in large amount by macrophages and granulocytes, and it is recently established as an important contributor to oxidative stress (Zheshuan *et al.*, 2011). Recent study done by Wang *et al.* (2018) identified H<sub>2</sub>O<sub>2</sub> as a source of reactive oxygen species (ROS) which can modify low-density lipoprotein (LDL) in the arterial wall and contribute to the development of atherosclerosis. Other studies have addressed H<sub>2</sub>O<sub>2</sub> as a vasoactive agent with ability to induce vasoconstriction of resistance vessels and increase vascular tone, hence contribute to the development of hypertension (Vidrio *et al.*, 2003; Zorzano *et al.*, 2003).

H<sub>2</sub>O<sub>2</sub> has also been recognised as an important signalling molecule involved in inflammatory damage, by inducing the expression of inflammatory cytokines and adhesion molecules such as the type I transmembrane glycoprotein CD62P in many cell types (Smith & Vainio, 2007; Johnston *et al.*, 1996). Zheshuan *et al.* (2011) have demonstrated an ability of H<sub>2</sub>O<sub>2</sub> to function as a secondary messenger and regulate activation of many important transcription factors, such as nuclear factor kappa-light-chain-enhancer of activated B cells (NF-κB), that control the inducible expression of genes regulating macrophage-effector functions and cytokines. H<sub>2</sub>O<sub>2</sub> has also been shown to activate phosphatidylinositol-3 kinase, and protein kinase B pathway which play a key role in insulin-induced glucose transport of adipocytes through GLUT4 translocation to the plasma membrane (El Hadri *et al.*, 2001).

## **8.2 Hydrogen peroxide (H<sub>2</sub>O<sub>2</sub>) in VSMCs**

Hydrogen peroxide is produced in VSMCs by multiple enzymatic systems, including SSAO and LOX activity. These systems have an important role in redox signalling under physiological conditions; however, can cause toxic cellular defects and various pathologies once their activity is dysfunctional. Intracellular H<sub>2</sub>O<sub>2</sub> production, however, is mainly driven by the mitochondria and its steady state levels in the vascular tissue are maintained through endogenous scavengers such as catalase and glutathione peroxidase (Chang *et al.*, 2016). Increased activity of multiple oxidase systems in the endothelium, media or adventitia can contribute to elevated H<sub>2</sub>O<sub>2</sub> levels. Being a cell permeable ROS that can diffuse easily between membranes, H<sub>2</sub>O<sub>2</sub> has relatively long half-life comparing to other ROS (Chang *et al.*, 2016). Furthermore, when produced exogenously, H<sub>2</sub>O<sub>2</sub> can induce its endogenous production by activating NADPH oxidase (NOX) proteins (Chang *et al.*, 2016). This could lead to chronic accumulation of H<sub>2</sub>O<sub>2</sub> and consequently VSMCs dysfunction in the vasculature.

### **8.3 Physiological roles of H<sub>2</sub>O<sub>2</sub> in VSMCs**

Under physiological conditions H<sub>2</sub>O<sub>2</sub> plays an important role in cellular signalling (Figure 22), and as such is an important mediator of VSMCs proliferation, migration, and differentiation (Brown *et al.*, 1999; Xiao *et al.*, 2009; Rezende *et al.*, 2012). H<sub>2</sub>O<sub>2</sub> has been identified as an early growth signal in VSMCs. Brown *et al.* (1999) have demonstrated that when produced endogenously within physiological levels, H<sub>2</sub>O<sub>2</sub> plays a fundamental role in VSMCs proliferation. Brown *et al.* (1999) have observed this by inhibiting rat VSMCs growth with catalase, an enzyme that hydrolyses H<sub>2</sub>O<sub>2</sub>. In another study done on rabbit VSMCs by Watanabe *et al.* (2001), H<sub>2</sub>O<sub>2</sub> synergistically enhanced angiotensin II induced VSMCs proliferation. Furthermore, in a study done on human VSMCs, H<sub>2</sub>O<sub>2</sub> induced the expression of placenta growth factor that regulates angiotensin II induced VSMCs proliferation (Shaw *et al.*, 2012; Pan *et al.*, 2010). H<sub>2</sub>O<sub>2</sub> has also been identified as an important mediator in PDGF induced VSMCs migration. A study done by Rezende *et al.* (2012) demonstrated an ability of H<sub>2</sub>O<sub>2</sub> to oxidase specific cysteine residues within the  $\alpha 7$  subunit of integrin  $\alpha 7\beta 1$ . Rezende *et al.* (2012) have suggested that this facilitates the formation of membrane protrusions in VSMCs by binding with laminin – 111, thereby enhancing the binding affinity of integrin to laminin, which increases VSMCs migration. The role of H<sub>2</sub>O<sub>2</sub> has also been mentioned in VSMCs differentiation. Xiao *et al.* (2009) demonstrated that NOX4 induced H<sub>2</sub>O<sub>2</sub> production mediates the differentiation of stem cells into VSMCs via activation of serum response factor and myocardin.

### **8.4 Pathological effects of H<sub>2</sub>O<sub>2</sub> in VSMCs**

Although the exact intracellular concentration of H<sub>2</sub>O<sub>2</sub> may vary depending on cell type, the physiological range in the cell is between 1 and 100nM (Chang *et al.*, 2016). At higher concentrations H<sub>2</sub>O<sub>2</sub> could initiate inflammatory responses, growth arrest and cell death. In VSMCs pathological concentrations of H<sub>2</sub>O<sub>2</sub> could accelerate the development and progression of atherosclerosis and vascular calcification (Chang *et al.*, 2016). This is mainly accomplished by regulating the expression of inflammatory molecules and infiltration of inflammatory cells in the vascular wall (Figure 22).

A study done by Sun *et al.* (2012) has demonstrated that H<sub>2</sub>O<sub>2</sub> can induce the expression of the receptor activator of nuclear factor kappa B ligand (RANKL) in VSMCs, which promotes macrophages infiltration. Infiltrated inflammatory cells such as macrophages would produce tumour necrosis factor- $\alpha$  (TNF- $\alpha$ ), a major pro-inflammatory cytokine in the development of atherosclerosis, which also promotes further H<sub>2</sub>O<sub>2</sub> generation via NOX or the mitochondria dependent pathways (Chatterjee *et al.*, 2011). Furthermore, an increased H<sub>2</sub>O<sub>2</sub> production because of enhanced expression and activity of amine oxidases could also initiate a signalling cascade which would lead to expression of inflammatory cytokines and adhesion molecules in the vascular wall (Chang *et al.*, 2016). In a study done on transgenic mice overexpressing a VSMCs specific catalase (an enzyme that hydrolyses H<sub>2</sub>O<sub>2</sub>), Parastatidis *et al.* (2013) have observed significant reduction in inflammatory molecules related to the progression and development of atherosclerosis, such as: TNF- $\alpha$ , TGF- $\beta$ , osteopontin, interleukin 1  $\beta$  (IL-1 $\beta$ ) and monocyte chemoattractant protein-1 (MCP-1). Regarding vascular calcification, Mody *et al.* (2001) have shown that H<sub>2</sub>O<sub>2</sub> produced through xanthine oxidase can induce osteogenic differentiation of bovine calcifying vascular cells. In another study using primary mouse VSMCs Byon *et al.* (2008) have demonstrated an ability of H<sub>2</sub>O<sub>2</sub> to directly induce calcification. Byon *et al.* (2008) have observed inhibition of VSMCs specific markers and upregulation of bone specific markers, indicating a phenotypic change of VSMCs to an osteogenic phenotype. Elevated H<sub>2</sub>O<sub>2</sub> levels in VSMCs have also been linked with protein glycation (Figure 22).

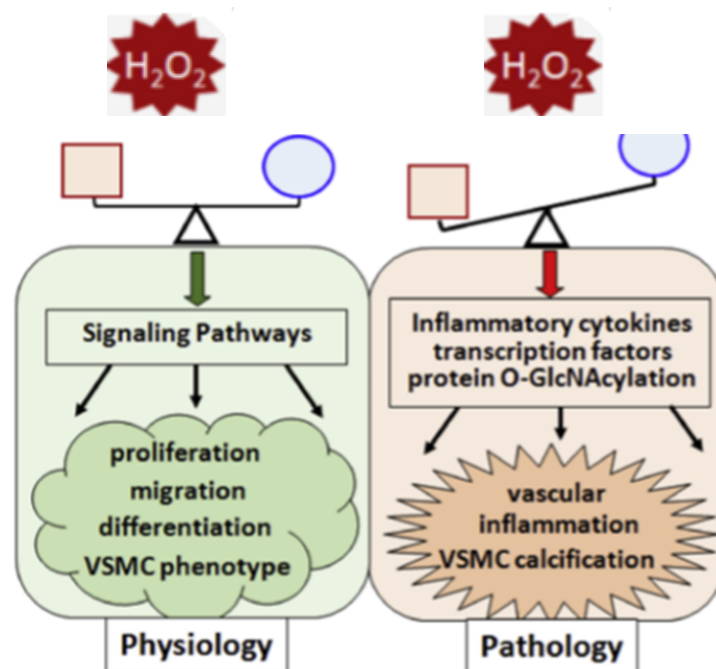


**Figure 22.** The role of H<sub>2</sub>O<sub>2</sub> in modulation VSMCs physiology and pathology (Chang *et al.*, 2016).

## 8.5 Aldehydes and biological consequences of aldehydes exposure

Apart from being produced endogenously through SSAO/VAP-1 and LOX activity and cellular metabolic pathways such as lipid oxidation, histone demethylation, carbohydrate, and ascorbate autoxidation; and the metabolism of amino acids, vitamins, carbohydrates and steroids, aldehydes can also have various exogenous sources (Figure 23).

Motor vehicle exhaust can generate aldehydes directly or because of hydrocarbons production in which hydrocarbons are converted to aldehydes through photochemical oxidation reactions (Dator *et al.*, 2019). Aldehydes can be generated in the atmosphere through the hydroxyl radical mediated – photochemical oxidation of hydrocarbons. Certain foods (flavourings), alcoholic drinks and tobacco smoke are also exogenous sources of aldehydes. The tobacco smoke has been identified to contain significant amounts of acetaldehyde, formaldehyde, acrolein and crotonaldehyde (Hecht, 2003). Exogenous exposure to aldehydes can also be a result of the metabolism of certain drugs including cyclophosphamide, ifosfamide and misonidazole (Dator *et al.*, 2019).

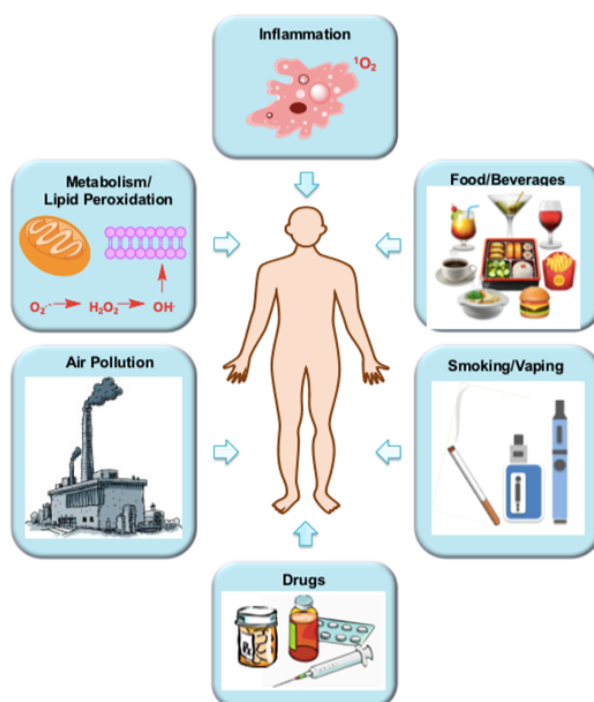
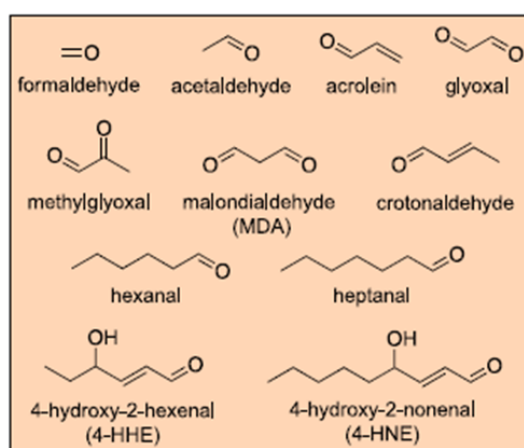


Figure 23. Exogenous and endogenous sources of human exposure to aldehydes (Dator *et al.*, 2019).

Human exposure to aldehydes has been implicated in various diseases including cardiovascular pathologies, diabetes, neurodegenerative diseases (Parkinson's and Alzheimer's) and cancer. Due to being strong electrophiles, aldehydes are highly reactive with nucleophilic sites in DNA and proteins with which they form reversible and irreversible modifications. Failure to eliminate or repair these modifications could lead to changes in cellular homeostasis and ultimately cell death (Dator *et al.*, 2019). Aldehydes (Figure 24) can also interact with various other biomolecules including enzymes, peptides, regulatory proteins, phospholipids, and DNA, forming covalent modifications, causing a disturbance in their normal functions, and leading to mutations and chromosomal aberrations (Dator *et al.*, 2019).



**Figure 24. Structure of common aldehydes (Dator *et al.*, 2019).**

Research indicates that endogenous aldehydes such as methylglyoxal, formaldehyde and acrolein are mediators of cardiovascular pathologies (Dator *et al.*, 2019; Matveychuk *et al.*, 2011). The toxicity of these aldehydes greatly depends on aldehyde metabolising enzymes in cells. There are several metabolic enzymatic pathways responsible for the detoxification of aldehydes. This includes the glutathione dependent aldehyde metabolising enzymes, aldehyde oxidizing enzymes, and aldehyde reducing enzymes (O'Brien *et al.*, 2005). Methylglyoxal is metabolized by glyoxalase (GLOX) and reduced by aldo-keto reductase (AKR) 1A2, and the metabolism of formaldehyde is mediated by glutathione, alcohol, and aldehyde dehydrogenase, ADH5 and ALDH2 respectively (O'Brien *et al.*, 2005). Reduced glutathione (GSH) levels could lead to significant increase in formaldehyde cytotoxicity. This is because formaldehyde reacts spontaneously with intracellular GSH, present in adequate amounts to form S-hydroxy methyl glutathione (HMGSH), which undergoes oxidation by ADH5 and NAD(P)<sup>+</sup> to generate S-formylglutathione (FGSH), which is subsequently converted by S-formyl glutathione hydrolase (FGH) regenerating GSH and yielding formate (ester of formic acid) (Dator *et al.*, 2019).

## 8.6 Oxidative stress and aldehydes

Endogenous aldehydes have also been linked with ROS induced post-translational modifications (Dator *et al.*, 2019). A balance between ROS production and the antioxidant defence system is crucial to maintain redox homeostasis, and a disturbance in this balance would result with elevated ROS and consequently oxidative stress. The most important source of endogenous ROS is the mitochondrial electron transport chain which leads to production of ROS by converting oxygen into superoxide anions (Boveris & Chance, 2013). Other sources of ROS production are various metabolic processes including oxidation of NADPH by NADPH oxidase and oxidation of xanthine by xanthine oxidase (Grimsrud *et al.*, 2008). It has been estimated that 1-8% of ROS produced in cells would form adducts with proteins within the mitochondria (Dator *et al.*, 2019). Overproduction of ROS has also been associated with mutations in the mitochondrial gene that encodes a component of the electron transport chain.

Oxidative stress caused by consistent over-production of ROS could lead to oxidation of cellular components and consequently modifications of DNA, proteins, lipids, and carbohydrates (Grimsrud *et al.*, 2008). Therefore, it has been highlighted as a main trigger for biological damage and as such is implicated in various diseases, including cardiovascular and inflammatory disorders (Finkel & Holbrook, 2000; Lin & Beal, 2006; Dator *et al.*, 2019).

In the case of proteins, oxidation reactions caused by oxidative stress could lead to various post-translational modifications that are results either from direct oxidation of amino acid residues, or through reactive intermediates formed by oxidation of other cellular components (Grimsrud *et al.*, 2008). Furthermore, a significant portion of ROS induced post-translational modifications would result from addition of reactive carbonyl functional groups on proteins known as “protein carbonylation” (Grimsrud *et al.*, 2008). The most common and reactive carbonyl groups are the aldehydes.

Direct protein carbonylation could be achieved through various reactions, however, the most prevalent protein carbonylation is formed through lipid derived aldehydes (Grimsrud *et al.*, 2008). Lipid peroxidation is an end-product of the reaction between reactive oxygen species (ROS) and/or reactive nitrogen species (RNS) and lipids containing carbon-carbon double bonds, such as polyunsaturated fatty acids (Pizzimenti *et al.*, 2013). In this process ROS and RNS oxidase polyunsaturated fatty acids, resulting with free radical chain reactions and subsequent formation of by-products such as aldehydes, lipid radicals and hydrocarbons (Pizzimenti *et al.*, 2013).

The most reactive aldehydes generated from polyunsaturated fatty acids oxidation are  $\alpha,\beta$ -unsaturated aldehydes, including 4-HNE, 4-ONE, and acrolein (Grimsrud *et al.*, 2008). Glutathione S-transferase A4 (GSTA4) catalyses the conjugation of the highly reactive  $\alpha,\beta$ -unsaturated aldehydes to glutathione, leading to their efflux from the cell by the glutathione conjugate transporter RLIP76 (Grimsrud *et al.*, 2008). In addition, when oxidised by aldehyde dehydrogenase or reduced by alcohol dehydrogenase, aldehyde reductase, or aldose reductase these aldehydes are converted into less toxic molecules (Figure 25). The  $\alpha,\beta$ -unsaturated aldehydes that escape cellular metabolism serve as electrophiles in the covalent modification of proteins *via* non-enzymatic Michael addition. Moreover, the double bond in these aldehydes, due the presence of electron - withdrawing functional groups, serves as a site for Michael addition with cysteine, histidine, or lysine residues. These additions could result with aliphatic carbonyl adducts being formed on cysteine, histidine, or lysine residues that may alter the activity of protein targets or cause them to become degraded by the proteasome (Grimsrud *et al.*, 2008).

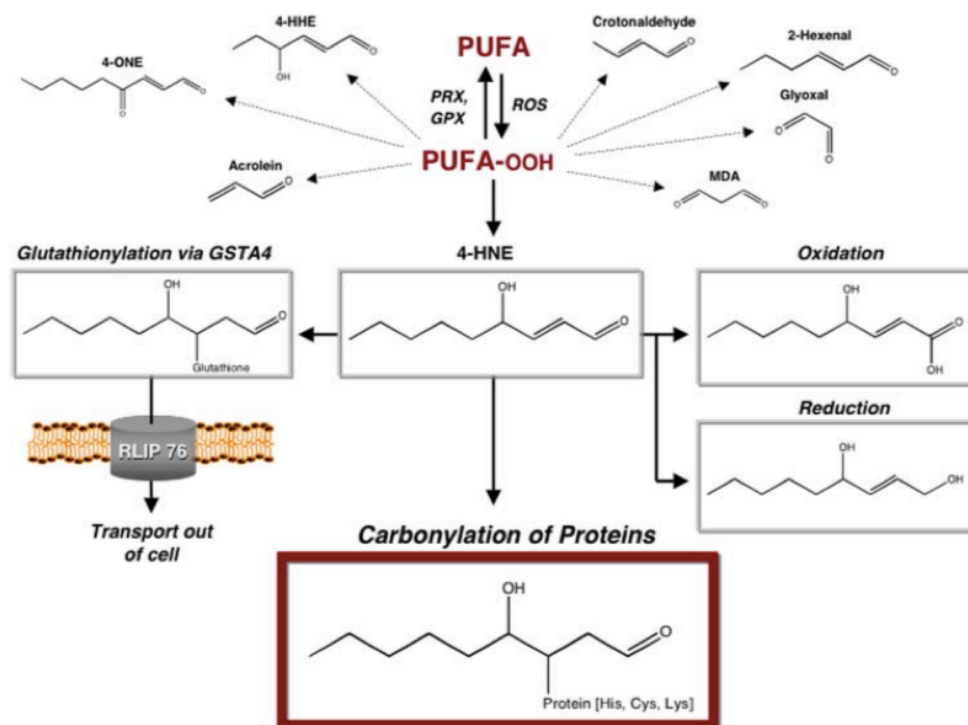


**Figure 25. Cellular fates of  $\alpha,\beta$ -unsaturated aldehydes and carbonylated proteins.** ROS stimulate peroxidation of polyunsaturated fatty acids (PUFA), an oxidative event that is reversible through reduction by peroxiredoxin (PRX) and glutathione peroxidase (GPX) enzymes. The lipid hydroperoxides (PUFA-OOH) generated are unstable and lead to a variety of reactive aldehydes. The lipid peroxidation products generated include the  $\alpha,\beta$ -unsaturated aldehydes 4-HNE, 4-ONE, 4-hydroxy-(2E)-hexanal (4-HHE), (2E)-hexenal, crotonaldehyde, and acrolein as well as the dialdehydes glyoxal and malondialdehyde (MDA) (Grimsrud *et al.*, 2008).

## SECTION 9. SSAO AND LOX INHIBITORS

### 9.1 SSAO inhibitors

The numerous similarities between the amine oxidase family of enzymes, especially their overlapping substrate specificity have been an obstacle in designing a very selective SSAO inhibitor. The several proposed approaches for inhibiting SSAO are small interfering RNA's, function blocking antibodies and small molecule inhibitors (Pannecoeck *et al.*, 2015). The most studied group are the small molecule inhibitors. This includes hydrazine derivatives, aminoglycoside antibiotics, benzamides, vitamin B1 derivatives, amino acid derivatives, oxime-based primary amine oxidase inhibitors and peptides (Pannecoeck *et al.*, 2015, Bligt-Linde *et al.*, 2013; Marttila-Ichihara *et al.*, 2010). A detailed list of well-known SSAO inhibitors, their mechanism of action, *in vitro* and *in vivo* studies associated with CVD, and their therapeutic potential is included in Table 3.

**Table 3. SSAO Inhibitors**

| Structure        | Compounds   | Mechanism of action   | Efficacy <i>in vitro</i> for CVD   | Efficacy <i>in vivo</i> for CVD  | Therapeutic potential |
|------------------|---|---|--|--|-----------------------|
| Allylamine based | MDL72974A (potent at nM – irreversible for SSAO and MAO-B)                                  | Forms a stable covalently bound enzyme-inhibitor adduct at the active site of the enzyme. | MDL-72974A inhibits SSAO activity in rat aortic smooth muscle cells (A7r5) (Hernandez <i>et al.</i> , 2006). | MDL-72974A reduces atherosclerotic lesions in KKAY diabetic mice fed with a cholesterol diet for 16 weeks (Yu <i>et al.</i> , 2002). | Anti-diabetic         |
|                  | MDL72145 (potent at nM – irreversible for SSAO and MAO-B, competitive reversible for MAO-A) | Forms a stable covalently bound enzyme-inhibitor adduct at the active site of the enzyme. | MDL72145 inhibits SSAO activity in cultured rat VSMCs (Langford <i>et al.</i> , 2002).                       | MDL72145 reduces SSAO activity acutely (6 and 24h) and chronically (21 days) in weanling   | Anti-Parkinson        |

---

|   |   |  |   |                       |
|---|---|--|---|-----------------------|
|   |   |  | sprague–<br>dawley rats<br>(Langford <i>et al.</i> , 1999).   |                       |
| MDL72527<br>(potent at $\mu\text{M}$ –<br>irreversible<br>and<br>mechanism<br>based for<br>SSAO and<br>PAO) | Forms a<br>stable<br>covalently<br>bound<br>enzyme-<br>inhibitor<br>adduct at the<br>active site of<br>the enzyme | MDL72527<br>protects the<br>myocytes<br>from<br>spermine<br>toxicity<br>(Tipnis & He,<br>1998).<br><br>100 $\mu\text{M}$ MDL<br>72527<br>inhibits<br>SSAO<br>activity in rat<br>aortic<br>VSMCs<br>(Ucal <i>et al.</i> ,<br>2018).<br><br>MDL72527<br>(100 $\mu\text{M}$ )<br>inhibits<br>platelets<br>activation,<br>apoptosis<br>and<br>aggregation<br>in platelets<br>isolated from<br>a wild type<br>mice (Liu <i>et al.</i> ,<br>2016). |   | Anti-cancer           |
| PXS-4728A<br>(potent at<br>nM –<br>irreversible<br>and<br>mechanism<br>based for<br>SSAO)                   | Forms a<br>stable<br>covalently<br>bound<br>enzyme-<br>inhibitor<br>adduct at the<br>active site of<br>the enzyme | PXS-4728A<br><i>in vitro</i> effect<br>has only<br>been studied<br>in relation to<br>chronic<br>obstructive<br>pulmonary<br>disease<br>(COPD) and<br>not CVD.  | In ApoE-<br>deficient<br>mice, SSAO<br>inhibition by<br>PXS-4728A<br>reduces athero-<br>sclerosis and<br>decreases<br>oxidative<br>stress<br>(Wang <i>et al.</i> ,<br>2018a).<br><br>PXS-4728A<br>reduces | Anti-<br>inflammatory |

---

---

|  |  |  |  |  |
|--|--|--|--|--|
|  |  |  |  | atherosclerosis in cholesterol-fed New Zealand White rabbits (Wang <i>et al.</i> , 2018b). |
|  |  |  |  | PXS-4728A reduces SSAO activity in diabetic mice (Wong <i>et al.</i> , 2020).              |

---

|                        |   |   |  |  |
|------------------------|---|---|--|--|
| <b>Hydrazine based</b> | Semicarbazide (potent at mM – reversible for SSAO, LOX and DAO) | Inactivates SSAO by forming hydrazones with TPQ | 1 mM semicarbazide inhibits SSAO activity in rat aortic smooth muscle cells (A7r5) (Hernandez <i>et al.</i> , 2006).<br><br>Semicarbazide inhibits allylamine-induced vascular toxicity in rat vascular endothelial and SMCs (Ramos <i>et al.</i> , 1998). | Inactivation of SSAO by semicarbazide promotes the stability of atherosclerotic lesions with less macrophages but more SMCs and collagen accumulations in LDLr <sup>-/-</sup> mice (Zhang <i>et al.</i> , 2016).<br><br>Semicarbazide (SCZ, 30 mg/kg) reduces myocardial infarct size in male Sprague–Dawley rats (Yang <i>et al.</i> , 2011). |
|------------------------|---|---|--|--|

---

---

|  |  |  |   |               |
|--|--|--|---|---------------|
|  |  |  | Semicarbazide (3h; 98 mg/kg) inhibits SSAO driven acrolein formation in allylamine-treated rats (Awasthi & Boor, 1993).   |               |
| Methylhydrazine (potent at nM – reversible for SSAO, potentiates hepatic MAO-B activity) | Inactivates SSAO by forming hydrazones with TPQ  | Methylhydrazine inhibits SSAO in rat aorta tissue homogenate (Holt & Callingham, 1994).  |   | Anti-cancer   |
|  |  | Methylhydrazine inhibits the SSAO driven deamination of benzylamine SSAO in rat adipose tissue (Holt & Callingham, 1992).  |   |               |
| Aminoguanidine (potent at nM – irreversible for SSAO, weak NOS and MAO inhibitor)        | Inactivates SSAO by forming hydrazones with TPQ<br><br>Trap carbonyl intermediates and block the formation of AGEs | Aminoguanidine inhibits SSAO activity in human umbilical arteries and rat aortae (Yu & Zuo, 1997).<br><br>Prevents the formation of AGE-modified apolipoproteins | Aminoguanidine reduces formaldehyde production by inhibiting SSAO activity in male CD1 Swiss white mice (Kazhkov <i>et al.</i> , 2007).<br><br>Aminoguanidine increases | Anti-diabetic |

---

---

|  |   |   |  |                   |
|--|---|---|--|-------------------|
|  |   | n A-1<br>(Bucala <i>et al.</i> , 1994).   | arterial elasticity and decreases vascular AGE accumulation as well as the severity of atherosclerotic plaques in streptozotocin-induced diabetic rats with diabetic nephropathy (Hu <i>et al.</i> , 2011).  |                   |
| LJP-1207<br>(potent at nM – irreversible for SSAO) | Inactivates SSAO by forming hydrazones with TPQ | LJP-1207 Reduces SSAO activity in rat aorta homogenate (Kubota <i>et al.</i> , 2020). | LJP-1207 (30 mg/kg) reduces the myocardial infarct size in male Sprague–Dawley rats (Yang <i>et al.</i> , 2011).<br><br>LJP 1207 reduces serum levels of tumour necrosis factor- $\alpha$ and interleukin 6 in lipopolysaccharide (LPS)-challenged mice (Luisa <i>et al.</i> , 2005).<br><br>LJP 1207 inhibits VAP-1 in diabetic, oestrogen-treated ovariectomized | Anti-inflammatory |

---

|                   |  |   |   |  |                   |
|-------------------|--|---|---|--|-------------------|
|                   |  |   |   | d female fats subjected to transient forebrain Ischemia (Hao-Liang <i>et al.</i> , 2006).                          |                   |
| <b>Antibodies</b> | mAb TK8-14 (Mouse IgG2a Isotype and antigen human VAP-1) | Cause conformational changes of VAP-1/SSAO molecule | Treatment of endothelial cells with mAb TK8-14 decreases SSAO facilitated benzylamine oxidation and the number of rolling lymphocytes (Salmi <i>et al.</i> , 2001).<br><br>mAb TK8-14 inhibits lymphocytes adhesion to VAP-1 on endothelial cells (Salmi <i>et al.</i> , 2000).<br><br>Lymphocytes rolling on endothelial cells is diminished by SSAO inhibitor mAb TK8-14 (Koskinen <i>et al.</i> , 2004). | mAb TK8-14 reduces SSAO driven vascular complications in mTIEhVAP-1 transgenic mice (Stolen <i>et al.</i> , 2004). | Anti-inflammatory |
|                   | mAb 1B2 (Mouse IgM and antigen human VAP-1)              |   | mAb 1B2 inhibits lymphocytes binding to VAP-1 on endothelial  |  | Anti-inflammatory |

|                              |  |   |  |  |                   |
|------------------------------|--|---|--|--|-------------------|
|                              |  |   | cells (Smith <i>et al.</i> , 1998).  |  |                   |
| <b>siRNAs</b>                | VAP-1<br>siRNA   | Cleaves and degrades AOC3 mRNA  | VAP-1 knockdown with VAP-1 siRNA impairs the migratory capacity of primary pericytes (Gharanei <i>et al.</i> , 2020).  | Inhibition of VAP-1 with siRNA attenuates cerebral oedema and improves neurological recovery in mice 24 h post-injury (Ma <i>et al.</i> , 2011).<br><br>Blocking VAP-1 with siRNA 24 h before inducing Intracerebral haemorrhage in mice inhibits leukocyte migration, decreases cerebral oedema, and improves neurobehavioral deficits (Almarghalani & Shah, 2021). | Anti-inflammatory |
| <b>Propargyl amine based</b> | $\beta$ -amino propionitrile – $\beta$ APN (weak and competitive reversible for SSAO; highly potent for LOX, at $\mu$ M as irreversible and mechanism based; | Forms intermediate which, isomerizes to a more stable product capable of forming a copper chelated species, which then form a | Endothelial permeability is increased by LOX inhibition in cells incubated with $\beta$ APN (Rodriguez <i>et al.</i> , 2008).<br><br>$\beta$ APN shows weak inhibitory | $\beta$ APN significantly attenuates the increase in body weight and cardiac hypertrophy observed in high-fat diet (HFD) rats (Rodriguez <i>et al.</i> , 2016).  | Anti-cancer       |

---

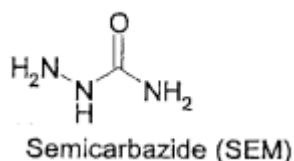
|   |   |   |
|---|---|---|
| <p>recently also defined as non-selective for all LOX enzymes (Ikenaga <i>et al.</i>, 2017; Hajdu <i>et al.</i>, 2018).</p> | <p>covalent adduct with the cofactor.</p> | <p>potential over SSAO and higher potency for LOX in arteries of growing Brown Norway (BN) rats (Mercier <i>et al.</i>, 2009).</p> <p><math>\beta</math>APN demonstrate s irreversible inhibition over LOX and weak competitive reversible inhibition over SSAO in lamb aorta (Pestov <i>et al.</i>, 2011).</p> |
|---|---|---|

---

## **9.2 Hydrazine based derivative inhibitors of SSAO**

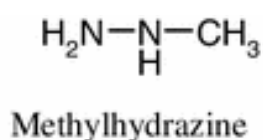
Hydrazine derivatives are generally ranked as one of the most potent SSAO inhibitors. Their mechanism of inhibition is primarily due to covalent binding to the prosthetic group at the cofactor site of the enzyme (Kinemuchi *et al.*, 2004). These inhibitors have been demonstrated effective for acute and chronic inflammatory diseases. Esteban *et al.* (2013) have identified a hydrazine compound (JL72) with multitarget ligand properties which was able to modulate monoaminergic transmission and exert a potent anti-inflammatory effect. Another group of effective hydrazine derivative are the well-studied LJP series of amine oxidase inhibitors. These inhibitors have been demonstrated successful in inhibiting neutrophils accumulation and reducing inflammation in a variety of disease models (Foot *et al.*, 2013; Salter-Cid *et al.*, 2005; Xu *et al.*, 2006; Wang *et al.*, 2006).

Semicarbazide, through which SSAO has been characterised, also belongs to the group of hydrazine derivatives; however, is considered weak inhibitor comparing to other compounds.



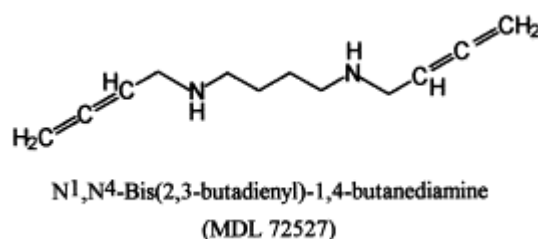
It has recently been identified to be less sensitive in rat comparing to human SSAO (Kubota *et al.*, 2020). In a study done by Kubota *et al.* (2020), where SSAO inhibition was compared between five known inhibitors (semicarbazide, hydralazine, LJP-1207, astellas compound 35c and PXS-4728A), in recombinant rat and human VAP-1, semicarbazide was identified as the least potent of the five inhibitors tested and with nearly a 10-fold difference in IC<sub>50</sub> between human and rat VAP-1 (85.9 μM vs. 993 μM). In this study, semicarbazide was selected as competitive inhibitor to study SSAO inhibition due to being the first recognised inhibitor of the enzyme with extensively validated inhibitory potential in various *in vitro* and *in vivo* studies (Table 3).

Methylhydrazine is another hydrazine-based inhibitor, more potent comparing to semicarbazide. In a study by Holt & Callingham (1994), methylhydrazine demonstrated a dose dependent SSAO inhibition in various rat homogenate tissues. Moreover, when compared to procarbazine, methylhydrazine was identified as more potent inhibitor; however, much more rapidly reversible (Holt & Callingham, 1994). Holt & Callingham (1994) also observed potentiated MAO-A and MAO-B activity in homogenates of brown adipose tissue from rats after treatment with methylhydrazine. In subsequent *in vivo* studies done by Kinemuchi *et al.* (2004), when injected to rats, methylhydrazine once again resulted with a dose dependent SSAO inhibition, with IC<sub>50</sub> values in most tissues of about 0.08 mg/kg. However, Kinemuchi *et al.* (2004) also detected potentiation of MAO-B activity to 140% in the liver and MAO-A activity to 350% in brown adipose tissue, after treatment with methylhydrazine. In this study methylhydrazine was also applied as competitive reversible inhibitor to study SSAO inhibition, predominantly due to its high potency (inhibits at nM, as previously documented in *in vitro* studies in rat), and selectivity (has no effect on NOS) over SSAO (Table 3).



### 9.3 Suicide (mechanism-based) inhibitors of SSAO

MDL72527 is a propenyl amine-based inhibitor which can irreversibly inhibit SSAO and polyamine oxidases (PO). It was initially designed in 1985 as a selective irreversible inhibitor for PO (Bey *et al.*, 1985). However, it has recently been also identified as a mechanism-based, suicide inhibitor of SSAO (Seiler *et al.*, 2000; Duranton *et al.*, 2002; Agostinelli *et al.*, 2006). Being a suicide inhibitor, MDL72527 is converted by SSAO to a highly reactive intermediate product. This leads to irreversible inhibition of SSAO due to formation of a stable covalently bound enzyme-inhibitor adduct at the active site of the enzyme (Kinemuchi *et al.*, 2004). Because of the lacking primary amino group, MDL72527 does not form a Schiff base with TPQ, as is the case for substrates, instead it forms a reversible adduct with TPQ, bringing the inactivator in a position that allows reaction of the double bond system with a nucleophile of the active site of the enzyme (Agostinelli *et al.*, 2005). Since the adduct in contrast with Schiff bases is unstable, TPQ is regenerated while the inactivator remains bound to the enzyme protein by a covalent bond (Agostinelli *et al.*, 2005).



Due to being extensively studied as an enzyme-activated irreversible inhibitor of PO, MDL72527 has already been identified as a compound with therapeutic potential (Duranton *et al.*, 2002). In a study done by Halline *et al.* (1990), MDL72527 successfully reduced 1,2-dimethylhydrazine induced colon tumour growth, and in another study done by Dogan *et al.* (1999) MDL72527 reduced the injury volume and oedema formation after brain ischemia. In this study MDL72527 was used as irreversible, mechanism-based inhibitor to study SSAO inhibition, due to having strong potency for SSAO and no selectivity for other vascular amine oxidases such as LOX (Table 3). Another mechanism-based SSAO inhibitor is 2-bromoethylamine (2-BEA). 2-BEA is a highly selective, potent and suicide inhibitor of the membrane-bound VAP-1 with no inhibitory effect on monoamine oxidase (MAO). This compound belongs to the halo-alkylamine group of inhibitors and has a bromine atom at the beta position which contributes for its high potency inhibition (Yu *et al.*, 2001). 2-BEA has been demonstrated as irreversible, mechanism based, and time-dependent inhibitor in both, *in vitro* and *in vivo* models (Yu *et al.*, 2001; Pannecoeck *et al.*, 2015).



## 9.4 Function blocking antibodies for SSAO

Function blocking antibodies are another group of SSAO inhibitors designed to inhibit the membrane bound VAP-1 and prevent adhesion and transmigration of neutrophils. Therefore, they are reported in the literature as therapeutic agents with anti-inflammatory properties (Salmi *et al.*, 2000; Salmi *et al.*, 2001; Stolen *et al.*, 2004; Koskinen *et al.*, 2004). The most successful are the mouse/human chimeric antibodies which consist of combination of variable domains of the parental mouse antibodies, with a modified human IgG2 constant region. These antibody inhibitors have many advantages such as: reduced binding to Fc receptors in comparison with natural IgG molecules, easier maintenance of specificity and affinity of the antigen-binding site and no activation of complement or initiation of antibody-dependent cell-mediated cytotoxicity (Kirton *et al.*, 2005).

## 9.5 LOX inhibitors

The LOX family of enzymes have also been targeted with small molecule inhibitors, mainly in the treatment of invasive cancers (Smithen *et al.*, 2019). However, targeting LOX enzymes with small molecule inhibitors has been proven challenging, mainly due to lack of crystal structures useful for drug design and difficulties with isolating several of the enzymes in an active form (Smithen *et al.*, 2019). Nevertheless, in recent years several LOX-selective inhibitors have been reported, including halo allylamine-based inhibitors PXS-S1A and the highly potent PXS-S2A, as well as dual LOXL2/LOXL3 inhibitor PXS-5153A (Figure 26.1), aminomethylenepyridine (Figure 26.2) and dual LOX/LOXL2 inhibitor CCT365623 (Figure 26.3a) which has been demonstrated to significantly reduce tumour growth in a LOX-dependent breast tumour transgenic mouse model (Smithen *et al.*, 2019). These novel inhibitors offer significant advantages over the prototypical pan-LOX inhibitor  $\beta$ -aminopropionitrile ( $\beta$ APN) (Figure 26) whose lack of sites amenable for chemical modification precludes preclinical optimization (Smithen *et al.*, 2019).

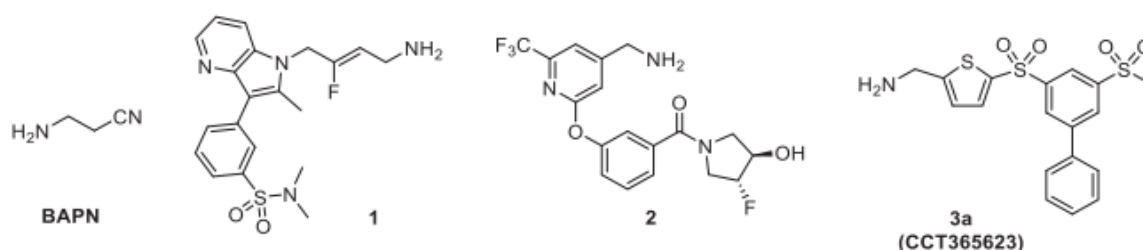
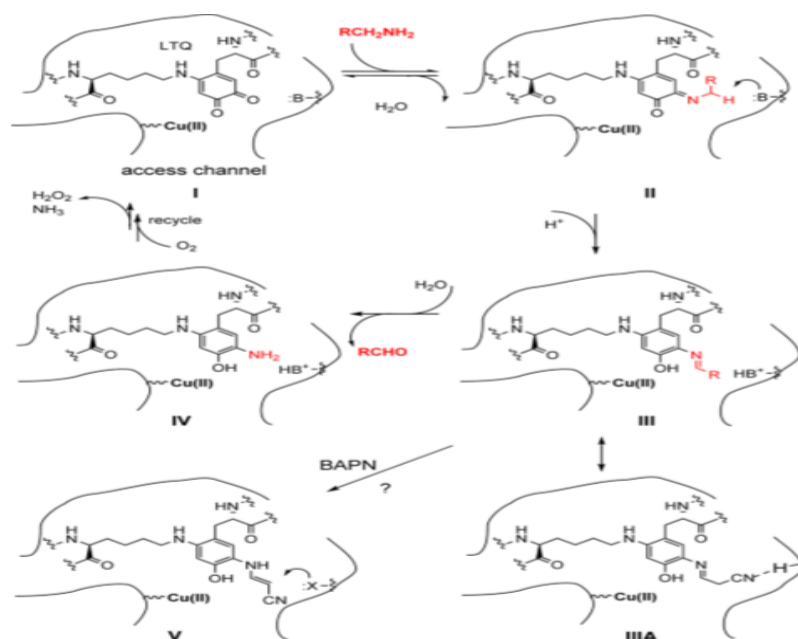


Figure 26. Small molecule inhibitors of LOX family enzymes (Smithen *et al.*, 2019)

## 9.6 $\beta$ -Aminopropionitrile ( $\beta$ APN)

$\beta$ -Aminopropionitrile ( $\beta$ APN) is a mechanism based - irreversible inhibitor for LOX (Hutchinson *et al.*, 2017; Leung *et al.*, 2019). Recently, it has also been suggested as non-selective for all LOX enzymes (Ikenaga *et al.*, 2017; Hajdu *et al.*, 2018). In the process of lysine oxidation catalysed by LOX the  $\epsilon$ -amino group reversibly reacts with the cofactor LTQ (Figure 27 I) to form an intermediate substrate Schiff base (Figure 27 II). During this process, a basic residue catalyse the irreversible rearrangement of II by proton abstraction, leading to a reduction of the quinoid ring to form the product Schiff base (Figure 27 III). Hydrolysis of III would result with an aldehyde (allysine) and intermediate (Figure 27 IV), which is then recycled via several steps involving  $O_2$  and Cu to I; this would lead to concomitant release of  $H_2O_2$  and  $NH_3$ . However, when  $\beta$ APN binds to LOX (Figure 27), the intermediate III isomerizes to a more stable product V, potentially capable of forming a copper chelated species, or a nearby nucleophilic residues, which then form a covalent adduct to irreversibly inactivate the enzyme (Hutchinson *et al.*, 2017).



**Figure 27. The oxidation mechanism by LOX and its inhibition by  $\beta$ APN (Hutchinson *et al.*, 2017).**

In this study,  $\beta$ APN was utilised to study LOX inhibition due to being reported as highly potent mechanism-based inhibitor, with strongest inhibitory potential for LOX in comparison to other copper amine oxidases present in the vasculature (Pestov *et al.*, 2011; Mercier *et al.*, 2009; Rodriguez *et al.*, 2008; Rodriguez *et al.*, 2016).

## SECTION 10. AIMS AND OBJECTIVES

SSAO levels have been observed to alter in various cardiovascular pathologies including atherosclerosis, hypertension, strokes, and congestive heart failure. However, the role of SSAO in cardiovascular pathologies has only been investigated in tissue culture. The aim of this study was to firstly investigate SSAO activity in cell culture by optimising a method that would effectively assess SSAO catalytic activity *in vitro* using benzylamine as model substrate, which has been previously mentioned as the most appropriate substrate for measuring *in vitro* SSAO activity in rodents and humans (Kubota *et al.*, 2020). The advantage of the proposed method is to allow a high throughput investigation of multiple areas of interest compared to a tissue culture model.

Secondly, apply the same method to explore the mechanism by which SSAO metabolism of its endogenous substrates' methylamine and aminoacetone causes vascular damage; and characterise SSAO inhibition with a well-proven reversible SSAO inhibitors, semicarbazide and methylhydrazine, and a more novel, irreversible, and mechanism-based inhibitor, MDL72527. These inhibitors have been previously validated as highly selective for SSAO, while demonstrating a potency over the enzyme within a different concentration range (semicarbazide in mM, methylhydrazine in nM, and MDL72527 in  $\mu$ M; see Table 3).

Thirdly, investigate the activity of SSAO and LOX, and their interconnection in VSMCs as cells were being passaged from lower to a higher passage number; and elucidate which enzyme has predominant contributory role in ROS formation in aged (late passage) cells.

Vascular SMCs were selected due to expressing high activity of SSAO in the vasculature. VSMCs are the main stromal cells in the medial layer of the vascular wall and are involved in many physiological functions and pathological changes that take place in the vasculature (Lacolley *et al.*, 2012). These cells produce the extracellular matrix (ECM) which is important to provide the arterial wall with the capacity to withstand the pressure from the circulating blood (Lacolley *et al.*, 2012). VSMCs are characterised with high plasticity which enables them to re-programme their expression pattern in response to external stimuli. Therefore, based on the signals present in their local environment these cells can change phenotype from quiescent – contractile to proliferative - synthetic phenotype. The acquired synthetic phenotype will enable these cells to migrate and proliferate inwardly from the medial to the intimal layer of the arteries, leading to intimal hyperplasia which is one of the main characteristics in the pathophysiology of atherosclerosis (Gimbrone & Garcia-Cardena, 2016).

**PHASE 1:** Develop and optimise an *in vitro* model to effectively measure SSAO activity in primary VSMCs from rat aorta using benzylamine as model substrate.

Furthermore:

- Evaluate the effectiveness of the model while exploring SSAO kinetics in the presence of its endogenous amine compounds methylamine and aminoacetone to understand the level of interaction between the enzyme and these amines in vascular pathologies. In doing that, SSAO's affinity ( $K_m$ ) for methylamine and aminoacetone, and the rate ( $V_{max}$ ) at which the enzyme converts the amines into aldehydes was assessed using the non-linear regression model of Michaelis Menten.
- Evaluate further the efficacy of the model while characterising SSAO inhibition with the standard competitive reversible inhibitors semicarbazide (potent within mM range), methylhydrazine (potent within nM range), and a newer inhibitor that acts through mechanism-based inhibition such as MDL72527 (potent in  $\mu$ M range). In doing that, SSAO kinetic parameters ( $K_m$  and  $V_{max}$ ) were once again assessed in the presence of the above-mentioned inhibitors, and the potency of each inhibitor was validated by comparing the inhibitor constant values ( $K_i$ ) using the non-linear regression model of Michaelis Menten.
- Investigate toxicological consequence of SSAO catalytic activity *in vitro* by measuring VSMCs viability after methylamine and aminoacetone treatment, before and after addition of MDL72527. Furthermore, assess potential synergism in the toxicological effect between SSAO derived products by measuring cell viability after direct exposure to an aldehyde, hydrogen peroxide, or an aldehyde and hydrogen peroxide.

**PHASE 2:** Apply the model characterised in Phase I to study SSAO and LOX in VSMCs, as cells were being passaged from lower to higher passage number. In doing that, the activity of both enzymes, their protein expression (VAP-1 and LOX), the expression of the VSMCs contractile markers SM22 $\alpha$  and ACTA2, and the expression of PDGFR $\beta$ , a G-protein coupled receptor involved in chemotaxis, were assessed at basal level and in the presence of SSAO and LOX respective substrates and inhibitors.

**PHASE 3:** Investigate the molecular interaction mechanism between SSAO and LOX in rat aortic VSMCs and establish which enzyme has predominant role in ROS formation and consequently vascular damage. In doing that, AOC3 and LOX mRNA levels were assessed in the presence of SSAO and LOX respective inhibitors; and ROS and total GSH levels were assessed in VSMCs with a greater passage number, in the presence of SSAO and LOX respective amine substrates.

# CHAPTER II: METHODOLOGY

## SECTION 2.1

### MATERIALS

*Table 4. Materials used in this thesis*

| Chemical  | Supplier        | Product Code |
|---|-----------------|--------------|
| $\alpha$ -Smooth Muscle Actin (D4K9N) XP <sup>®</sup> Rabbit mAb (20 $\mu$ L) | Cell signalling | 19245        |
| Aminoacetone Hydrochloride 5MG  | Sigma           | CDS020585    |
| Amplex <sup>®</sup> Red Monoamine Oxidase Assay Kit                           | Thermo Fisher   | A12214       |
| Ampliflu <sup>™</sup> red (10-Acetyl-3,7-dihydroxyphenoxazine) 5MG-F          | Sigma           | 90101        |
| Anti-SM22 $\alpha$ antibody (100 $\mu$ L)                                     | Abcam           | Ab124964     |
| Anti-PDGF Receptor $\beta$ (28E1) Rabbit mAb (20 $\mu$ L)                     | Cell Signalling | 3169         |
| $\beta$ actin HRP conjugated antibody (100 $\mu$ L)                           | Abcam           | Ab20272      |
| $\beta$ -aminopropionitrile ( $\beta$ APN) fumarate salt 5G                   | Sigma           | A3134        |
| Benzylamine hydrochloride 25G   | Sigma           | B5136        |
| Bolt <sup>®</sup> 8% (1.0mm X 10well) Bis-Tris Plus Gels                      | Thermo Fisher   | NW00080BOX   |
| Bolt <sup>®</sup> NuPAGE <sup>®</sup> LDS sample buffer (4X) 250ML            | Thermo Fisher   | NP0008       |
| Bolt <sup>®</sup> /NuPAGE <sup>®</sup> reducing agent (10X) 10ML              | Thermo Fisher   | NP0009       |
| Bolt <sup>®</sup> MOPS and MES SDS running buffers (20X) 500ml                | Thermo Fisher   | B002         |
| Bovine serum albumin (BSA) 100G   | Sigma           | A7906        |

|  |                   |             |
|--|-------------------|-------------|
| Bradford reagent 500ML   | Thermo Fisher     | 15424109    |
| Cadaverine (1,5 diamino pentane dihydrochloride) 5G                                      | Sigma             | D22606      |
| Clorgyline - N-Methyl-N-propargyl-3-(2,4-dichlorophenoxy) propylamine hydrochloride 50MG | Sigma             | M3778       |
| DMSO 500ML   | Fisher Scientific | D/4121/PB08 |
| Dulbecco's modified eagle medium (DMEM), with low (1 g/L) glucose 500ML                  | Gibco             | 41965-039   |
| Foetal Bovine Serum (FBS) 500ML  | Fisher Scientific | 15799170    |
| Formaldehyde 250ML-F   | Sigma             | 47608       |
| Goat anti-rabbit IgG (Alexa Fluor <sup>®</sup> 647 conjugate) secondary antibody 250µL   | Cell Signalling   | 4414S       |
| Glutathione (GSH) assay kit  | Abcam             | Ab239727    |
| Horseradish peroxidase (HRPO) lyophilized, powder, ~150 U/mg 100MG                       | Sigma             | 77332       |
| HS AllStars Cell death control 1nmol   | Qiagen            | SI04381048  |
| Hydrogen peroxide (H <sub>2</sub> O <sub>2</sub> ) 500ML                                 | Sigma             | 516813      |
| Isopropanol 1L   | Sigma             | 563935      |
| Methanol 500ML   | Fisher Scientific | 11472854    |
| Methylamine Hydrochloride 100G   | Sigma             | M0505       |
| Methylglyoxal 25ML   | Sigma             | M0252       |
| Methylhydrazine 5G   | Sigma             | 699101      |
| MDL72527 5MG   | Sigma             | M2949       |
| MTT [(3-(4,5-dimethylthiazol-2-yl)-2,5-diphenyl tetrazolium bromide) 1G                  | Sigma             | 1117140001  |
| Penicillin/streptomycin 20ML   | Sigma             | P4333       |
| Phosphate Buffer Saline (PBS 1X) 500ML   | Sigma             | D8537       |
| Pierce BCA Protein Assay kit 500ML   | Thermo Fisher     | 23227       |
| Precision Plus Protein <sup>®</sup> Standards kaleidoscope ladder 500µL                  | Bio Rad           | 1610374     |

|  |                   |            |
|--|-------------------|------------|
| Primers 100µM Actb – Left                                | Sigma             | HA14301489 |
| Primers 100µM Actb – Right                               | Sigma             | HA14301490 |
| Primers 100µM SSAO – Left                                | Sigma             | HA14220322 |
| Primers 100µM SSAO – Right                               | Sigma             | HA14220323 |
| Primers 100µM LOX – Left                                 | Sigma             | HA14220324 |
| Primers 100µM LOX – Right                                | Sigma             | HA14220325 |
| Protease inhibitor cocktail 1ML                          | Sigma             | P8340      |
| Phosphatase inhibitor cocktail 1ML                       | Sigma             | P2850      |
| qPCR BIO SyGreen 1-Step Go Kit                           | PCR Biosystems    | PB25.31    |
| Rabbit monoclonal to LOX<br>(EPR4025) 100µL              | Abcam             | Ab174316   |
| Radiance Plus ECL reagents 100mL                         | Azure Biosystems  | AC0024     |
| ReliaPrep™ RNA cell miniprep<br>system kit               | Promega           | Z6010      |
| Resorufin sodium 5G                                      | Sigma             | R3257      |
| Restore Plus western blot stripping<br>buffer 500ML      | Thermo Fisher     | 46430      |
| ROS assay kit (Red)                                      | Abcam             | Ab186027   |
| VAP-1 antibody conjugated with<br>Alexa Fluor® 200 µg/ml | Santa Cruz        | SC373924   |
| Semicarbazide Hydrochloride 5G                           | Sigma             | S2201      |
| siRNA5_LOX 5nmol   | Qiagen            | SI03039267 |
| siRNA6_LOX 5nmol   | Qiagen            | SI03045959 |
| siRNA8_LOX 5nmol   | Qiagen            | SI03114433 |
| Si AllStars Negative Control 5nmol                       | Qiagen            | 324458133  |
| Sodium Phosphate 25G                                     | Sigma             | 342483     |
| Tris-base 1KG  | Fisher Scientific | 10785341   |
| Trypsin 20ML   | Sigma             | T4174      |
| Tween-20 100ML   | Sigma             | P7949      |

## SECTION 2.2

### METHODS – CELL CULTURE

#### 2.2.1 Animals

The care and use of all animals in this study was carried out in accordance with Home Office regulations following the Animal and Scientific Procedures Act of 1986 under PPL70/7732. The male Wistar rats (180-220g) were housed in pairs in standard cages (Tecniplast 2000P) with sawdust (Datesand grade 7 substrate) and shredded paper wool bedding with water and food (5LF2 10% protein LabDiet) in the Biological Services Unit at the University of Hertfordshire. The housing environment was maintained at a constant temperature ( $21 \pm 2^{\circ}\text{C}$ ) and light-dark cycle (12:12 hours). The rat model was used due to being closely similar with humans in terms of aortic SSAO activity. A study done by Boomsma *et al.* (2000) which investigated variations in SSAO activity in plasma and tissues of mammals demonstrated not significant difference in aortic SSAO activity between human and rat. Wistar strain was selected over other strains such as Sprague-Dawley<sup>®</sup> due to having smaller body size and would therefore incur smaller cost.

Furthermore, to support the principle of the 3R's (replacement, reduction, and refinement) tissues were mostly shared from teaching and research studies; this minimised the numbers of animals being used. The small number of rats that were purchased were sourced from Charles River (Harlow, UK) and the same supplier was maintained throughout the project. Moreover, male rats were used as previously been demonstrated that there are no significant gender-related differences in SSAO activity between rat, cattle, horse, sheep, and goat regardless of species (Al-Wabel, 2008). All experiments were carried out in accordance with the University of Hertfordshire animal welfare ethical guidelines and European directive 2010/63/EU. Rats were euthanised by CO<sub>2</sub> asphyxiation and the aorta was removed and placed in a DMEM solution supplemented with 10% Foetal Bovine Serum (FBS (v/v)), 1% penicillin (100units ml<sup>-1</sup>), streptomycin (100µg ml<sup>-1</sup>) and 2mM L-Glutamine.

### 2.2.2 Cells

The VSMCs were selected due to expressing high levels of both, SSAO and LOX. Due to being an enzyme with functional diversity SSAO distinguishes itself with a different role in different vascular cells. In VSMCs, unlike the enzyme expressed in vascular endothelial cells, SSAO does not bind lymphocytes but rather it mediates toxicological effects (El Hadri *et al.*, 2002). Since the aim of this study was to investigate the toxicological consequence of overactive SSAO, its interaction with LOX, and how this contributes to the early developing stages of atherosclerosis, VSMCs were the preferred choice of cell. Moreover, it has previously been noted that cultured cells represent essential tools to investigate SSAO pharmacology, biochemistry, and function (El Hadri *et al.*, 2002).

This study used primary VSMCs because primary cell cultures most closely represent the tissue of origin. However, primary cultured VSMCs can lose the capacity to contract and transform into synthetic phenotype after several passages (Chi *et al.*, 2017). These cells can also prematurely undergo induction of cellular senescence earlier than other cells, causing early cultures to contain a mixture of both young and senescent cells (Ogrodnik, 2021). Therefore, the VSMCs used in these experiments were between passage 3 and 8. In a study by Chang *et al.* (2014), VSMCs at early passage (passage 4) have shown better migration probability and VSMCs at late passage (passage 10) have demonstrated a decrease in size and less elongated morphology, with loss in parallel organization of actin filament, and a randomized actin filament distribution.

Cellular aging has been defined as a gradual decline in cell function and an increase in probability of cell death (Ogrodnik, 2021). Primary cells require several passages to fully develop receptors and maintain a consistent and fast proliferation rate (Chang *et al.*, 2014). In this study, VSMCs at passage 3 & 4 were considered as young cells because of their observed optimum cell function distinguished by elongated morphology and fast proliferation rate. Furthermore, VSMCs at passage 8 were considered as old cells because of reduced cell function distinguished by change in morphology (broad and flat rather than elongated) and declined cell proliferation. These changes were observed when the VSMCs were grown beyond passage 8 (passage 9 and 10).

### **2.2.3 Preparation of cell culture reagents**

Rat aortic vascular smooth muscle cells (VSMCs) were cultured in Dulbecco's Modified Eagle's Medium (DMEM; Gibco®), supplemented with 10% Foetal Bovine Serum (FBS (v/v)), 1% penicillin (100units ml<sup>-1</sup>), streptomycin (100µg ml<sup>-1</sup>) and 2mM L-Glutamine. The complete culture media was stored at 4°C and used within three weeks from opening. Phosphate buffer saline (PBS) was used as purchased with 1X concentration. Trypsin-EDTA (without Ca<sup>2+</sup>, Mg<sup>2+</sup>; Gibco®) was diluted to 10X in PBS for the routine subculture.

### **2.2.4 Isolation of rat aortic VSMCs**

The rats were euthanized by CO<sub>2</sub> asphyxiation followed by cervical dislocation. The aorta was removed and placed in a DMEM solution supplemented with 10% Foetal Bovine Serum (FBS (v/v)), 1% penicillin (100units ml<sup>-1</sup>), streptomycin (100µg ml<sup>-1</sup>) and 2mM L-Glutamine. VSMCs were isolated from the rat's aorta, as described by Jufang *et al.* (2017). Aortas were washed three times with PBS and the fat tissue was removed. The artery was cut into small blocks (1 mm<sup>2</sup>) and transferred to a T-25 cell culture flask, with the medial layer facing down. The flask was placed upright in a CO<sub>2</sub> incubator (5% CO<sub>2</sub> and 95% humidified air) at 37°C for 2 - 4 hours to facilitate explant attachment. After firm adherence of the explants, 5ml DMEM was added to the flask and the flask was placed horizontally in a CO<sub>2</sub> incubator (5% CO<sub>2</sub> and 95% humidified air) at 37°C for 48h. After 48h, the flask was replenished with fresh culture media. In the following 7-10 days, after reaching ~80% confluence, the explants were removed from the cells with Pasteur glass pipette and the media was replaced with 5ml fresh media. Figure 28 shows an early micrograph of the cells beginning to migrate from the explant after 4 (A) and 7 (B) days incubation. After 10-15 days the explants were removed, and the fully confluent cells were sub-cultured as described in the methods section 2.2.5.

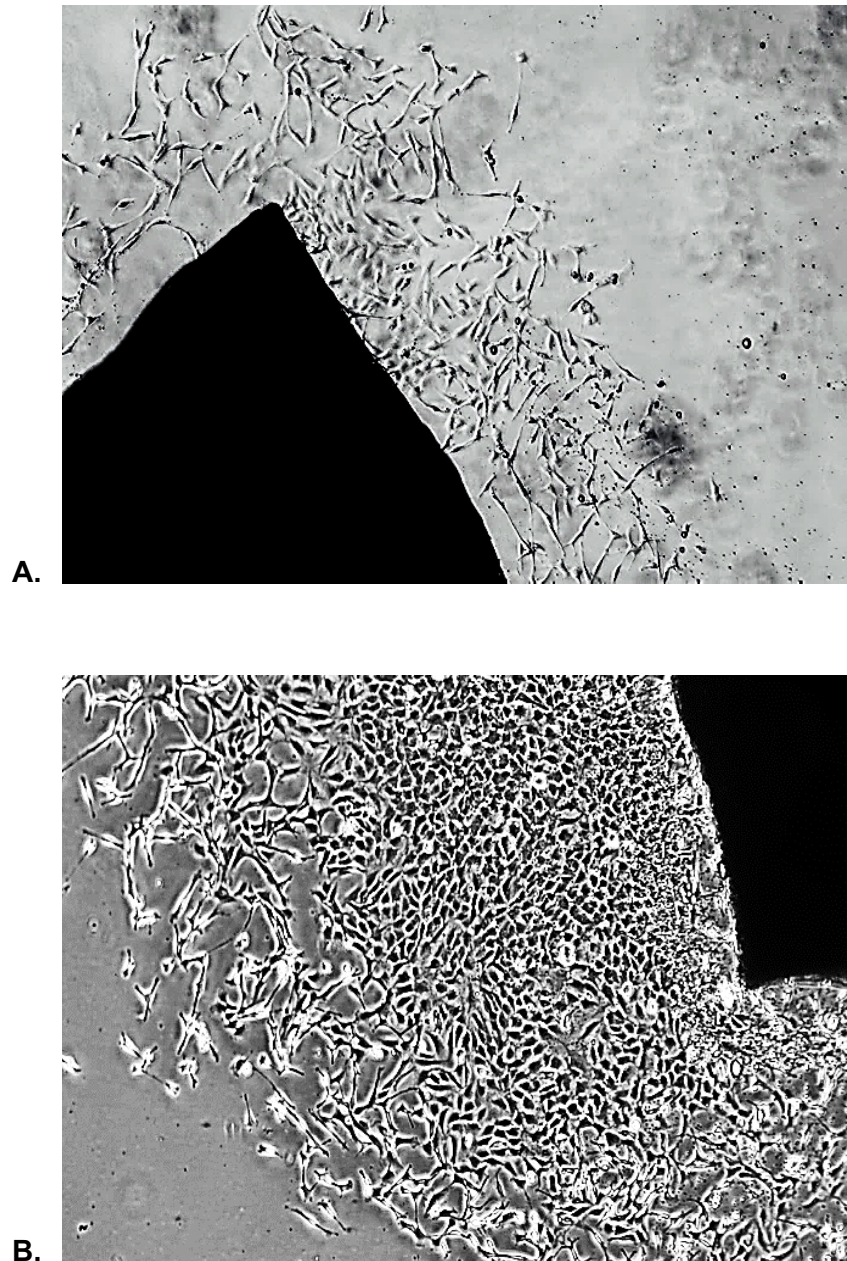


**Figure 28. *In vitro* culture of rat SMCs from aortic explants viewed at 160X magnification (10X E-PL, 4X objective lens, 40X image magnification) under an inverted Olympus light microscope. A) Cell growth after 4 days incubation; B) Cell growth after 7 days incubation (scale bar: 27.2851 $\mu$ m).**

### **2.2.5 Sub-culture of rat aortic VSMCs**

After reaching ~80-90% confluence the media was removed by aspiration and the cells were washed twice with 5ml of 1XPBS followed by addition of 3ml Trypsin/EDTA (diluted in 10X PBS) for 2 minutes to initiate cell detachment.

When majority of cells were detached, 6ml of fresh media was added to neutralise the Trypsin/EDTA. The cell suspension was then centrifuged in a sterile centrifuge tube (220 G) for 5 minutes. After centrifugation, the supernatant was aspirated, and the cell pellet was re-suspended with fresh media (3ml). Suspended cells were counted using haemocytometer as described in section 2.2.6 and plated in plates for experimentation or in flasks for further expansion. With every trypsinisation the number of passage was increased by one. Rat VSMCs between passage 3 to 8 were used for experimentation or cryopreserved as described in section 2.2.7.

### **2.2.6 Cell Counting Using a Haemocytometer**

After being re-suspended with fresh culture media to ensure single cell suspension, 20 $\mu$ l of cell suspension was mixed with 20 $\mu$ l of 0.4% Trypan blue in small Eppendorf tube. 10 $\mu$ l of cell suspension was added into the well of the chamber (allowing capillary action to draw it inside) and counted with inverted Olympus light microscope at 10X magnification. Both, viable (unstained) and dead (blue cells) were counted in four corner squares and averaged. The below calculations were performed to determine the following:

- % Cell Viability = [Total Viable cells (Unstained) / Total cells (Viable +Dead)] X 100.
- Viable Cells/ml = Average viable cell count per square x Dilution Factor x 10<sup>4</sup>
- Average viable cell count per square = Total number of viable cells in 4 squares / 4.
- Dilution Factor = Total Volume (Volume of sample + Volume of diluting liquid) / Volume of sample
- Cell density (Cells per ml) = No of cells counted / 10<sup>4</sup> x dilution factor
- Total number of cells = cells per ml x volume of cell suspension

Cells were sub-cultured up to passage 8, as described in section 2.2.5.

### **2.2.7 Cryopreservation of rat aortic VSMCs**

Cells were routinely cryopreserved for future use. Cells were trypsinised and centrifuged in complete culture medium for 5 minutes. The supernatant was discarded, and the cell pellet was re-suspended in 3ml freezing media per flask, consisting of 20% FBS (v/v), 10% Dimethyl Sulfoxide (DMSO; (v/v), 9% DMEM (v/v), and 1% penicillin/streptomycin (v/v). Cell suspensions were then transferred to cryovials (1-1.5 ml cell suspension in each cryovial) and kept in isopropanol layered Mr Frosty<sup>®</sup> freezing container at -80<sup>o</sup>C overnight to prevent ice crystal formation. The following day, cells were transferred into liquid nitrogen.

### **2.2.8 Resuscitation of rat aortic VSMCs**

Cells were thawed as previously described (Suowen *et al.*, 2009). 5ml complete DMEM was added to T-25 flask which was then kept for 30 min in a CO<sub>2</sub> incubator (5% CO<sub>2</sub> and 95% humidified air) at 37°C. Once removed from the liquid nitrogen, the lower half of the vial was placed in a 37°C water bath and watched closely during the thawing process. The vial was removed from the water bath when only small amount of ice was left inside; it was then decontaminated with 70% IMS, in a sterile biological safety cabinet. The cells in the vial were resuspended by gently pipetting 5 times, and the cell suspension (1ml) from the vial was added into the T-25 flask containing 5ml complete DMEM. The flask was then returned in a CO<sub>2</sub> incubator (5% CO<sub>2</sub> and 95% humidified air) at 37°C and kept overnight, after which complete media was added to the flask to remove all traces of DMSO.

### **2.2.9 Phenotypic characterisation of rat aortic VSMCs**

*In vitro* cultured rat VSMCs were stained for the smooth muscle cell marker SM22 $\alpha$ . Freshly cultured cells were plated at  $2 \times 10^4$  in 24-well plate and allowed to grow for 48 hours to reach 70-80% confluence. Cells were then washed twice with 1XPBS and incubated with ice-cold methanol for 30 minutes for fixing, at room temperature. After fixing, cells were incubated for 60 minutes with 200 $\mu$ l of blocking buffer (100mM TRIS-Base, 100mM of NaCl, 100 $\mu$ l Tween-20 and 5% (w/v) Bovine Serum Albumin (BSA), at pH 7.5.

Cells were then incubated with the SM22 $\alpha$  primary antibody diluted 1:500 in blocking buffer and placed on orbital shaker for 60 minutes. Cells were washed three times with 1XPBS, followed by incubation with anti-rabbit IgG secondary antibody conjugated with Alexa Flour<sup>®</sup> at a dilution of 1:1000 in blocking buffer.

The cell monolayer was again washed in excess 1X PBS to remove unbound antibody, followed by incubation with increasing concentration of glycerol at 10, 30, 60 and 90%. Cell monolayers with glycerol were wrapped in a foil and kept on a room temperature in the dark to protect from light; or, kept overnight at -4°C. Cells were then observed and imaged on a fluorescent microscope. Figure 29 (A & B) is a visual presentation of the stained rat aortic VSMCs depicting the presence of SM22 $\alpha$  actin fibres.

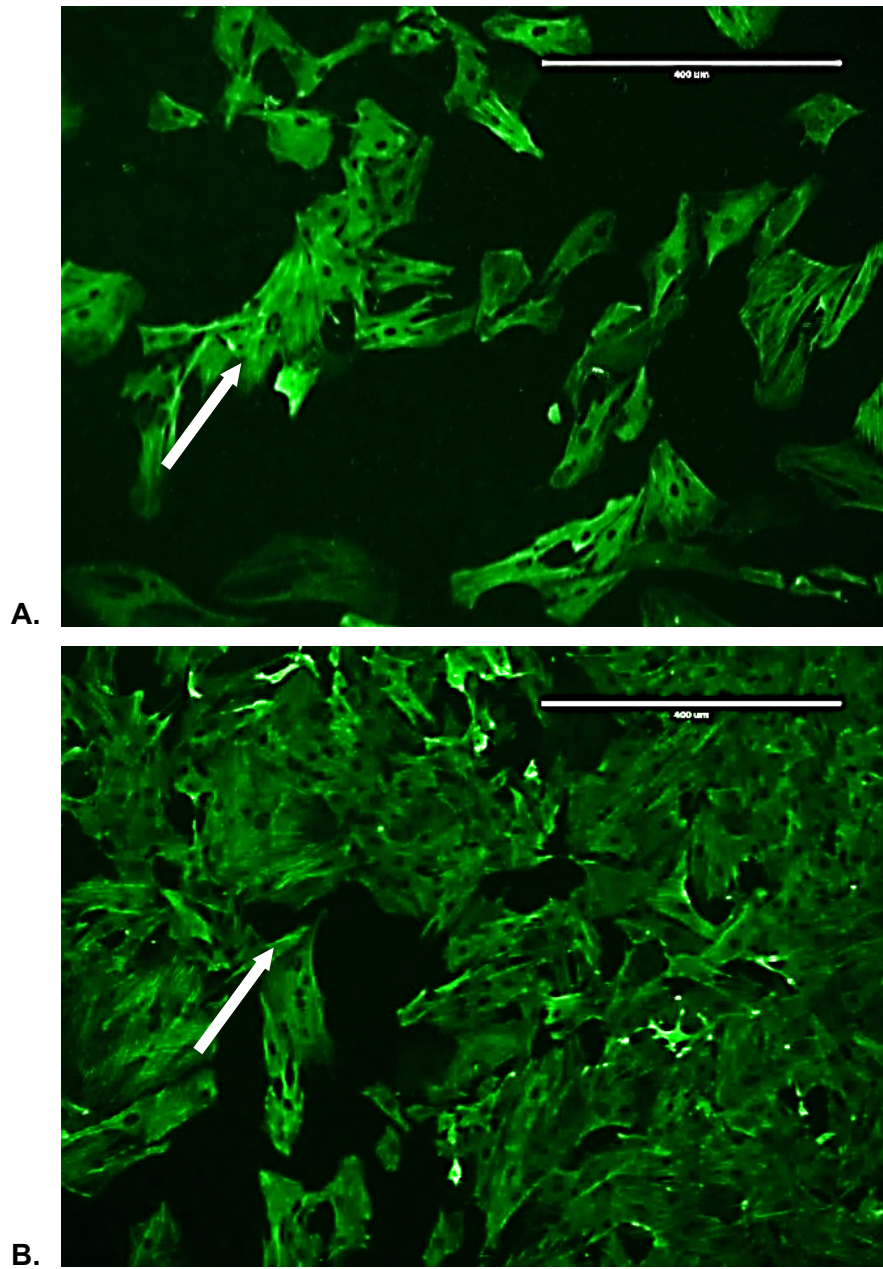


**Figure 29. Immuno-stained microscopic image of rat aortic smooth muscle cells depicting the presence of SM22 $\alpha$  actin fibres (scale bar: 400 $\mu$ m, magnification: X10).**

### 2.2.10 Protein quantification using BCA assay

To express SSAO and LOX activity as  $\text{nmolH}_2\text{O}_2/\text{h}/\text{mg}$  protein, the protein concentration ( $\text{mg}/\text{ml}$ ) in cell samples was calculated using the Bicinchoninic acid (BCA) assay. This assay was selected because of its high sensitivity and tolerance of interfering species (Huang *et al.*, 2010). BCA assay is based on two chemical reactions:

- The first is the reduction of cupric ions ( $\text{Cu}^{2+}$ ) to cuprous ions ( $\text{Cu}^{1+}$ ) by the peptide bonds, known as the biuret reaction (Huang *et al.*, 2010).
- The second step is the chelation of one  $\text{Cu}^{1+}$  with two BCA molecules forming an intense purple complex, which has a peak absorbance at 620nm (Huang *et al.*, 2010).

The peptide bonds and specific residues reduce cupric ions to cuprous ions, which form two complexes with peptide bonds and BCA (Figure 30).

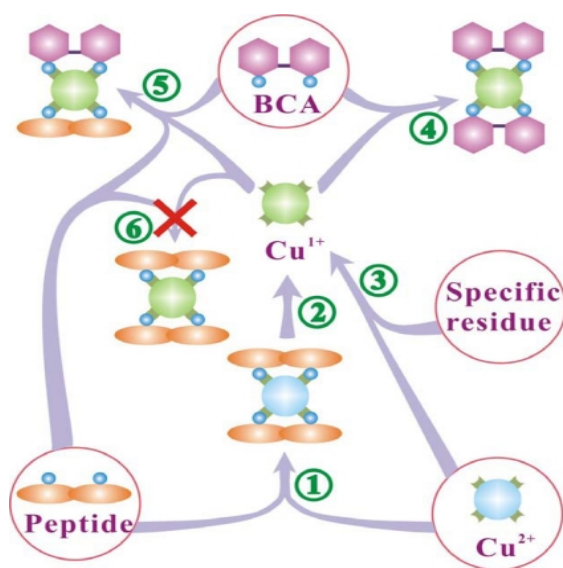


Figure 30. Schematic drawing to display the chemical species in a solution during the BCA protein assay (Huang *et al.*, 2010).

Prior to performing the BCA assay, cells were lysed with 0.5M NaOH and kept on a room temperature for 2 hours. Stock of BSA was diluted to a concentration of 10mg/ml and standards were prepared as shown in Table 5. The BCA reagent was prepared freshly in 50:1 ratio with reagent A and B respectively. Samples, (5µl sample + 5µl distilled water) were added in 80 wells from 96-well plate. The remaining 16 wells were filled with standards, (5µl standard + 5µl, 0.5M NaOH), which were added in duplicate. Additionally, 100µl of freshly prepared BCA reagent was added to each well of the plate.

The 96-well plates were incubated for 45 minutes on a room temperature, on a shaker, and the absorbance was read on Clario Star<sup>®</sup> plate reader (BMG Labtech), at 620nm. The data was transferred to an Excel spreadsheet and analysed before plotting absorbance versus concentration of standards (µg/µl). The protein concentrations of samples were determined from the graph and used to convert absorbance values of samples to protein concentrations using the straight-line equation as shown below in Figure 31. Equation was rearranged to calculate the amount of protein (mg/ml).

**Table 5. Standards for BCA protein assay**

| <b>No</b> | <b>Working stock<br/>10mg/ml BSA (µl)</b> | <b>Distilled<br/>water (µl)</b> | <b>Final<br/>concentration of<br/>protein (µg/µl)</b> |
|-----------|---|---------------------------------|---|
| <b>1</b>  | 0   | 1000                            | 0   |
| <b>2</b>  | 20  | 980                             | 0.2   |
| <b>3</b>  | 40  | 960                             | 0.4   |
| <b>4</b>  | 60  | 940                             | 0.6   |
| <b>5</b>  | 100                                       | 900                             | 1   |
| <b>6</b>  | 200                                       | 800                             | 2   |
| <b>7</b>  | 300                                       | 700                             | 3   |
| <b>8</b>  | 400                                       | 600                             | 4   |

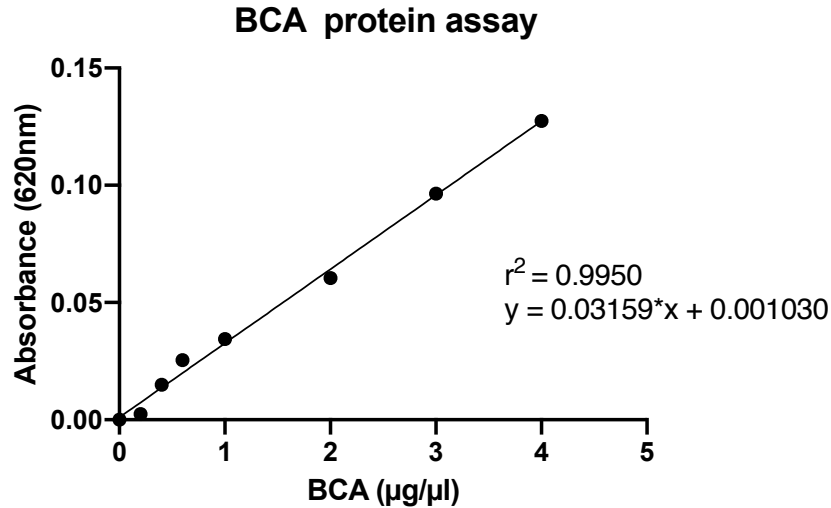


**Figure 31. A linear regression of a protein standard curve. The plate was incubated at room temperature, for 45min, on a shaker. Absorbance readings were taken at 620nm, on a Clario Star<sup>®</sup> Microplate Reader (BMG Labtech).**

### **2.2.11 Protein quantification using Bradford assay**

The Bradford assay was used to determine the concentration of protein in cell samples prior to performing the western blot analysis. This method measures the presence of the amino acid residues lysine, arginine, and histidine, which contributes to formation of protein-dye complex (Ernst & Zor, 2010). Prior to performing the Bradford assay cells were washed twice with 1XPBS and lysed with 40µl RIPA buffer (0.5M TRIS at pH 7.4, 0.9g NaCl, 0.1g SDS, 1ml TRITON x 100, 5mM EDTA) which was supplemented with 10% protease and phosphatase inhibitor cocktail. Cells were then scraped using a pipette tip; vortexed and sonicated for 5 minutes in ice cold water. Stock of BSA was diluted to a concentration of 10mg/ml and standards were prepared as shown in Table 6. Samples, (3µl sample + 47µl distilled water) were added in triplicates and standards, (3µl standard + 3µl RIPA buffer + 44µl distilled water) were added in duplicate in 96-well plate.

Additionally, 200µl of Bradford reagent was added to each well of the plate. The plate was incubated for 15 minutes at room temperature and the absorbance was read on Clario Star<sup>®</sup> plate reader (BMG Labtech), at 570nm and 450nm. The data was transferred to an Excel spreadsheet and analysed before plotting absorbance ratio (570nm / 450nm) versus concentration of standards (µg/µl).

The protein concentrations of samples were determined from the graph and used to convert absorbance values of samples to protein concentrations using the straight-line equation as shown below in Figure 32. Equation was rearranged to calculate the amount of protein ( $\mu\text{g}/\mu\text{l}$ ).

**Table 6. Standards for Bradford protein assay**

| No | Working stock<br>10mg/ml BSA ( $\mu\text{l}$ ) | Distilled<br>water ( $\mu\text{l}$ ) | Final<br>concentration of<br>protein ( $\mu\text{g}/\mu\text{l}$ ) |
|----|--|--------------------------------------|--|
| 1  | 0  | 1000                                 | 0  |
| 2  | 50   | 950                                  | 0.5  |
| 3  | 100  | 900                                  | 1  |
| 4  | 200  | 800                                  | 2  |
| 5  | 400  | 600                                  | 4  |

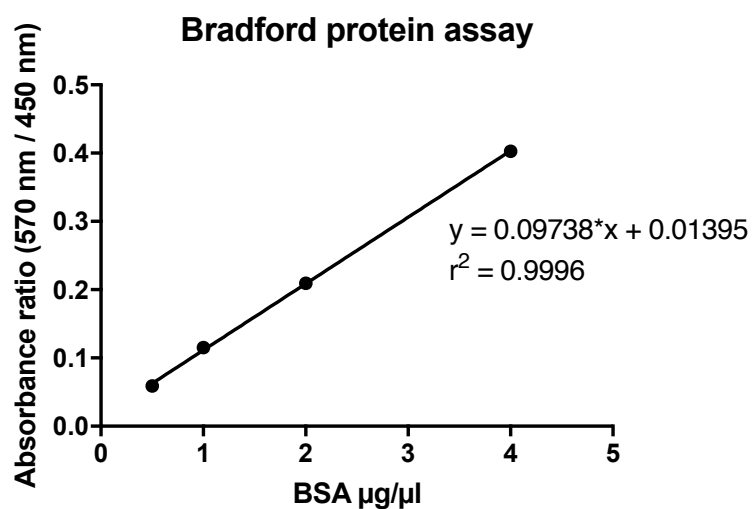


**Figure 32. A linear regression of a protein standard curve. The plate was incubated at room temperature for 5 – 10 minutes. Absorbance readings were taken at 570nm and 450nm, on a Clario Star<sup>®</sup> Microplate Reader (BMG Labtech).**

### 2.2.12 Measurement of SSAO activity in rat aortic VSMCs

SSAO activity in rat aortic VSMCs was measured with the Amplex<sup>®</sup> Red Monoamine Oxidase assay kit (Molecular Probes, UK), using a fluorescence microplate reader (BMG Labtech). Amplex<sup>®</sup> Red is a non-fluorescent and colourless compound that upon enzymatic oxidation catalysed by the enzyme horseradish peroxidase (HRP), is transformed into resorufin, a highly absorbing and fluorescing compound. HRP uses Amplex<sup>®</sup> red as an electron donor during the reduction of hydrogen peroxide to water (Figure 33).

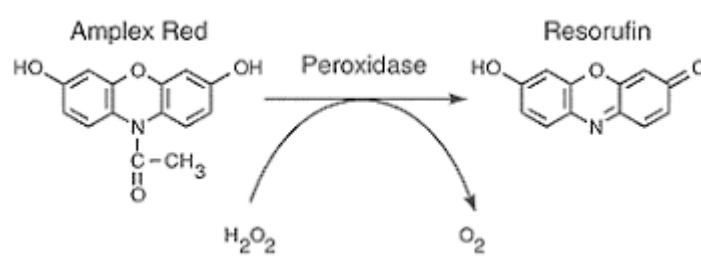


**Figure 33. Amplex<sup>®</sup> Red, a non-fluorescent substrate, produces a highly fluorescent product resorufin, in response to H<sub>2</sub>O<sub>2</sub> upon the oxidation by HRP (Debski *et al.*, 2016).**

Rat aortic vascular smooth muscle cells were plated at  $5 \times 10^4$  in a black-walled, clear-bottom 96-well plate and allowed to grow for 24-48 hours to reach confluence. The cells were treated with a reaction mixture containing 20mM Amplex<sup>®</sup> Red - a highly sensitive and stable probe for H<sub>2</sub>O<sub>2</sub> (200 $\mu$ l; Sigma Aldrich, UK), 200U/ml HRPO - an enzyme that catalyse the oxidation of Amplex<sup>®</sup> Red to resorufin (100 $\mu$ l; Sigma Aldrich, UK), 100mM benzylamine hydrochloride - substrate for SSAO (200 $\mu$ l; Sigma Aldrich, UK) and 0.5mM clorgyline - inhibitor of MAO-A & MAO-B (20 $\mu$ l; Sigma Aldrich, UK), supplemented with 0.25M sodium phosphate buffer at pH 7.4. 100 $\mu$ l of the reaction mixture was added to the first 80 wells; the cells in the last two columns were left without reaction mixture. The plate was incubated at 37<sup>o</sup>C and the fluorescence units (RFU) were read on a Clario Star<sup>®</sup> Microplate Reader (BMG Labtech), using excitation 540nm and emission 590nm. During the oxidative process SSAO first catalyse the conversion of benzylamine to benzaldehyde with consumption of O<sub>2</sub> and H<sub>2</sub>O, while also producing H<sub>2</sub>O<sub>2</sub> and NH<sub>4</sub>. In the presence of H<sub>2</sub>O<sub>2</sub>, Amplex<sup>®</sup> Red undergoes enzymatic oxidation catalysed by HRPO and is transformed into resorufin, a highly absorbing and fluorescing compound (Figure 34).

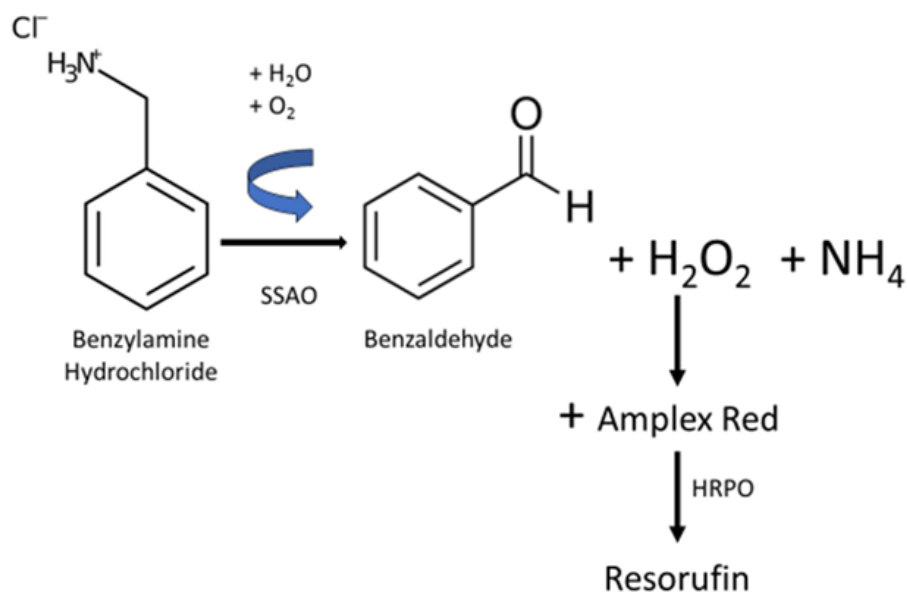


**Figure 34. Principle of the assay.**

### 2.2.13 Western blot analysis

Western blot analysis was performed as previously described (Mahmood & Yang, 2012) by using Bolt® 8% (1.0mm X 10well) Bis-Tris Plus Gels (Thermo Fisher Scientific) and the iBlot® 2 Gel Transfer Device with the iBlot® 2 Transfer Stacks. Bolt® MOPS SDS running buffer (20X) was used for proteins with high molecular weight and Bolt® MES SDS running buffer (20X) was used for proteins with low molecular weight. The amount of protein from frozen cell samples was calculated using the Bradford assay, as explained in the methods section 2.2.11. Cell samples were thawed, vortexed and kept on ice while preparing the loading mixture. The loading sample mixture was prepared with deionized water, Bolt® LDS sample buffer (4X), Bolt®/NuPAGE® reducing agent (10X) and cell sample protein ( $\mu\text{l}$ ). The loading sample mixture was then vortexed and heated on  $70^\circ\text{C}$  for 10 minutes. 1XSDS running buffer was prepared by adding 50ml of 20X Bolt® MES or MOPS SDS running buffer to 950ml of deionized water.

After preparing the sample loading mixture and the buffers, the gel (Bolt® 8% (1.0mm X 10well) Bis-Tris Plus) was prepared by removing the comb and rinsing it three times with 1X running buffer. The gel was then placed in Bolt® Mini Gel Tank and filled with 1X running buffer. The anode and cathode chambers of the tank were also filled with the appropriate 1X running buffer. The samples were then loaded in the following order: Precision Plus Protein® Standards kaleidoscope ladder ( $5\mu\text{l}$ ), samples ( $40\mu\text{l}$ ), Precision Plus Protein® Standards kaleidoscope ladder ( $10\mu\text{l}$ ).

The Bolt® Mini Gel Tank was filled to the top with more 1X running buffer and the gel was run for 45 minutes at 200V constant for MOPS, and 35 minutes at 200V constant for MES. The gel was then transferred to nitrocellulose (NC) membrane using the iBlot® 2 Gel Transfer Device. The membrane was cut in several places based on the protein of interest and was firstly incubated with 5% w/v milk powder, for one hour, at room temperature, on a shaker. The primary antibodies were then diluted with 5% w/v BSA, which was previously diluted in TBS washing solution (TRIS base, NaCl, 10% Tween® 20 and deionized water), at 4°C with gentle shaking, overnight. The next day the membrane blots with primary antibodies were washed (x3) with TBS and incubated with secondary antibodies diluted with 5% w/v milk powder and TBS, for one hour, at room temperature, on a shaker.  $\beta$ -actin was detected with every western blot analysis. The HRP conjugated  $\beta$ -actin antibody was diluted at 1:15000 in 5% w/v milk powder, 1XTBS, 10% Tween®20 and was placed at room temperature with gentle shaking, for one hour. In the last step, the membrane blot with  $\beta$ -actin as well as the membrane blots with the other antibodies were washed (x3) with TBS and observed on myECL imager (Thermo Fisher Scientific) after addition of Radiance Plus ECL reagents (Azure Biosystems).

#### **2.2.14 Protein quantification with Image J**

The image J software was applied to quantify protein bands from western blot analysis. Firstly, a single region of interest was defined for each protein band. To do that a frame was drawn around the largest band. The same frame was then used for all the protein bands within a row. "Ctr" + "1", "Ctr" + "2", and "Ctr" + "3", was used to record measurement for each band. The same frame used for the protein bands was also applied to take a background measurement. The data was then exported into an Excel spreadsheet and the pixel density was inverted for all data (protein bands and their background). The net value of a protein band was then obtained by deducting the inverted background from the inverted band value. Finally, a ratio was derived from the net band value over the net loading control, which was considered as a final relative quantification value.

## SECTION 2.3

### STATISTICS

The data was analysed with the statistical software GraphPad Prism 7. Results are presented as means  $\pm$  SEM and means  $\pm$  SD. A correlation analysis was performed to identify statistical difference between passage number and  $K_m$  values. For more than two groups, statistical analysis was performed by one or two-way ANOVA. One-way ANOVA was used to compare variance in a group means within a sample whilst considering only one independent factor. Two-way ANOVA was used to examine the effect of two factors on a dependent variable, while also examine whether the two factors affect each other to influence the continuous variable. Furthermore, Dunnett's multiple comparison test was applied to compare a set of treatments against a single control mean and Tukey's multiple comparison test was applied to compare differences between treatments (every mean with every other mean). Additionally, Sidak's multiple comparison test was applied for a set of means, to adjust significance level for multiple comparisons. The Michaelis - Menten model with quotation  $Y = V_{max} * X / (K_m + X)$  was applied to determine  $K_m$  and  $V_{max}$ . The competitive enzyme equation  $K_{mObs} = K_m * (1 + [I]/K_i)$   $Y = V_{max} * X / (K_{mObs} + X)$  was employed to investigate the effect of competitive inhibitors; and the non-competitive enzyme equation  $V_{maxinh} = V_{max} / (1 + I/K_i)$   $Y = V_{maxinh} * X / (K_m + X)$  was employed to study the effect of non-competitive inhibitors. Probability values  $< 0.05$  were considered as being statistically significant.

# CHAPTER III: RESULTS

## SECTION 3.1 DEVELOPMENT OF *IN VITRO* MODEL TO CHARACTERISE SSAO ACTIVITY IN RAT AORTIC VASCULAR SMOOTH MUSCLE CELLS

### 3.1.1 INTRODUCTION

SSAO is a multifunctional enzyme that exists in soluble, and membrane bound form. This contributes for its diverse function that varies depending on the tissue where it is expressed. Despite being found in almost all mammalian tissues this enzyme shows high activity in vascular endothelial and smooth muscle cells. The role of SSAO has been extensively investigated in various pathophysiological conditions. It has been reported that soluble SSAO activity is altered in conditions such as atherosclerosis, diabetes, inflammatory liver disease, obesity, and congestive heart failure (Gella *et al.*, 2013; Obata, 2006; Wang *et al.*, 2018). A well-established method to assess SSAO activity is the radiometric method which incorporates radioactivity to determine the amount of product made over time (Castlilio *et al.*, 1998). The advantage of this method is the high sensitivity in detecting low levels of enzymatic activity. However, it has innumerable disadvantages including the use of radioactive compounds, high cost, and unsuitability to be used in routine clinical practice (Peet *et al.*, 2011, Yraola *et al.*, 2006).

Recently, the fluorometric and luminometric methods are more commonly used, while some authors have also investigated SSAO activity through its protein expression (Salmi & Jalkanen, 2006). The fluorometric method allows continuous time-dependent following of the enzymatic reaction (Bisswanger, 2014). In a study by Gella *et al.* (2013) the radiometric and fluorometric method were compared in their efficiency to measure SSAO activity using plasma samples. Gella *et al.* (2013) have used radiolabelled benzylamine to measure SSAO activity radiochemically, and the Amplex<sup>®</sup> Red monoamine oxidase assay to measure SSAO activity fluorometrically. Gella *et al.* (2013) have demonstrated an excellent linear correlation between SSAO activity obtained in both methods and observed no significant difference between the two.

However, in comparison to radiometric methods the fluorometric approach is better choice to detect SSAO activity, mainly due to being equally effective as the radiometric method, less time-consuming and suitable to be used in routine clinical practice (Gella *et al.*, 2013; Bisswanger, 2014). The fluorometric Amplex<sup>®</sup> Red Monoamine Oxidase assay measures SSAO activity based on the detection of H<sub>2</sub>O<sub>2</sub> in a horseradish peroxidase coupled reaction using 10-acetyl-3,7-dihydroxyphenoxazine (Amplex<sup>®</sup> Red reagent), a highly sensitive and stable probe for H<sub>2</sub>O<sub>2</sub> (Zhao *et al.*, 2012). Advantages of the Amplex<sup>®</sup> Red reagent over other H<sub>2</sub>O<sub>2</sub> sensitive probes include its stability, the stability of the reaction product resorufin, and the long wave-length spectra of resorufin (Zhao *et al.*, 2012).

This assay has been demonstrated as being 20 times more sensitive to detect hydrogen peroxide than the spectrophotometric ferrous thiocyanate method (Mishin *et al.*, 2010). The Amplex<sup>®</sup> Red monoamine oxidase assay has been previously implemented to investigate SSAO activity in serum samples (Aalto *et al.*, 2010; Bisswanger, 2012), and tissue culture (Wang *et al.*, 2018; Jarnicki *et al.*, 2016; Peng *et al.*, 2016); however, has not been utilized to assess SSAO catalytic efficiency in cell culture. This assay uses benzylamine as model substrate to study SSAO activity. Benzylamine is the most appropriate substrate for measuring *in vitro* SSAO activity in rodents and humans (Kubota *et al.*, 2020). Hernandez *et al.* (2006) compared SSAO kinetic parameters in rat aortic A7r5 cells using different SSAO substrates, including benzylamine and methylamine, and demonstrated higher SSAO affinity for benzylamine with V<sub>max</sub> = 87 ± 5 nmol/min and K<sub>m</sub> = 0.8 ± 0.1 mM, comparing to methylamine V<sub>max</sub> = 7.32 ± 0.44 nmol/min and K<sub>m</sub> = 1.04 ± 0.28 mM.

The Amplex<sup>®</sup> Red monoamine oxidase assay also includes the use of clorgyline. This is because benzylamine is a common substrate for not only SSAO, but also MAO-A and MAO-B. Since clorgyline is MAO-A and MAO-B selective inhibitor, and SSAO is not sensitive to clorgyline, it has been included in this assay to confirm the identity of the enzyme responsible for the metabolism of benzylamine. Clorgyline is a mechanism-based inhibitor for MAO-A and B, with higher potency for MAO-A (clorgyline inhibited MAO-A by 95%, and MAO-B by 30%, as detected by Lamensdorf *et al.*, 1996). Clorgyline binds covalently to the flavin cofactor of the enzyme while it is in the enzyme-substrate complex (Fowler *et al.*, 2009); and has previously been used to inhibit MAO enzymes in assays detecting SSAO activity (Nemcsik *et al.*, 2007; Quelhas-Santos *et al.*, 2015).

Moreover, benzylamine can also act as substrate for LOX; however, since the Amplex<sup>®</sup> Red monoamine oxidase assay was optimised to detect SSAO activity in line with earlier references (Iglesias-Osma *et al.*, 2005; Peter *et al.*, 2006; Gella *et al.*, 2013; Foot *et al.*, 2013; Rcheulishvili *et al.*, 2021), in this study  $\beta$ APN (irreversible, mechanism-based inhibitor for LOX) was not added in the reaction mixture while measuring SSAO activity. Furthermore, since  $\beta$ APN can also act as weak inhibitor for SSAO (Table 3), it would impair the enzyme and therefore, the SSAO activity detected with this assay would not be a clear presentation of a total SSAO activity.

Overall, this section aims to investigate SSAO activity in cell culture by optimising the Amplex<sup>®</sup> Red monoamine oxidase assay. Objectives:

1. Identify an optimal signal to noise ratio (%), time (h), and substrate concentration (mM) for the measurement of SSAO catalytic activity in cell culture using primary VSMCs of a rat.
2. Observe changes in SSAO kinetic parameters ( $K_m$  and  $V_{max}$ ) as cells were being passaged from lower (3) to a higher (8) passage number.

### 3.1.2 METHODS

#### ***SSAO fluorometric enzyme activity in rat aortic VSMCs – gain optimisation***

SSAO activity was measured with the Amplex<sup>®</sup> Red Monoamine Oxidase assay, as described in the methods section 2.2.12. To optimise the gain for this assay, the 96-well plate containing cells with and without reaction mixture was first incubated for 24 hours at 37°C, and the fluorescence units (RFU) were read at different gain percentages (10%, 50% and 90%), using excitation 540nm and emission 590nm, on a Clario Star<sup>®</sup> Microplate Reader (BMG Labtech).

#### ***SSAO fluorometric enzyme activity in rat aortic VSMCs - time optimisation***

To optimise the assay for time continuous measurement of SSAO activity was performed over different time intervals. Samples were treated with reaction mixture as explained in the methods section 2.2.12. The RFU were read at different time intervals (0h, 0.5h, 1h, 2h, 4h, 6h, 8h, 24h), using excitation 540nm and emission 590nm, on a Clario Star<sup>®</sup> Microplate Reader (BMG Labtech). The data was transferred to an Excel spreadsheet and analysed before plotting fluorescence (RFU) against time (h).

The end-point fluorescence was measured with resorufin. 2mM of resorufin stock solution was diluted to a concentration of 1000 $\mu$ M (Table 7), in 1X reaction buffer [2ml of 5X reaction buffer (0.25 M sodium phosphate at pH 7.4), 10ml distilled water] to yield resorufin standards ranging from 0 to 20 $\mu$ M. 100 $\mu$ l of each resorufin standard was added in duplicate into individual empty wells of a 96-well microplate. The plate was incubated for 1 hour at 37<sup>0</sup>C prior to measuring fluorescence using excitation 540nm and emission 590nm, on a Clario Star<sup>®</sup> Microplate Reader (BMG Labtech). The data was transferred and analysed on Excel spreadsheet before preparing a standard curve of resorufin fluorescence (RFU) versus concentration ( $\mu$ M) (Figure 35).

To express SSAO activity in nmolH<sub>2</sub>O<sub>2</sub>/ml, the fluorescence readings from different time intervals were multiplied by the slope and added by the intercept (both calculated from the linear equation of the resorufin standard curve). To express SSAO activity in nmolH<sub>2</sub>O<sub>2</sub>/mg protein, the nmolH<sub>2</sub>O<sub>2</sub>/ml values were divided over the protein concentration (mg/ml) which was calculated with the BCA assay, as described in the methods section 2.2.10 (Figure 31).

**Table 7. Standards for resorufin**

| <b>No</b> | <b>Working stock<br/>100<math>\mu</math>M resorufin<br/>(<math>\mu</math>l)</b> | <b>1X reaction<br/>buffer (<math>\mu</math>l)</b> | <b>Concentration<br/>of resorufin<br/>(<math>\mu</math>M)</b> |
|-----------|---|---|---|
| <b>1</b>  | 0   | 1000  | 0 $\mu$ M   |
| <b>2</b>  | 2   | 998   | 2 $\mu$ M   |
| <b>3</b>  | 5   | 995   | 5 $\mu$ M   |
| <b>4</b>  | 10  | 990   | 10 $\mu$ M  |
| <b>5</b>  | 15  | 985   | 15 $\mu$ M  |
| <b>6</b>  | 20  | 980   | 20 $\mu$ M  |
|           |   |   |   |

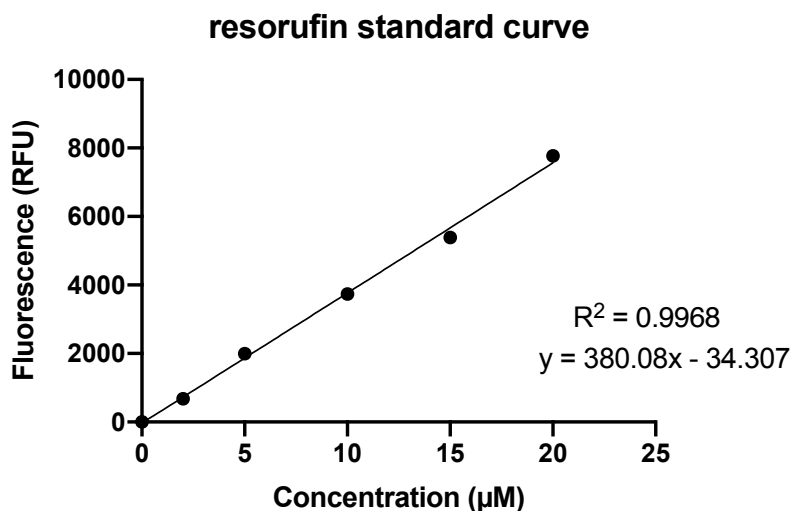


**Figure 35. A linear regression of resorufin standard curve. The plate was incubated for 1 hour at 37°C prior to measuring fluorescence using excitation 540 nm and emission 590 nm, on a Clario Star<sup>®</sup> Microplate Reader (BMG Labtech).**

### ***SSAO fluorometric enzyme activity in rat aortic VSMCs - substrate optimisation***

To optimise the assay for substrate concentration, at initial comparison cells at passage 3 to 8 and confluency of ~80-90% were treated with reaction mixture containing 20mM Amplex<sup>®</sup> Red (20µl), 200U/ml HRPO (10µl) and 0.5mM clorgyline (10µl), supplemented with 0.25M sodium phosphate buffer at pH 7.4. Several reaction mixtures were prepared using different benzylamine hydrochloride concentrations (0, 0.5, 2, 10, & 20mM), and the fluorescence was measured at 0h, 0.5h, 1h, 2h, 4h and 6h using excitation 540nm and emission 590nm, on a Clario Star<sup>®</sup> Microplate Reader (BMG Labtech). The same was repeated (n = 5) with smaller benzylamine concentrations (0, 0.02, 0.05, 0.1, 0.5, 1 & 5mM). The data for each substrate concentration (mM) was transferred to an Excel spreadsheet and analysed as explained in the methods section 3.1.2, before plotting SSAO activity (nmolH<sub>2</sub>O<sub>2</sub>/h/mg protein) against time (h). The reaction velocity (V) expressed as (nmolH<sub>2</sub>O<sub>2</sub>/h) was derived from the slope of the linear part of the progress curve from the SSAO activity (nmolH<sub>2</sub>O<sub>2</sub>/h/mg protein) vs time graph for each substrate concentration (Figure 86, Appendix 1). SSAO's affinity (Km) and Vmax were determined with GraphPad Prism 7 by plotting reaction velocity (nmolH<sub>2</sub>O<sub>2</sub>/h) versus substrate concentration, using the non-linear regression model of Michaelis-Menten  $Y = \frac{V_{max} * X}{(K_m + X)}$ .

### 3.1.3 RESULTS

#### **SSAO fluorometric enzyme activity in rat aortic VSMCs – gain optimisation**

To detect SSAO fluorometric activity within 24h VSMCs were treated with reaction mixture, as explained in the methods section 2.2.12. Cells without reaction mixture were used as control. Figure 36 is a presentation of a 24h SSAO fluorescence measurements in rat aortic VSMCs with three different gain percentages (10, 50 and 90%). Figure 36 demonstrates significant SSAO fluorescence activity (RFU) detected in rat aortic VSMCs over 24h (\*\*\*\* $p < 0.0001$  compared to control group) and excellent signal to noise ratio in all gain levels. There was no statistical difference in fluorescent activity detected between different gains. Therefore, 10% was selected as an optimal gain to be used in future experiments.

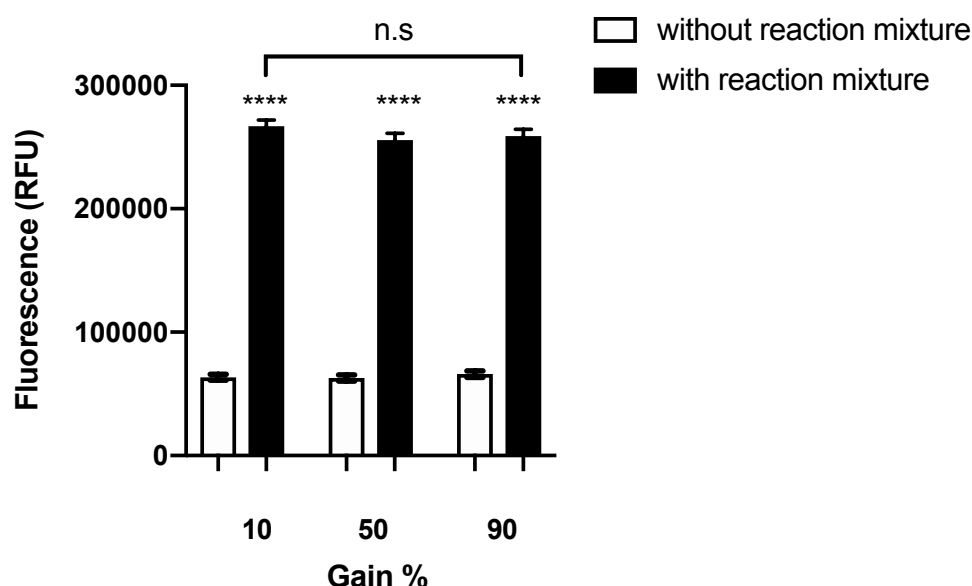


**Figure 36. 24h SSAO fluorescence measurements with three different gain percentages (10%, 50%, 90%), in cells without reaction mixture (open bars) and cells with reaction mixture (solid bars). Reaction mixture was prepared with 0.25M sodium phosphate buffer (pH7.4), containing Amplex<sup>®</sup> Red (200 $\mu$ l; Sigma Aldrich, UK), horseradish peroxidase (100 $\mu$ l; Sigma Aldrich, UK), benzylamine (200 $\mu$ l; Sigma Aldrich, UK) and clorgyline (10 $\mu$ l; Sigma Aldrich, UK). The data was analysed by two-way ANOVA (\*\*\*\* $p < 0.0001$ ) followed by Dunnett's multiple comparison test. Significant difference in fluorescent activity (RFU) was detected between control and treated cells in all three gain levels (\*\*\*\* $p < 0.0001$  for cells without reaction mixture vs cells with reaction mixture at gain 10, 50 and 90%). There was no statistical difference in fluorescent activity (RFU) detected between 10, 50 and 90% gain ( $p > 0.05$ ). The data was presented as means  $\pm$  S.E.M. of three independent experiments with five replicates in each. The asterisk (\*) indicates statistical significance compared to controls at each gain percentage.**

### SSAO fluorometric enzyme activity in rat aortic VSMCs - time optimisation

To identify an optimal time for SSAO measurement in rat aortic VSMCs, continuous measurements of SSAO activity were performed over different time intervals, as described in the methods section 3.1.2. Figure 37 demonstrates a linear progress curve of the SSAO activity observed from 0 to 8 h which increases over time. Figure 38 demonstrates a linear progress curve (0 to 12h) followed by a non-linear later progression (12 to 24h) of the SSAO activity observed from 0 to 24h. 6 hours after addition of reaction mixture was established as an optimal time to measure SSAO enzymatic activity in rat aortic VSMCs. The enzymatic SSAO activity expressed as nmol of the product  $\text{H}_2\text{O}_2$  formed per hour, per mg protein (nmol  $\text{H}_2\text{O}_2$ /h/mg protein) was consistent with previous studies (Aalto *et al.*, 2012; Mercier, 2009; Mathys *et al.*, 2002).

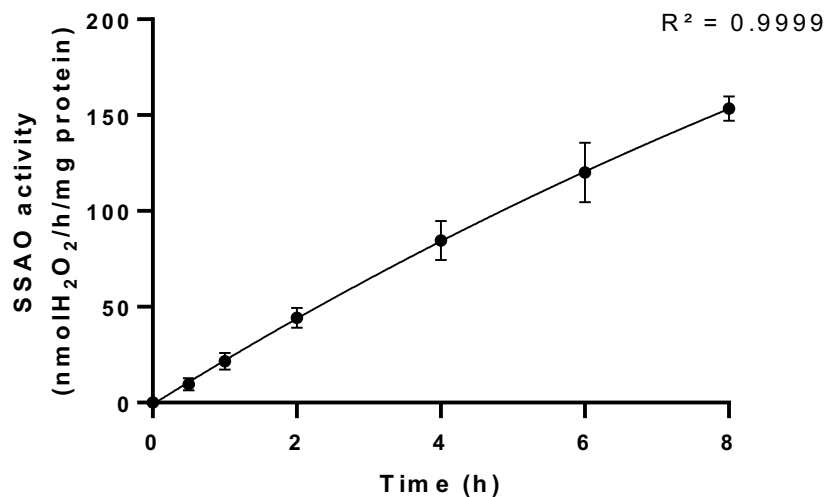


**Figure 37. SSAO activity (nmol  $\text{H}_2\text{O}_2$ /h/mg protein) over different time intervals (0h, 0.5h, 1h, 2h, 4h, 6h, 8h) in rat aortic VSMCs. Fluorescence readings were taken with a fluorescence microplate reader using excitation 540nm and emission 590nm, on a Clario Star<sup>®</sup> Microplate Reader (BMG Labtech). The plate was kept at 37<sup>o</sup>C between time measurements. The data is presented as means  $\pm$  S.E.M. of three independent experiments with five replicates in each.**

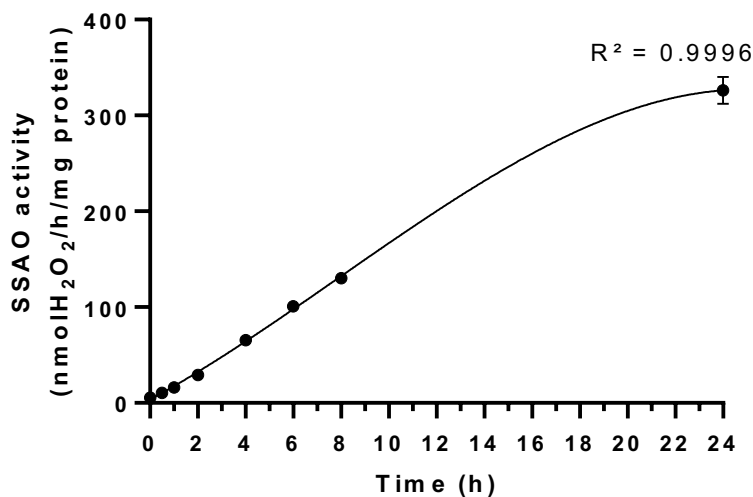


**Figure 38. SSAO activity (nmol H<sub>2</sub>O<sub>2</sub>/h/mg protein) over different time intervals (0h, 0.5h, 1h, 2h, 4h, 6h, 8h, 24h) in rat aortic SMCs. Fluorescence readings were taken with a fluorescence microplate reader using excitation 540nm and emission 590nm, on a Clario Star<sup>®</sup> Microplate Reader (BMG Labtech). The plate was kept at 37<sup>0</sup>C between time measurements. The data is presented as means  $\pm$  SD of three independent experiments with five replicates in each.**

### ***SSAO fluorometric enzyme activity in rat aortic VSMCs - substrate optimisation***

To optimise the assay for substrate concentration, at initial comparison samples were treated with different benzylamine hydrochloride concentrations (0, 0.5, 2, 10, & 20mM) and the fluorescence was measured at different time intervals, as explained in the methods section 3.1.2. Figure 39 demonstrates the highest activity (V<sub>max</sub>) of SSAO and its affinity (K<sub>m</sub>) for the substrate benzylamine in rat aortic VSMCs from passage 3 to 8, determined with Michaelis-Menten.

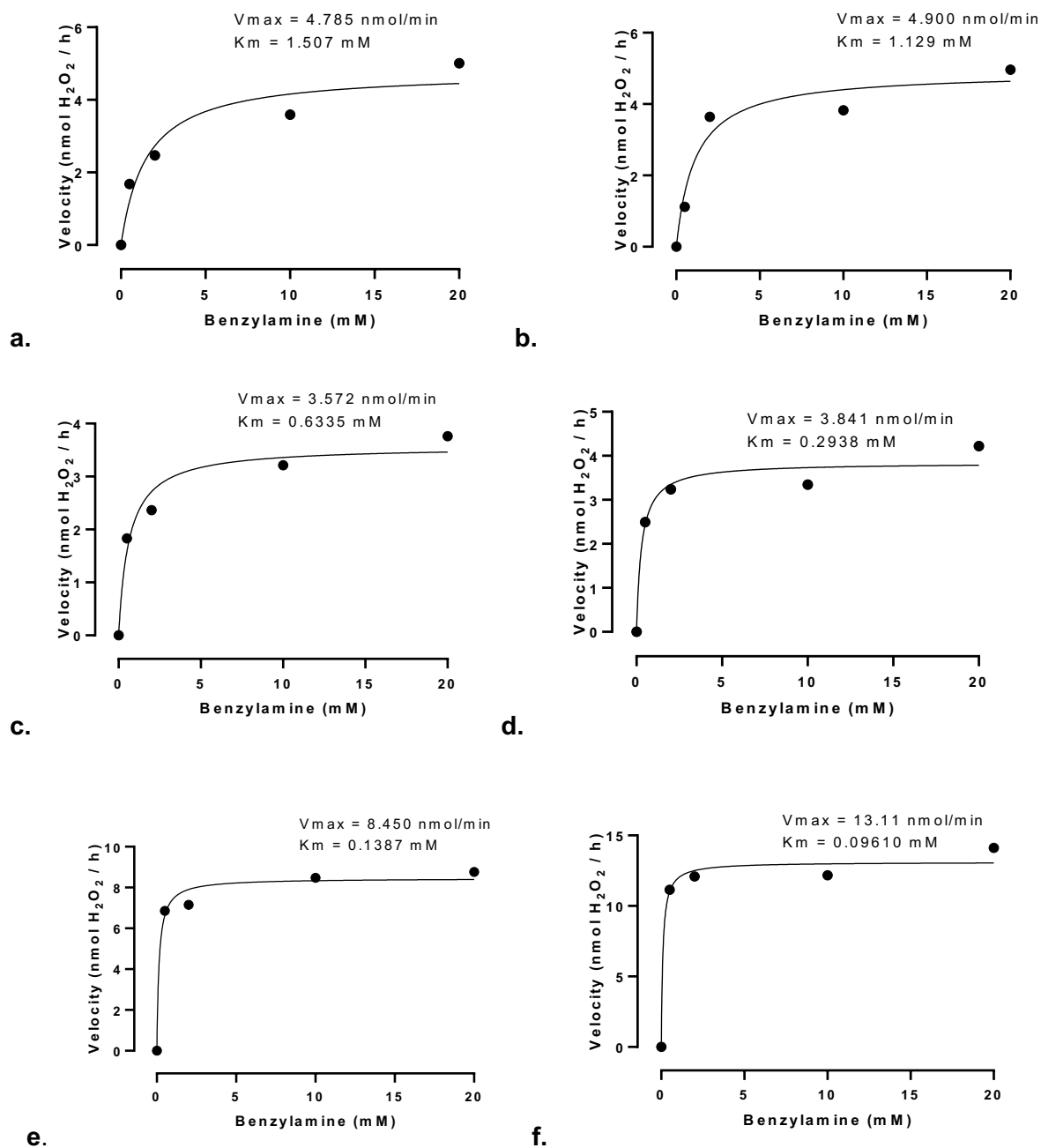


**Figure 39.** The highest activity ( $V_{\text{max}}$ ) of SSAO and its affinity ( $K_m$ ) for the substrate benzylamine (0, 0.5, 2, 10, and 20mM) in rat aortic VSMCs. The data was analyzed with the non-linear regression model of Michaelis-Menten  $Y = V_{\text{max}} \cdot X / (K_m + X)$  ( $n = 1$ ). Passage 3 (a), passage 4 (b), passage 5 (c), passage 6 (d), passage 7 (e), passage 8 (f).

Subsequently, samples were treated with smaller substrate concentrations (0, 0.02, 0.05, 0.1, 0.5, 1, 5mM) and the fluorescence was measured at different time intervals (0h, 0.5h, 1h, 2h, 4h, 6h), as explained in the methods section 3.1.2. Figure 40 demonstrates the highest activity ( $V_{\text{max}}$ ) of SSAO and its affinity ( $K_m$ ) for the substrate benzylamine in rat aortic VSMCs from passage 3 to 8, determined with Michaelis-Menten.

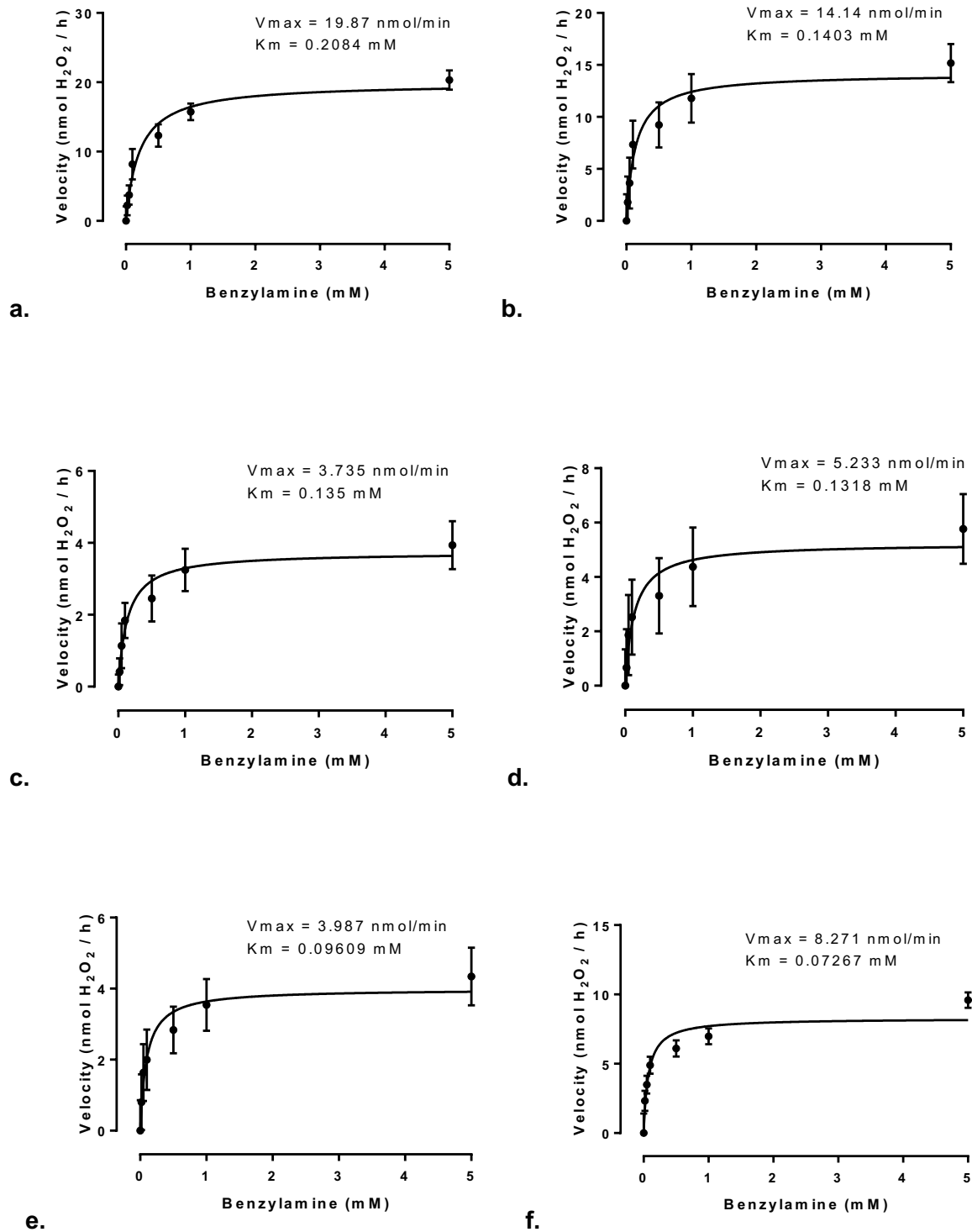


**Figure 40.** The highest activity ( $V_{\text{max}}$ ) of SSAO and its affinity ( $K_m$ ) for the substrate benzylamine (0, 0.02, 0.05, 0.1, 0.5, 1, and 5mM) in rat aortic VSMCs. Passage 3 (a), passage 4 (b), passage 5 (c), passage 6 (d), passage 7 (e), passage 8 (f). The data was analyzed with the non-linear regression model of Michaelis-Menten  $Y = V_{\text{max}} \cdot X / (K_m + X)$  and is presented as means  $\pm$  S.E.M. of five independent experiments with five replicates in each.

### 3.1.4 DISCUSSION

SSAO activity was measured with a continuous and highly sensitive hydrogen peroxide assay based on Amplex<sup>®</sup> Red oxidation. The Amplex<sup>®</sup> Red in this assay was used as a probe for the measurement of extracellular H<sub>2</sub>O<sub>2</sub>, but because H<sub>2</sub>O<sub>2</sub> is freely diffusible, this measurement was taken as indication of intracellular H<sub>2</sub>O<sub>2</sub> production (Zhao *et al.*, 2012). The chemical reaction between Amplex<sup>®</sup> Red and H<sub>2</sub>O<sub>2</sub> was catalysed by HRP at which Amplex<sup>®</sup> Red reacts with H<sub>2</sub>O<sub>2</sub> at 1:1 ratio to form a coloured and highly fluorescent compound resorufin, as explained in the methods section 2.2.10.

The Amplex<sup>®</sup> Red monoamine oxidase assay was optimised for gain, time, and substrate concentration. Significant fluorescence activity (RFU) was detected in rat aortic VSMCs over 24h (\*\*\*\*p < 0.0001 compared to control group), and an excellent signal to noise ratio was demonstrated in all gain levels (Figure 36). Moreover, no statistical difference in fluorescence activity was detected between all three gain levels (10, 50, and 90%); therefore, 10% gain was selected as an optimal gain to be taken in future experiments. During time optimisation SSAO activity was measured continuously over different time intervals; this allowed continuous time-dependent following of the enzymatic reaction. The linear increase of the reaction over time observed in the first set of experiments (Figure 37) showed significant, but incomplete progression.

The second set of experiments resulted with linear increase over time, followed by non-linear progression of the reaction course observed at later time (Figure 38). The latter non-linear progression observed in Figure 38 suggests that the reaction was becoming saturated at this point at which most SSAO molecules have become engaged with substrate, meaning less SSAO molecules were available for further substrate binding. The data from Figure 37 and 38 demonstrates peak in SSAO activity at 6h from addition of reaction mixture. The detected SSAO activity (nmolH<sub>2</sub>O<sub>2</sub> /h) at 6h was comparable with previous *in vitro* studies (Aalto *et al.*, 2012; Mercier, 2009; Mathys *et al.*, 2002).

While optimising the substrate concentration changes in SSAO kinetic parameters (K<sub>m</sub> and V<sub>max</sub>) were observed with each cell passage. The findings from the preliminary study showed lower K<sub>m</sub> values with each cell passage, suggesting higher enzyme-substrate affinity in cells at a greater passage number (Figure 39). These findings also conveyed an increase in the rate at which SSAO converts the substrate to product (V<sub>max</sub>) as the cells age with passage (Figure 39).

Novel findings like this have not been previously reported in the literature. El Hadri *et al.* (2002) have examined SSAO activity during differentiation of rat aortic VSMCs and demonstrated a differentiation dependent emergence of SSAO activity; however, have not compared SSAO kinetic parameters with each cell passage. A passage dependent increase in SSAO affinity for its substrate benzylamine (\*\*p < 0.01) was also observed with the smaller substrate concentrations (Figure 40), as shown by a 3-fold reduction in the Km as passage increased from 3 (Km = 0.2084) to 8 (Km = 0.07267).

However, the data for Vmax did not correlate with the preliminary findings (Figure 39 & 40). As per Figure 40, Vmax did not simultaneously increase with the Km values. This is because substrate binding and catalysis are two different and sequential steps in enzymatic reaction (Bisswanger, 2014). Km is (inversely) related to substrate binding to the enzyme, and Vmax is (directly) related to the catalytic power of the enzyme in converting the substrate to products. Therefore, the enzyme has both a substrate binding site, and a substrate catalytic site, each composed of specific amino acids in the enzyme active site (Bisswanger, 2014). Some amino acid residues may be common to both, binding and catalytic sites, while some may be exclusive to either site (Bisswanger, 2014).

The increase in SSAO affinity shown in Figure 39 & 40 suggests that in rat aortic cell culture model there is an efficient binding of SSAO with its substrate benzylamine, which increases in cells at a greater passage number. This suggests that in rat aortic VSMCs at a higher passage number the production of H<sub>2</sub>O<sub>2</sub>, aldehyde, and ammonia happens at a greater rate because of SSAO catalysed reaction. Being identified as a source of oxidative stress in the vasculature, when produced at a fast speed, H<sub>2</sub>O<sub>2</sub> would generate countless reactive oxygen species that could engulf LDL and form foam cells. In their recent paper Wang *et al.* (2018) suggested that when produced at high concentrations H<sub>2</sub>O<sub>2</sub> (≥100nM) could exhibit cytotoxic effect to vascular cells, induce expression of inflammatory cytokines and contribute to increased migration and proliferation of the VSMCs from the medial to the intimal layer of the arteries.

Furthermore, the preliminary as well as subsequent findings pointed towards consistency in the optimal concentration of the substrate benzylamine. As observed in Figure 39, the higher concentrations (2, 10 & 20mM) of the substrate brought the reaction close to saturation point, indicating that at these concentrations the reaction starts slowing down and finally ceases. As per Figure 40 this effect was observed with substrate concentrations 1 & 5mM. Benzylamine with concentration 0.5mM showed an increase in the rate of reaction and efficient occupation of the enzyme binding sites without causing saturation, in the preliminary and subsequent findings (Figure 39 & 40). It was therefore taken as an optimal substrate concentration to be implemented in the upcoming set of experiments. These findings were similar with previous studies which have demonstrated an optimal benzylamine concentration of 1mM (Morin *et al.*, 2001; Ochiai *et al.*, 2006; Zhexuan *et al.*, 2011). The advantage of this model, however, is that it was able to establish smaller benzylamine concentration as an optimal concentration comparing to previous studies.

### **3.1.5 CONCLUSION**

The data generated thus far has established an *in vitro* cell culture model that can effectively measure SSAO activity in rat aortic VSMCs. This provides good comparison with previous tissue culture models (Wang *et al.*, 2018; Jarnicki *et al.*, 2016). The data obtained here demonstrates higher enzyme-substrate affinity in cells with a greater passage number comparing to early passage cells (\*\*p < 0.01). Thus, the model characterised here is a promising vehicle for assessing SSAO activity in rat aortic VSMCs and can be used as an appropriate method to investigate the role of SSAO and LOX in cardiovascular pathology, which has previously relied upon less standardised, animal tissue models.

## SECTION 3.2 FURTHER EVALUATION OF THE MODEL USING REVERSIBLE AND IRREVERSIBLE SSAO INHIBITORS AND METHYLAMINE AND AMINOACETONE AS SUBSTRATES

### 3.2.1 INTRODUCTION

After successful optimisation of the model, the same was applied further to characterise SSAO inhibition with reversible and irreversible inhibitors and investigate SSAO kinetics in the presence of methylamine and aminoacetone as substrates. However, prior to validating the model further a set of cytotoxicity studies were performed to identify safe inhibitor and optimal substrate concentrations. As mentioned earlier, the small molecule inhibitors are the most studied group of SSAO inhibitors (Pannecoeck *et al.*, 2015). Therefore, before characterising SSAO inhibition with the competitive hydrazine-based inhibitors semicarbazide and methylhydrazine, potential cytotoxic effects of these inhibitors were investigated on rat aortic VSMCs. In doing that rat aortic VSMCs viability was observed after 1h incubation with semicarbazide (0.1, 1, & 10mM) and methylhydrazine (1, 10, & 100nM). A study by Fernandez de Arriba *et al.* (1996) demonstrated almost 90% SSAO inhibition in bovine lung tissue homogenate and no cytotoxic effect after 30min incubation with hydrazine based SSAO inhibitors. Furthermore, these inhibitors have been previously shown as selective SSAO inhibitors *in vitro* and *ex vivo* (Holt & Callingham, 1994; Floris & Mondovi, 2009) and are known to inactivate SSAO by forming hydrazones with TPQ (Agostinelli *et al.*, 2006). Moreover, millimolar concentrations of semicarbazide and nanomolar concentrations of methylhydrazine have shown potency in inhibiting SSAO in a dose dependent manner (Holt & Callingham, 1994; O'Rourke *et al.*, 2007; O'Rourke *et al.*, 2008; Floris & Mondovi, 2009).

SSAO inhibition was also characterised with the propenyl amine-based inhibitor, N1, N4-bis(2,3-butadienyl)-1,4-butanediamine (MDL 72527). This inhibitor has been designed in 1985 as a selective irreversible inhibitor of polyamine oxidases (PO) (Bey *et al.*, 1985). It has been shown to inactivate SSAO at micromolar concentrations and time-dependently in *in vitro* studies involving cells and tissues (Seiler *et al.*, 2000; Duranton *et al.*, 2002; Agostinelli *et al.*, 2006) and *in vivo* with dose of 50mg/kg in rodents (Duranton *et al.*, 2002). Therefore, before applying it to characterise SSAO inhibition in rat aortic VSMCs, cell viability was first determined after 1h incubation with 10, 50 & 100µM MDL72527. This inhibitor has previously been reported effective and non-toxic to cells after 1h incubation (Quemener *et al.*, 1992).

Being known as a suicide inhibitor, MDL 72527 irreversibly inactivates SSAO by forming an unstable adduct with TPQ. Due to being unstable the adduct would lead to regeneration of TPQ, while MDL72527 remains bound to SSAO by covalent bond (Agostinelli *et al.*, 2006).

Before continuing with the second set of model validation experiments to study the level of interaction between SSAO and the model amines, rat aortic VSMCs viability was observed once again after 24h treatment with methylamine and aminoacetone. It has previously been reported that after being deaminated to methylglyoxal and formaldehyde because of SSAO catalysed reaction, aminoacetone and methylamine can exert cytotoxic effect in homogenates of various guinea pig tissues (Pizzimenti *et al.*, 2013), human umbilical artery (Deng & Yu, 1999), and plasma samples (Thornalley, 1996).

To investigate this effect in rat aortic VSMCs, fully confluent cells were treated for 24h with different concentrations of methylamine and aminoacetone before assessing cellular viability. A combination of an amine and MDL72527 with concentration 100 $\mu$ M (previously established effective to irreversibly inhibit SSAO) was also added to the cells to confirm whether cell toxicity was mediated through SSAO catalyzed reaction that has led to production of methylglyoxal and formaldehyde because of amine deamination. The cell viability assay was further utilized to investigate a direct cytotoxicity of methylglyoxal and formaldehyde on rat aortic VSMCs. The toxicity of these aldehydes has been widely implicated in age related diseases, including cardiovascular pathologies (Uchida *et al.*, 2000; Maynard *et al.*, 2015; Yang *et al.*, 2018). Unlike free radicals, aldehydes are more stable with half-life ranging from minutes to hours (Dator *et al.*, 2019).

This high stability could enable methylglyoxal and formaldehyde to diffuse easily and attack intracellular targets distant from the point of origin, consequently leading to cytotoxicity. It has previously been highlighted that the deamination reaction catalysed by SSAO produces equal molar concentrations of cytotoxic aldehyde and H<sub>2</sub>O<sub>2</sub> (Lin *et al.*, 2005). Lin *et al.* (2005) have further suggested that SSAO mediated products (aldehydes and H<sub>2</sub>O<sub>2</sub>) act in synergism in inducing cell damage and death. Therefore, while investigating a direct cytotoxic effect from methylglyoxal and formaldehyde, rat aortic VSMCs were also exposed to equal molar concentrations of an aldehyde and H<sub>2</sub>O<sub>2</sub> to identify potential synergistic mechanism between SSAO derived products in inducing cell death.

Overall, this section aims to evaluate the effectiveness of the model optimised in section 3.1, investigate toxicological consequence of SSAO catalytic activity in rat aortic VSMCs and identify potential synergism between SSAO derived products in inducing cell death. Objectives:

1. Apply the Amplex<sup>®</sup> Red monoamine oxidase assay optimised in section 3.1 to study SSAO inhibition with reversible competitive inhibitors semicarbazide and methylhydrazine, and the irreversible, mechanism-based inhibitor MDL72527.
2. Apply the Amplex<sup>®</sup> Red monoamine oxidase assay to compare SSAO kinetic parameters in the presence of aminoacetone and methylamine as substrates.
3. Perform cytotoxicity assay to observe changes in VSMCs viability after 24h treatment with aminoacetone and methylamine, in the presence and absence of MDL72527.
4. Perform cytotoxicity assay to observe changes in VSMCs viability after 24h direct exposure to formaldehyde and methylglyoxal alone, and in combination with hydrogen peroxide.

### 3.2.2 METHODS

#### *Cell viability*

Cell viability was determined with the MTT (3-(4,5-dimethylthiazol-2-yl)-2,5-diphenyltetrazolium bromide) tetrazolium reduction assay, as previously described (Riss *et al.*, 2016). Colour formation in this assay serves as a useful marker for viable cells. The principle is that the tetrazolium salt is metabolised into insoluble purple formazan by active mitochondrial enzyme. The cellular mechanism of MTT reduction into formazan involves reaction with NADPH that transfers electrons to MTT (Figure 41).

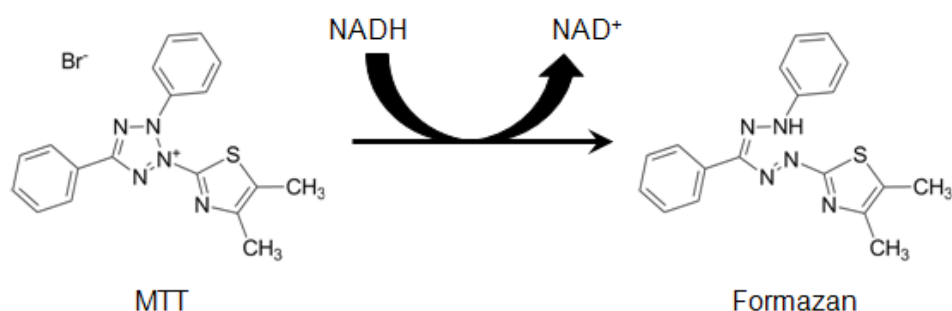


**Figure 41. Structure of MTT and coloured product formazan (Riss *et al.*, 2016).**

Firstly, rat aortic VSMCs were plated at  $5 \times 10^4$  in a 96-well plate and allowed to grow for 24-48 hours to reach confluence. After reaching confluence cells were incubated with serum free DMEM and semicarbazide (0.1, 1 & 10mM), or serum free DMEM and methylhydrazine (1, 10 & 100nM), or serum free DMEM and MDL72527 (10, 50 & 100 $\mu$ M), for 1h in a CO<sub>2</sub> incubator (5% CO<sub>2</sub> and 95% humidified air) at 37°C. After 1h the old media was removed, and cells were washed with 1XPBS. MTT substrate was prepared with serum free medium at final concentration 5mg/ml. 20 $\mu$ l of MTT solution + 180 $\mu$ l of serum free media was added to each well and the plate was incubated for 4h in a CO<sub>2</sub> incubator (5% CO<sub>2</sub> and 95% humidified air) at 37°C.

After incubation the media containing MTT was carefully removed and the formazan crystals were dissolved by adding 200 $\mu$ l isopropanol. The plate was then wrapped in a foil and placed on a shaker for 15 minutes. The quantity of formazan directly proportional to the number of viable cells was measured by recording changes in absorbance at 570nm, using a spectrophotometric Clario Star<sup>®</sup> Microplate Reader (BMG Labtech). The same was repeated after 24h cell incubation with serum free DMEM and aminoacetone (AA 5, 10, 50, 100 $\mu$ M), or serum free DMEM, AA and MDL72527 (100 $\mu$ M). Additionally, different cells were incubated with serum free DMEM and methylamine (M 50, 100, 500, 1000 $\mu$ M), or serum free DMEM, M and MDL72527 (100 $\mu$ M) for 24h.

After 24h the old media was removed, and cells were washed with 1XPBS before applying MTT solution prepared by dissolving MTT in serum free DMEM at final concentration 5mg/ml. MTT assay was also utilized to determine cell viability after addition of methylglyoxal and methylglyoxal + H<sub>2</sub>O<sub>2</sub>, as well as formaldehyde and formaldehyde + H<sub>2</sub>O<sub>2</sub>. Confluent cells were incubated with serum free DMEM and 50 $\mu$ M methylglyoxal, or 50 $\mu$ M H<sub>2</sub>O<sub>2</sub>, or 50 $\mu$ M M + H<sub>2</sub>O<sub>2</sub> for 24h. In the case of formaldehyde, confluent cells were incubated with serum free DMEM and 1000 $\mu$ M formaldehyde, or 1000 $\mu$ M H<sub>2</sub>O<sub>2</sub>, or 1000 $\mu$ M F + H<sub>2</sub>O<sub>2</sub> for 24h, before performing the MTT assay. Changes in absorbance were recorded at 570nm, using a spectrophotometric Clario Star<sup>®</sup> Microplate Reader (BMG Labtech).

### **SSAO inhibition with semicarbazide, methylhydrazine and MDL72527**

SSAO inhibition was characterised with the Amplex<sup>®</sup> Red assay using semicarbazide, methylhydrazine and MDL72527 as inhibitors. Cells were plated at  $5 \times 10^4$  in a black-walled, clear-bottom 96-well plate, and allowed to grow for 24-48 hours to reach confluence. A preliminary set of experiments was conducted first to establish the optimal inhibition time for each inhibitor. Cell samples were incubated for 5, 15 and 30 minutes at 37°C with semicarbazide (0.1, 1 & 10mM), methylhydrazine (1, 10 & 100nM), and MDL72527 (10, 50 & 100µM), prior to adding a reaction mixture containing different benzylamine concentrations (0, 0.02, 0.05, 0.1, 0.5, 1mM), 260µl of 0.25M sodium phosphate buffer (pH 7.4), 20µl Amplex<sup>®</sup> Red (20mM), 10µl horseradish peroxidase (200U/ml), and 10µl clorgyline (0.5mM). The inhibition time for each inhibitor was optimised by comparing the inhibition constant (K<sub>i</sub>) values derived by GraphPad Prism 7, which were obtained by measuring substrate-velocity curves in the presence of different inhibitor concentrations. After identifying an optimal inhibition time for each inhibitor, in the following set of experiments cell samples were incubated for 15 minutes at 37°C with semicarbazide (0.1, 1 & 10mM), methylhydrazine (1, 10 & 100nM), and MDL72527 (10, 50 & 100µM), prior to addition of reaction mixture containing different benzylamine concentrations (0, 0.02, 0.05, 0.1, 0.5, 1mM), 260µl of 0.25M sodium phosphate buffer (pH 7.4), 20µl Amplex<sup>®</sup> Red (20mM), 10µl horseradish peroxidase (200U/ml) and 10µl clorgyline (0.5mM). The reaction velocity (nmol H<sub>2</sub>O<sub>2</sub>/h) was derived from the slope of the linear part of the progress curve from the SSAO activity (nmolH<sub>2</sub>O<sub>2</sub>/h/mg protein) vs time graph for each substrate concentration (mM), in the presence of inhibitor. The inhibition constant (K<sub>i</sub>) for each inhibitor was obtained by plotting the reaction velocity (nmolH<sub>2</sub>O<sub>2</sub>/h) values measured at different inhibitor concentrations versus substrate concentration (0, 0.02, 0.05, 0.1, 0.5 & 1mM). For semicarbazide and methylhydrazine, the data was analysed with GraphPad Prism 7 using the competitive enzyme inhibition equation:  $K_{mObs} = K_m \cdot (1 + [I]/K_i)$   $Y = V_{max} \cdot X / (K_{mObs} + X)$ . For MDL72527, the data was analysed with GraphPad Prism 7 using the non-competitive enzyme equation:  $V_{maxinh} = V_{max} / (1 + I/K_i)$   $Y = V_{maxinh} \cdot X / (K_m + X)$ .

### **SSAO kinetics with methylamine and aminoacetone as substrates**

After establishing non-toxic amine concentrations, SSAO kinetic parameters in the presence of methylamine and aminoacetone were compared using the model optimised in section 3.1. Rat aortic VSMCs with confluency of ~80-90% were treated with reaction mixture (20µl Amplex<sup>®</sup> Red, 10µl HRPO, supplemented with 0.25M sodium phosphate buffer at pH 7.4) and methylamine as substrate, with concentrations 0, 0.02, 0.05, 0.1, 0.5, 0.7, & 0.9 mM; or aminoacetone as substrate with concentrations 0, 2, 5, 10, 20, 35 & 45µM.

0.5mM clorgyline was also added to the reaction mixture to maintain consistency. The data for each substrate concentration was transferred to an Excel spreadsheet and analysed before plotting SSAO activity (nmolH<sub>2</sub>O<sub>2</sub>/h/mg protein) against time (h). The reaction velocity (V) expressed as (nmolH<sub>2</sub>O<sub>2</sub>/h) was derived from the slope of the linear part of the progress curve from the SSAO activity (nmolH<sub>2</sub>O<sub>2</sub>/h/mg protein) vs time graph for each substrate concentration. SSAO's affinity (K<sub>m</sub>) and V<sub>max</sub> were determined by plotting reaction velocity (nmolH<sub>2</sub>O<sub>2</sub>/h) versus substrate concentration using the non-linear regression model of Michaelis-Menten  $Y = V_{max} * X / (K_m + X)$ .

### 3.2.3 RESULTS

#### ***Cell viability after addition of semicarbazide, methylhydrazine, and MDL72527***

Cell viability was assessed after addition of semicarbazide (0.1, 1 & 10mM), methylhydrazine (1, 10 & 100nM), and MDL72527 (10, 50 & 100μM), as explained in the methods section 3.2.2. Figure 42 demonstrates measured cell viability (%) after 1h treatment with semicarbazide (A), methylhydrazine (B), and MDL72527 (C).

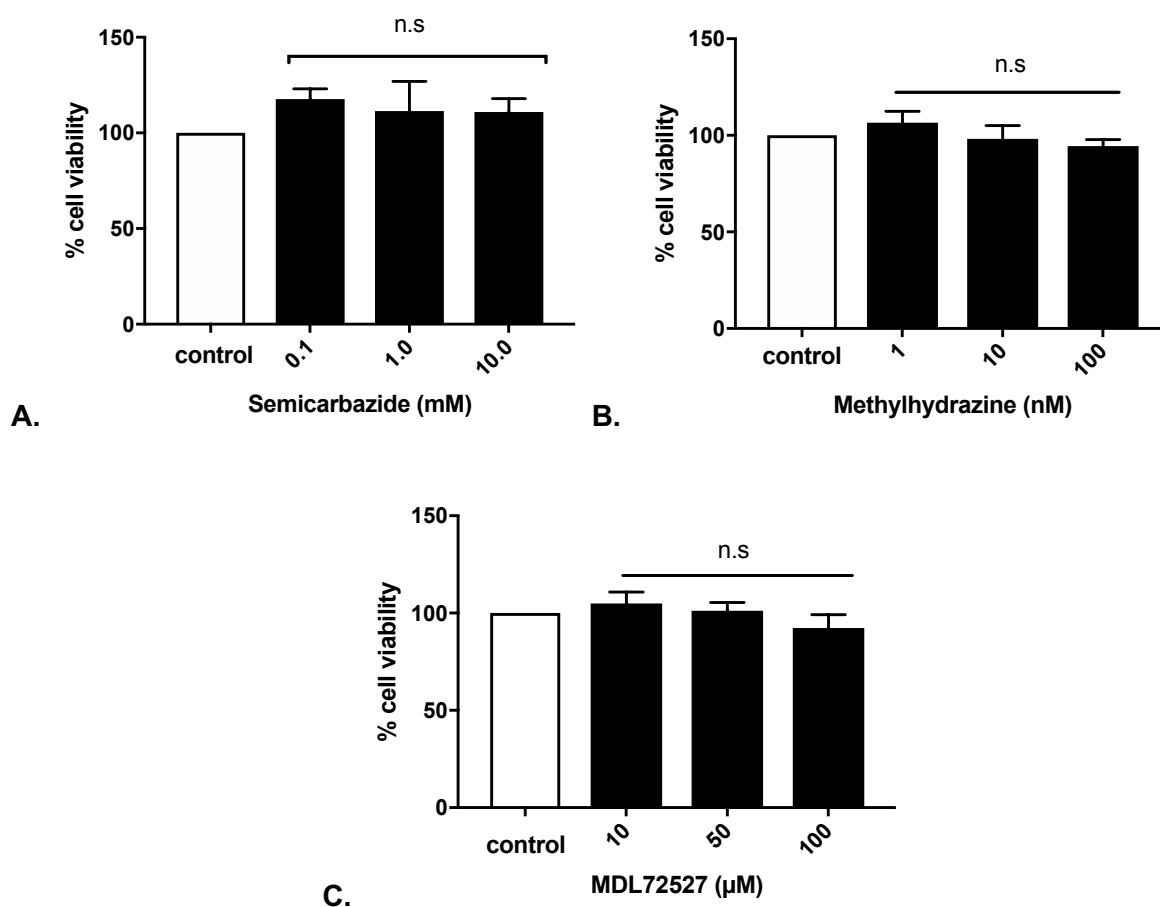


**Figure 42. Viability of rat aortic VSMCs after 1h treatment with A) 0.1, 1, and 10mM semicarbazide, B) 1, 10 and 100nM methylhydrazine, and C) 10, 50 and 100µM MDL72527. The data was analysed by one-way ANOVA followed by Dunnett's multiple comparison test. There was no significant difference ( $p > 0.05$ ) detected between controls (open bars) and A) semicarbazide treated (solid bars), B) methylhydrazine treated (solid bars), and C) MDL72527 treated cells (solid bars). The data is presented in percentages of cell viability as means  $\pm$  S.E.M. of five independent experiments with five replicates in each.**

### ***SSAO inhibition with semicarbazide, methylhydrazine and MDL72527***

After identifying safe inhibitor concentrations SSAO inhibition was characterized applying the model optimized in section 3.1. Firstly, an optimal inhibition time was established for each inhibitor. In doing that cell samples were incubated for 5, 15 and 30 minutes at 37°C with semicarbazide (0.1, 1 & 10mM), methylhydrazine (1, 10 & 100nM), and MD72527L (10, 50 & 100 µM), as described in the methods section 3.2.2. The kinetic parameters in the presence of each inhibitor were obtained by applying the equation for competitive ( $K_{mObs} = K_m \cdot (1 + [I]/K_i)$   $Y = V_{max} \cdot X / (K_{mObs} + X)$ ), and non-competitive enzyme inhibition ( $V_{maxinh} = V_{max} / (1 + I/K_i)$   $Y = V_{maxinh} \cdot X / (K_m + X)$ ), using GraphPad Prism 7 (Figure 87, Appendix 2). The competitive enzyme inhibition equation was applied for semicarbazide and methylhydrazine, and the non-competitive enzyme inhibition equation was applied for MDL72527. Table 8 presents SSAO kinetic parameters obtained after 5-, 15-, and 30-minutes incubation with semicarbazide, methylhydrazine and MDL72527. Most significant inhibition with semicarbazide, methylhydrazine and MDL72527 was detected after 15 minutes incubation, as observed in the  $K_i$  value (Table 8).

**Table 8. SSAO kinetic parameters after 5-, 15-, and 30-minutes incubation at 37°C with semicarbazide (0.1, 1 & 10mM), methylhydrazine (1, 10 & 100nM), and MD72527 (10, 50 & 100µM)**

|                        |                                 |                |                |                                 |
|------------------------|---------------------------------|----------------|----------------|---------------------------------|
| <b>Semicarbazide</b>   | <b>Time of incubation (min)</b> | <b>Km (mM)</b> | <b>Ki (mM)</b> | <b>Vmax (nmol/h/mg protein)</b> |
|                        | <b>5</b>                        | 0.3046         | 8.888          | 19.59                           |
|                        | <b>15</b>                       | 0.2982         | 7.813          | 14.17                           |
|                        | <b>30</b>                       | 0.3409         | 10.39          | 12.67                           |
| <b>Methylhydrazine</b> | <b>Time of incubation (min)</b> | <b>Km (mM)</b> | <b>Ki (nM)</b> | <b>Vmax (nmol/h/mg protein)</b> |
|                        | <b>5</b>                        | 0.06216        | 6.556          | 168.7                           |
|                        | <b>15</b>                       | 0.1543         | 4.507          | 175.6                           |
|                        | <b>30</b>                       | 0.08577        | 25.25          | 158                             |
| <b>MDL72572</b>        | <b>Time of incubation (min)</b> | <b>Km (µM)</b> | <b>Ki (µM)</b> | <b>Vmax (nmol/h/mg protein)</b> |
|                        | <b>5</b>                        | 0.3892         | 136.8          | 33.79                           |
|                        | <b>15</b>                       | 0.4249         | 77.13          | 47.45                           |
|                        | <b>30</b>                       | 0.6164         | 181.4          | 21.09                           |

After establishing an optimal time of 15 minutes for all three inhibitors, cell samples were incubated for 15 minutes at 37°C with semicarbazide SCZ (0.1, 1 & 10mM), methylhydrazine MHZ (1, 10 & 100nM), and MDL72527 (10, 50 & 100µM), as described in the methods section 3.2.2. Figure 43 is a presentation of SSAO kinetic activity observed after 15 minutes incubation with semicarbazide, methylhydrazine and MDL72527. Cells without inhibitor were used as control. The Velocity (nmolH<sub>2</sub>O<sub>2</sub>/h) was derived from the slope of the linear part of the progress curve from the SSAO activity (nmolH<sub>2</sub>O<sub>2</sub>/h/mg protein) vs time graph for each substrate concentration in the presence of (A) semicarbazide, (B) methylhydrazine, and (C) MDL72527.

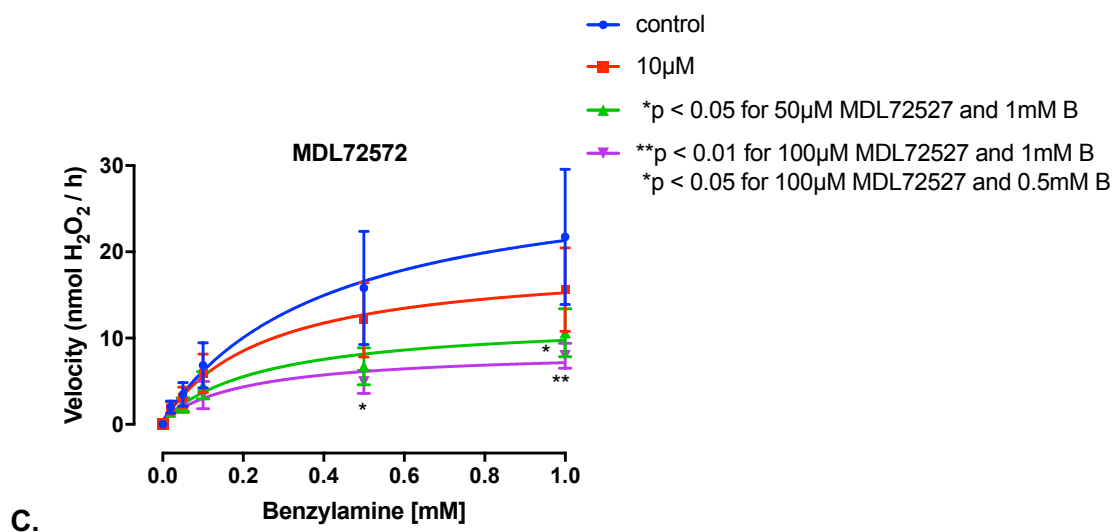
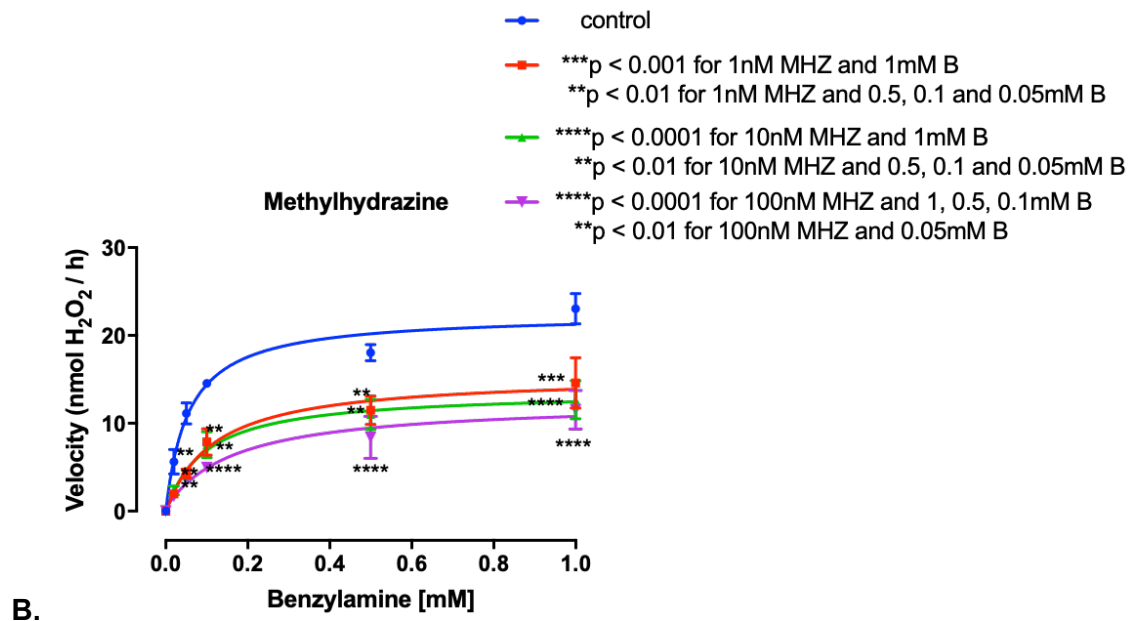
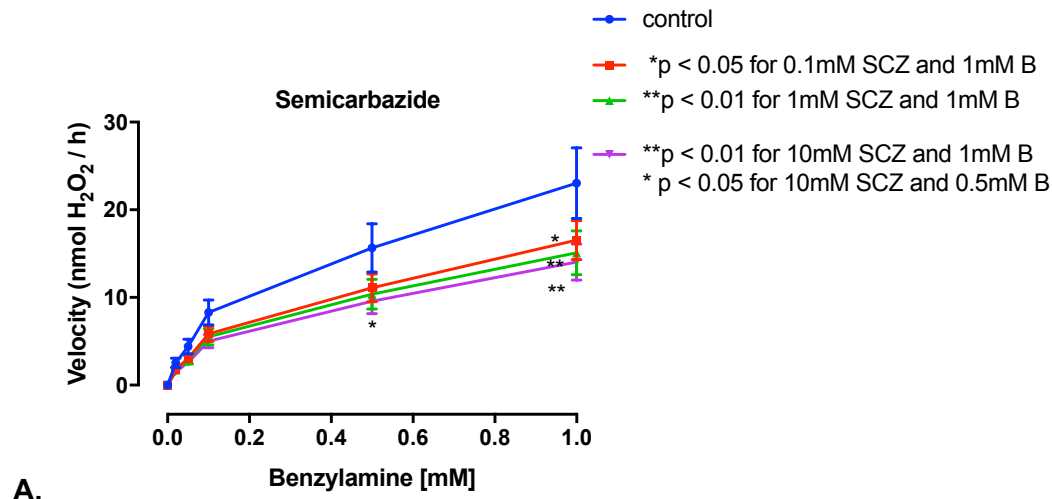
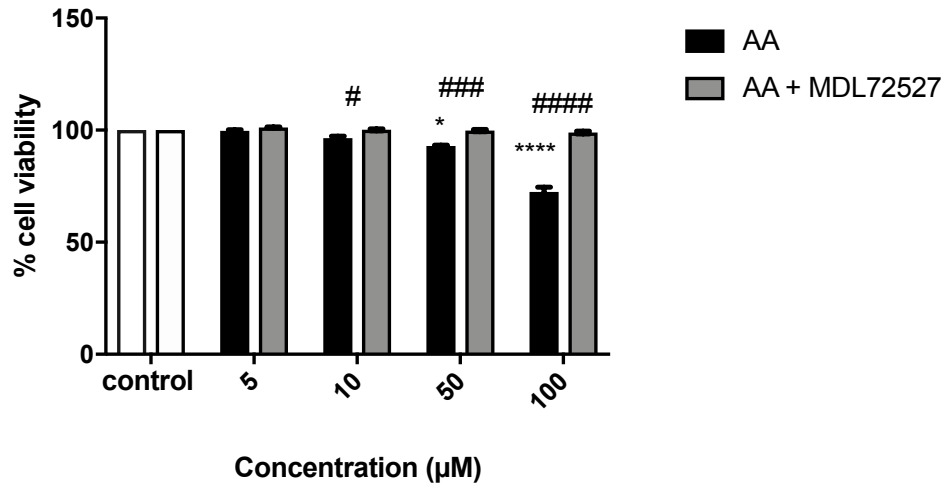


Figure 43. SSAO inhibition with (A) semicarbazide - SCZ, (B) methylhydrazine - MHZ, and (C) MDL72527 after 15 min incubation. The data is presented with curve fitting algorithm, using the GraphPad Prism 7 competitive enzyme equation  $KmObs=Km*(1+[I]/Ki)$   $Y=Vmax*X/(KmObs+X)$  for semicarbazide and methylhydrazine, and the non-competitive enzyme equation  $Vmaxinh=Vmax/(1+I/Ki)$   $Y=Vmaxinh*X/(Km+X)$  for MDL72527. The data was analyzed by two-way ANOVA (\*\*\*\* $p < 0.0001$ ), followed by Dunnett's multiple comparison tests. For semicarbazide (A), at 1mM benzylamine (B) \* $p < 0.05$  for control vs 0.1mM SCZ, and \*\* $p < 0.01$  for control vs 1mM and 10mM SCZ; at 0.5mM benzylamine \* $p < 0.05$  for control vs 10mM SCZ. For methylhydrazine (B), at 1mM benzylamine \*\*\* $p < 0.001$  for control vs 1nM MHZ and \*\*\*\* $p < 0.0001$  for control vs 10 and 100nM MHZ; at 0.5mM benzylamine \*\* $p < 0.01$  for control vs 1 and 10nM MHZ, and \*\*\*\* $p < 0.0001$  for control vs 100nM MHZ; at 0.1mM benzylamine \*\* $p < 0.01$  for control vs 1 and 10nM MHZ, and \*\*\*\* $p < 0.0001$  for control vs 100nM MHZ; at 0.05mM benzylamine \*\* $p < 0.01$  for control vs 1, 10 and 100nM MHZ. For MDL72527 (C), at 1mM benzylamine \* $p < 0.05$  for control vs 50 $\mu$ M MDL72527 and \*\* $p < 0.01$  for control vs 100 $\mu$ M MDL; at 0.5mM benzylamine \* $p < 0.05$  for control vs 100 $\mu$ M MDL. The data is presented as means  $\pm$  S.E.M. of five independent experiments with five replicates in each. The asterisk (\*) indicates statistical significance compared to control at each inhibitor and substrate concentration.

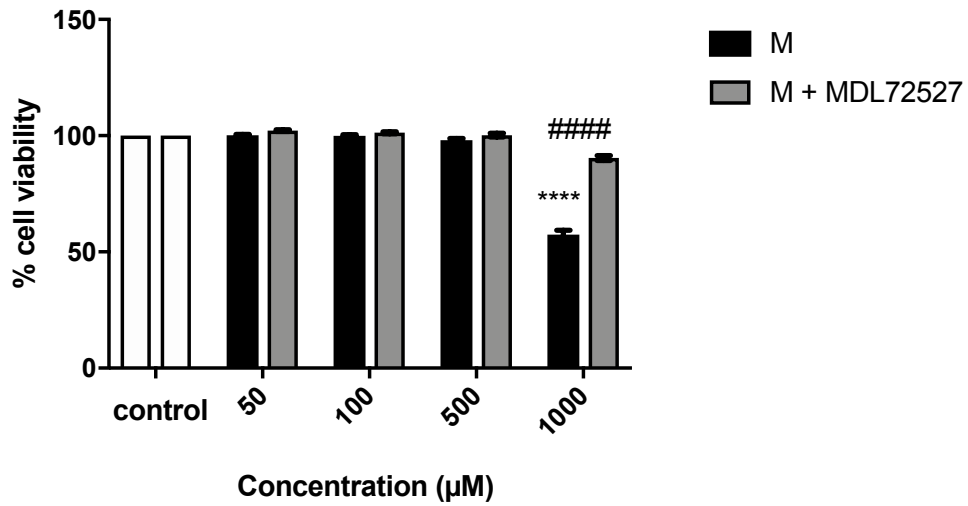
### ***Cell viability after addition of aminoacetone and methylamine***

Cell viability was assessed after addition of SSAO amine (aminoacetone or methylamine), or SSAO amine (aminoacetone or methylamine) + SSAO inhibitor (MDL72527), as explained in the methods section 3.2.2. Figure 44 demonstrates the effect of increasing concentrations of aminoacetone (AA) and methylamine (M) on VSMCs viability (%) after 24h treatment, and the MDL72527 suppressive treatment effect on cytotoxicity induced by both amines. Reduction in VSMCs viability was detected after 24h treatment with both, aminoacetone and methylamine.

Aminoacetone at 50 $\mu$ M caused 15% and at 100 $\mu$ M resulted with 30% cell death comparing to control (\* $p < 0.05$  for control vs 50 $\mu$ M AA; \*\*\*\* $p < 0.0001$  for control vs 100 $\mu$ M AA) (Figure 44A); methylamine at 1000 $\mu$ M caused 40% cell death comparing to control (\*\*\*\* $p < 0.0001$  for control vs 1000 $\mu$ M M (Figure 44B). This effect was almost completely abolished with 100 $\mu$ M MDL72527 (# $p < 0.05$  for 10 $\mu$ M AA and AA + 100 $\mu$ M MDL; (### $p < 0.001$  for 50 $\mu$ M AA and AA + 100 $\mu$ M MDL; ##### $p < 0.0001$  for 100 $\mu$ M AA and AA + 100 $\mu$ M MDL (Figure 44A); and (##### $p < 0.0001$  for 1000 $\mu$ M M and M + 100 $\mu$ M MDL) (Figure 44B).



A.

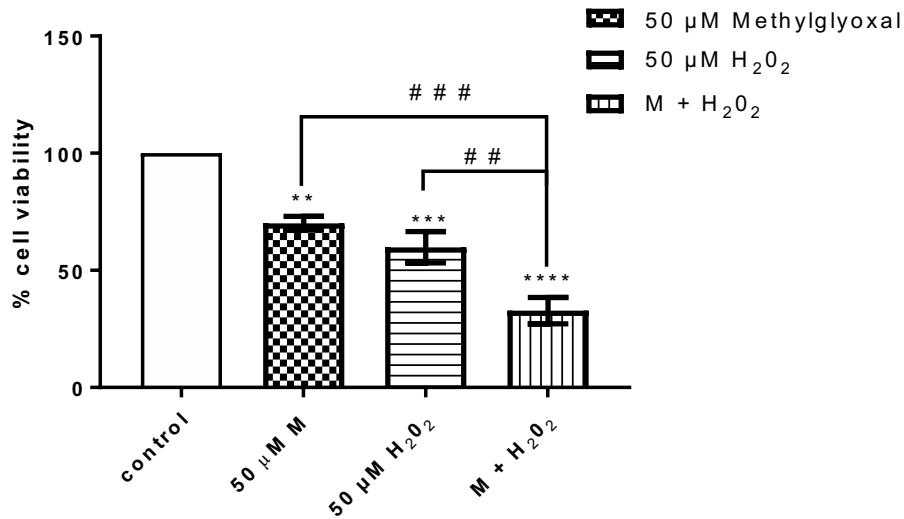


B.

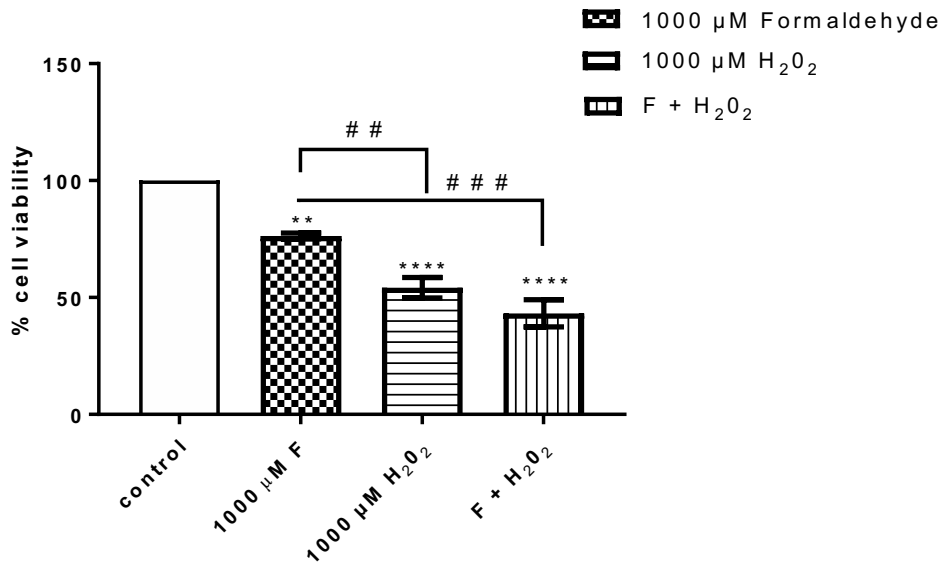
Figure 44. (A) Viability of rat aortic VSMCs treated with increasing concentrations of aminoacetone (black bars), or AA + 100µM MDL72527 (grey bars). The data was analyzed by two-way ANOVA (\*\*\*\* $p < 0.0001$ ), followed by Dunnett's multiple comparison test (\* $p < 0.05$  for control vs 50µM AA; \*\*\*\* $p < 0.0001$  for control vs 100µM AA), and Sidak's multiple comparison test (# $p < 0.05$  for 10µM AA and AA + 100µM MDL; (### $p < 0.001$  for 50µM AA and AA + 100µM MDL; #### $p < 0.0001$  for 100µM AA and AA + 100µM MDL). (B) Viability of rat aortic VSMCs treated with increasing concentrations of methylamine (black bars), or M + 100µM MDL72527 (grey bars). The data was analyzed by two-way ANOVA (\*\*\*\* $p < 0.0001$ ), followed by Dunnett's multiple comparison test (\*\*\*\* $p < 0.0001$  for control vs 1000µM M), and Sidak's multiple comparison test (#### $p < 0.0001$  for 1000µM M and M + 100µM MDL). The data is presented in percentages of control cell viability as means  $\pm$  S.E.M. of five independent experiments with five replicates in each. The asterisk (\*) indicates statistical significance compared to control at each concentration. The hash (#) indicates statistical significance between treatments.

### ***Cell viability after addition of methylglyoxal, formaldehyde and H<sub>2</sub>O<sub>2</sub>***

Cell viability was also assessed after addition of methylglyoxal, formaldehyde and H<sub>2</sub>O<sub>2</sub> or combination of an aldehyde (methylglyoxal or formaldehyde) + H<sub>2</sub>O<sub>2</sub> in 1:1 ratio. Figure 45 demonstrates measured VSMCs viability (%) after 24h treatment with 50μM methylglyoxal (M), 50μM H<sub>2</sub>O<sub>2</sub>, and M + H<sub>2</sub>O<sub>2</sub> in 1:1 ratio (A), or 1000μM formaldehyde (F), 1000μM H<sub>2</sub>O<sub>2</sub>, and F + H<sub>2</sub>O<sub>2</sub> in 1:1 ratio (B). Direct cytotoxic effect was observed after 24h treatment with M, F, H<sub>2</sub>O<sub>2</sub>; and the combination of both (M + H<sub>2</sub>O<sub>2</sub>) and (F + H<sub>2</sub>O<sub>2</sub>). Methylamine (50μM) and formaldehyde (1000μM) caused 30 – 40% cell death comparing to control. H<sub>2</sub>O<sub>2</sub> at 50μM caused 30% and at 1000μM 40% cell death comparing to control (Figure 45A & B). Methylamine and H<sub>2</sub>O<sub>2</sub> combined caused 70% cell death, with formaldehyde and H<sub>2</sub>O<sub>2</sub> causing 60% cell death above control (Figure 45A & B). Moreover, an enhanced cytotoxic effect was observed after addition of methylamine (M) + H<sub>2</sub>O<sub>2</sub>, (####p < 0.001 for 50μM M + H<sub>2</sub>O<sub>2</sub> vs 50μM M; ##p < 0.01 for 50μM M + H<sub>2</sub>O<sub>2</sub> vs 50μM H<sub>2</sub>O<sub>2</sub>), and formaldehyde (F) + H<sub>2</sub>O<sub>2</sub> (###p < 0.001 for 1000μM F + H<sub>2</sub>O<sub>2</sub> vs 1000μM F; ##p < 0.01 for 1000μM H<sub>2</sub>O<sub>2</sub> vs 1000μM F). This could indicate additive rather than synergistic effect between SSAO derived products.



A.



B.

**Figure 45. A) Viability of rat aortic VSMCs treated with methylglyoxal (squared bars), H<sub>2</sub>O<sub>2</sub> (horizontal line bars) and M + H<sub>2</sub>O<sub>2</sub> (vertical line bars) in 1:1 ratio. The data was analyzed by one-way ANOVA (\*\*\*\**p* < 0.0001), followed by Dunnett's multiple comparison test (\**p* < 0.01 for control vs 50μM M, \**p* < 0.001 for control vs 50μM H<sub>2</sub>O<sub>2</sub>, \*\*\*\**p* < 0.0001 for control vs 50μM M + H<sub>2</sub>O<sub>2</sub>), and Tukey's multiple comparison test (###*p* < 0.001 for 50μM M + H<sub>2</sub>O<sub>2</sub> vs 50μM M; ##*p* < 0.01 for 50μM M + H<sub>2</sub>O<sub>2</sub> vs 50μM H<sub>2</sub>O<sub>2</sub>). B) Viability of rat aortic VSMCs treated with formaldehyde (squared bars), H<sub>2</sub>O<sub>2</sub> (horizontal line bars) and F + H<sub>2</sub>O<sub>2</sub> (vertical line bars) in 1:1 ratio. The data was analyzed by one-way ANOVA (\*\*\*\**p* < 0.0001), followed by Dunnett's multiple comparison test (\*\**p* < 0.01 for control vs 1000μM F, \*\*\*\**p* < 0.0001 for control vs 1000μM H<sub>2</sub>O<sub>2</sub> and \*\*\*\**p* < 0.0001 for control vs 1000μM F + H<sub>2</sub>O<sub>2</sub>) and Tukey's multiple comparison test (##*p* < 0.01 for 1000μM H<sub>2</sub>O<sub>2</sub> vs 1000μM F; ###*p* < 0.001 for 1000μM F + H<sub>2</sub>O<sub>2</sub> vs 1000μM F). The data is presented in percentages of control cell viability as means ± S.E.M. of five independent experiments with five replicates in each. The asterisk (\*) indicates statistical significance compared to control at each treatment. The hash (#) indicates statistical significance between treatments.**

### SSAO kinetics with methylamine and aminoacetone as substrates

After identifying optimal substrate concentration of aminoacetone and methylamine that is not cytotoxic to rat aortic VSMCs, to understand the level of interaction between SSAO and these amines, SSAO kinetic parameters were assessed with the model optimised in section 3.1. Figure 46 demonstrates the highest activity ( $V_{max}$ ) of SSAO and its affinity ( $K_m$ ) for the substrate aminoacetone (A) and methylamine (B) in rat aortic VSMCs, using the non-linear regression model of Michaelis-Menten  $Y = V_{max} \cdot X / (K_m + X)$ .

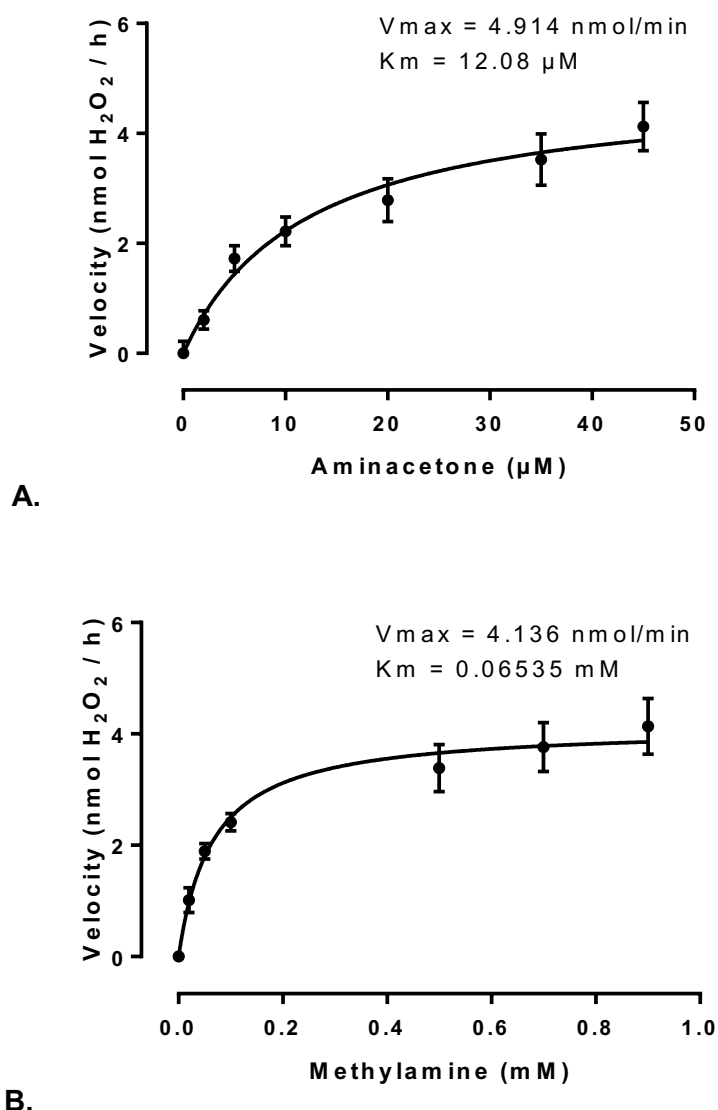


Figure 46. SSAO kinetic parameters ( $V_{max}$  and  $K_m$ ) in the presence of aminoacetone (A) and methylamine (B) The data was analyzed with the non-linear regression model of Michaelis-Menten  $Y = V_{max} \cdot X / (K_m + X)$  and is presented as means  $\pm$  S.E.M. of five independent experiments with five replicates in each.

### 3.2.4 DISCUSSION

To further validate the model optimised in section 3.1 the Amplex<sup>®</sup> Red monoamine oxidase assay was applied to characterise SSAO inhibition with two standard reversible inhibitors (semicarbazide and methylhydrazine) and the irreversible inhibitor MDL72527. After demonstrating a safe concentration range of all three inhibitors, as presented with the cytotoxicity data (Figure 42A, B, and C), an optimal inhibition time of 15 minutes was established as the most effective to inhibit SSAO. This was reflected in the  $K_i$  values (Table 8). This inhibition time is congruent with previous studies that have used lung, liver, and aorta tissue homogenates to study SSAO inhibition (Deng & Yu, 1999; Duranton *et al.*, 2002; Agostinelli *et al.*, 2006; O'Rourke *et al.*, 2008; Floris & Mondovi, 2009). In this study, semicarbazide at millimolar range (0.1, 1 & 10mM) demonstrated SSAO inhibition in the presence of 1 and 0.5mM benzylamine, with no cytotoxic effect on cell growth (Figure 43A). This finding is consistent with previous studies that have identified semicarbazide as the weakest inhibitor from the hydrazine group of inhibitors, with ability to trap carbonyls once they are formed thus blocking enzyme activity in a non - specific manner (Floris & Mondovi, 2009; Pannecoeck *et al.*, 2015).

Furthermore, in this study methylhydrazine achieved SSAO inhibition at 1, 10 and 100nM, in the presence of 1, 0.5, 0.1 and 0.05mM benzylamine (Figure 43B). The ability of methylhydrazine to inhibit SSAO within a nanomolar range was in accordance with previous studies that have examined the effectiveness of methylhydrazine in homogenates of various rat tissues (Holt & Callingham, 1994; O'Rourke *et al.*, 2007; O'Rourke *et al.*, 2008). This study also demonstrated successful and irreversible SSAO inhibition with 50 & 100 $\mu$ M MDL72527 in the presence of 1 and 0.5mM benzylamine (Figure 43C). This finding is also comparable with previous studies that have demonstrated time dependent potency of MDL72527 in inhibiting not only SSAO, but also PAO (Seiler *et al.*, 2000; Duranton *et al.*, 2002; Agostinelli *et al.*, 2006). Duranton *et al.* (2002) have demonstrated complete inhibition of PAO and SSAO with 50 $\mu$ M MDL72527, with no cytotoxic effect on cell growth. Before assessing the model further by applying it to understand the level of interaction between the endogenous amines (methylamine and aminoacetone) and SSAO, the cytotoxic effect of these amines and their corresponding products (aldehydes) was investigated in rat aortic VSMCs. Considering that an irreversible, mechanism - based inhibitor would be the most suitable candidate for clinical progression due to generating a chemically reactive intermediate that irreversibly inactivates the enzyme comparing to reversible competitive inhibitors, MDL72527 at 100 $\mu$ M was added to the cells as it was demonstrated effective in irreversibly inhibiting SSAO in the presence of 0.5mM substrate (Figure 43C).

Serum free media was used as it has previously been highlighted that protein antioxidants present in the serum could increase cell resistance to aminoacetone and methylamine triggered cell death (Sartori *et al.*, 2008). These findings demonstrate induced VSMCs death after 24h exposure to 50 & 100 $\mu$ M aminoacetone, and 1000 $\mu$ M methylamine (Figure 44A & B). The cytotoxicity was reversed with the SSAO specific and irreversible inhibitor MDL72527, which completely abolished cell death (<sup>#</sup>p < 0.05 for 10 $\mu$ M AA and AA + 100 $\mu$ M MDL; (<sup>###</sup>p < 0.001 for 50 $\mu$ M AA and AA + 100 $\mu$ M MDL; (<sup>####</sup>p < 0.0001 for 100 $\mu$ M AA and AA + 100 $\mu$ M MDL (Figure 44A); and (<sup>#####</sup>p < 0.0001 for 1000 $\mu$ M M and M + 100 $\mu$ M MDL) (Figure 44B). Therefore, this data suggests that the induced cytotoxicity observed in rat aortic VSMCs was mediated through SSAO metabolic products (methylglyoxal and formaldehyde), because of SSAO catalysed reaction.

When present within a high micromolar range, aminoacetone and methylamine have previously been reported as triggers for cell death in human aortic VSMCs and insulin producing cells (Sartori *et al.*, 2008; 2010; Hernandez *et al.*, 2006). In a study done by Sartori *et al.* (2008) aminoacetone was demonstrated toxic to insulin producing RINm5f cells with concentrations between 100 and 500 $\mu$ M. This data agrees with the findings by Sartori *et al.* (2008); however, it also signifies a cytotoxic effect at lower AA concentrations (50 $\mu$ M) in rat aortic VSMCs (Figure 44A). In relation to methylamine, Hernandez *et al.* (2006) have demonstrated a dose dependent toxic effect of methylamine starting at 1mM in human aortic smooth muscle cells because of SSAO mediated deamination. Hernandez *et al.* (2006) have confirmed this by observing Caspase-3 activation, PARP cleavage and cytochrome c release. This data enhances the findings by Hernandez *et al.* (2006) shown in HASMCs by also indicating a methylamine driven cytotoxicity at 1mM in rat aortic VSMCs (Figure 44B).

Furthermore, the data in this section demonstrates direct cytotoxic effect caused by SSAO generated aldehydes (methylglyoxal and formaldehyde), and H<sub>2</sub>O<sub>2</sub> (Figure 45A & B). In these findings both, methylglyoxal (50 $\mu$ M) and formaldehyde (1000 $\mu$ M) caused 30 – 40% cell death comparing to control (<sup>\*\*</sup>p < 0.01). Furthermore, H<sub>2</sub>O<sub>2</sub> alone, with concentration 50 $\mu$ M caused 30% cell death comparing to control (<sup>\*\*\*</sup>p < 0.001), and at concentration 1000 $\mu$ M led to 40% cell death comparing to control (<sup>\*\*\*\*</sup>p < 0.0001). The observed cytotoxic effect of methylglyoxal and formaldehyde detected here is congruent with previous studies (Lin *et al.*, 2005; Braun *et al.*, 2018). Formaldehyde has been reported cytotoxic in rat aortic endothelial cells (Lin *et al.*, 2005). Lin *et al.* (2005) have demonstrated that at high micromolar concentrations formaldehyde can induce covalent binding between functional groups in lysine residues of protein, and DNA base.

Additionally, Lin *et al.* (2005) have further reported that at high concentrations (1 and 2mM) H<sub>2</sub>O<sub>2</sub> alone can also contribute to cell death by increasing DNA protein crosslinks. Regarding methylglyoxal, Braun *et al.* (2018) have suggested that at high micromolar concentrations (400 – 800μM) methylglyoxal can induce cell death in human umbilical vein endothelial cells by downregulating cell cycle associated genes and upregulating the heme-oxygenase 1 (HO-1).

The data in this section further shows an additive rather than synergistic effect between H<sub>2</sub>O<sub>2</sub> and SSAO produced aldehydes (methylglyoxal and formaldehyde) in inducing cell death. In these findings, methylglyoxal and H<sub>2</sub>O<sub>2</sub> combined caused 70% cell death (\*\*\*\*p < 0.0001), with formaldehyde and H<sub>2</sub>O<sub>2</sub> causing 60% cell death above control (\*\*\*\*p < 0.0001) (Figure 45A & B). Moreover, when comparing the effect between treatments, in the presence of methylglyoxal a higher percentage of cell death was detected by methylglyoxal + H<sub>2</sub>O<sub>2</sub>, comparing to methylglyoxal and H<sub>2</sub>O<sub>2</sub> on its own (####p < 0.001 for 50μM M + H<sub>2</sub>O<sub>2</sub> vs 50μM M; ##p < 0.01 for 50μM M + H<sub>2</sub>O<sub>2</sub> vs 50μM H<sub>2</sub>O<sub>2</sub>). Furthermore, in the presence of formaldehyde a higher percentage of cell death was detected by formaldehyde + H<sub>2</sub>O<sub>2</sub>, and H<sub>2</sub>O<sub>2</sub> on its own, comparing to formaldehyde (####p < 0.001 for 1000μM F + H<sub>2</sub>O<sub>2</sub> vs 1000μM F; ##p < 0.01 for 1000μM H<sub>2</sub>O<sub>2</sub> vs 1000μM F). In light with these findings, previous studies have already confirmed potential interactions between SSAO generated aldehydes and H<sub>2</sub>O<sub>2</sub> (Lin *et al.*, 2005; Conklin *et al.*, 2004; Gubisne-Haberle *et al.*, 2004). Conklin *et al.* (2004) have suggested that H<sub>2</sub>O<sub>2</sub> interacts with formaldehyde and converts the same to excited formaldehyde which can penetrate easily into the smallest reactive regions of biomolecules; causing various reactions on lysine- rich histone proteins on DNA and RNA. However, to differentiate between a synergistic and additive interaction additional studies are needed that would use smaller concentration range and different ratios between the SSAO derived aldehydes and hydrogen peroxide. Furthermore, additional cytotoxicity assays such as lactate dehydrogenase (LDH) and presto blue could also be implemented to confirm additive or synergistic effect between SSAO derived aldehydes and hydrogen peroxide.

After identifying a safe concentration range at which SSAO endogenous amines (methylamine and aminoacetone) failed to exert cytotoxic effect on rat aortic VSMCs, another set of kinetic experiments was performed using the Amplex<sup>®</sup> Red monoamine oxidase assay, to understand the level of interaction between SSAO and these amines. The data presented in this section demonstrates higher SSAO affinity for aminoacetone comparing to methylamine (12μM vs 60μM) in rat aortic VSMCs, as observed in the Km values (Figure 46A & B). Furthermore, the rate at which SSAO converts the amines into their corresponding products aldehydes was also slightly higher in the case of aminoacetone (5nmol/min vs 4nmol/min), as observed in the Vmax values (Figure 46A & B).

SSAO kinetic parameters were compared in a study by Hernandez *et al.* (2006) which investigated the kinetics of soluble SSAO in rat aortic A7r5 cells after addition of methylamine, benzylamine and tyramine as substrates. Hernandez *et al.* (2006) have demonstrated higher Vmax (7.32 nmol/min) and smaller SSAO affinity for methylamine (1.04 mM). This data differs from the findings published by Hernandez *et al.* (2006), and the reason for that could be the use of a primary cell line, with focus on the membrane bound form of the enzyme and not soluble SSAO.

Furthermore, Figure 46A & B indicates that in rat aortic VSMCs the conversion of aminoacetone and methylamine into methylglyoxal and formaldehyde, because of SSAO catalysed reaction, happens at a fast rate (~ 4 nmol/min). The fast generation of methylglyoxal and formaldehyde could cause damage to the cell membrane due to auto-oxidation of lipids and fatty acids within the cell. As per Figure 46A & B, in rat aortic VSMCs there is a greater production of methylglyoxal comparing to formaldehyde, because of SSAO catalysed reaction. Cellular concentrations of methylglyoxal are estimated to be between 1 – 5  $\mu$ M and higher concentrations than this can have damaging effect to the cell, mainly due to its highly reactive nature (Dator *et al.*, 2019). Being a highly reactive glycation agent, methylglyoxal could also act as a precursor for the formation of AGE (Braun *et al.*, 2018).

### **3.2.5 CONCLUSION**

The data presented here shows a successful validation of the model optimised in section 3.1, which once more confirms the efficacy of the same. SSAO inhibition was characterised with reversible and irreversible inhibitors potent in inhibiting SSAO with no cytotoxic effect on cell growth. Methylhydrazine was identified as the most potent reversible, and MDL72572 as the most potent irreversible inhibitor. Furthermore, this data demonstrates cellular toxicity because of SSAO catalysed reaction and enhanced cytotoxicity after simultaneous addition of SSAO derived products (aldehydes and H<sub>2</sub>O<sub>2</sub>), which indicates additive rather than synergistic relationship between the same. These findings also demonstrate fast generation of methylglyoxal and formaldehyde in rat aortic VSMCs because of SSAO catalysed reaction; and higher SSAO affinity for aminoacetone comparing to methylamine, which indicates a greater production of methylglyoxal comparing to formaldehyde in these cells.

## **SECTION 3.3 SSAO AND LOX ACTIVITY DURING RAT AORTIC VASCULAR SMOOTH MUSCLE CELLS AGING**

### **3.3.1 INTRODUCTION**

Following the successful optimisation and validation of the model in section 3.1 and 3.2 the same was applied further to explore the physiological and pathological role of SSAO and LOX during VSMCs aging, as cells were being passaged from lower to higher passage number. VSMCs are the main stromal cells in the medial layer of the vascular wall that produce the extracellular matrix (ECM) which is important to provide the arterial wall with the capacity to withstand the pressure from the circulating blood (Lacolley *et al.*, 2012). These cells also maintain a variable contractile tone which is responsible for the regulation of blood pressure and redistribution of blood flow. When mechanical stress is generated within the arterial wall a hydraulic conductance occurs across the wall, delivering soluble substances from the blood outwards. Found in the medial layer of the arterial wall VSMCs are highly sensitive to mechanical stress and are accessible to soluble plasma components which are outwardly transferred from the circulating blood through the vascular wall (Lacolley *et al.*, 2012).

The movement of VSMCs inwardly from the medial to the intimal layer of the arteries (VSMCs intimal proliferation) depends on the ability of these cells to adhere, migrate, and proliferate in response to specific growth factors. Furthermore, these cells can perform additional functions in response to the stimuli to which they are subjected. This ability of VSMCs to adapt is mainly related to its high plasticity to re-programme their expression pattern in response to acute stimuli (mediated by ligand–receptor interactions), and chronic stimuli that trigger epigenetic modulations (Lacolley *et al.*, 2012). VSMCs can exist in a proliferative and migratory – synthetic, and quiescent - contractile phenotype. However, it has been suggested that differentiation and proliferation of VSMCs are not mutually exclusive (Alexander & Owens, 2012; Owens *et al.*, 2004). These cells can undergo profound changes between two phenotypes: a quiescent one with differentiated VSMCs, and a proliferating one with dedifferentiated VSMCs (Wang *et al.*, 2015). This would greatly depend on the signals present in their local environment through which contractile VSMCs can acquire the ability to migrate and proliferate, promote ECM production, inflammatory signals, and/or calcification.

SSAO, being highly expressed in the vasculature is mainly predominant in the medial and intimal layer of the arterial wall (O'Sullivan *et al.*, 2002). Furthermore, being an enzyme with functional diversity SSAO manifests different role depending on the nature of the cell type. In endothelial cells SSAO mediates lymphocytes binding; however, in VSMCs its role has not been explored in detail. Lyles & Pino (1998) have suggested that membrane bound SSAO mediates toxicological effects in tunica media through aliphatic amine metabolism and exerts cytotoxic effects on smooth muscle cells *in vitro*. This was later confirmed by El Hadri *et al.* (2001) that have identified the SSAO generated H<sub>2</sub>O<sub>2</sub> as a signalling molecule with an ability to exert pleiotropic functions in VSMCs and mediate apoptosis. In accordance with these findings the data presented in section 3.2 also demonstrates cellular toxicity because of SSAO catalysed reaction; as well as enhanced cytotoxic effect caused by simultaneous addition of SSAO derived products, aldehydes and H<sub>2</sub>O<sub>2</sub>. However, in addition to its cytotoxic effect, SSAO's high expression in VSMCs might also indicate its potential involvement in other physiological or pathological functions, including cell proliferation, differentiation, and migration.

The role of SSAO in VSMCs proliferation and differentiation has not been explicitly studied. Sung *et al.* (2005) have associated the enhanced SSAO driven H<sub>2</sub>O<sub>2</sub> production in VSMCs with an acceleration of switch from contractile to synthetic phenotype in these cells. Recent research has also pointed towards the involvement of another copper reach amine oxidase (LOX) in VSMCs differentiation and migration (Lucero *et al.*, 2008; Rodrigez *et al.*, 2008; 2002; Raposo *et al.*, 2004). In the study by Lucero *et al.* (2008), it was demonstrated that the enzymatic activity of LOX and the H<sub>2</sub>O<sub>2</sub> product of its enzymatic reaction are responsible for chemotactic response in VSMCs. Lucero *et al.* (2008) have attributed this effect to the activation of the platelet derived growth factor receptor  $\beta$  (PDGFR $\beta$ ) and further demonstrated that inhibition of LOX activity with  $\beta$ -aminopropionitrile ( $\beta$ APN) reduces the binding affinity of the platelet-derived growth factor- $\beta$  (PDGF $\beta$ ) to its receptor PDGFR $\beta$ .  $\beta$ APN is a well-known irreversible inhibitor which inhibits LOX activity by a catalysis-dependent suicidal inactivation mechanism. This process is triggered by an initial oxidation of the - amino group of  $\beta$ APN (H<sub>2</sub>NCH<sub>2</sub>CH<sub>2</sub>CN) which then generates an intermediate that remains covalently bound to the active site, thus irreversibly inactivating the enzyme (Lucero *et al.*, 2008).

Activation of platelet derived growth factors and their receptors are known to drive mesenchymal pathological responses in many vascular disorders, including atherosclerosis (Andrae *et al.*, 2008). The platelet-derived growth factor- $\beta$  (PDGF $\beta$ ) is well-known mediator of VSMCs phenotypic switching (Tang *et al.*, 2011). PDGF $\beta$  is a dimeric molecule that when binds to its receptor promotes receptor dimerization (Figure 47). Being a receptor tyrosine kinase (RTK), when activated the PDGFR $\beta$  triggers cascade of events that contribute to differentiation, proliferation, and migration of VSMCs (Tallquist *et al.*, 2000). During their migration and intimal proliferation, VSMCs partially lose their contractile phenotype and acquire a pro-inflammatory and matrix remodelling phenotype, which is a critical process behind peripheral vascular disease and atherosclerosis (Tang *et al.*, 2011).

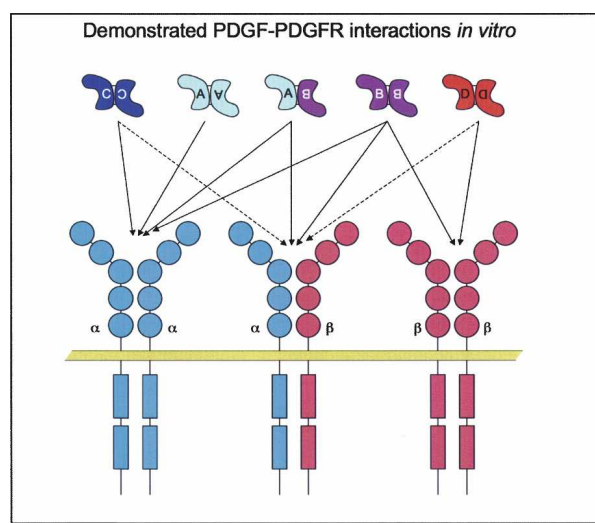


**Figure 47. PDGF–PDGFR interactions. Each chain of the PDGF dimer interacts with one receptor subunit. The active receptor configuration is therefore determined by the ligand dimer configuration. These are interactions that have been demonstrated in cell culture (Andrae *et al.*, 2008).**

In their natural quiescent (contractile) phenotype VSMCs express a set of up-regulated smooth muscle markers which are necessary for the main function of these cells to contract the vessel wall. These markers are cytoskeleton and contractile proteins such as: actin  $\alpha$  2 (ACTA2), smooth muscle myosin heavy chain (SMMHC), calponin and SM22 $\alpha$ . The expression of the smooth muscle markers is normally downregulated in differentiated VSMCs and is often regarded as a sign for VSMCs phenotypic switch (Wang *et al.*, 2015). During the pathophysiology of atherosclerosis, dedifferentiated VSMCs participate in the formation of intimal hyperplasia by decreasing the expression of contractile proteins and increasing proliferation, migration, and matrix protein synthesis (Yoshida *et al.*, 2008).

Ageing is a prominent risk factor for the development of atherosclerosis and other cardiovascular disease. Therefore, it is important to assess passage related changes in SSAO and/or LOX activity which could suggest their potential involvement in vascular remodelling - an important factor in the development and progression of atherosclerosis. Moreover, this study already demonstrated a passage dependent increase in SSAO affinity (\*\*p < 0.01) in section 3.1, which could indicate changes in enzymatic activity as the cells age with passage. Furthermore, the interaction between SSAO and LOX in this process has been previously posed as an important unexplored area which required further research.

Overall, this section aims to investigate changes in SSAO and LOX enzymatic activity and expression during VSMCs proliferation, their interaction, and their contributory role in vascular remodelling as cells were being passaged from lower to a higher passage number. Objectives:

1. Investigate SSAO activity and expression at basal level, and in the presence of MDL72527 (mechanism-based inhibitor for SSAO) and  $\beta$ APN (mechanism-based inhibitor for LOX) using benzylamine as substrate.
2. Investigate LOX activity and expression at basal level, and in the presence of  $\beta$ APN MDL72527 (mechanism-based inhibitor for LOX) and MDL72527 (mechanism-based inhibitor for SSAO) using cadaverine as substrate.
3. Investigate the expression of both, SSAO and LOX after 1h treatment with  $\beta$ APN and MDL72527, and 6h treatment with benzylamine and cadaverine.
4. Investigate the expression of the VSMCs contractile markers ACTA2 and SM22 $\alpha$  after 1h treatment with  $\beta$ APN and MDL72527, and 6h treatment with benzylamine and cadaverine.
5. Investigate the expression of PDGFR $\beta$  after 1h treatment with  $\beta$ APN and MDL72527, and 6h treatment with benzylamine and cadaverine.

## SECTION 3.3.2 METHODS

### ***SSAO activity in rat aortic VSMCs from passage 3 to 8***

To compare SSAO activity (expressed as H<sub>2</sub>O<sub>2</sub> production) at rat aortic VSMCs from passage 3 to 8, cells were plated at 5 x 10<sup>4</sup> in a black-walled, clear-bottom 96-well plate, and allowed to grow for 24-48 hours to reach confluence. Cell samples from passage 3 to 8 were treated with reaction mixture containing 860µl of 0.25M sodium phosphate buffer (pH 7.4), 20µl Amplex<sup>®</sup> Red (20mM), 10µl horseradish peroxidase (200U/ml), 10µl clorgyline (0.5mM) and 200µl benzylamine at concentration 0.5mM. Cells containing reaction mixture without benzylamine were considered as control. SSAO activity was measured after 6h from addition of reaction mixture using excitation 540nm and emission 590nm, on a Clario Star<sup>®</sup> Microplate Reader (BMG Labtech).

### ***SSAO and LOX activity in rat aortic VSMCs from passage 3, 5 and 8***

To investigate the possibility of LOX interference with SSAO activity during rat aortic VSMCs aging, the activity of both enzymes was first studied at basal level, in cells from passage 3, 5 and 8. To compare the activity between SSAO and LOX expressed as H<sub>2</sub>O<sub>2</sub> production, rat aortic VSMCs from passage 3, 5 and 8 were treated with reaction mixture containing 860µl of 0.25M sodium phosphate buffer (pH7.4), 20µl Amplex<sup>®</sup> Red (20mM), 10µl horseradish peroxidase (200U/ml), 10µl clorgyline (0.5mM), and 200µl (0.5mM) benzylamine, or 1,5 diamino pentane dihydrochloride (cadaverine) respectively. SSAO activity (expressed as H<sub>2</sub>O<sub>2</sub> production) was also studied in the presence of MDL72527 and βAPN. Cells were treated with reaction mixture containing 860µl of 0.25M sodium phosphate buffer (pH 7.4), 20µl Amplex<sup>®</sup> Red (20mM), 10µl horseradish peroxidase (200U/ml), 10µl clorgyline (0.5mM), and 200µl (0.5mM) benzylamine or 200µl (0.5mM) benzylamine and 10µl (100µM) MDL72527 - irreversible SSAO inhibitor, or 200µl (0.5mM) benzylamine and 10µl (200µM) βAPN - irreversible LOX inhibitor. LOX activity was also assessed in the presence of MDL72527 and βAPN. Cells were treated with reaction mixture containing 860µl of 0.25M sodium phosphate buffer (pH7.4), 20µl Amplex<sup>®</sup> Red (20mM), 10µl horseradish peroxidase (200U/ml), and 200µl (0.5mM) 1,5 diamino pentane dihydrochloride (cadaverine - LOX substrate), or 200µl (0.5mM) cadaverine and 10µl (100µM) MDL72527, or 200µl (0.5mM) cadaverine and 10µl (200µM) βAPN. 0.5mM (10µ) clorgyline was also added to the reaction mixture to maintain consistency.

Cells containing reaction mixture without benzylamine or cadaverine were considered as control. SSAO and LOX activity were measured after 6h from addition of reaction mixture using excitation 540nm and emission 590nm, on a Clario Star<sup>®</sup> Microplate Reader (BMG Labtech).

### ***SSAO kinetics in rat aortic VSMCs (passage 3, 5 and 8) in the presence of $\beta$ APN***

A second set of experiments was performed where SSAO kinetic parameters ( $V_{max}$  and  $K_m$ ) were assessed once more in the presence of LOX irreversible and specific inhibitor,  $\beta$ APN. Cells from passage 3, 5 and 8 were treated with reaction mixture containing 860 $\mu$ l of 0.25M sodium phosphate buffer (pH7.4), 20 $\mu$ l Amplex<sup>®</sup> Red (20mM), 10 $\mu$ l horseradish peroxidase (200U/ml), 10 $\mu$ l clorgyline (0.5mM), SSAO substrate (benzylamine) at different concentrations (0, 0.02, 0.05, 0.1, 0.5, 1 and 5mM) and LOX irreversible and specific inhibitor (200 $\mu$ M  $\beta$ APN). SSAO activity was measured at different time intervals (0h, 0.5h, 1h, 2h, 4h, 6h), using excitation 540nm and emission 590nm, on a Clario Star<sup>®</sup> Microplate Reader (BMG Labtech). The reaction velocity ( $V$ ) expressed as (nmolH<sub>2</sub>O<sub>2</sub>/h) was derived from the slope of the linear part of the progress curve from the SSAO activity (nmolH<sub>2</sub>O<sub>2</sub>/h/mg protein) vs time graph for each substrate concentration (mM), as explained in the methods section 3.1.2. SSAO's affinity ( $K_m$ ) and  $V_{max}$  were determined by plotting reaction velocity (nmolH<sub>2</sub>O<sub>2</sub>/h) versus substrate concentration using the non-linear regression model of Michaelis-Menten  $Y = V_{max} * X / (K_m + X)$ .

### ***LOX kinetics in rat aortic VSMCs (passage 3, 5 and 8)***

LOX kinetic parameters ( $V_{max}$  and  $K_m$ ) were also assessed in rat aortic VSMCs from passage 3, 5 and 8. In doing that cell samples were treated with reaction mixture containing 860 $\mu$ l of 0.25M sodium phosphate buffer at pH7.4, 20 $\mu$ l Amplex<sup>®</sup> Red (20mM), 10 $\mu$ l horseradish peroxidase (200U/ml), as well as different concentrations of cadaverine (0, 0.02, 0.05, 0.1, 0.5, 1 and 5mM) as LOX substrate. To maintain consistency, 0.5mM (10 $\mu$ ) clorgyline was also added to the reaction mixture. LOX activity was measured at different time intervals (0h, 0.5h, 1h, 2h, 4h, 6h), using excitation 540nm and emission 590nm, on a Clario Star<sup>®</sup> Microplate Reader (BMG Labtech). The reaction velocity ( $V$ ) expressed as (nmolH<sub>2</sub>O<sub>2</sub>/h) was derived from the slope of the linear part of the progress curve from the LOX activity (nmolH<sub>2</sub>O<sub>2</sub>/h/mg protein) vs time graph for each substrate concentration (mM), as explained in the methods section 3.1.2. LOX's affinity ( $K_m$ ) and  $V_{max}$  were determined by plotting reaction velocity (nmolH<sub>2</sub>O<sub>2</sub>/h) versus substrate concentration using the non-linear regression model of Michaelis-Menten  $Y = V_{max} * X / (K_m + X)$ .

### **Western blot analysis**

The protein expression of VAP-1, Pro-LOX, ACTA2, SM22 $\alpha$  and PDGFR $\beta$  was observed in rat aortic VSMCs from passage 3, 5 and 8 with western blot analysis, as described in the methods section 2.2.13. The expression of VAP-1 was detected with Alexa Fluor<sup>®</sup> conjugated VAP-1 antibody at dilution 1:1000 in 5% w/v BSA, 1XTBS, 10% Tween<sup>®</sup>20. The expression of Pro-LOX was detected with rabbit monoclonal to Pro-LOX antibody at dilution 1:1000 in 5% w/v BSA, 1XTBS, 10% Tween<sup>®</sup>20. The expression of SM22 $\alpha$  was detected with rabbit monoclonal to SM22 $\alpha$  antibody at dilution 1:2000 in 5% w/v BSA, 1XTBS, 10% Tween<sup>®</sup>20. The expression of ACTA2 was detected with rabbit monoclonal to ACTA2 antibody at dilution 1:1000 in 5% w/v BSA, 1XTBS, 10% Tween<sup>®</sup>20. The expression of PDGFR $\beta$  was detected with rabbit monoclonal to PDGFR $\beta$  diluted 1:1000 in 5% w/v BSA, 1XTBS, 10% Tween<sup>®</sup>20. HRP conjugated  $\beta$ -actin diluted at 1:15000 in 5% w/v milk powder, 1XTBS, 10% Tween<sup>®</sup>20 was used like a control. The protein bands were quantified with ImageJ software, as explained in the methods section 2.2.14.

### **SECTION 3.3.3 RESULTS**

#### ***SSAO activity in rat aortic VSMCs from passage 3 to 8***

SSAO activity in rat aortic VSMCs from passage 3 to 8 was studied as explained in the methods section 3.3.2, by utilising the optimised Amplex<sup>®</sup> Red monoamine oxidase assay. Reaction mixture was prepared with 0.25M sodium phosphate buffer (pH 7.4), Amplex<sup>®</sup> Red (20mM), horseradish peroxidase (200U/ml), clorgyline (0.5mM) and 0.5mM benzylamine. VSMCs without benzylamine were used as control. Figure 48 demonstrates measured SSAO activity expressed as H<sub>2</sub>O<sub>2</sub> production in early (3 & 4) versus late passage VSMCs treated with reaction mixture containing SSAO substrate (with 0.5mM benzylamine), and control (without substrate). Significant difference in SSAO activity (nmolH<sub>2</sub>O<sub>2</sub>/h/mg protein) was observed between early passage cells (3 & 4), and cells with a greater passage number, as presented by two-way ANOVA (\*\*\*\*p < 0.0001). Moreover, significant difference at each passage was also detected between control cells and cells treated with 0.5mM benzylamine (#### p < 0.0001).

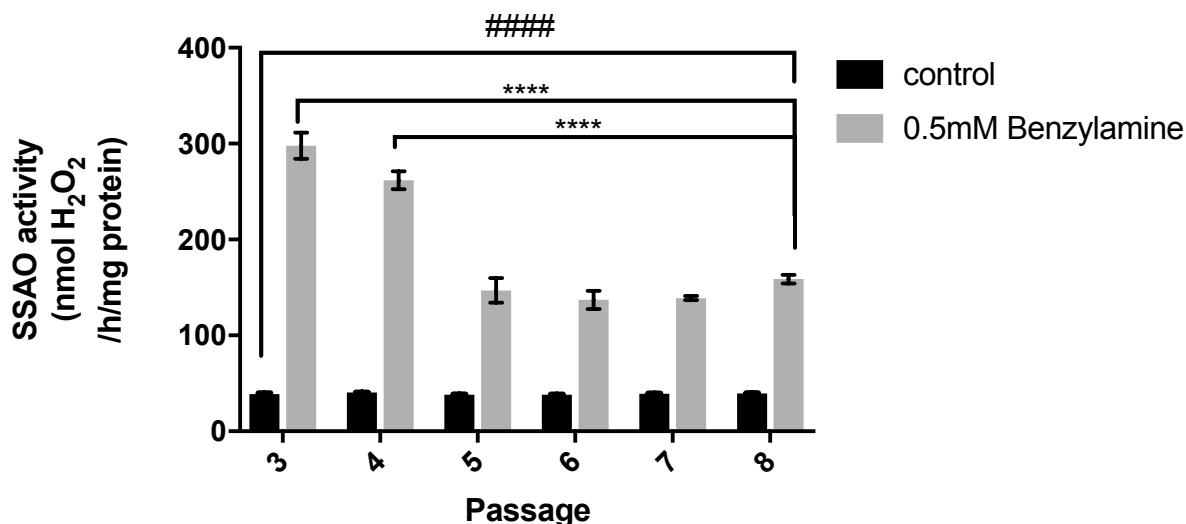
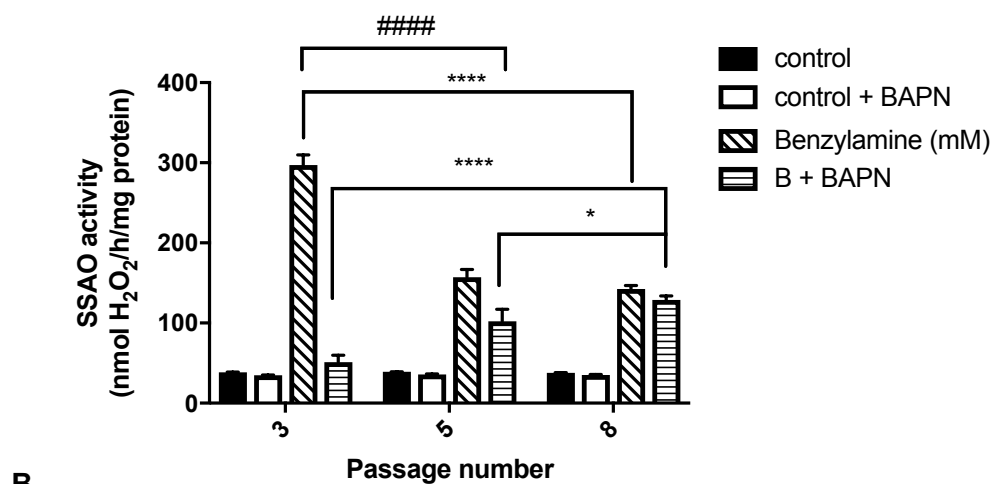
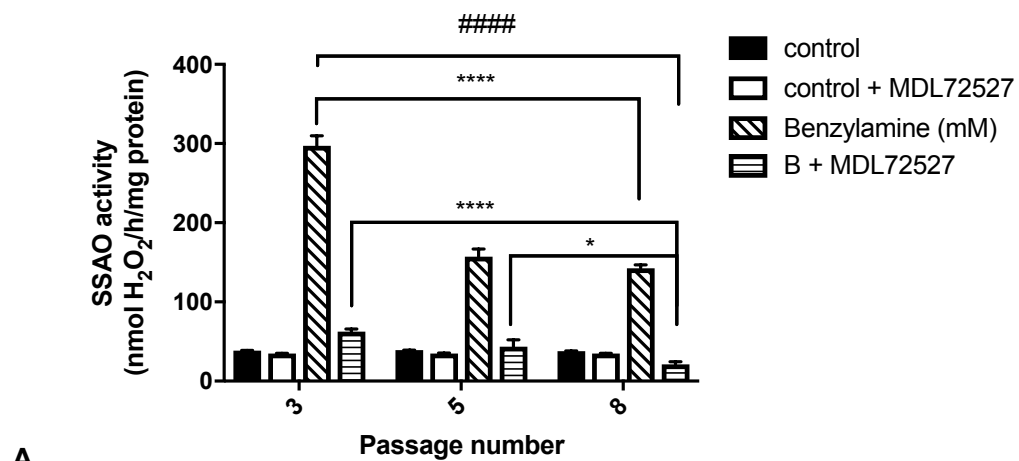


**Figure 48.** SSAO activity expressed as H<sub>2</sub>O<sub>2</sub> production (nmolH<sub>2</sub>O<sub>2</sub>/h/mg protein) in rat aortic VSMCs from passage 3, 4, 5, 6, 7, & 8. Cells were treated with reaction mixture containing 0.5mM SSAO substrate benzylamine (grey bars) and reaction mixture without substrate (control; solid bars). The activity was measured after 6h from addition of reaction mixture. The data was analysed by two-way ANOVA (\*\*\*\*p < 0.0001), followed by Tukey's multiple comparison test (\*\*\*\*p < 0.0001 for cells passage 3 vs 4, 5, 6, 7, & 8 after treatment with benzylamine; \*\*\*\*p < 0.0001 for cells passage 4 vs 5, 6, 7 & 8 after treatment with benzylamine); and Sidak's multiple comparison test (####p < 0.0001 for control vs 0.5mM benzylamine treated cells at each passage. The data is presented as means ± S.E.M. of five independent experiments with five replicates in each. The asterisk (\*) indicates statistical significance between early vs late passage cells treated with benzylamine. The hash (#) indicates statistical difference between control and benzylamine treated cells in different passages.

### **SSAO and LOX activity in rat aortic VSMCs from passage 3, 5 and 8.**

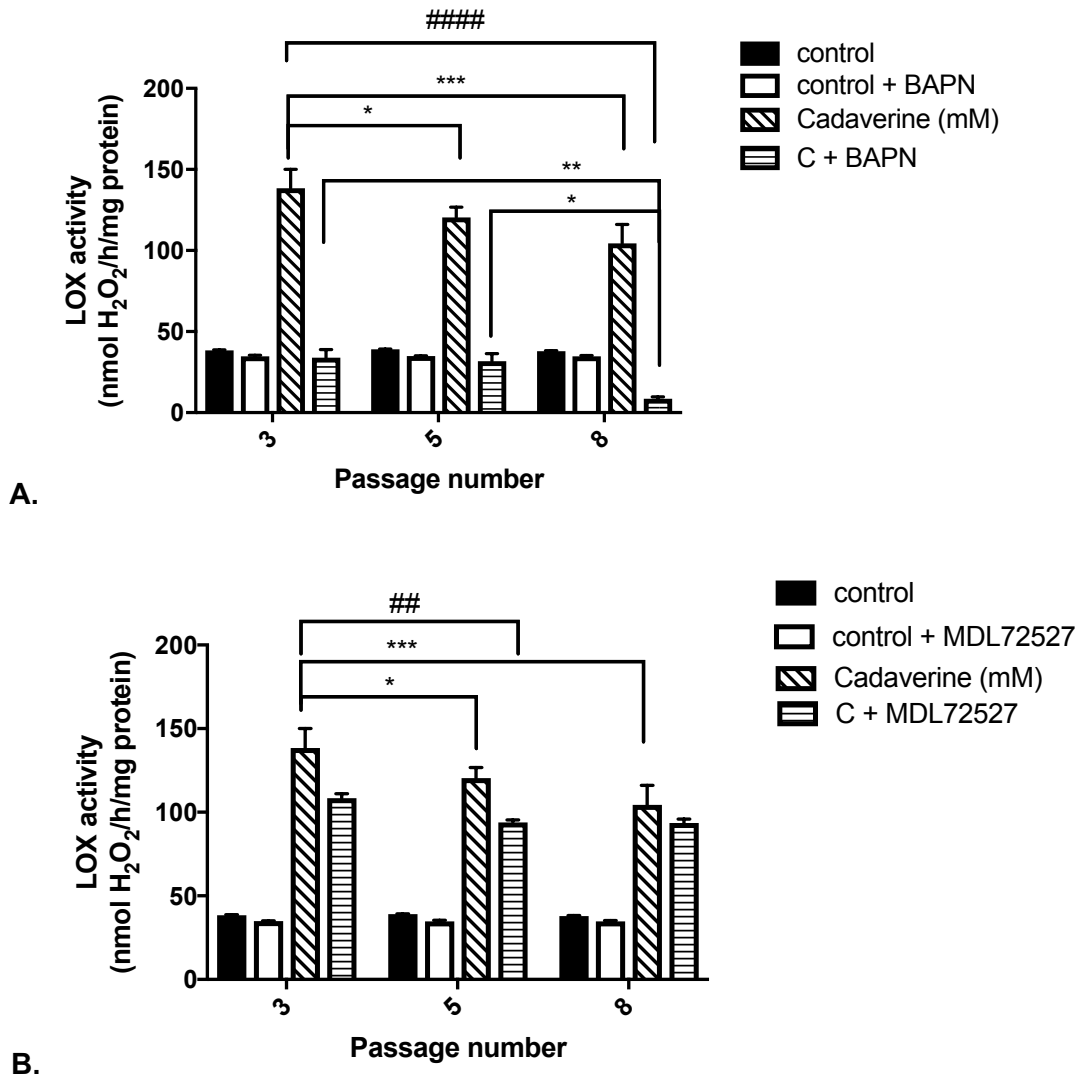
SSAO and LOX activity were compared in rat aortic VSMCs from passage 3, 5 and 8 with the Amplex<sup>®</sup> Red monoamine oxidase assay based on H<sub>2</sub>O<sub>2</sub> production. SSAO activity expressed as H<sub>2</sub>O<sub>2</sub> production (nmolH<sub>2</sub>O<sub>2</sub>/h/mg protein) was measured after 6h from addition of reaction mixture containing 860µl of 0.25M sodium phosphate buffer (pH7.4), 20µl Amplex<sup>®</sup> Red (20mM), 10µl horseradish peroxidase (200U/ml), 10µl clorgyline (0.5mM), and 200µl (0.5mM) benzylamine; reaction mixture containing 200µl (0.5mM) benzylamine + 10µl (100µM) MDL72527; reaction mixture without substrate (control) and reaction mixture without substrate + 10µl (100µM) MDL72527 (control + MDL72527) (A); or, reaction mixture containing 200µl (0.5mM) benzylamine; reaction mixture containing 200µl (0.5mM) benzylamine + 10µl (200µM) βAPN; reaction mixture without substrate (control) and reaction mixture without substrate + 10µl (200µM) βAPN (control + βAPN) (B).

Figure 49 presents detected SSAO activity in benzylamine treated cells, with and without the presence of MDL72527, and with and without the presence of  $\beta$ APN. For benzylamine and MDL72527 treated cells (Figure 49A) statistical difference was detected for cells at passage 3 vs 5 and 3 vs 8 after treatment with benzylamine (\*\*\*\* $p < 0.0001$ ); cells passage 3 vs 8 (\*\*\*\* $p < 0.0001$ ) and 5 vs 8 (\* $p < 0.05$ ) after treatment with benzylamine + MDL72527. Statistical difference was also detected between benzylamine and B + MDL72527 at passage 3, 5 and 8 (#### $p < 0.0001$ ). For benzylamine and  $\beta$ APN treated cells (Figure 49B) statistical difference was detected for cells at passage 3 vs 5 and 3 vs 8 after treatment with benzylamine (\*\*\*\* $p < 0.0001$ ); cells passage 3 vs 5 and 3 vs 8 (\*\*\*\* $p < 0.0001$ ) and cells passage 5 vs 8 (\* $p < 0.05$ ) after treatment with benzylamine +  $\beta$ APN. Statistical difference was also detected between benzylamine and B +  $\beta$ APN at passage 3 and 5. (#### $p < 0.0001$ ).



**Figure 49. SSAO activity expressed as H<sub>2</sub>O<sub>2</sub> production (nmolH<sub>2</sub>O<sub>2</sub>/h/mg protein) in rat aortic VSMCs from passage 3, 5, & 8. A) The cells were treated with reaction mixture containing 0.5mM benzylamine (B - hatched bars); 0.5mM benzylamine + 100μM MDL72527 (horizontal line bars); reaction mixture without benzylamine (control - solid bars) and reaction mixture without benzylamine + MDL72527 (control + MDL72527, open bars). The data was analyzed by two-way ANOVA (\*\*\*\*p < 0.0001), followed by Tukey's multiple comparison test (\*\*\*\*p < 0.0001 for cells passage 3 vs 5 and 3 vs 8 after treatment with benzylamine; \*\*\*\*p < 0.0001 for cells passage 3 vs 8 and \*p < 0.05 for cells passage 5 vs 8 after treatment with benzylamine + MDL72527; (#### p < 0.0001 for benzylamine vs B + MDL at passage 3, 5 and 8). B) The cells were treated with reaction mixture containing 0.5mM benzylamine (hatched bars); 0.5mM benzylamine + 200μM βAPN (horizontal line bars); reaction mixture without benzylamine (control - solid bars) and reaction mixture without benzylamine + βAPN (control + βAPN, open bars). The data was analyzed by two-way ANOVA (\*\*\*\*p < 0.0001), followed by Tukey's multiple comparison test (\*\*\*\*p < 0.0001 for cells passage 3 vs 5 and 3 vs 8 after treatment with benzylamine; \*\*\*\*p < 0.0001 for cells passage 3 vs 5 and 3 vs 8 and \*p < 0.05 for cells passage 5 vs 8 after treatment with benzylamine + βAPN); (####p < 0.0001 for benzylamine vs B + βAPN at passage 3 and 5). The data is presented as means ± S.E.M. of five independent experiments with five replicates in each. The asterisk (\*) indicates statistical significance between treatments at each passage. The hash (#) indicates statistical difference between combination of treatments (benzylamine vs B + MDL72527, or benzylamine vs B + βAPN) at each passage.**

LOX activity expressed as H<sub>2</sub>O<sub>2</sub> production was measured after 6h from addition of reaction mixture containing 860μl of 0.25M sodium phosphate buffer (pH 7.4), 20μl Amplex<sup>®</sup>Red (20mM), 10μl horseradish peroxidase (200U/ml), 10μl clorgyline (0.5mM – added to maintain consistency), and 200μl (0.5mM) cadaverine; reaction mixture containing 200μl (0.5mM) cadaverine + 10μl (200μM) βAPN, reaction mixture without substrate (control) and reaction mixture without substrate + 10μl (200μM) βAPN (control + βAPN) (A); or, reaction mixture containing 200μl (0.5mM) cadaverine; reaction mixture containing 200μl (0.5mM) cadaverine + 10μl (100μM) MDL72527, reaction mixture without substrate (control) and reaction mixture without substrate + 10μl (100μM) MDL72527 (control + MDL72527) (B). Figure 50 presents detected LOX activity in cadaverine treated cells, with and without the presence of MDL72527, and with and without the presence of βAPN. For cadaverine and βAPN treated cells (Figure 50A), statistical difference was detected for cells at passage 3 vs 5 (\*p < 0.05) and 3 vs 8 (\*\*\*p < 0.001) after treatment with cadaverine; cells passage 3 vs 8 (\*\*p < 0.01) and 5 vs 8 (\*p < 0.05) after treatment with cadaverine + βAPN. Statistical difference was also detected between cadaverine and C + βAPN at passage 3, 5 and 8 (#### p < 0.0001). For cadaverine and MDL72527 treated cells (Figure 50B) statistical difference was detected for cells at passage 3 vs 5 (\*p < 0.05) and 3 vs 8 (\*\*\*p < 0.001) after treatment with cadaverine. Statistical difference was also detected between cadaverine and C + MDL72527 at passage 3 and 5 (## p < 0.01) (Figure 50B).



**Figure 50.** LOX activity expressed as H<sub>2</sub>O<sub>2</sub> production (nmolH<sub>2</sub>O<sub>2</sub>/h/mg protein) in rat aortic VSMCs from passage 3, 5, & 8. **A)** The cells were treated with reaction mixture containing 0.5mM cadaverine (hatched bars); 0.5mM cadaverine + 200μM βAPN (horizontal line bars); reaction mixture without cadaverine (control - solid bars) and reaction mixture without cadaverine + 200μM βAPN (control + βAPN, open bars). The data was analyzed by two-way ANOVA (\*\*\*\*p < 0.0001), followed by Tukey's multiple comparison test (\*p < 0.05 for cells passage 3 vs 5 and \*\*\*p < 0.001 for cells passage 3 vs 8 after treatment with cadaverine; \*\*p < 0.01 for cells passage 3 vs 8 and \*p < 0.05 for cells passage 5 vs 8 after treatment with cadaverine + βAPN); (####p < 0.0001 for cadaverine vs C + βAPN at passage 3, 5 and 8). **B)** The cells were treated with reaction mixture containing 0.5mM cadaverine (hatched bars); 0.5mM cadaverine + 100μM MDL72527 (horizontal line bars); reaction mixture without cadaverine (control - solid bars) and reaction mixture without cadaverine + MDL72527 (control + MDL72527, open bars). The data was analyzed by two-way ANOVA (\*\*\*p < 0.001), followed by Tukey's multiple comparison test (\*p < 0.05 for cells passage 3 vs 5 and \*\*\*p < 0.001 for cells passage 3 vs 8 after treatment with cadaverine); (##p < 0.01 for cadaverine vs C + MDL72527 at passage 3 and 5). The data is presented as means ± S.E.M. of five independent experiments with five replicates in each. The asterisk (\*) indicates statistical significance between treatments at each passage. The hash (#) indicates statistical difference between combination of treatments (cadaverine vs C + βAPN, or cadaverine vs C + MDL72527) at each passage.

### SSAO kinetics in rat aortic VSMCs (passage 3, 5 and 8) in the presence of $\beta$ APN

SSAO kinetic parameters were assessed in the presence of the irreversible LOX inhibitor,  $\beta$ APN. The cells samples were treated with reaction mixture containing 860 $\mu$ l of 0.25M sodium phosphate buffer (pH7.4), 20 $\mu$ l Amplex<sup>®</sup> Red (20mM), 10 $\mu$ l horseradish peroxidase (200U/ml), 10 $\mu$ l clorgyline (0.5mM), 200 $\mu$ l different benzylamine concentrations (0, 0.02, 0.05, 0.1, 0.5, 1 and 5mM) and 10 $\mu$ l (200 $\mu$ M)  $\beta$ APN, as explained in the methods section 3.3.2. Figure 51 demonstrates the highest activity ( $V_{max}$ ) of SSAO and its affinity ( $K_m$ ) for the substrate benzylamine in the presence of LOX inhibitor –  $\beta$ APN, in rat aortic VSMCs from passage 3 (A), 5 (B), and 8 (C).

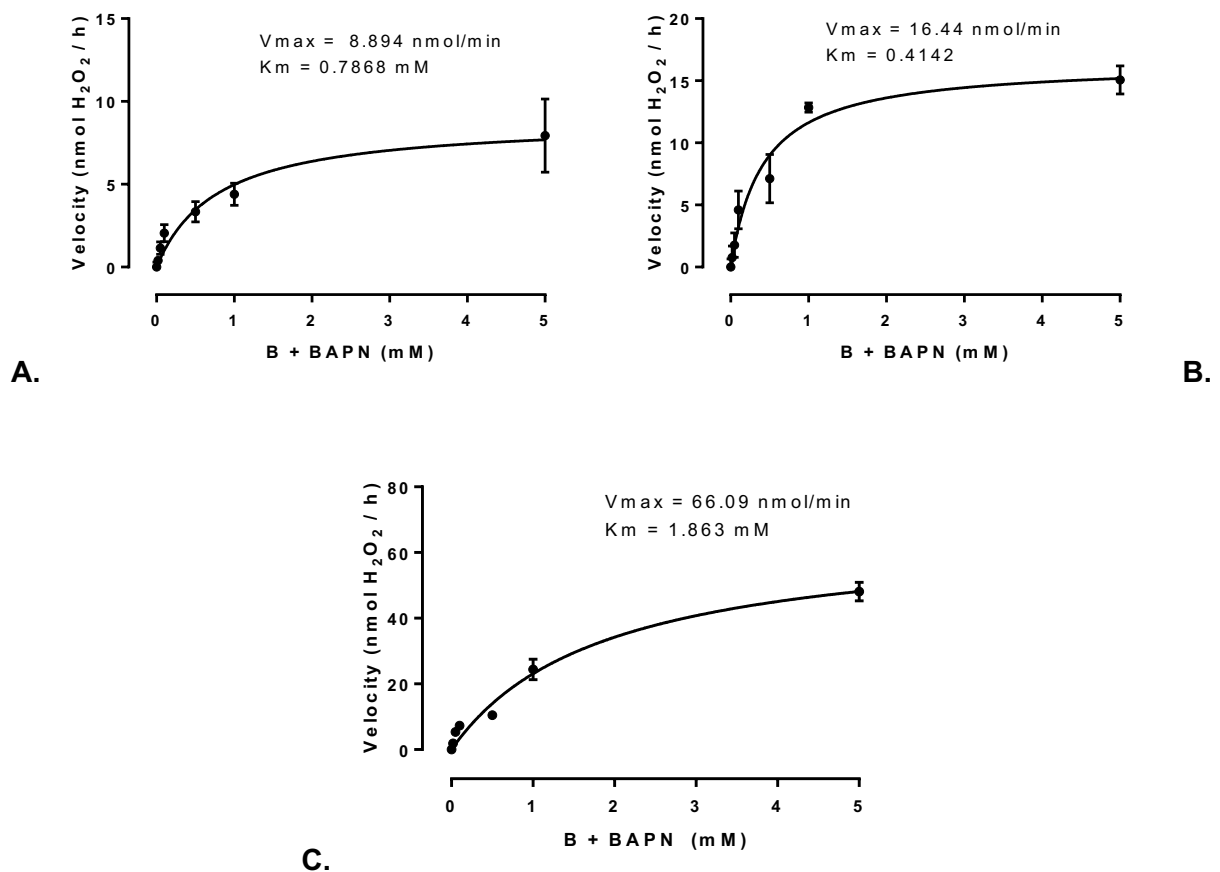
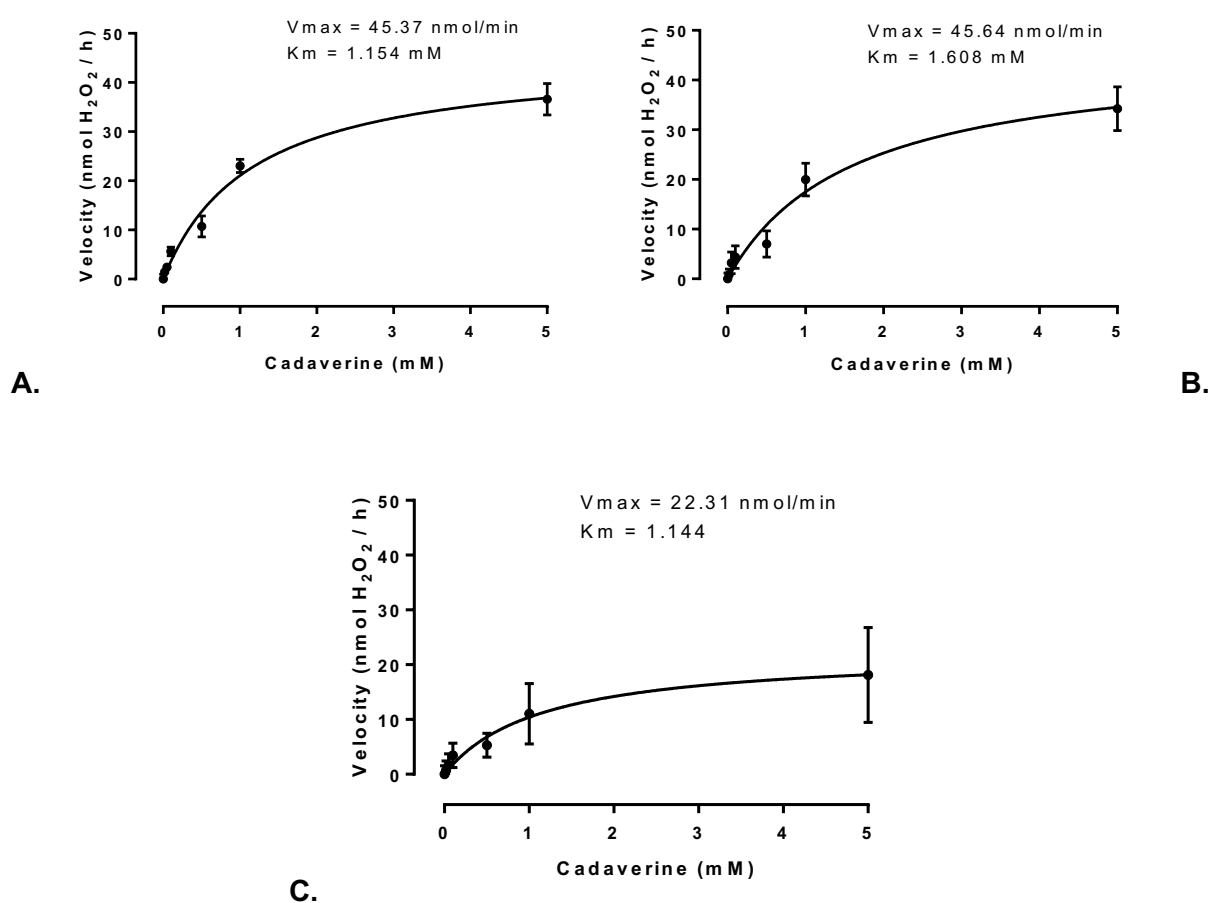


Figure 51. SSAO kinetic parameters in the presence of 200 $\mu$ M  $\beta$ APN. A) passage 3, B) passage 5, C) passage 8. The data was analyzed with the non-linear regression model of Michaelis-Menten  $Y = V_{max} * X / (K_m + X)$  and is presented as means  $\pm$  S.E.M. of five independent experiments with five replicates in each.

### **LOX kinetics in rat aortic VSMCs (passage 3, 5 and 8)**

LOX kinetic parameters were assessed in rat aortic VSMCs from passage 3, 5 and 8. The cells samples were treated with reaction mixture containing 860 $\mu$ l of 0.25M sodium phosphate buffer (pH7.4), 20 $\mu$ l Amplex<sup>®</sup> Red (20mM), 10 $\mu$ l horseradish peroxidase (200U/ml), 10 $\mu$ l clorgyline (0.5mM – added to maintain consistency), and 200 $\mu$ l different cadaverine concentrations (0, 0.02, 0.05, 0.1, 0.5, 1 and 5mM), as explained in the methods section 3.3.2. Figure 52 demonstrates the highest activity (Vmax) of LOX and its affinity (Km) for the substrate cadaverine in rat aortic VSMCs from passage 3 (A), 5 (B), and 8 (C).



**Figure 52. LOX kinetic parameters in rat aortic VSMCs. A) passage 3, B) passage 5, C) passage 8. The data was analyzed with the non-linear regression model of Michaelis-Menten  $Y = V_{max} * X / (K_m + X)$  and is presented as means  $\pm$  S.E.M. of five independent experiments with five replicates in each.**

## Western blot analysis and densitometry

The protein expression of VAP-1 and Pro-LOX in rat aortic VSMCs was analyzed with western blot analysis, as explained in the methods section 2.2.13. Cell samples from passage 3, 5 and 8 were lysed without being previously treated (control - A), or after 1h treatment with 200 $\mu$ M  $\beta$ APN (B).  $\beta$ -actin from each cell sample was detected to normalize the level of protein. The protein was quantified using ImageJ software, as explained in the methods section 2.2.14.

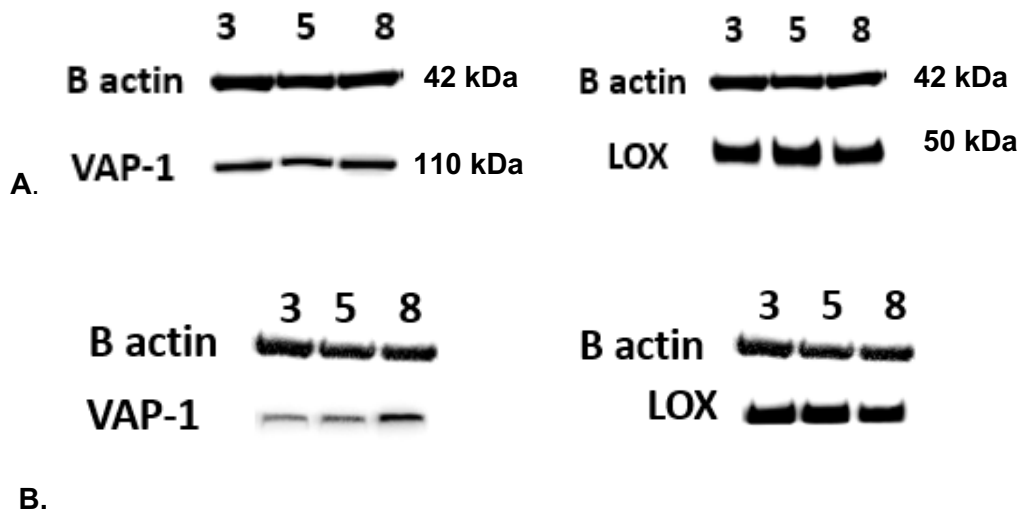


**Figure 53. Western blot analysis of VAP-1 and Pro-LOX in rat aortic VSMCs from passage 3, 5 and 8 (n = 3). A) Detection of VAP-1 and Pro-LOX protein in non-treated (control) rat aortic VSMCs. B) Detection of VAP-1 and Pro-LOX protein in  $\beta$ APN treated rat aortic VSMCs.  $\beta$ -actin was used as loading control.**

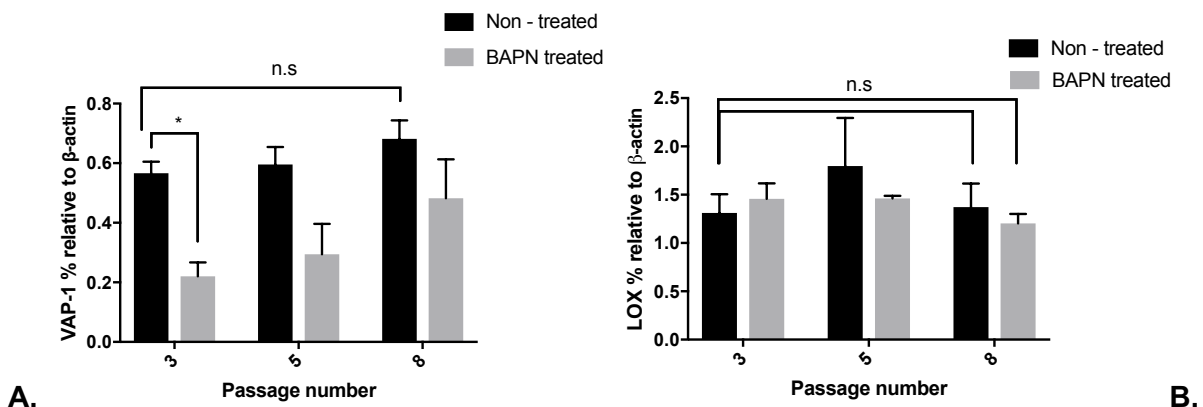


**Figure 54.** VAP-1 (A) and Pro-LOX (B) protein expression (expressed as percentage relative to  $\beta$ -actin) in non-treated (control: black bars) and  $\beta$ APN treated (grey bars) rat aortic VSMCs from passage 3, 5 and 8.  $\beta$ APN treated cells were exposed to 200 $\mu$ M  $\beta$ APN 1h prior to lysing. The optical density was quantified using the image densitometer ImageJ. The data was analyzed by two-way ANOVA (\*\* $p < 0.001$ ), followed by Sidak's and Tukey's multiple comparison tests. There was no significant difference in VAP-1 expression over passage ( $p > 0.05$ ). Significant difference in VAP-1 expression was detected between non-treated vs  $\beta$ APN treated cells at passage 3 (\* $p < 0.05$ ) (A). There was no significant difference in Pro-LOX expression over passage ( $p > 0.05$ ), and between non-treated vs  $\beta$ APN treated cells at passage 3, 5 and 8 ( $p > 0.05$ ) (B). The data is presented as means  $\pm$  S.E.M. of three independent experiments with three replicates in each. The asterisk (\*) indicates statistical significance compared to control at each passage.

The protein expression of the smooth muscle cells markers ACTA2 and SM22 $\alpha$ , was also analyzed with western blot analysis, as explained in the methods section 2.2.13. Cell samples from passage 3, 5 and 8 were lysed without being previously treated (control - A), or after 1h treatment with 200 $\mu$ M  $\beta$ APN (B).  $\beta$ -actin from each cell sample was detected to normalize the level of protein. The protein was quantified using ImageJ software, as explained in the methods section 2.2.14.

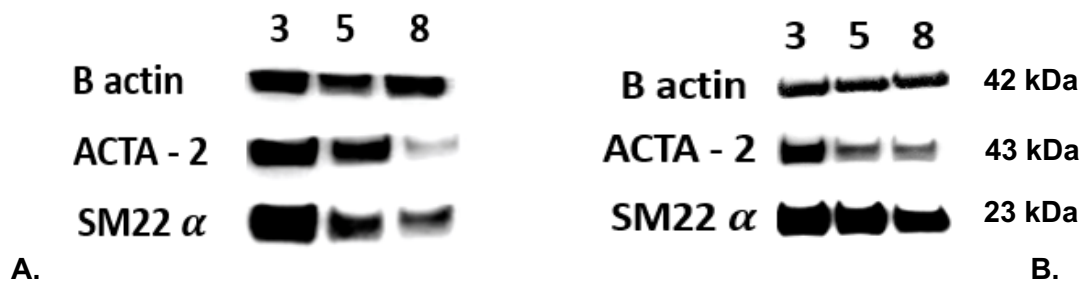


**Figure 55.** Western blot analysis of ACTA2 and SM22 $\alpha$  in rat aortic VSMCs from passage 3, 5 and 8 ( $n = 3$ ). A) Detection of ACTA2 and SM22 $\alpha$  protein in non-treated (control) rat aortic VSMCs. B) Detection of VAP-1 and LOX protein in  $\beta$ APN treated rat aortic VSMCs.  $\beta$ -actin was used as loading control.

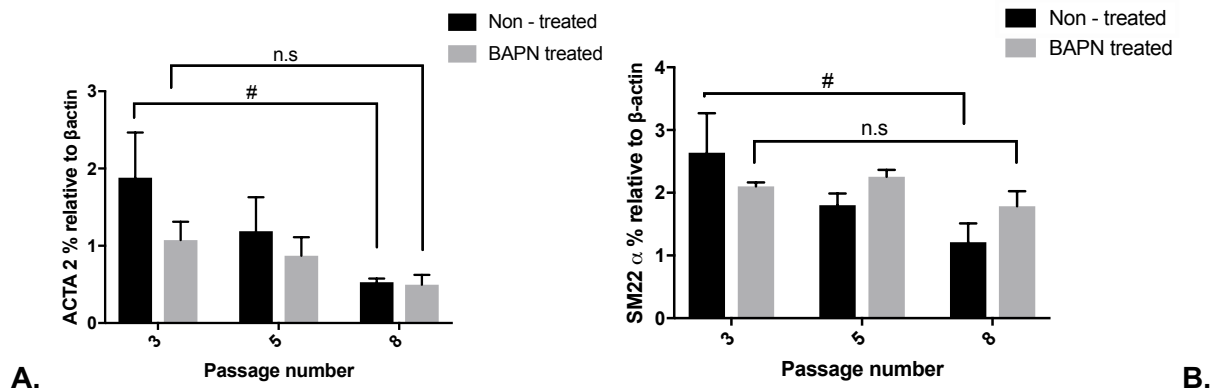


**Figure 56.** ACTA2 (A) and SM22α (B) protein expression (expressed as percentage relative to β-actin) in non-treated (control) and βAPN treated rat aortic VSMCs from passage 3, 5 and 8. βAPN treated cells were exposed to 200μM βAPN 1h prior to lysing. The optical density was quantified using the image densitometer ImageJ. The data was analyzed by two-way ANOVA (\*p < 0.05), followed by Sidak's and Tukey's multiple comparison tests. Significant difference in ACTA2 expression was detected in non-treated cells over passage (#p < 0.05 for 3 vs 8). There was no significant difference in ACTA2 expression between non-treated vs βAPN treated cells (p > 0.05) (A). Significant difference in SM22α expression was detected in non-treated cells over passage (#p < 0.05 for 3 vs 8), There was no significant difference in SM22α expression detected between non-treated vs βAPN treated cells (p > 0.05) (B). The data is presented as means ± S.E.M. of three independent experiments with three replicates in each. The hash (#) indicates statistical significance between passages.

The protein expression of PDGFRβ was analyzed with western blot analysis, as explained in the methods section 2.2.13. Cell samples from passage 3, 5 and 8 were lysed without being previously treated (control - A), or after 1h treatment with 200μM βAPN (B). β-actin from each cell sample was detected to normalize the level of protein. The protein was quantified using ImageJ software, as explained in the methods section 2.2.14.



**Figure 57.** Western blot analysis of PDGFR β in rat aortic VSMCs from passage 3, 5 and 8 (n = 3). A) Detection of PDGFR β protein in non-treated (control) rat aortic VSMCs. B) Detection of PDGFR β protein in βAPN treated rat aortic VSMCs. β-actin was used as loading control.

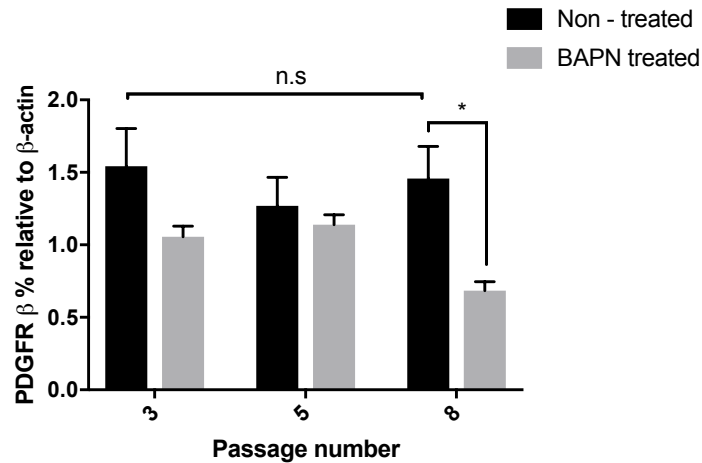


**Figure 58.** PDGFR $\beta$  protein expression (expressed as percentage relative to  $\beta$ -actin) in non-treated (control) and  $\beta$ APN treated rat aortic VSMCs from passage 3, 5 and 8.  $\beta$ APN treated cells were exposed to 200 $\mu$ M  $\beta$ APN for 1h prior lysing. The optical density was quantified using the image densitometer ImageJ. The data was analyzed by two-way ANOVA (\*\* $p < 0.01$ ), followed by Sidak's and Tukey's multiple comparison tests. There was no significant difference in PDGFR $\beta$  expression over passage ( $p > 0.05$ ). Significant difference in PDGFR $\beta$  expression was detected between non-treated vs  $\beta$ APN treated cells at passage 8 (\* $p < 0.05$ ). The data is presented as means  $\pm$  S.E.M. of three independent experiments with three replicates in each. The asterisk (\*) indicates statistical significance compared to control at each passage.

Western blot analysis was further utilized to detect the expression of VAP-1, Pro-LOX, ACTA2, SM22 $\alpha$  and PDGFR $\beta$  in rat aortic VSMCs previously treated with MDL72527. Cell samples from passage 3, 5 and 8 were lysed without being previously treated (control - A), or after 1h treatment with 100 $\mu$ M MDL72527 (B).  $\beta$ -actin from each cell sample was detected to normalize the level of protein. The protein was quantified using ImageJ software, as explained in the methods section 2.2.14.

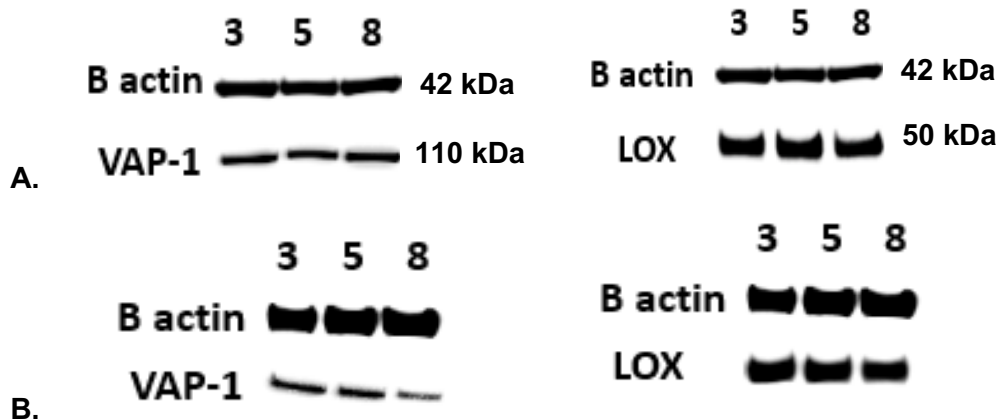


**Figure 59.** Western blot analysis of VAP-1 and Pro-LOX in rat aortic VSMCs from passage 3, 5 and 8 ( $n = 3$ ). A) Detection of VAP-1 and Pro-LOX protein in non-treated (control) rat aortic VSMCs. B) Detection of VAP-1 and Pro-LOX protein in MDL72527 treated rat aortic VSMCs.  $\beta$ -actin was used as loading control.

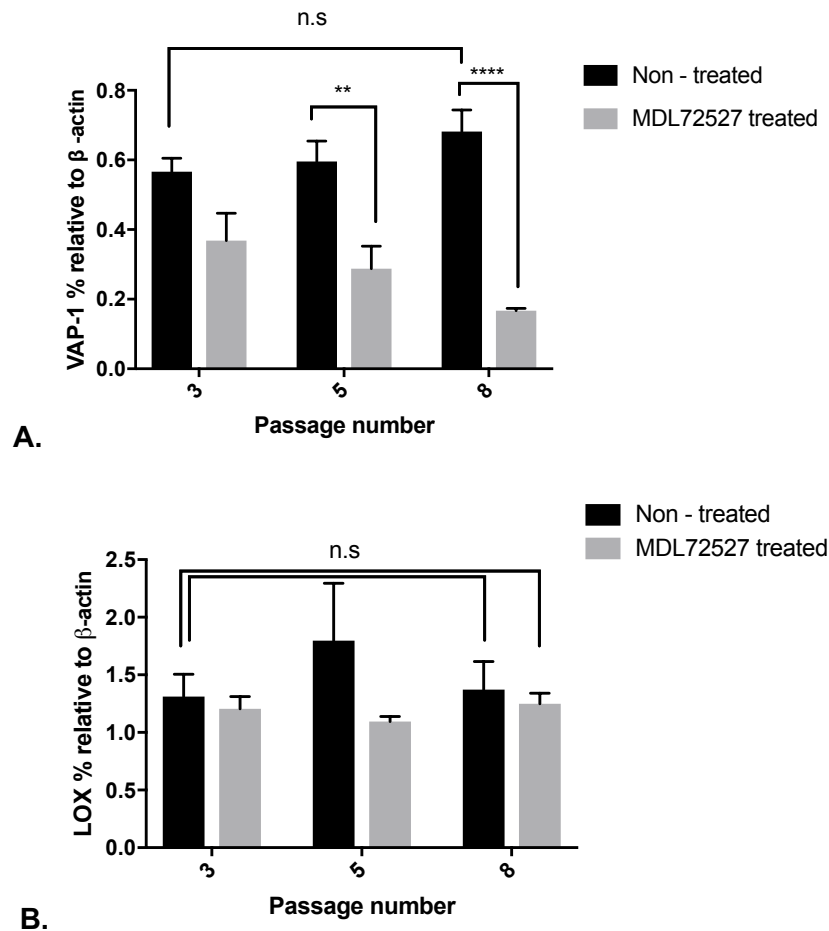


**Figure 60. VAP-1 (A) and Pro-LOX (B) protein expression (expressed as percentage relative to  $\beta$ -actin) in non-treated (control: black bars) and MDL72527 treated (grey bars) rat aortic VSMCs from passage 3, 5 and 8. MDL72527 treated cells were exposed to 100 $\mu$ M MDL72527 1h prior to lysing. The optical density was quantified using the image densitometer ImageJ. The data was analyzed by two-way ANOVA (\*\*\*\* $p < 0.0001$ ), followed by Sidak's and Tukey's multiple comparison tests. There was no significant difference in VAP-1 expression over passage ( $p > 0.05$ ). Significant difference in VAP-1 expression was detected between non-treated vs MDL72527 treated cells at passage 5 (\*\* $p < 0.01$ ) and passage 8 (\*\*\*\* $p < 0.0001$ ) (A). There was no significant difference in Pro-LOX expression over passage, and between non-treated vs MDL72572 treated cells at passage 3, 5 and 8 ( $p > 0.05$ ) (B). The data is presented as means  $\pm$  S.E.M. of three independent experiments with three replicates in each. The asterisk (\*) indicates statistical significance compared to control at each passage.**

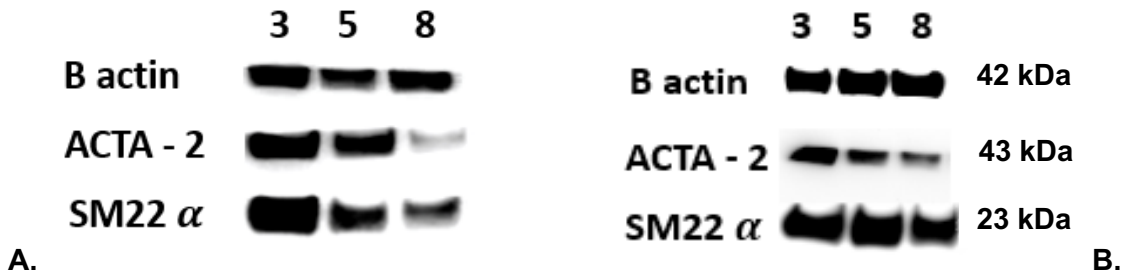


Figure 61. Western blot analysis of ACTA2 and SM22 $\alpha$  in rat aortic VSMCs from passage 3, 5 and 8 (n = 3). A) Detection of ACTA2 and SM22 $\alpha$  protein in non-treated (control) rat aortic VSMCs. B) Detection of ACTA2 and SM22 $\alpha$  protein in MDL72527 treated rat aortic VSMCs.  $\beta$ -actin was used as loading control.

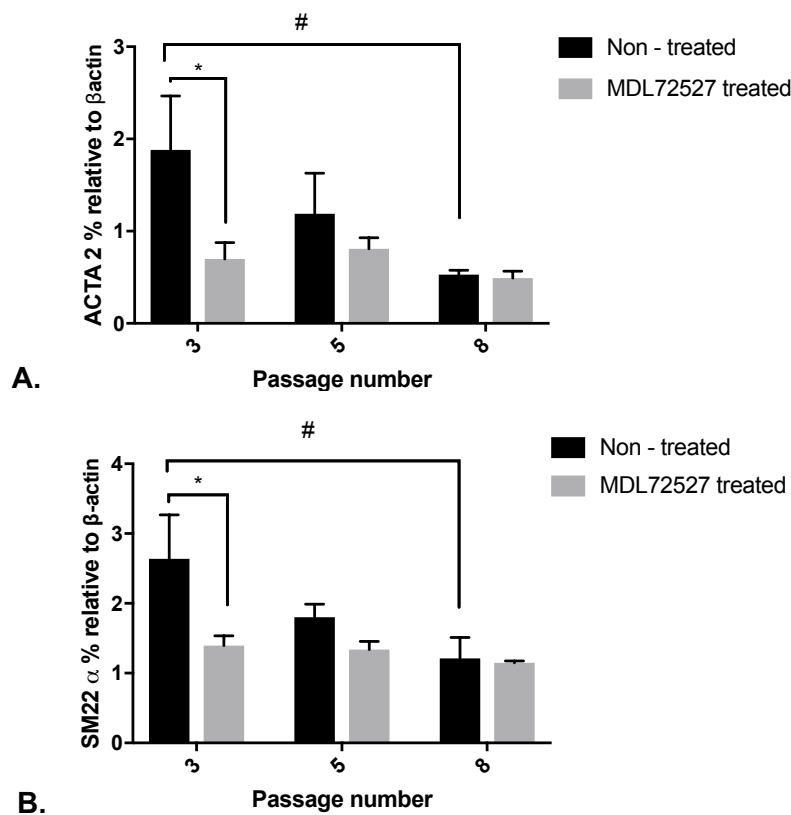


Figure 62. ACTA2 (A) and SM22 $\alpha$  (B) protein expression (expressed as percentage relative to  $\beta$ -actin) in non-treated (control) and MDL72527 treated rat aortic VSMCs from passage 3, 5 and 8. MDL72527 treated cells were exposed to 100 $\mu$ M MDL72527 1h prior to lysing. The optical density was quantified using the image densitometer ImageJ. The data was analyzed by two-way ANOVA (\* $p < 0.05$ ), followed by Sidak's and Tukey's multiple comparison tests. Significant difference in ACTA2 expression was detected between non-treated cells over passage (# $p < 0.05$  for 3 vs 8), and between non-treated vs MDL72527 treated cells at passage 3 (\* $p < 0.05$ ) (A); Significant difference in SM22 $\alpha$  expression was detected between non-treated cells over passage (# $p < 0.05$  for 3 vs 8), and between non-treated vs MDL72527 treated cells at passage 3 (\* $p < 0.05$ ) (B). The data is presented as means  $\pm$  S.E.M. of three independent experiments with three replicates in each. The asterisk (\*) indicates statistical significance compared to control at each passage. The hash (#) indicates statistical significance between passages.

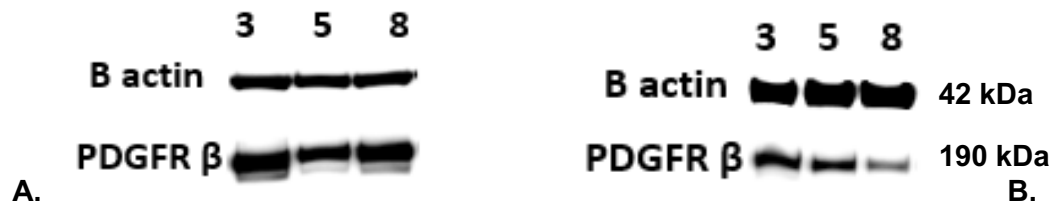


Figure 63. Western blot analysis of PDGFR $\beta$  in rat aortic VSMCs from passage 3, 5 and 8 (n = 3). A) Detection of PDGFR $\beta$  protein in non-treated (control) rat aortic VSMCs. B) Detection of PDGFR $\beta$  protein in MDL72527 treated rat aortic VSMCs.  $\beta$ -actin was used as loading control.

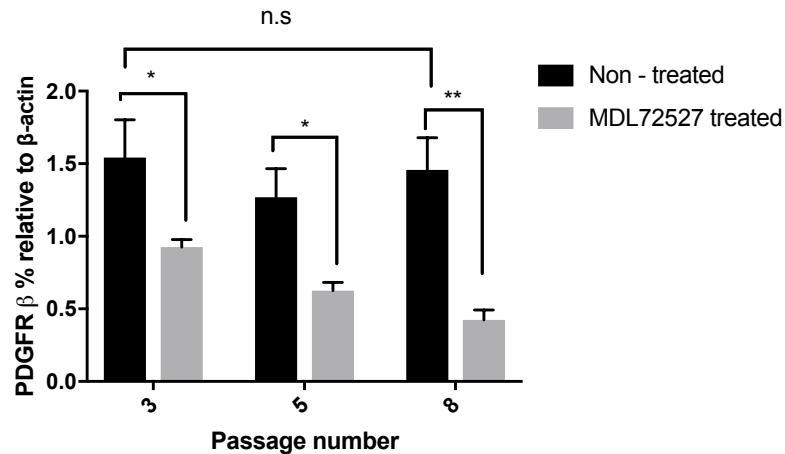


Figure 64. PDGFR $\beta$  protein expression (expressed as percentage relative to  $\beta$ -actin) in non-treated (control) and MDL72527 treated rat aortic VSMCs from passage 3, 5 and 8. MDL72527 treated cells were exposed to 100 $\mu$ M MDL72527 1h prior to lysing. The optical density was quantified using the image densitometer ImageJ. The data was analyzed by two-way ANOVA (\*\* $p$  < 0.001), followed by Sidak's and Tukey's multiple comparison test. There was no significant difference in PDGFR $\beta$  expression over passage ( $p$  > 0.05). Significant difference in PDGFR $\beta$  expression was detected between non-treated vs MDL72527 treated cells at passage 3 (\* $p$  < 0.05), passage 5 (\* $p$  < 0.05), and passage 8 (\*\* $p$  < 0.01). The data is presented as means  $\pm$  S.E.M. of three independent experiments with three replicates in each. The asterisk (\*) indicates statistical significance compared to control at each passage.

Western blot analysis was also utilized to detect the expression of VAP-1, Pro-LOX, ACTA2, SM22 $\alpha$  and PDGFR $\beta$  in rat aortic VSMCs previously treated with benzylamine or cadaverine. Cell samples from passage 3, 5 and 8 were lysed without being previously treated (control - A), or after 6h treatment with 0.5mM benzylamine (B), or 0.5mM cadaverine (C) respectively.  $\beta$ -actin from each cell sample was detected to normalize the level of protein. The protein was quantified using ImageJ software, as explained in the methods section 2.2.14.



**Figure 65.** Western blot analysis of VAP-1 and Pro-LOX in rat aortic VSMCs from passage 3, 5 and 8 (n = 3). **A)** Detection of VAP-1 and Pro-LOX protein in non-treated (control) rat aortic VSMCs. **B)** Detection of VAP-1 and Pro-LOX protein in benzylamine treated rat aortic VSMCs. **C)** Detection of VAP-1 and Pro-LOX protein in cadaverine treated rat aortic VSMCs.  $\beta$ -actin was used as loading control.

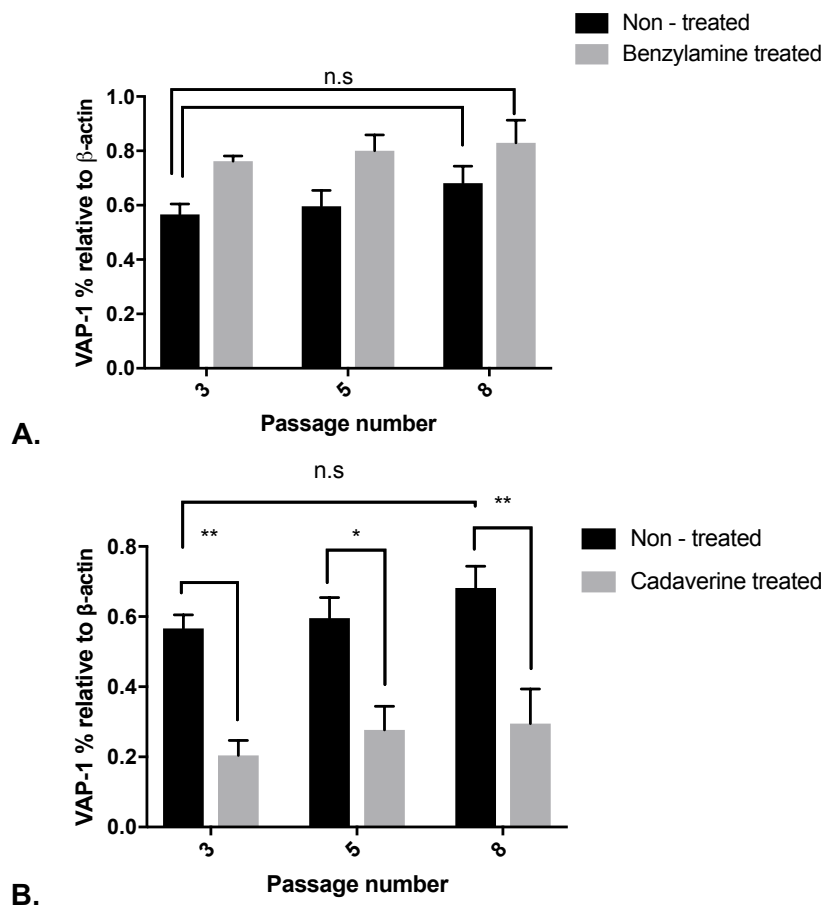


Figure 66. VAP-1 protein expression (expressed as percentage relative to  $\beta$ -actin) in (A) benzylamine (grey bars) and (B) cadaverine (gray bars) treated cells comparing to non-treated (control: black bars) rat aortic VSMCs from passage 3, 5 and 8. Benzylamine and cadaverine treated cells were exposed to 0.5mM benzylamine or cadaverine 6h prior to lysing. The optical density was quantified using the image densitometer ImageJ. data was analyzed by two-way ANOVA (\*\*\*\* $p < 0.0001$ ), followed by Sidak's and Tukey's multiple comparison tests. There was no significant difference detected in VAP-1 expression over passage, and in non-treated vs benzylamine treated cells ( $p > 0.05$ ) (A). There was no significant difference in VAP-1 expression over passage ( $p > 0.05$ ). Significant difference in VAP-1 expression was detected between non-treated vs cadaverine treated cells at passage 3 (\*\* $p < 0.01$ ), passage 5 (\* $p < 0.05$ ) and passage 8 (\*\* $p < 0.01$ ) (B). The data is presented as means  $\pm$  S.E.M. of three independent experiments with three replicates in each. The asterisk (\*) indicates statistical significance compared to control at each passage.

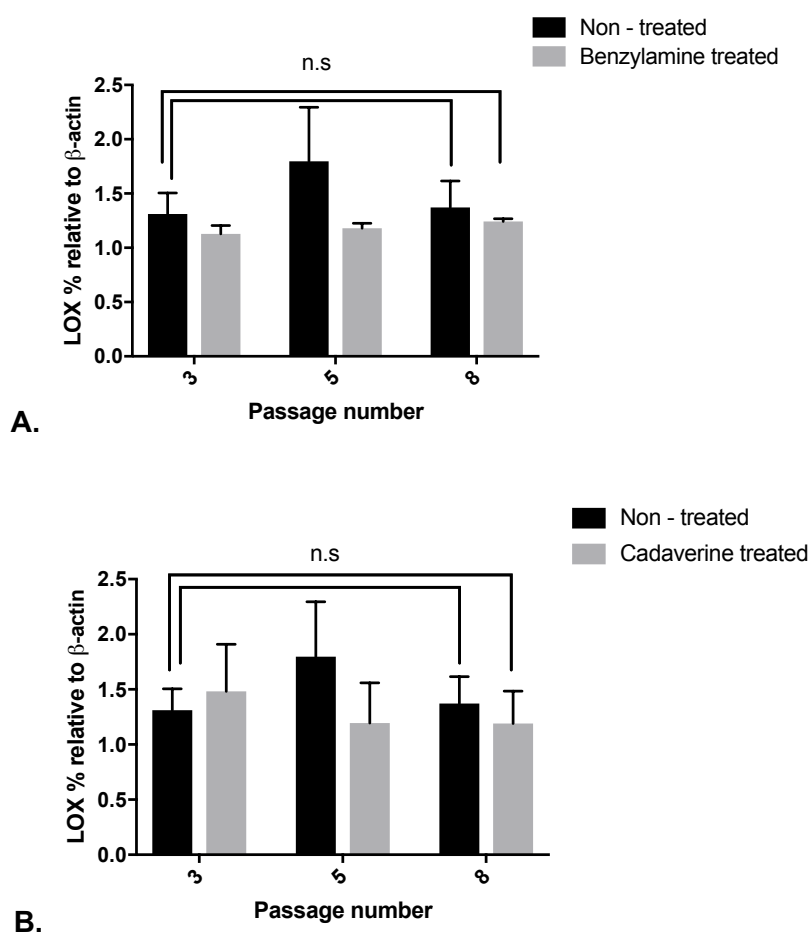


Figure 67. Pro-LOX protein expression (expressed as percentage relative to  $\beta$ -actin) in (A) benzylamine (grey bars) and (B) cadaverine (gray bars) treated cells comparing to non-treated (control: black bars) rat aortic VSMCs from passage 3, 5 and 8. Benzylamine and cadaverine treated cells were exposed to 0.5mM benzylamine or cadaverine 6h prior to lysing. The optical density was quantified using the image densitometer ImageJ. The data was analyzed by two-way ANOVA, followed by Sidak's and Tukey's multiple comparison test. There was no significant difference in Pro-LOX expression over passage, and between non-treated vs benzylamine and vs cadaverine treated cells ( $p > 0.05$ ) (A & B). The data is presented as means  $\pm$  S.E.M. of three independent experiments with three replicates in each.

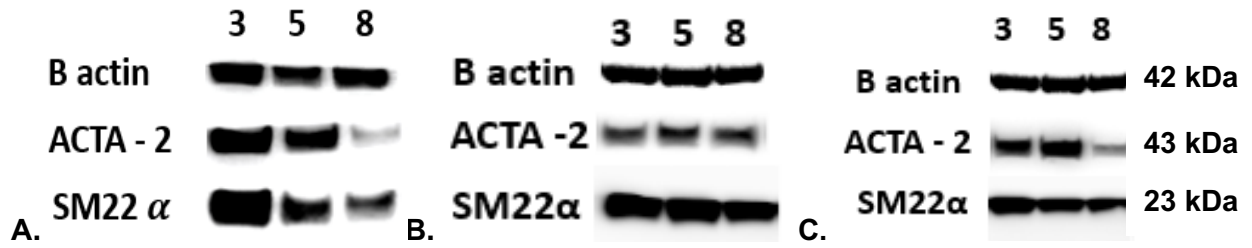


Figure 68. Western blot analysis of ACTA2 and SM22 $\alpha$  in rat aortic VSMCs from passage 3, 5 and 8 (n = 3). A) Detection of ACTA2 and SM22 $\alpha$  protein in non-treated (control) rat aortic VSMCs. B) Detection of ACTA2 and SM22 $\alpha$  protein in benzylamine treated rat aortic VSMCs. C) Detection of ACTA2 and SM22 $\alpha$  protein in cadaverine treated rat aortic VSMCs.  $\beta$ -actin was used as loading control.

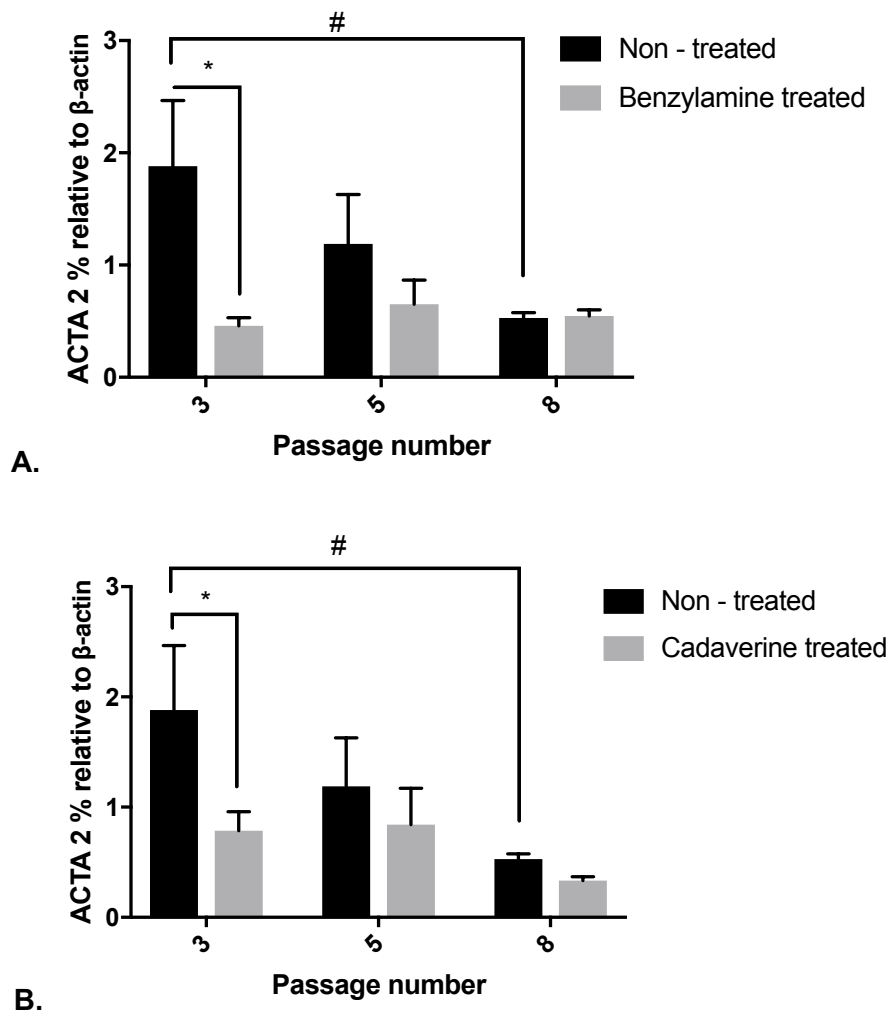


Figure 69. ACTA2 protein expression (expressed as percentage relative to  $\beta$ -actin) in (A) benzylamine (grey bars) and (B) cadaverine (gray bars) treated cells comparing to non-treated (control: black bars) rat aortic VSMCs from passage 3, 5 and 8. Benzylamine and cadaverine treated cells were exposed to 0.5mM benzylamine or cadaverine 6h prior to lysing. The optical density was quantified using the image densitometer ImageJ. The data was analyzed by two-way ANOVA (\* $p < 0.05$ ), followed by Sidak's and Tukey's multiple comparison tests. Significant difference in ACTA2 expression was detected in non-treated cells over passage (# $p < 0.05$  for 3 vs 8), and between non-treated vs benzylamine treated cells at passage 3 (\* $p < 0.05$ ) (A). Significant difference in ACTA2 expression was detected in non-treated cells over passage (# $p < 0.05$  for 3 vs 8), and between non-treated vs cadaverine treated cells at passage 3 (\* $p < 0.05$ ) (B). The data is presented as means  $\pm$  S.E.M. of three independent experiments with three replicates in each. The asterisk (\*) indicates statistical significance compared to control at each passage. The hash (#) indicates statistical significance between passages.

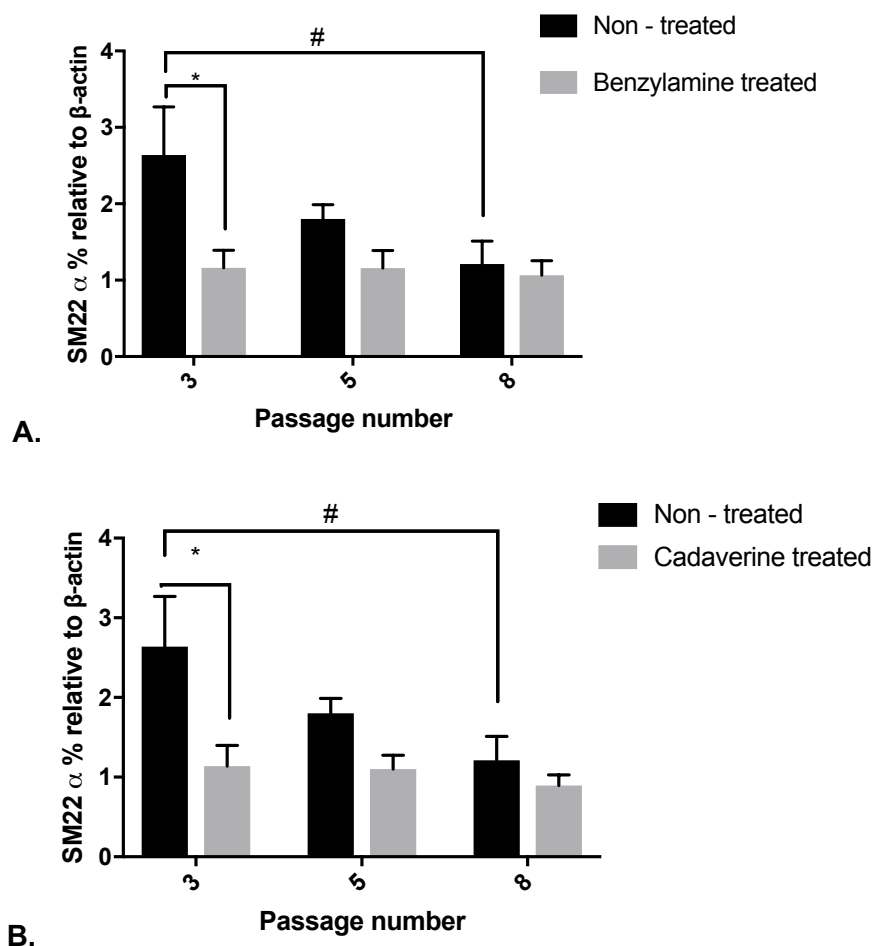


Figure 70. SM22 $\alpha$  protein expression (expressed as percentage relative to  $\beta$ -actin) in (A) benzylamine (grey bars) and (B) cadaverine (gray bars) treated cells comparing to non-treated (control: black bars) rat aortic VSMCs from passage 3, 5 and 8 (n = 3). Benzylamine and cadaverine treated cells were exposed to 0.5mM benzylamine or cadaverine 6h prior to lysing. The optical density was quantified using the image densitometer ImageJ. The data are presented as a percentage of SM22 $\alpha$  relative to  $\beta$ -actin. The data was analyzed by two-way ANOVA (\*\*p < 0.01), followed by Sidak's and Tukey's multiple comparison tests. Significant difference in SM22 $\alpha$  expression was detected over passage (#p < 0.05 for 3 vs 8), and between non-treated vs benzylamine treated cells at passage 3 (\*p < 0.05) (A). Significant difference in SM22 $\alpha$  expression was detected over passage (#p < 0.05 for 3 vs 8), and between non-treated vs cadaverine treated cells at passage 3 (\*p < 0.05) (B). The data is presented as means  $\pm$  S.E.M. of three independent experiments with three replicates in each. The asterisk (\*) indicates statistical significance compared to control at each passage. The hash (#) indicates statistical significance between passages.

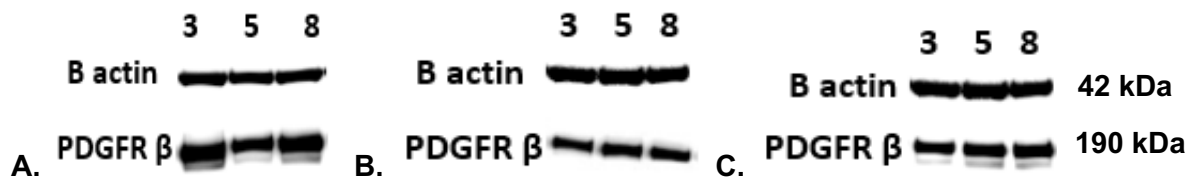
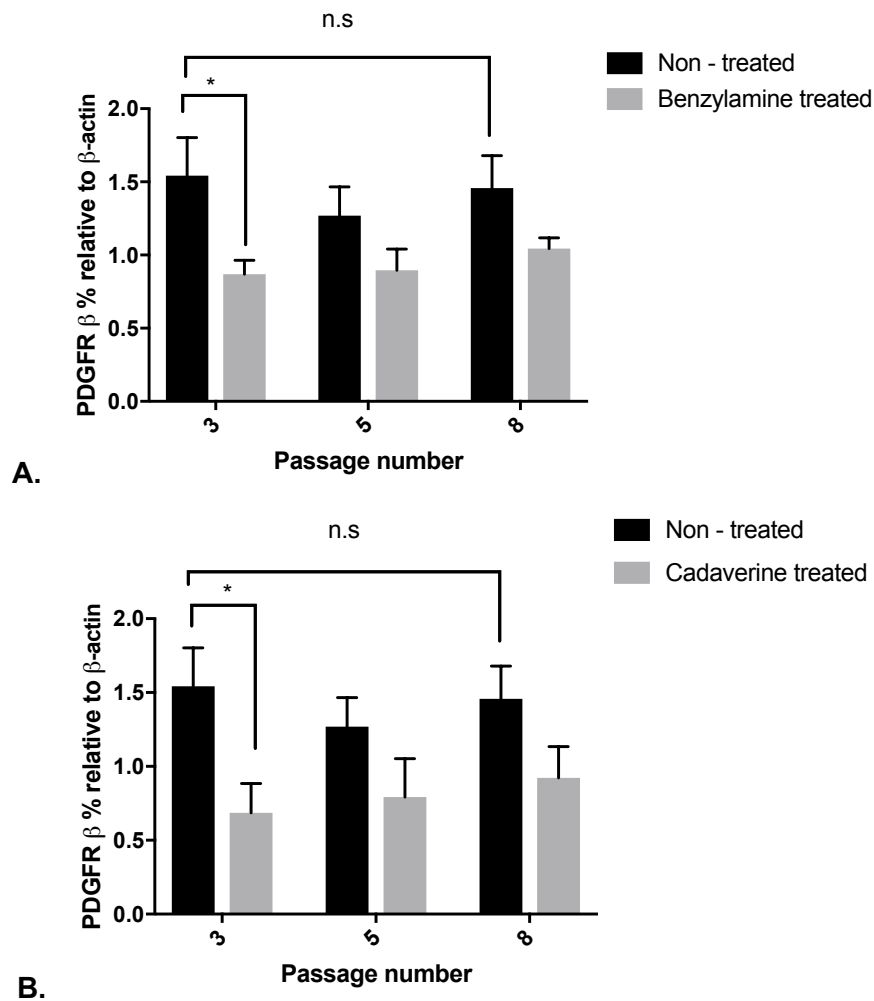


Figure 71. Western blot analysis of PDGFR  $\beta$  in rat aortic VSMCs from passage 3, 5 and 8 (n = 3). A) Detection of PDGFR  $\beta$  protein in non-treated (control) rat aortic VSMCs. B) Detection of PDGFR  $\beta$  protein in benzylamine treated rat aortic VSMCs. C) Detection of PDGFR  $\beta$  protein in cadaverine treated rat aortic VSMCs.  $\beta$ -actin was used as loading control.



**Figure 72. PDGFR $\beta$  protein expression (expressed as percentage relative to  $\beta$ -actin) in (A) benzylamine (grey bars) and (B) cadaverine (gray bars) treated cells comparing to non-treated (control: black bars) rat aortic VSMCs from passage 3, 5 and 8. Benzylamine and cadaverine treated cells were exposed to 0.5mM benzylamine or cadaverine 6h prior to lysing. The optical density was quantified using the image densitometer ImageJ. The data was analyzed by two-way ANOVA (\*\* $p < 0.01$ ), followed by Sidak's and Tukey's multiple comparison tests. There was no significant difference in PDGFR $\beta$  expression over passage ( $p > 0.05$ ). Significant difference in PDGFR $\beta$  expression was detected between non-treated vs benzylamine treated cells at passage 3 (\* $p < 0.05$ ) (A). There was no significant difference in PDGFR $\beta$  expression over passage ( $p > 0.05$ ). Significant difference in PDGFR $\beta$  expression was detected between non-treated vs cadaverine treated cells at passage 3 (\* $p < 0.05$ ) (B). The data is presented as means  $\pm$  S.E.M. of three independent experiments with three replicates in each. The asterisk (\*) indicates statistical significance compared to control at each passage.**

### SECTION 3.3.4 DISCUSSION

While investigating SSAO activity during VSMCs proliferation, higher enzymatic activity (expressed as  $\text{H}_2\text{O}_2$  production) was detected in early in comparison to late passage VSMCs (Figure 48). Moreover, there was a significant difference in SSAO activity between early (3 & 4) and late passage (5, 6, 7, & 8) cells, as presented in Figure 48 (\*\*\*\* $p < 0.0001$  for cells passage 3 vs 4, 5, 6, 7, & 8 after treatment with benzylamine; \*\*\*\* $p < 0.0001$  for cells passage 4 vs 5, 6, 7 & 8 after treatment with benzylamine). Additionally, at each passage the enzymatic activity detected in benzylamine treated cells was significantly higher (#### $p < 0.0001$  for benzylamine treated vs control at passage 3, 4, 5, 6, 7, & 8) in comparison to control cells (treated without benzylamine).

However, not knowing whether the high activity measured at early passage cells was mainly SSAO driven, or it was also a consequence of another VSMCs abundant copper amine oxidase such as LOX, which can also deaminate benzylamine, additional set of experiments were performed in cells from passage 3, 5 & 8 in which SSAO activity was measured at basal level, in the presence of its corresponding suicide inhibitor (MDL72527), and an inhibitor ( $\beta$ APN) that can induce suicide inhibition of LOX (Figure 49A & B). At basal level SSAO activity was found to decrease as the cells aged with passage (\*\*\*\* $p < 0.0001$  for cells passage 3 vs 5 and 3 vs 8 after treatment with benzylamine). Furthermore, complete inhibition of SSAO activity was observed after addition of its specific inhibitor MDL72527 (Figure 49A). Moreover, MDL72527 presented stronger inhibitory potential over SSAO as the passage number increased (\*\*\*\* $p < 0.0001$  for cells passage 3 vs 8 and \* $p < 0.05$  for cells passage 5 vs 8 after treatment with benzylamine + MDL72527). Statistical difference was also detected between benzylamine vs benzylamine + MDL72527 treated cells at passage 3, 5 and 8 (#### $p < 0.0001$ ).

In the presence of a specific LOX inhibitor ( $\beta$ APN), SSAO activity was once again significantly reduced at passage 3, to the same extend as with MDL72527 treatment; followed by gradual increase between passage 3, 5 and 8 (Figure 49B). Despite being known as a very specific LOX inhibitor, some studies have classified  $\beta$ APN as reversible, competitive inhibitor of SSAO (Mercier, 2009; Lyles & Singh, 1995). In light with this, Figure 49B also demonstrates inhibitory potential of  $\beta$ APN over SSAO, which declines as the cells age with passage (\*\*\*\* $p < 0.0001$  for cells passage 3 vs 5 and 3 vs 8, and \* $p < 0.05$  for cells passage 5 vs 8 after treatment with benzylamine +  $\beta$ APN). Additionally, (#### $p < 0.0001$  for benzylamine vs B +  $\beta$ APN treated cells at passage 3 and 5), could indicate LOX and SSAO interaction in early passage VSMCs.

Previous studies have suggested that as inhibitor,  $\beta$ APN has higher affinity for LOX comparing to SSAO (Mercier, 2009; Lyles & Singh, 1995). Therefore, the inhibition of  $H_2O_2$  production observed at early passage cells in the presence of benzylamine could be a result of  $\beta$ APN predominant inhibition over LOX (Figure 49B). In addition, the observed decline in  $\beta$ APN inhibitory potential over SSAO in late passage cells (Figure 49B) could also be attributed to reduced LOX activity and increased SSAO activity in aged VSMCs. This could suggest that the benzylamine metabolised at late passage cells is mainly SSAO driven, which is why  $\beta$ APN does not demonstrate full inhibitory potential over SSAO, as reflected in the  $H_2O_2$  production (Figure 49B).

In the next set of experiments using cadaverine as substrate LOX activity was assessed at basal level, in the presence of its corresponding suicide inhibitor ( $\beta$ APN), and inhibitor (MDL72527) that can irreversibly inhibit SSAO (Figure 50A & B). At basal level LOX activity was also found to decrease as the cells aged with passage (\* $p < 0.05$  for cells passage 3 vs 5 and \*\*\* $p < 0.001$  for cells passage 3 vs 8 after treatment with cadaverine). Furthermore, complete inhibition of LOX activity was detected after addition of its corresponding suicide inhibitor  $\beta$ APN (Figure 50A), with the most significant reduction observed at passage 8 (\*\* $p < 0.01$  for cells passage 3 vs 8 and \* $p < 0.05$  for cells passage 5 vs 8 after treatment with cadaverine +  $\beta$ APN). Additionally, statistical difference was also detected between cadaverine vs cadaverine +  $\beta$ APN treated cells at passage 3, 5 and 8 (#### $p < 0.0001$ ).

There was no significant difference in LOX activity after addition of the specific SSAO inhibitor MDL72527 (Figure 50B). Since cadaverine is mainly deaminated by LOX and not SSAO, an addition of SSAO's suicide inhibitor MDL72527 did not significantly alter  $H_2O_2$  production. Moreover, MDL compounds being developed initially as derivatives of allylamine in the search for specific inhibitors of monoamine oxidase B (MAO B), contain a 3-fluoro or 3-chloro moiety which confers relatively specific and irreversible SSAO-inhibitory qualities to the compounds (Langford *et al.*, 2002); hence, these compounds have relatively little or no effect on LOX. However, when compared to cadaverine treated cells, the cadaverine + MDL72527 treatment demonstrated statistical significance in early passage cells (## $p < 0.01$  for cadaverine vs cadaverine + MDL72527 at passage 3 and 5). This data also supports the notion of possible interaction between SSAO and LOX in early passage VSMCs.

SSAO kinetics were observed once again, this time in the presence of  $\beta$ APN. In the cells treated with  $\beta$ APN SSAO affinity was found to increase between passage 3 and 5 (Figure 51A & B); however, it was reduced at passage 8 (Figure 51C). Its  $V_{max}$  on the other hand was increased as the cells aged in passage, which means that the rate at which SSAO converts the substrate to product in the presence of  $\beta$ APN is faster in aged VSMCs. Moreover, the affinity of LOX was also investigated in cells treated with its substrate cadaverine. LOX affinity for its substrate cadaverine was found to be consistent between passage 3, 5 & 8 (Figure 52 A, B & C). Overall, this data might suggest that in primary rat aortic VSMCs at early passage, LOX is the predominant enzyme responsible for  $H_2O_2$  production; however, as the cells age with passage SSAO becomes the predominant active enzyme whose activity leads to higher  $H_2O_2$  production comparing to LOX (Figure 49A & B; Figure 50A & B).

The predominant SSAO activity over LOX in aged VSMCs (Figure 49B; Figure 50A) supports the finding from section 3.1 which demonstrates higher SSAO affinity in cells with a greater passage number (Figure 39 & 40). Passage dependent changes in SSAO activity were reported in other studies (Trent *et al.*, 2002; El Hadri *et al.*, 2002). Trent *et al.* (2002) compared SSAO activity in rat aortic VSMCs from passage 8, 12, 14 & 16 using DMEM with varying glucose concentrations and have identified a passage dependent increase in SSAO activity in cells grown in high glucose DMEM. However, despite being congruent with the data presented in section 3.1, the findings reported by Trent *et al.* (2002) are not comparable, mainly because difference in culture conditions. Trent *et al.* (2002) have used later passage cells grown in high glucose DMEM, while this study uses early passage cells grown in low glucose DMEM. In another study by El Hadri *et al.* (2002) cultured VSMCs were used to study SSAO activity and expression during their differentiation process. El Hadri *et al.* (2002) used a serum-free medium permissive for *in vitro* VSMC differentiation, and observed a differentiation dependent increase in SSAO activity, mRNA, and protein levels.

After identifying higher SSAO activity in cells with a greater passage number and predominant LOX activity in early passage cells, additional set of experiments were performed to elucidate whether the activity of SSAO and LOX correlates with the expression of VAP-1 (the membrane bound form of SSAO) and Pro-LOX (the membrane bound pro-enzyme form of LOX); and investigate further whether changes in SSAO and LOX activity and expression contribute to phenotypic changes in VSMCs. This decision was supported with the observation that cells with a greater passage number were proliferating with a faster rate comparing to early passage cells.

Therefore, western blot experiments were performed to observe the expression of the membrane bound VAP-1, Pro-LOX, the VSMCs contractile markers (ACTA2 and SM22 $\alpha$ ) and PDGFR $\beta$ , in cells from passage 3, 5 & 8 previously treated with  $\beta$ APN or MDL72527, as well as benzylamine or cadaverine, respectively. The western blot data shows a consistent expression of VAP-1 and Pro-LOX in non-treated (control) cells between passage 3, 5 & 8 (Figure 53A & B). Furthermore, VAP-1 expression was reduced after treatment with  $\beta$ APN, with the most significant reduction observed at passage 3 (\* $p < 0.05$  for controls vs  $\beta$ APN treated cells), and no significant difference in Pro-LOX expression was detected comparing to controls at passage 3, 5 & 8 (Figure 53A & B; Figure 54A & B). In light with the finding presented in Figure 50A, this data indicates that  $\beta$ APN, as specific LOX inhibitor successfully inhibits LOX activity, without altering its protein expression. Therefore, the Pro-LOX protein detected after  $\beta$ APN treatment is probably a non-enzymatically active protein (Figure 53A & B; Figure 54A & B).

VAP-1 expression was also reduced in MDL72527 treated cells (Figure 59A & B; Figure 60A), with the most significant reduction observed at passage 5 (\*\* $p < 0.01$ ) and 8 (\*\*\*\* $p < 0.0001$ ) and no significant difference in Pro-LOX expression was detected comparing to controls at passage 3, 5 & 8 (Figure 59A & B; Figure 60B). In light with the data presented in Figure 50B where no changes in LOX activity were observed after MDL72527 treatment, this data also suggests that MDL72527 has no inhibitory effect on Pro-LOX protein expression in VSMCs from passage 3, 5 & 8; however, it can downregulate SSAO activity and reduce VAP-1 protein expression in cells with a greater passage number (Figure 49A; Figure 59A & B; Figure 60A).

In terms of ACTA2 and SM22 $\alpha$  expression, a passage-dependent reduction (\* $p < 0.05$  for passage 3 vs 8) was observed in non-treated cells (Figure 55A & B; Figure 56A & B). The passage dependent reduction was also visible in  $\beta$ APN treated cells; however, with no significant difference comparing to controls (Figure 55A & B; Figure 56A & B). In MDL72527 treated cells (Figure 61A & B), significant difference in ACTA2 and SM22 $\alpha$  expression was detected at passage 3 between non-treated vs MDL72527 treated cells (\* $p < 0.05$ ). The reason for detected reduction in contractile markers in non-treated cells, as the cells aged with passage, could be the use of primary cell line (Bennett *et al.*, 2016; Owens, 1995). Owens (1995) suggested that primary cultured VSMCs prepared from explants are prone to undergo dedifferentiation under standard culture conditions, with a consistent decrease in several smooth muscle contractile proteins. Taking this into account, the rat aortic VSMCs from passage 3, 5 & 8 were stained once again with SM22 $\alpha$  to confirm phenotype (Appendix 3, Figure 88A, B & C).

Furthermore, the data presented in this section shows consistent expression of PDGFR $\beta$  in non-treated cells and reduced expression at passage 8 in  $\beta$ APN treated cells (Figure 57A & B); as per Figure 58, (\*p < 0.05 for non-treated vs  $\beta$ APN treated cells). Reduced PDGFR $\beta$  expression was also detected after MDL72527 treatment (Figure 63A & B); as per Figure 64, (\*p < 0.05 for non-treated vs MDL72527 treated cells at passage 3 and 5; \*\*p < 0.01 for non-treated vs MDL72527 treated cells at passage 8). Overall, this data demonstrates that inhibition of both enzymes reduces PDGFR $\beta$  expression in VSMCs; which after inhibition of LOX was observed only at passage 8, and after inhibition of SSAO was observed at passage 3, 5, and 8. These findings are in accordance with the study by Lucero *et al.* (2008) that has highlighted the importance of LOX in oxidizing the PDGFR $\beta$  and consequently inducing chemotactic response in VSMCs. However, the data presented here extends further by also suggesting a potential, and more significant involvement of SSAO in this process, which has not been previously mentioned.

In cells treated with benzylamine the expression of VAP-1 and Pro-LOX was consistent between passage 3, 5, and 8 (Figure 65A & B), without significant difference comparing to controls (Figure 66A; Figure 67A). However, in cells treated with cadaverine the expression of VAP-1 was reduced at passage 3, 5 & 8 (Figure 65A & C), with a significant difference detected between non-treated vs cadaverine treated cells (\*\*p < 0.01 for passage 3; \*p < 0.05 for passage 5; and \*\*p < 0.01 for passage 8) (Figure 66B). The expression of Pro-LOX was maintained between passage 3, 5 & 8 (Figure 65A & C), with being slightly higher at passage 3 comparing to control; however, without significant difference detected at each passage (Figure 67B). This data suggests that active LOX, or cadaverine on its own might alter VAP-1 protein expression in VSMCs from passage 3, 5, and 8 (Figure 67C).

Furthermore, in benzylamine treated cells, ACTA2 and SM22 $\alpha$  expression were almost consistent between passage 3, 5 & 8 (Figure 68B). In cadaverine treated cells, there was a reduced expression in both markers at passage 8, however not statistically significant (Figure 68C). Additionally, the protein quantification data demonstrates reduced expression in ACTA2 at passage 3 after benzylamine and cadaverine treatment (\*p < 0.05 for non-treated vs benzylamine and vs cadaverine treated cells) (Figure 69A & B), and reduced expression in SM22 $\alpha$  at passage 3 after benzylamine and cadaverine treatment (\*p < 0.05 for non-treated vs benzylamine and vs cadaverine treated cells) (Figure 70A & B). Despite the loss of contractile markers observed in non-treated cells over passage (Figure 69A & B; Figure 70A & B), the data presented here demonstrates additional loss of markers in early passage VSMCs triggered after activation of both amines. This could suggest that both, SSAO and LOX might contribute to phenotypic modulation in primary rat aortic VSMCs.

The PDGFR $\beta$  expression was consistent in non-treated cells over passage (Figure 71A). Significant difference in PDGFR $\beta$  expression was detected between non-treated vs benzylamine and vs cadaverine treated cells at passage 3 (\*p < 0.05) (Figure 72A & B). This data demonstrates that an addition of LOX and VAP-1 substrate inhibits PDGFR $\beta$  expression in early passage cells. This could be a consequence of a potential interaction between the two enzymes in young VSMCs during which overactive LOX suppresses SSAO activity, and this consequently leads to reduced PDGFR $\beta$  expression in early passage VSMCs; or, it could also suggest a direct inhibitory potential of cadaverine and benzylamine over PDGFR $\beta$ .

### **3.3.5 CONCLUSION**

The data presented in this section confirms the activity of SSAO and LOX in primary rat aortic VSMCs and suggests a possible interaction between these two enzymes in young (early passage) VSMCs. At basal level, LOX activity was found to decrease as the cells aged with passage and its affinity and protein expression were maintained between passages. In the presence of cadaverine,  $\beta$ APN significantly abolished LOX activity, with the most significant reduction observed at passage 8, and MDL72527 had no effect on LOX activity and expression in VSMCs from passage 3, 5 and 8. At basal level, SSAO activity was also found to decrease as the cells aged with passage and its protein expression was maintained between passages. In the presence of benzylamine, MDL72527 significantly abolished SSAO activity, with the most significant inhibition observed at passage 8. Furthermore, in the presence of benzylamine,  $\beta$ APN demonstrated predominant inhibitory potential over SSAO at early passage cells which was reduced as the cells aged with passage; and resulted with a significant reduction in VAP-1 protein expression at passage 3. Since benzylamine is a common substrate and  $\beta$ APN has higher affinity for LOX, the observed reduction in SSAO activity and protein expression after  $\beta$ APN treatment might indicate interaction between LOX and SSAO in early passage VSMCs, during which altered LOX activity might impact SSAO activity and expression. Treatment with benzylamine did not increase or reduce VAP-1 and LOX expression comparing to controls. In cadaverine treated cells LOX expression was not altered; however, VAP-1 expression was significantly reduced comparing to controls. A noticeable loss of contractile markers was observed in non-treated cells. In early passage cells there was additional reduction in contractile markers after treatment with MDL72527, cadaverine and benzylamine. A reduction in PDGFR $\beta$  expression was observed after LOX (passage 8) and SSAO (passage 3, 5 and 8) inhibition, and after benzylamine and cadaverine treatment in VSMCs at passage 3. This might suggest potential involvement of SSAO and LOX in VSMCs phenotyping modulation and consequently vascular remodeling.

## **SECTION 3.4 MOLECULAR STUDIES ON THE INTERACTION BETWEEN SSAO AND LOX IN RAT AORTIC VASCULAR SMOOTH MUSCLE CELLS**

### **SECTION 3.4.1 INTRODUCTION**

To understand further the relationship between SSAO and LOX during VSMCs aging and discern which of these two enzymes is prevalent and more active in young and aged cells, additional molecular studies were required to recognise the interaction between SSAO and LOX in in young (early passage) VSMCs. Being known as ectoenzymes with a catalytically active domain outside the cell surface, SSAO and LOX have the capacity to catalyse enzymatic reactions in the immediate vicinity of the cell surface, and thereby regulate the concentration and functions of their substrates and end-products (Salmi & Jalkanen, 2001). The very close similarity between these two enzymes in terms of substrates and inhibitors is posing a great challenge when studying interactions between the two. Although, despite sharing common substrates and inhibitors, LOX is considerably smaller, its primary sequence lacks copper-coordinating histidines, and it has LTQ instead of TPQ as a cofactor. Intriguingly, Salmi & Jalkanen (2001) suggested that the molecular mechanism of LOX during which epsilon amino groups of lysine are catalysed leading to covalent cross-linking of two molecules is notably comparable to that proposed for VAP-1 in leukocyte extravasation.

Previous studies have already indicated potential interactions between these two copper-dependent amine oxidases regarding various biological functions within the VSMCs (Lucero *et al.*, 2008; Mercier, 2009); however, have not suggested which one of the two is more predominant in early comparing to late passage cells. This is very important to fully understand the role of these enzymes, and their interaction in VSMCs physiology and pathology. The data presented in section 3.3 demonstrates predominant LOX activity in early passage cells and reduced LOX activity in cells with a greater passage number (Figure 50A). Moreover, it indicates higher SSAO activity in aged cells; which was reflected in the reduced inhibitory potential of  $\beta$ APN over SSAO in cells with the greater passage number (Section 3.3; Figure 49B), in the passage dependent increase of SSAO's affinity for the substrate benzylamine (Section 3.1), and in the passage dependent increase of SSAO's  $V_{max}$  after  $\beta$ APN treatment (Section 3.3; Figure 51).

Elevated SSAO activity has previously been associated with many cardiovascular pathologies, including atherosclerosis. In addition, downregulated LOX activity has been associated with the early stages of atherosclerosis. Rodriguez *et al.* (2008; 2002) have observed downregulated LOX activity and expression in endothelial cells and have contributed this to the presence of oxidised LDL. Therefore, the reduction in LOX activity seen in late passage cells might be attributed to elevated SSAO activity in aged VSMCs which has led to excessive H<sub>2</sub>O<sub>2</sub> production, and consequently oxidised LDL because of elevated ROS levels.

The interdependent relationship between SSAO and LOX has previously been highlighted in VSMCs pathology (Mercier, 2009; Lucero *et al.*, 2008; Langford *et al.*, 2002). Lucero *et al.* (2008) have indicated that the membrane bound VAP-1 could be one of the cell membrane proteins oxidised by LOX, and as such critically involved in chemotaxis of these cells. Mercier (2009) suggested that SSAO plays a minor role in extracellular matrix stability through its synergistic relationship with LOX. The involvement of SSAO in the normal physiological development of elastin was also mentioned in a study by Langford *et al.* (2002) in which chronic SSAO inhibition with MDL compounds produced lesions of disorganisation of elastin fibres within tunica media, which was accompanied by degenerative medial changes and metaplastic changes in the VSMCs.

Alterations in ECM and cell-cell interactions within the wall are critical determinants of vascular remodelling (Smolock & Berk, 2012). Being important contributing factors in the formation and stability of ECM would also mean that alterations in the levels of SSAO and LOX might promote VSMCs phenotypic modulation and consequently vascular remodelling. Previous studies have already suggested that SSAO could contribute to vascular remodelling observed in age-related pathologies by inducing unwanted cross-linking of extracellular matrix proteins, and its crucial role in oxidative stress formation and inflammation (Mercier, 2009). LOX has also been identified as active participant in vascular remodelling by inducing chemotactic response in VSMCs and having control over other cellular process such as cell transformation and gene expression (Rodriguez *et al.*, 2008). In this study reduced PDGFR $\beta$  expression was observed after LOX and SSAO inhibition, and after treatment with benzylamine and cadaverine, which could suggest a potential role of these enzymes in VSMCs phenotypic modulation. PDGFRs expression in cultured cells is dynamic and responsive to a variety of stimuli, including hypoxia, thrombin, cytokines, and growth factors (Andrae *et al.*, 2008). Therefore, active LOX and SSAO could certainly act as players of external stimuli for PDGFR $\beta$  expression, probably though their by-products produced because of their respective catalysed reactions.

Overall, this section aims to elucidate further whether the reduced H<sub>2</sub>O<sub>2</sub> production observed in early passage VSMCs (Section 3.3; Figure 49B), in the presence of benzylamine, is caused by direct inhibition of SSAO, or rather due to indirectly inhibited SSAO because of reduced LOX activity. Furthermore, to investigate whether suppressed SSAO activity (whether it is through direct or indirect inhibition) is detectable only on protein level, or it extends to mRNA level. Objectives:

1. Assess mRNA expression levels of the gene that encodes for SSAO (AOC3) and the gene that encodes for LOX (LOX) in VSMCs from passage 3, 5 and 8 after treatment with MDL72527 and  $\beta$ APN, by applying a quantitative polymerase chain reaction (qPCR). qPCR was chosen because it allows sensitive, specific, and reproducible quantification of nucleic acids (Arya *et al.*, 2005).
2. Investigate changes in LOX and AOC3 mRNA levels in early passage VSMCs previously treated with short interfering RNAs (siRNAs) directed to LOX gene. RNAi is often very effective at minimal concentrations (Scacheri *et al.*, 2004); therefore, the lowest possible concentration of siRNA was applied to prevent saturation of the RNAi machinery and unwanted side effects.

The RNA interference (RNAi) pathway was first detected as a response to exogenously introduced long double-stranded RNA (dsRNA) (Fire *et al.*, 1998). An RNase III enzyme, Dicer, cleaves the dsRNA into duplexes of 21–23 nucleotides (nt) termed short interfering RNAs (siRNAs), which then guide a multicomponent complex known as RISC (RNA induced silencing complex), which is complementary to mRNAs and target their cleavage. Once an mRNA is cleaved, it is expected to be promptly degraded (Doench *et al.*, 2003). In recent years, the transfection of mammalian cells with exogenous siRNAs has rapidly been adopted as a technology for targeted gene silencing (Elbashir *et al.*, 2001).

## SECTION 3.4.2 METHODS

### *RNA extraction*

Primary rat aortic vascular smooth muscle cells were plated at  $5 \times 10^4$ /well in a 24-well plate and allowed to grow for 24-48 hours to reach confluence. After reaching confluence some of the cells were left as non-treated (reference samples), others were treated with 100 $\mu$ M (20 $\mu$ l per well) MDL72527, and the rest were treated with 200 $\mu$ M (20 $\mu$ l per well)  $\beta$ APN. The RNA from each well containing cells (non-treated, as well as MDL72527 and  $\beta$ APN treated) was extracted by applying the ReliaPrep™ RNA cell miniprep system kit (Promega). This protocol is based on four essential steps: effective disruption of cells, denaturation of nucleoprotein complexes, inactivation of endogenous ribonuclease (RNase) activity, and removal of contaminating DNA and proteins.

The culture media was removed from the wells and the cells were washed with ice-cold, sterile 1XPBS (500 $\mu$ l per well). After that 100 $\mu$ l of lysis buffer (prepared by adding 325 $\mu$ l of 1-Thioglycerol to 32.5ml of BL buffer, which was supplied with the kit) was added to each well and the lysate was repeatedly pipetting over the well surface 7-10 times. The lysate was then collected and transferred to a microcentrifuge tube. 35 $\mu$ l isopropanol (100%) was added to each centrifuge tube and the tubes were mixed by vortexing for 5 seconds. The lysate from each centrifuge tube was then transferred to a ReliaPrep™ minicolumn placed in a collection tube and centrifuged at 13,000 x g for 30 seconds at 22°C. After centrifugation, the liquid was discarded and the minicolumn was placed in a different collection tube.

500 $\mu$ l of RNA wash solution (prepared by adding 60ml of 95% ethanol to a 35ml concentrated RNA wash solution - RWA) was added to the minicolumn and the collection tube containing the minicolumn was centrifuged again at 13,000 x g for 30 seconds. After that 30 $\mu$ l of DNase I incubation mix (24 $\mu$ l yellow core buffer, 3 MnCl<sub>2</sub> at 0.09M, and 3 $\mu$ l DNase I) was added to the minicolumn membrane and the minicolumn was incubated for 15 minutes at 22°C. After the incubation, 200 $\mu$ l of column wash solution (prepared by adding 7.5ml of 95% ethanol to a 5ml concentrated column wash solution - CWE) was added to the minicolumn and the minicolumn was centrifuged at 13,000 x g for 15 seconds; after that 500 $\mu$ l RNA wash solution was added again, and the minicolumn was centrifuged at 13,000 x g for 30 seconds.

The wash solutions and the collection tube were then discarded. The minicolumn was placed to a new collection tube. 300µl of RNA wash solution was added again followed by centrifugation at 20,000 x g for 2 minutes. The minicolumn was then transferred from the collection tube to an elution tube. 15µl of nuclease-free water was added to the minicolumn and the elution tube containing the minicolumn was centrifuged at 13,000 x g for 1 minute. The purified RNA was quantified with NanoDrop Spectrophotometer (NanoDrop Technologies) and stored at -80°C until further use.

### **SSAO and LOX gene expression in rat aortic VSMCs using qPCR method**

SSAO and LOX gene expression levels were detected and quantified with a quantitative polymerase chain reaction (qPCR) based on a relative quantification method, also known as comparative threshold method. QPCR BIO SyGreen 1-Step Go Kit (PCR Biosystems) was used to perform the PCR reaction. This kit uses antibody-mediated hot start technology that prevents the formation of primer-dimers and improves reaction sensitivity and specificity. The primers for VAP-1, LOX and  $\beta$  – actin (Table 9) were designed through Roche Life Sciences, by inserting their respective reference sequences (NM\_017061.2 *Rattus norvegicus* lysyl oxidase (LOX), mRNA; NM\_031582.2 *Rattus norvegicus* amine oxidase, copper containing 3 (AOC3), mRNA), which were obtained from ncbi.nlm.nih.gov website.

**Table 9. Primers sequence for *Rattus norvegicus* amine oxidase, copper containing 3 (AOC3), *Rattus norvegicus* lysyl oxidase (LOX), and *Rattus norvegicus*  $\beta$ -actin.**

| <b>Gene name</b>                | <b>Forward primer (5' – 3')</b> | <b>Reverse primer (5' – 3')</b> |
|---------------------------------|---------------------------------|---------------------------------|
| <b>AOC3</b>                     | ACCCACAACGCTCACTTCA             | TTCATAGGGACAAAAGCCAAA           |
| <b>LOX</b>                      | AGGATCCACGGAGGATGG              | GGGAGGCCAGGAGACT                |
| <b><math>\beta</math>-actin</b> | CCCGCGAGTACAACCTTCT             | CGTCATCCATGGCGAACT              |

Master mix (with final volume 10µl/well) was prepared for all reference (non-treated) and target (MDL72527 and  $\beta$ APN treated) samples (Table 10).  $\beta$ -actin was used as a reference gene due to demonstrating relatively stable expression levels in response to any treatment (Rao *et al.*, 2013); and AOC3 and LOX were the genes of interest (target genes). Each target gene was run in triplicates, simultaneously with the reference gene  $\beta$ -actin; and was analyzed separately for all reference and target samples.

**Table 10. An illustration of the qPCR experimental design**

|                       | <b>Reference sample</b>   | <b>Target sample</b>   |
|-----------------------|---|--|
| <b>Reference gene</b> | $\beta$ -actin expression in non-treated RASMCs from passage 3, 5 and 8 | $\beta$ -actin expression in MDL72527 and $\beta$ APN treated RASMCs from passage 3, 5 and 8 |
| <b>Target gene 1</b>  | AOC3 expression in non-treated RASMCs from passage 3, 5 and 8           | AOC3 expression in MDL72527 and $\beta$ APN treated RASMCs from passage 3, 5 and 8           |
| <b>Target gene 2</b>  | LOX expression in non-treated RASMCs from passage 3, 5 and 8            | LOX expression in MDL72527 and $\beta$ APN treated RASMCs from passage 3, 5 and 8            |

The master mix per well for each gene was prepared with: 1X qPCRBIO SyGreen 1-Step Mix (5 $\mu$ l), forward primer at concentration 10 $\mu$ M (0.4 $\mu$ l), reverse primer at concentration 10 $\mu$ M (0.4 $\mu$ l), 1X RTaseGo - which contains RNase inhibitor (0.5 $\mu$ l), 20ng/ $\mu$ l template RNA (1 $\mu$ l) and 2.7 $\mu$ l qPCR grade water. Samples prepared without 1X RTaseGo were used as a negative control. After loading, the plate was centrifuged at 1000 RPM for 1min, and readings were taken on QuantStudio™ 7 Flex Real-Time PCR System (Thermo Fisher Scientific). The thermal cycling protocol is listed in Table 11.

**Table 11. qPCR thermal cycling protocol**

| <b>Cycles</b> | <b>Temperature</b> | <b>Time</b> | <b>Notes</b>          |
|---------------|--------------------|-------------|-----------------------|
| <b>1</b>      | 45 <sup>o</sup> C  | 10 minutes  | Reverse transcription |
| <b>1</b>      | 95 <sup>o</sup> C  | 2 minutes   | Polymerase activation |
| <b>40</b>     | 95 <sup>o</sup> C  | 5 seconds   | Denaturation          |
| <b>40</b>     | 60 <sup>o</sup> C  | 25 seconds  | Annealing/extension   |

The data was analysed with the  $2^{-\Delta\Delta CT}$  method of relative quantification. This method uses the threshold cycle (CT) value, which is the cycle at which the fluorescence level reaches a threshold (Rao *et al.*, 2013). The CT values were used to calculate relative gene expression in target and reference samples by using  $\beta$ -actin as the reference gene.

Firstly,  $\Delta\text{CT}$  (difference in threshold cycle between the target and reference genes) was calculated with the following formula:  $\Delta\text{CT} = \text{CT (a target gene)} - \text{CT (a reference gene)}$ . Secondly, the  $\Delta\Delta\text{CT}$  (difference in  $\Delta\text{CT}$  as described in the above formula between the target and reference samples) was calculated with the following formula:  $\Delta\Delta\text{CT} = \Delta\text{CT (a target sample)} - \Delta\text{CT (a reference sample)}$ . And finally, the  $2^{-\Delta\Delta\text{CT}}$  was calculated as the fold change of the target gene expression in the target sample relative to the reference sample and normalised to the reference gene  $\beta$ -actin. The relative gene expression was set to 1 for reference samples because  $\Delta\Delta\text{CT}$  is equal to 0.

### ***siRNA knockdown of LOX gene in primary rat aortic VSMCs using reverse transfection – protocol optimisation***

The interplay between LOX and SSAO in early passage rat aortic VSMCs was studied with gene knockdown using reverse transfection and lipofectamine - RNAiMAX transfection reagent. Lipofectamine transfection reagent was chosen due to having high transfection efficiency for a wide range of cells. The aim of this experiment was to reduce LOX gene expression in early passage (2 & 3) rat aortic VSMCs and observe what changes this would bring on AOC3 gene expression, and consequently VAP-1 protein expression. The transfection protocol was first performed in a sterile 6 well plate to identify the best siRNAs (which resulted with  $\geq 50\%$  inhibition), as well as optimise the cell density and time of transfection.

Firstly, to establish an optimal VSMCs density for transfection, cells with confluency ~80-90% were washed with 1XPBS, harvested by trypsinisation, and counted using haemocytometer, as explained in the methods section 2.2.5 and 2.2.6. Cells with different densities ( $2 \times 10^4$ ,  $5 \times 10^4$ ,  $3 \times 10^5$ ,  $4 \times 10^6$ ) were then re-suspended in 10ml antibiotic free DMEM supplemented with 10% FCS. The cell pellets were centrifuged at  $21^\circ\text{C}$  for 3 minutes at 1800 RPM. The supernatant was removed, and the cells were re-suspended in 20ml antibiotic free DMEM supplemented with 10% FCS. The re-suspended cells were plated in a sterile 6 well plate (4ml/well) and their growth was observed between 24h and 72h. The rat aortic VSMCs plated at  $3 \times 10^5$  density were actively dividing cells at 48h and 72h with confluency between ~60-80%, therefore, this density was chosen as an optimal density in the next stage of the experiment.

In the second phase of optimization, we observed the knockdown effect of LOX over 48h and 72h using three siRNAs that target LOX gene. SiRNA\_LOX\_5, SiRNA\_LOX\_6 and SiRNA\_LOX\_8 were selected based on their target sequences (Table 12). More details on the selected siRNAs are listed in Figure 89, Appendix 4. All three siRNAs were purchased from QIAGEN as 5nmol lyophilized powder and were dissolved with 250µl RNase free water to obtain a 20µM solution. The solutions were aliquoted in small aliquots and stored at -20°C.

**Table 12. LOX siRNAs and their target sequences**

| <i>SiRNA</i>       | <i>Target sequence</i> |
|--------------------|------------------------|
| <i>SiRNA_LOX_5</i> | ACCCGGAAATTACATTCTAAA  |
| <i>SiRNA_LOX_6</i> | AGGGCGGATGTCAGAGACTAT  |
| <i>SiRNA_LOX_8</i> | TCCCGGATGTTATGATACTTA  |

To confirm successful knockdown, HS cell death was used like a positive control. It was prepared as a 10µM solution by dissolving 1nmol lyophilized siRNA with 100µl RNase free water. HS cell death was selected due to being a blend of highly potent siRNAs targeting ubiquitously expressed rat genes that are indispensable for cell survival (Kim & Eberwine, 2010). Knockdown of these genes induces a high degree of cell death, therefore death cells after treatment with HS death siRNA and RNAiMax transfection reagent were used to confirm a successful knockdown. Si control was used as a negative control due to being composed of random sequences that do not target any gene inside the cells (Kim & Eberwine, 2010). It was prepared as a 20µM solution by dissolving 5nmol lyophilized siRNA with 250µl RNase free water. In addition, a MOCK transfection control was also set up which contained only transfection reagent and OptiMEM – a reduced serum medium that allows for a reduction of FBS supplementation by at least 50% with no change in cell growth rate or morphology. MOCK was included to observe (if any) phenotypic changes to the cells caused by the transfection.

Confluent cells were first washed with 1XPBS, harvested by trypsinisation, and counted using haemocytometer, as explained in the methods section 2.2.5 and 2.2.6. Cells with density  $3 \times 10^5$  were then re-suspended in 10ml antibiotic free DMEM supplemented with 10% FCS. The cell pellets were centrifuged at 21°C for 3 minutes at 1800 RPM. The supernatant was removed, and the cells were re-suspended in 20ml antibiotic free DMEM supplemented with 10% FCS and placed in incubator at 37°C/5% CO<sub>2</sub> until further use. 3µl (20µM) from all three siRNAs were added to three wells from a six well plate, thus obtaining a final concentration of 20nM.

In addition, 3µl (20µM) Si control and 6µl (10µM) HS death were added in two wells from a six well plate, following by addition of 490µl OPTIMEM in all six wells (one well contained only 490µl OPTIMEM). The solutions in each well were mixed by pipetting up and down and rocking the plate. 3µ lipofectamine RNAiMAX transfection reagent was then added to all wells containing OPTIMEM on its own, SiRNAs and OPTIMEM, Si control and OPTIMEM, HS death and OPTIMEM; and the plate was incubated at room temperature for 20 minutes. After incubation 2.5ml of cells (previously counted and kept in an incubator at 37°C/5% CO<sub>2</sub>) was added to each well and the plate was incubated at 37°C/5%CO<sub>2</sub>. To see the effect of knockdown the cells were monitored between 24h and 72h. The RNA from cells containing MOCK, Si control, SiRNA\_LOX\_5, SiRNA\_LOX\_6 and SiRNA\_LOX\_8 was extracted after 48h and after 72h and qPCR was performed to identify changes in LOX's gene expression. The qPCR data was analysed with the  $2^{-\Delta\Delta CT}$  method of relative quantification. The CT values were used to calculate relative gene expression in target (SiRNA\_LOX\_5, SiRNA\_LOX\_6 and SiRNA\_LOX\_8) and reference samples (MOCK and Si control) by using β-actin as the reference gene.

Firstly,  $\Delta CT$  (difference in threshold cycle between the target and reference genes) was calculated with the following formula:  $\Delta CT = CT \text{ (a target gene)} - CT \text{ (a reference gene)}$ . Secondly, the  $\Delta\Delta CT$  (difference in  $\Delta CT$  as described in the above formula between the target and reference samples) was calculated with the following formula:  $\Delta\Delta CT = \Delta CT \text{ (a target sample)} - \Delta CT \text{ (a reference sample)}$ . And finally, the  $2^{-\Delta\Delta CT}$  was calculated as the fold change of the target gene expression in the target sample relative to the reference sample and normalised to the reference gene - β-actin. The  $2^{-\Delta\Delta CT}$  value was first calculated using MOCK as a reference sample and then Si control.

### ***siRNA knockdown of LOX gene in primary rat aortic VSMCs performed in T-75 flask***

After identifying the best siRNAs to take forward, and successfully optimising the cell density and time of transfection siRNA knockdown of LOX gene was performed in a T-75 flask. Separate flasks were used for transfection with individual siRNAs, Si control and HS death. Four reaction mixtures were prepared with: individual siRNAs, Si control and HS death. In doing that 8µl RNAiMAX was added to 8µl SiRNA\_LOX\_6 or SiRNA\_LOX\_8 at concentration 20µM and supplemented with 1350µl OptiMEM. In addition, 8µl RNAiMAX was also added to 8µl Si control (20µM) or 16µl HS cell death (10µM) and supplemented with 1350µl OptiMEM.

The reaction mixtures were incubated for 20 minutes at room temperature during which early passage (2 & 3), fully confluent rat aortic VSMCs were harvested and resuspended in antibiotic free DMEM (supplemented with 10% FBS) at concentration  $3 \times 10^5$  cells/ml. 6.650ml of cells were then added to each T-75 flask following by addition of the reaction mixture previously prepared, thus obtaining a final siRNA concentration of 20nM and  $2 \times 10^6$  cells/flask. Cells were distributed evenly through the flask by swirling in a figure of eight and the flasks were incubated at 37°C/5%CO<sub>2</sub>. The following day 6ml of antibiotic free DMEM (supplemented with 10% FBS) was added to each flask.

72h post transfection the cells were harvested by trypsinisation and re-suspended in two falcon tubes with 2ml antibiotic free DMEM (supplemented with 10% FBS) at concentration  $5 \times 10^4$  cells/ml. One falcon tube with cells was used for extraction of protein samples and the other for the extraction of RNA. To extract protein samples, cells were first centrifuged at 2000 RCF for 6 minutes at 4°C. The supernatant was removed, and cells were washed with 1XPBS and centrifuged again at 2000 RCF for 6 minutes at 4°C. After the removal of the supernatant the cells were re-suspended with 1ml RIPA buffer (0.5M TRIS at pH 7.4, 0.9g NaCl, 0.1g SDS, 1ml TRITON x 100, 5mM EDTA) supplemented with 10% protease and phosphatase inhibitor cocktail. The samples were then moved to a centrifuge tube, vortexed for 30 seconds, sonicated in icy water for 5 minutes, and stored at -20°C until further use.

To extract RNA, cells were centrifuged at 300 RCF for 5minutes and re-suspended in 1XPBS after which were centrifuged again at 300 RCF for 5minutes. The supernatant was then removed, and cells were re-suspended in 250µl lysis buffer (prepared by adding 325µl of 1-Thioglycerol to 32.5ml of BL buffer, which was supplied with the ReliaPrep™ RNA cell miniprep system kit (Promega). The lysate was mixed well by repeatedly pipetting 7-10 times and was then transferred to a microcentrifuge tube. 85µl isopropanol (100%) was added to each centrifuge tube and the tubes were mixed by vortexing for 5 seconds.

The lysate from each centrifuge tube was then transferred to a ReliaPrep™ minicolumn placed in a collection tube and centrifuged at 13,000 x g for 30 seconds at 22°C. After centrifugation, the liquid was discarded and the minicolumn was placed in a different collection tube. 500µl of RNA wash solution (previously prepared by adding 60ml of 95% ethanol to a 35ml concentrated RNA wash solution - RWA) was added to the minicolumn and the collection tube containing the minicolumn was centrifuged again at 13,000 x g for 30 seconds. After that 30µl of DNase I incubation mix (24µl yellow core buffer, 3 MnCl<sub>2</sub> at 0.09M, and 3µl DNase I) was added to the minicolumn membrane and the minicolumn was incubated for 15 minutes at 22°C.

After the incubation, 200µl of column wash solution (prepared by adding 7.5ml of 95% ethanol to a 5ml concentrated column wash solution - CWE) was added to the minicolumn and the minicolumn was centrifuged at 13,000 x g for 15 seconds; after that 500µl RNA wash solution was added again, and the minicolumn was centrifuged at 13,000 x g for 30 seconds. The wash solutions and the collection tube were then discarded. The minicolumn was placed to a new collection tube. 300µl of RNA wash solution was added again followed by centrifugation at 20,000 x g for 2 minutes. The minicolumn was then transferred from the collection tube to an elution tube. 30µl of nuclease-free water was added to the minicolumn and the elution tube containing the minicolumn was centrifuged at 13,000 x g for 1 minute. The purified RNA was quantified with NanoDrop Spectrophotometer (NanoDrop Technologies) and stored at -80°C until further use.

### ***SSAO and LOX gene expression in rat aortic VSMCs after gene knockdown using qPCR method***

SSAO and LOX gene expression levels were detected and quantified once again after LOX gene knockdown, by applying the quantitative polymerase chain reaction (qPCR) threshold method as described above. QPCR BIO SyGreen 1-Step Go Kit (PCR Biosystems) was used once again to perform the PCR reaction. The data was analysed with the  $2^{-\Delta\Delta CT}$  method of relative quantification, and the CT values were used to calculate relative gene expression in target (SiRNA\_LOX\_6 and SiRNA\_LOX\_8) and reference samples (Si control) by using  $\beta$ -actin as the reference gene. Firstly,  $\Delta CT$  (difference in threshold cycle between the target and reference genes) was calculated with the following formula:  $\Delta CT = CT \text{ (a target gene)} - CT \text{ (a reference gene)}$ . Secondly, the  $\Delta\Delta CT$  (difference in  $\Delta CT$  as described in the above formula between the target and reference samples) was calculated with the following formula:  $\Delta\Delta CT = \Delta CT \text{ (a target sample)} - \Delta CT \text{ (a reference sample)}$ . And finally, the  $2^{-\Delta\Delta CT}$  was calculated as the fold change of the target gene expression in the target sample relative to the reference sample and normalised to the reference gene -  $\beta$ -actin. The relative gene expression was set to 1 for reference samples (Si control) because  $\Delta\Delta CT$  is equal to 0.

### ***Western blot analysis after gene knockdown***

Western blot analysis was applied once again, as described in the methods section 2.2.13, to observe changes in Pro-LOX and VAP-1 protein expression after LOX gene knockdown. The expression of VAP-1 was detected with Alexa Fluor® conjugated VAP-1 antibody at dilution 1:1000 in 5% w/v BSA, 1XTBS, 10% Tween®20. The expression of Pro-LOX was detected with rabbit monoclonal to Pro-LOX antibody at dilution 1:1000 in 5% w/v BSA, 1XTBS, 10% Tween®20. HRP conjugated B-actin diluted at 1:15000 in 5% w/v milk powder, 1XTBS, 10% Tween®20 was used as control. The protein bands were quantified with ImageJ software, as explained in the methods section 2.2.14.

## **SECTION 3.4.3 RESULTS**

### ***SSAO and LOX gene expression in rat aortic VSMCs***

After studying SSAO and LOX activity, affinity, and protein expression in rat aortic VSMCs from passage 3, 5 and 8, additional qPCR experiments were performed to identify changes in gene expression between these two enzymes. In doing that, RNA was extracted from non-treated, MDL72527 and  $\beta$ APN treated cells at passage 3, 5 & 8, and QPCR BIO SyGreen 1-Step Go Kit (PCR Biosystems) was applied to perform the qPCR reaction, as explained in the methods section 3.4.2. Figure 73A presents the AOC3 mRNA levels relative to  $\beta$ -actin in non-treated, MDL72527 and  $\beta$ APN treated cells at passage 3, 5 & 8. Figure 73B presents the LOX mRNA levels relative to  $\beta$ -actin in non-treated, MDL72527 and  $\beta$ APN treated cells at passage 3, 5 & 8. The  $2^{-\Delta\Delta CT}$  was calculated as the fold change of the target gene expression in the target sample (LOX expression in MDL72527 and  $\beta$ APN treated RASMCs from passage 3, 5 and 8 and AOC3 expression in MDL72527 and  $\beta$ APN treated RASMCs from passage 3, 5 and 8) relative to the reference sample (LOX expression in non-treated RASMCs from passage 3, 5 and 8 and AOC3 expression in non-treated RASMCs from passage 3, 5 and 8) and normalised to the reference gene  $\beta$ -actin. The relative gene expression was set to 1 for reference samples because  $\Delta\Delta CT$  is equal to 0.

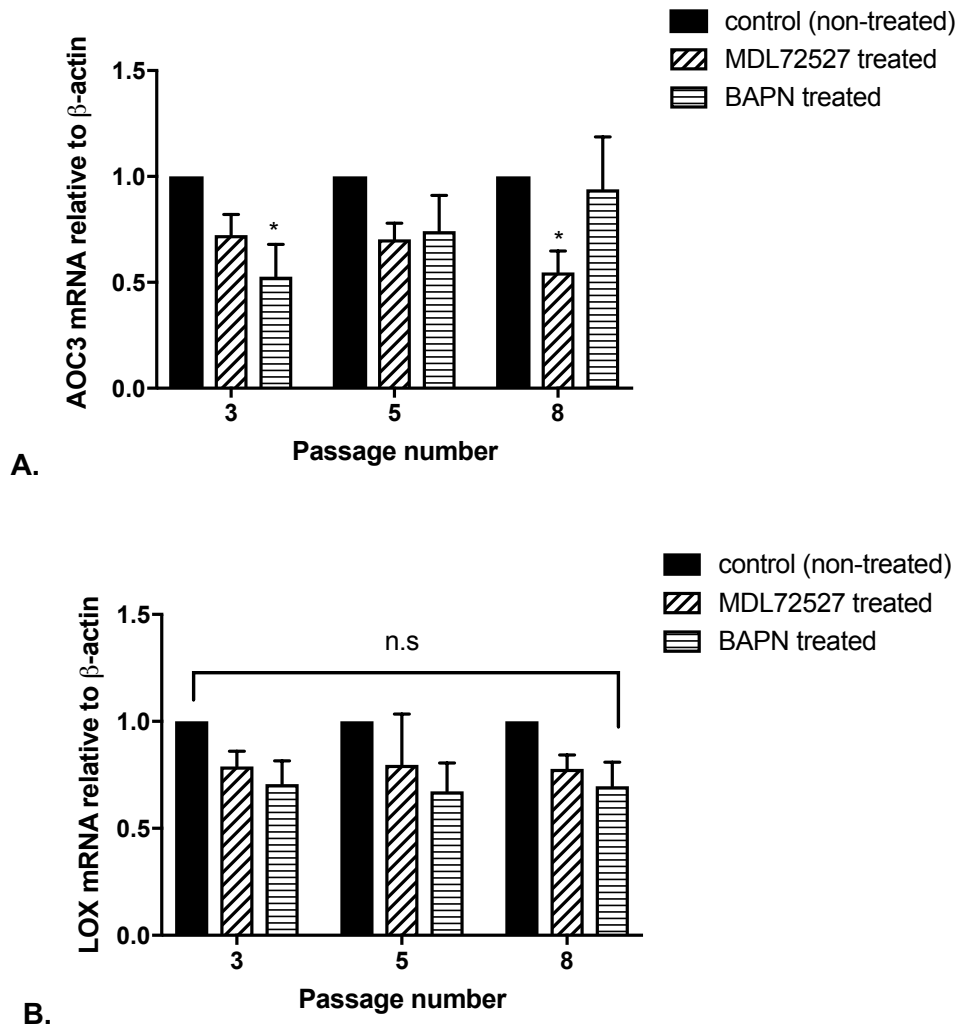


**Figure 73.** AOC3 (A) and LOX (B) gene expression (expressed as fold-change compared with control after normalization to the housekeeping gene  $\beta$ -actin) in non-treated (control: black bars), MDL72527 treated (hatched bars) and  $\beta$ APN treated (horizontal line bars) in rat aortic VSMCs from passage 3, 5, & 8. The data was analyzed by two-way ANOVA ( $***p < 0.001$ ), followed by Dunnett's multiple comparison test. Significant difference in AOC3 gene expression was detected at passage 3 ( $*p < 0.05$  for non-treated vs  $\beta$ APN treated cells), and passage 8 ( $*p < 0.05$  for non-treated vs MDL72527 treated cells) (A). There was no significant difference ( $p > 0.05$ ) detected in LOX gene expression after MDL72527 and  $\beta$ APN treatment between passage 3, 5 and 8 comparing to controls (B). The data is presented as means  $\pm$  S.E.M. of five independent experiments with three replicates in each. The asterisk (\*) indicates statistical significance compared to control at each passage.

### ***siRNA knockdown of LOX gene in primary rat aortic VSMCs using reverse transfection – protocol optimisation***

During protocol optimisation a preliminary experiment was first conducted during which the transfection was performed in a sterile 6 well plate to identify the best siRNAs, as well as optimise the cell density and time of transfection. Figure 74 presents the LOX mRNA levels relative to  $\beta$ -actin in rat aortic VSMCs treated with Si control, SiRNA5, SiRNA6, and SiRNA8 after 48h and 72h post transfection.

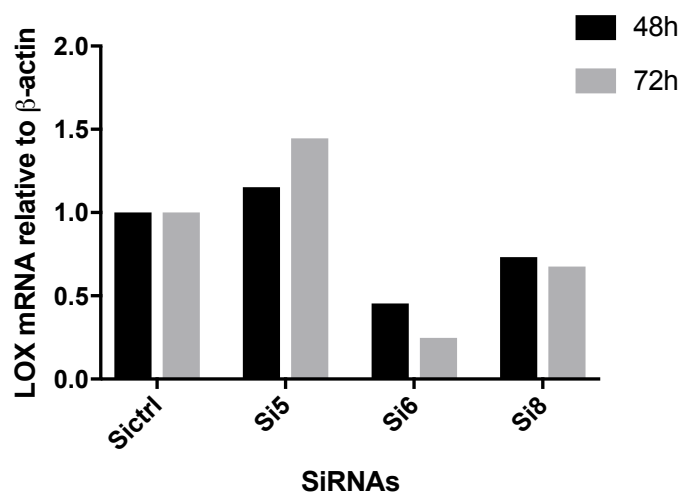


**Figure 74.** LOX gene expression (expressed as fold-change compared with control after normalization to the housekeeping gene  $\beta$ -actin) after treatment with Si control, SiRNA5, SiRNA6, and SiRNA8 48h (black bars) and 72h (grey bars) post transfection (n = 1).

### ***SSAO and LOX gene expression in rat aortic VSMCs after gene knockdown using qPCR method***

To observe potential interactions between SSAO and LOX in early passage rat aortic VSMCs, LOX and AOC3 gene expression levels were detected and quantified after LOX gene knockdown in rat aortic VSMCs from passage 2 and 3. Figure 75 demonstrates LOX and AOC3 gene expression after 72h transfection using lipofectamine - RNAiMAX transfection reagent and two individual siRNAs (SiRNA6 and SiRNA8). Cells transfected with Si control were used as control. The  $2^{-\Delta\Delta CT}$  was calculated as the fold change of the target gene expression in the target sample (Si6 and Si8) relative to the reference sample (SiCtrl) and normalised to the reference gene -  $\beta$ -actin. The relative gene expression was set to 1 for reference samples (SiCtrl) because  $\Delta\Delta CT$  is equal to 0.

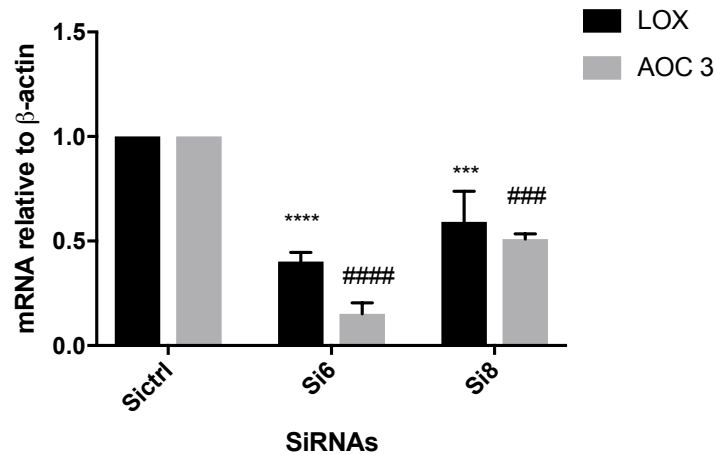


**Figure 75.** LOX (black bars) and AOC3 (grey bars) gene expression (expressed as fold-change compared with control after normalization to the housekeeping gene  $\beta$ -actin) in early passage (2 & 3) VSMCs cells treated with Si control, SiRNA6 and SiRNA8. The data was analyzed by two-way ANOVA (\*\*\*\* $p < 0.0001$ ), followed by Dunnett's multiple comparison test. Significant difference in LOX gene expression was detected with SiRNA6 (\*\*\*\* $p < 0.0001$  for Sictrl vs Si6 treated cells), and SiRNA8 (\*\* $p < 0.01$  for Sictrl vs Si8 treated cells). Significant difference in AOC3 gene expression was also detected with SiRNA6 (#### $p < 0.0001$  for Sictrl vs Si6 treated cells), and SiRNA8 (### $p < 0.001$  for Sictrl vs Si8 treated cells). The data is presented as means  $\pm$  S.E.M. of four independent experiments with three replicates in each. The asterisk (\*) indicates statistical significance for LOX compared to control at each passage. The hash (#) indicates statistical significance for AOC3 compared to control at each passage.

### **Western blot analysis after gene knockdown**

Western blot analysis was performed to detect the expression of Pro-LOX and VAP-1 in early passage (2 & 3) rat aortic VSMCs transfected with Si control (Sictrl), SiRNA6 (Si6) and SiRNA8 (Si8).  $\beta$ -actin was detected to normalize the level of protein. The protein was quantified using ImageJ software, as explained in the methods section 2.2.14.

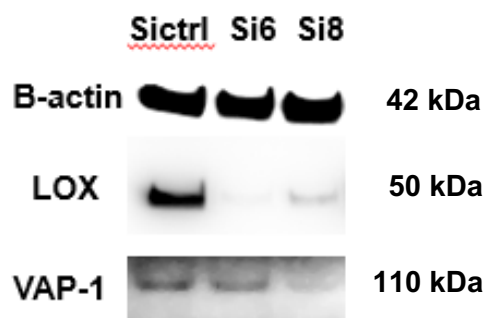


**Figure 76.** Western blot analysis of Pro-LOX and VAP-1 in rat aortic VSMCs 72h post transfection with Si control (Sictrl), SiRNA6 (Si6) and SiRNA8 (Si8) (n = 4).  $\beta$ -actin was used as loading control.

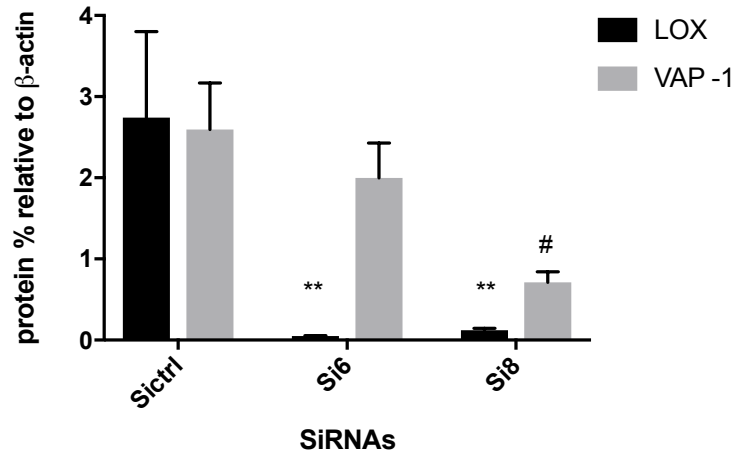


**Figure 77.** LOX (black bars) and VAP-1 (grey bars) protein expression (expressed as percentage relative to  $\beta$ -actin) in early passage (2 & 3) VSMCs cells treated with Si control, SiRNA6 and SiRNA8. The optical density was quantified using the image densitometer ImageJ. Significant difference in LOX protein expression was detected with SiRNA6 and SiRNA8 (\*\* $p < 0.01$  for Sictrl vs Si6 treated cells and Sictrl vs Si8 treated cells). Significant difference in VAP-1 protein expression was detected with SiRNA8 (# $p < 0.05$  for Sictrl vs Si8 treated cells). The data is presented as means  $\pm$  S.E.M. of four independent experiments with three replicates in each. The asterisk (\*) indicates statistical significance for LOX compared to control at each passage. The hash (#) indicates statistical significance for VAP-1 compared to control at each passage.

#### SECTION 3.4.4 DISCUSSION

To understand the interaction between SSAO and LOX in VSMCs physiology and pathology, changes in AOC3 and LOX mRNA levels were firstly observed after MDL72527 and  $\beta$ APN treatment. In VSMCs from passage 3, 5 and 8  $\beta$ APN and MDL72527 resulted with no significant difference in LOX mRNA expression levels (Figure 73B); however, changes in AOC3 mRNA levels were detected at passage 3 after  $\beta$ APN treatment (\* $p < 0.05$  for non-treated vs  $\beta$ APN treated cells), and passage 8 (\* $p < 0.05$  for non-treated vs MDL72527 treated cells) after MDL72527 treatment (Figure 73A). This data is consistent with the previous finding from section 3.3 which demonstrates significant reduction in SSAO activity (seen as  $H_2O_2$  production) in early passage VSMCs previously treated with  $\beta$ APN (Figure 49B). Furthermore, it complements the western blot data which shows reduced VAP-1 expression in VSMCs from passage 3 previously treated with  $\beta$ APN (Section 3.3; Figure 53A & B). The  $\beta$ APN inhibitory potential over AOC3 mRNA expression levels was diminished in cells with a greater passage number (Figure 73A); this effect is consistent with  $\beta$ APN's effect on SSAO activity and VAP-1 protein expression previously observed (Section 3.3; Figure 49B; Figure 53 A & B).

This data suggests that  $\beta$ APN acts as inhibitor of SSAO and successfully inhibits its activity while also reducing its protein expression and mRNA levels in early passage primary VSMCs; however, is losing its inhibitory potential in cells with a greater passage number.  $\beta$ APN has different inhibitory effects on LOX and SSAO. Although the exact effects of this compound on the two enzymes have been variably reported, depending on the doses, conditions (*in vitro* or *in vivo*) and species studied, it appears from previous work that  $\beta$ APN is a potent irreversible inhibitor of LOX and a reversible competitive inhibitor of SSAO (Mercier, 2009). In this study  $\beta$ APN demonstrated higher potency in inhibiting SSAO, as it suppressed not only its activity (Section 3.3; Figure 49B) but also VAP-1 expression (Section 3.3; Figure 53A & B) and AOC3 mRNA levels (Figure 73A). This inhibition was more pronounced in early passage VSMCs. In cells with a greater passage number  $\beta$ APN inhibitory potential over SSAO (activity, protein expression and mRNA levels) was reduced. Since SSAO has the capacity to regulate the concentration of its substrates by catalysing enzymatic reactions in an immediate vicinity of the cell surface (Salmi & Jalkanen, 2001), elevation of its activity in aged VSMC might increase the concentration of its substrate (in this case benzylamine), which would consequently result with suppressed inhibitory potential of  $\beta$ APN. This is because  $\beta$ APN inhibits SSAO through competitive reversible mechanism; therefore, increasing the concentration of the substrate would decrease the possibility of the inhibitor binding to the enzyme.

Interestingly,  $\beta$ APN demonstrated inhibitory effect only on LOX activity (Section 3.3; Figure 50A), without affecting its protein expression (Section 3.3; Figure 53A & B), and mRNA levels (Figure 73B). It is important to mention here that in addition to the first characterized LOX, the other four LOX-like proteins (LOXL 1–4) are also likely to catalyze cross-link formation in the vasculature, as does LOX (Mäki *et al.*, 2005) and their degree of inhibition by  $\beta$ APN are not yet established. Therefore, the less potent effect of  $\beta$ APN over LOX in comparison to SSAO might be attributed to the presence of other LOX active enzymes. In addition to that, it is also known that once the extracellular form of LOX is processed, it can re-enter the cells and localize in the nucleus. This localization is independent of the catalytic activity of the protein and cannot be blocked by a specific LOX inhibitor ( $\beta$ APN) (Iturbide *et al.*, 2014). Nuclear localizations of LOX have been previously detected within the nuclei of cultured rat aortic smooth muscle cells (Iturbide *et al.*, 2014; Li *et al.*, 1997); once again, this could be another reason why  $\beta$ APN was successful in inhibiting LOX activity but failed to succeed in reducing its protein expression and mRNA levels.

MDL72527 treatment did not reduce LOX mRNA levels (Figure 73B) in VSMCs from passage 3, 5 and 8. This result is consistent with the previous findings from section 3.3 where no changes in LOX activity and protein expression were observed after MDL72527 treatment (Section 3.3; Figure 50B; Figure 59A & B). Regarding AOC3 mRNA expression levels, MDL72527 inhibitory potential over SSAO was only significant at passage 8 (Figure 73A). This once again is in accordance with previous data from section 3.3 where most pronounced MDL72527 inhibitory potential over SSAO activity (Section 3.3; Figure 49A) and VAP-1 expression (Section 3.3; Figure 59A & B) was detected in late passage VSMCs. Overall, the data in this thesis confirms MDL72527 to be a specific irreversible inhibitor of SSAO, with no inhibitory effect over LOX. Despite being known as selective inhibitor of FAD-dependent polyamine oxidases, MDL72527 has previously been demonstrated effective in inhibiting copper-containing amine oxidases such as SSAO (Agostinelli *et al.*, 2005). However, at this stage the reason for its accelerated inhibitory potential over SSAO in aged VSMCs, in comparison to young cells, is still unknown.

LOX knockdown was firstly evaluated at 48h and 72h post transfection with siRNAs (SiRNA5, SiRNA6, and SiRNA8) targeted against LOX, or non-targeted Sictrl. The preliminary data from this section shows successful silencing with SiRNA6 and SiRNA8, as observed in LOX mRNA levels, with SiRNA6 being more efficient in silencing LOX gene (Figure 74). At 48h VSMCs presented an approximate 60% decrease in LOX mRNA levels with SiRNA6 comparing to Sictrl, and at 72h 80% decrease in LOX mRNA levels was observed with SiRNA6 comparing to Sictrl (Figure 74). Additionally, at 48h VSMCs presented an approximate 20% decrease in LOX mRNA levels with SiRNA8 comparing to Sictrl, and at 72h 30% decrease in LOX mRNA levels was observed with SiRNA8 comparing to Sictrl (Figure 74).

However, an opposite effect was observed with SiRNA5. At 48h VSMCs presented an approximate 20% increase in LOX mRNA levels with SiRNA5 comparing to Sictrl, and at 72h 40% increase in LOX mRNA levels was observed with SiRNA5 comparing to Sictrl (Figure 74). The reason for that could be that siRNA5 has not led to mRNA cleavage/degradation, but rather blocked translation of the protein, which in turn has triggered a feedback loop mechanism, leading to increased transcription of the gene (Dana *et al.*, 2017). It could also be an off-target effect such as increased interferon signaling, or stress signaling, which has led to upregulation of the gene; that has constituted with the siRNA not working well on the target gene (Jackson & Linsley, 2004). siRNAs might affect targets by blocking the translation of transcripts with partial homology, thereby affecting unintended targets at the level of translation (Jackson & Linsley, 2004).

Furthermore, during the optimization stage, elongated VSMCs morphology was observed after transfection with SiRNA6 and SiRNA8, which was not detected with SiRNA5. SiRNA5 transfected cells exhibited less elongated morphology and spread randomly on the culture flask without an organised structure. Therefore, based on these observations and the data presented in Figure 74 only SiRNA6 and SiRNA8 were taken forward in the second stage of knockdown experiments. This is because both SiRNAs manifested same phenotype and resulted with decrease in LOX mRNA expression levels, an effect which was not detected with SiRNA5. Moreover, since both SiRNAs (SiRNA6 and SiRNA8) demonstrated higher reduction in LOX mRNA expression after 72h, this time was adopted as an optimal transfection time in the second stage of knockdown experiments.

In the second stage of knockdown experiments early passage (2 & 3) VSMCs were transfected with SiRNA6 and SiRNA8 targeted against LOX, or non-targeted Sicontrol; after which LOX and AOC3 mRNA expression levels were observed once again by applying the qPCR method. The data in this section demonstrates successful silencing of LOX gene 72h post transfection with SiRNA6 (\*\*\*\* $p < 0.0001$  for Sicontrol vs Si6 treated cells), and SiRNA8 (\*\*\* $p < 0.001$  for Sicontrol vs Si8 treated cells), comparing to control (Figure 75). Significant reduction in AOC3 gene expression was also detected with SiRNA6 (##### $p < 0.0001$  for Sicontrol vs Si6 treated cells), and SiRNA8 (### $p < 0.001$  for Sicontrol vs Si8 treated cells), comparing to control (Figure 75). 72h post transfection an approximate 60% decrease in LOX mRNA levels was observed with SiRNA6 and 30% decrease in LOX mRNA levels was detected with SiRNA8 (Figure 75). Additionally, 72h post transfection an approximate 80% decrease in AOC3 mRNA levels was observed with SiRNA6 and 40% decrease in AOC3 mRNA levels was detected with SiRNA8 (Figure 75).

The protein expression from LOX was also significantly abolished 72h post transfection with SiRNA6 and SiRNA8, and VAP-1 protein expression was only significantly reduced with SiRNA8 comparing to control (Figure78). Moreover, the protein quantification data shows significant reduction in LOX protein expression with both, SiRNA6 and SiRNA8 (\*\* $p < 0.01$  for Sicontrol vs Si6 treated cells and Sicontrol vs Si8 treated cells); additionally, significant reduction in VAP-1 protein expression was detected only with SiRNA8 (# $p < 0.05$  for Sicontrol vs Si8 treated cells) (Figure 77). Therefore, in the presence of SiRNA6, the protein knockdown for VAP-1 does not correlate with the mRNA knockdown (Figure 77; 78; 79). If SiRNA6 was targeting VAP-1, these results could indicate a potential off-target activity that might have led to regulation at the protein level that is independent of mRNA downregulation. Complementary siRNAs can cause a spectrum of actions (Aleman *et al.*, 2007).

At one end of the spectrum, complementary interactions can yield mRNA degradation with little or no translational repression. Conversely, some interactions result in significant protein reduction with little or no change in mRNA levels, while others fall in the middle of the spectrum, resulting with some degree of mRNA degradation and translational repression (Aleman *et al.*, 2007). However, in this case this reasoning is not applicable as SiRNA6 is only targeting LOX gene.

The data in this section demonstrates successful knockdown of LOX gene in early passage rat aortic VSMCs, and a reduction in AOC3 mRNA and protein expression levels because of that. This finding supports our hypothesis of interrelation between these two enzymes and highlights potential synergism between LOX and SSAO in young (early passage) rat aortic VSMCs. Since LOX belongs to the same family as SSAO it is reasonable to suspect synergism between the two enzymes, which has already been highlighted in previous literature (Mercier, 2009; Lucero *et al.*, 2008; Langford *et al.*, 2002). This data substantiates an important finding and indicates interrelation between these two enzymes in VSMCs physiology and pathology.

### **3.4.5 CONCLUSION**

Overall, this section confirms molecular interactions between SSAO and LOX in primary rat aortic VSMCs and suggests potential synergism in their enzymatic activity in early passage VSMCs. This was verified with the reduction of AOC3 mRNA and protein levels after silencing LOX gene. Prior to that VAP-1 and LOX mRNA levels were observed after MDL72527 and  $\beta$ APN treatment.  $\beta$ APN demonstrated inhibitory potential over AOC3 mRNA levels in early passage VSMCs and MDL72527 in late passage VSMCs. Furthermore,  $\beta$ APN and MDL72527 did not result with inhibition of LOX mRNA levels in VSMCs from passage 3, 5 and 8. LOX gene was successfully silenced 72h post transfection with two pre-selected SiRNAs (SiRNA6 and SiRNA8), as seen by the reduction in LOX mRNA and protein expression levels. From the two SiRNAs, SiRNA6 demonstrated more prominent effect in silencing LOX gene. AOC3 mRNA expression levels were also reduced after silencing LOX gene. Reduction in AOC3 mRNA expression was observed with both SiRNAs, while VAP-1 protein was only significantly reduced with SiRNA8.

## SECTION 3.5 SSAO AND LOX IN ROS FORMATION

### 3.5.1 INTRODUCTION

After investigating SSAO and LOX activity throughout VSMCs aging, during which a synergistic interaction was identified between both enzymes in young (early passage cells), the contribution of SSAO and LOX was studied in ROS formation, in aged (late passage cells). A balance between ROS production and the antioxidant defence system is crucial to maintain redox homeostasis, and a disturbance in this balance would result with elevated ROS and consequently oxidative stress. However, an oxidative challenge or a loss of antioxidants alone does not constitute for oxidative stress. Oxidative stress is defined in situations where increased formation of oxidant(s) is accompanied by a loss of antioxidant(s) and/or accumulation of oxidized forms of the antioxidant(s) (Bonomini *et al.*, 2008).

The most important source of endogenous ROS is the mitochondrial electron transport chain which leads to production of ROS by converting oxygen into superoxide anions (Boveris & Chance, 2013). Other sources of ROS production are various metabolic processes including oxidation of NADPH by NADPH oxidase and oxidation of xanthine by xanthine oxidase (Grimsrud *et al.*, 2008). For example, an overproduction of NADPH, may result in increased redox cycling of substances that can undergo repetitive rounds of oxidation/reduction, ultimately leading to the increased generation of superoxide anion radical ( $O_2^-$ ) and secondary oxidants (Bonomini *et al.*, 2008). Oxidative stress caused by consistent overproduction of ROS could lead to oxidation of cellular components and consequently modifications of DNA, proteins, lipids, and carbohydrates (Grimsrud *et al.*, 2008). Therefore, it has been highlighted as a main trigger for biological damage and as such is implicated in various diseases, including cardiovascular and inflammatory disorders (Finkel & Holbrook, 2000; Lin & Beal, 2006; Dator *et al.*, 2019).

The increase of free radical production is closely associated with the development of the cardiovascular disorder atherosclerosis. After being generated in the endothelial layer of the vascular wall the radicals provoke an oxidative modification from low-density lipoprotein (LDL) to oxidized low-density lipoprotein (ox-LDL). The formation of ox-LDL stimulates circulating monocytes to migrate to the subendothelial space, causing further endothelial injury. The modified LDL is further taken up by macrophages which then become foam cells, leading to the formation of atherosclerotic plaque (Bonomini *et al.*, 2008).

It has been previously suggested that endothelial SSAO contributes to ROS formation through H<sub>2</sub>O<sub>2</sub> dependent mechanism (Wang *et al.*, 2018). In this study, SSAO activity was higher in comparison to LOX, in VSMCs with a greater passage number; and a gradual increase in SSAO affinity for its substrate benzylamine was detected as the cells aged with passage. High SSAO activity and affinity in aged cells would mean higher production of aldehydes and H<sub>2</sub>O<sub>2</sub>. Enhanced H<sub>2</sub>O<sub>2</sub> production has already been associated with increased VSMC migration rate (Li *et al.*, 2000; Lucero *et al.*, 2008). Lucero *et al.* (2008) have demonstrated LOX's driven H<sub>2</sub>O<sub>2</sub> as an effective chemotactic mediator in inducing VSMCs migration. As mentioned earlier, H<sub>2</sub>O<sub>2</sub> alone is not reactive; however, when produced in large amounts, in the presence of transition metals (particularly iron) it can be converted to toxic hydrogen free hydroxyl radical (OH<sup>•</sup>) *via* the Fenton reaction ( $H_2O_2 + Fe^{2+} \rightarrow \cdot OH + OH^- + Fe^{3+}$ ) (Obata, 2006). Hydroxyl radicals pose a greater risk comparing to H<sub>2</sub>O<sub>2</sub> because of their very short half-life (nanosecond comparing to half-life of minutes like in the case of H<sub>2</sub>O<sub>2</sub>). Since the lifetime of a radical relates to its reactivity and the amount of damage it can cause, hydroxyl radicals are short-lived and highly reactive with ability to execute most of the damage locally once they are formed.

It has long been suspected that ROS generate secondary products that spread injury and accelerate damage. Aldehydes, formed by the oxidation of unsaturated lipids, are the most common secondary products generated through ROS (Hill & Bhatnagar, 2009). These aldehydes possess high reactivity and are more stable than ROS, so they can diffuse to sites distant from their site of formation, thereby accelerating oxidative injury. Moreover, these aldehydes possess a rich variety of structural features, or they acquire additional ones by conjugating with receptive nucleophiles, which allows them to be recognized by cell constituents as signalling molecules (Hill & Bhatnagar, 2009).

Like ROS, aldehydes are metabolized and detoxified by several nonenzymatic and enzymatic processes (Hill & Bhatnagar, 2009). Converting aldehydes to less reactive products prevent the direct toxicity of the same; however, metabolic conversion could also enhance stability of aldehydes and thereby augment their ability to stimulate cell signalling (Hill & Bhatnagar, 2009). Previous work has shown that in most cells' aldehydes are either reduced (to alcohols), oxidized (to acids), or conjugated with cellular nucleophiles such as glutathione, carnosine ( $\beta$ -alanine-L-histidine), or proteins (Hill & Bhatnagar, 2009). Aldehyde dehydrogenases (ALDHs) catalyse the oxidation of aldehydes and glutathione S-transferases facilitates their glutathione conjugation.

Glutathione (GSH) is one of the most abundant (1 to 10mM in most cells) low molecular weight non-protein tripeptide thiol (cysteine, glycine, and glutamic acid) antioxidant, and its intracellular concentration is an indicator of oxidative stress. GSH is synthesized *in vivo*, by the consecutive action of two ATP-dependent enzymes, glutamate cysteine ligase (GCL) and glutathione synthase (GS); and the amino acids cysteine, glutamate, and glycine (Aquilano *et al.*, 2014). All cells synthesize GSH, however the main source is the liver where cysteine is metabolised. After being synthesised, GSH is delivered to the mitochondria, endoplasmic reticulum, nucleus, and the extracellular space. Mitochondrial GSH is most relevant for the disposal of ROS (Schulz *et al.*, 2000). Within the cells, GSH exists in two different forms: the reduced sulfhydryl form (GSH) and the glutathione disulphide (GSSG), oxidized form (Rahman *et al.*, 2007). As seen in Figure 78, oxidized glutathione is 2 reduced glutathione's bound together at the sulphur atoms (Pizzorno, 2014).

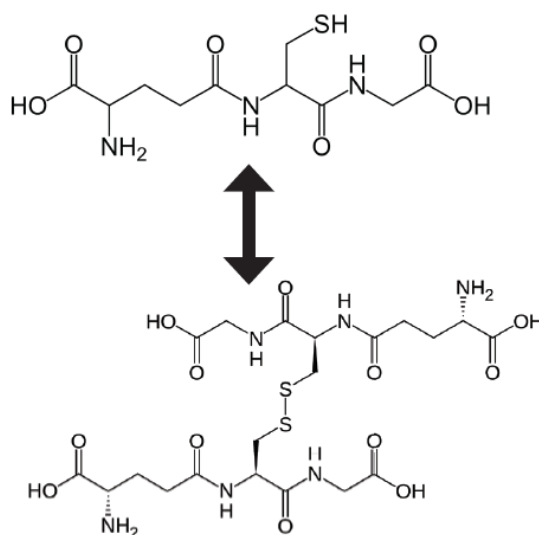


**Figure 78. Balance between GSH and GSSG (Pizzorno, 2014).**

GSH modulates intracellular ROS through its protective defence against the damaging effects of oxidative stress and its role in facilitating ROS cell signalling (Presnell *et al.*, 2013). However, it also has an important role as antioxidant in the detoxification of products derived from ROS-promoted oxidation of lipids such as aldehydes (Aquilano *et al.*, 2014). In the early stage of increased ROS, GSH manifest enhanced action to maintain redox signalling; however, in the case of prolonged ROS the amount of free GSH decreases leading to irreversible cell degeneration and death (Aquilano *et al.*, 2014). The ratio of GSH to GSSG is also important to determine healthy cell redox status of cells. Healthy cells at rest have a GSH/GSSG ratio >100 while the ratio drops to 1 to 10 in cells exposed to oxidant stress (Pizzorno, 2014).

Since both SSAO and LOX produce H<sub>2</sub>O<sub>2</sub> and aldehydes because of their respective catalysed reactions, their contribution in ROS formation was assessed in aged rat aortic VSMCs. This study already identified H<sub>2</sub>O<sub>2</sub> as a cytotoxic agent in VSMCs at concentration 50 and 1000µM (Section 3.2; Figure 45A & B) and demonstrated enhanced cytotoxicity in VSMCs after simultaneous addition of SSAO's produced aldehydes and H<sub>2</sub>O<sub>2</sub> (Section 3.2; Figure 45A & B). The cytotoxic and ROS formation ability of SSAO derived by-products has previously been highlighted in other studies (Saito *et al.*, 2005., Desai *et al.*, 2010, Kim *et al.*, 2020). Desai *et al.* (2010) have shown that methylglyoxal increases ROS through AGEs formation and Kim *et al.* (2020) have established ROS to be the crucial mechanism for methylglyoxal induced cytotoxicity in brain endothelial cells. Moreover, Kim *et al.* (2020) observed methylglyoxal driven mitochondrial ROS production and suppressed Akt/hypoxia-inducible factor 1 alpha (HIF-1α) pathway in these cells. On the other hand, Saito *et al.* (2005) have observed synergistic effect between formaldehyde and free radicals in increasing oxidative stress levels and reducing cell viability.

Overall, this section aims to investigate the contribution of SSAO and LOX in mitochondrial ROS production (in the form of superoxide and hydroxyl radicals), in aged rat aortic VSMCs (passage 7 & 8) in the presence of SSAO (benzylamine, methylamine, aminoacetone) and LOX (benzylamine and cadaverine) substrate amines with a sensitive fluorometric one-step assay which uses a ROS red dye to quantify ROS. Furthermore, relate the production of ROS with changes in GSH level. Objectives:

1. Establish an optimal time for assessing ROS, and identify which enzyme is predominant in ROS formation by measuring ROS over different time intervals after treatment with SSAO and LOX amine substrates.
2. Investigate changes in SSAO and LOX driven ROS production after addition of MDL72527 and βAPN.
3. Assess total GSH production in the presence of SSAO and LOX amine substrates before and after the addition of MDL72527 and βAPN, with the glutathione recycling assay based on the glutathione recycling system by DTNB and glutathione reductase.

2, 3 dimethoxynaphthoquinone (DMNQ) was used like a positive control (Figure 79). DMNQ is a redox cycling agent that generates both superoxide and hydrogen peroxide intracellularly; It does not react with free thiol groups, is non alkylating and non-adduct forming in contrast to other quinones (Tchivilev *et al.*, 2008).

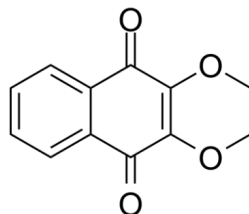


**Figure 79. DMNQ chemical structure (Tchivilev *et al.*, 2008).**

Previous studies have already demonstrated the efficacy of DMNQ in causing increased ROS generation (Chacko *et al.*, 2016; Tchivilev *et al.*, 2008). In a study by Chacko *et al.* (2016) this was evident by the elevation in non-mitochondrial respiration when monocytes were treated with various DMNQ concentrations (1 and 5 $\mu$ M).

## **SECTION 3.5.2 METHODS**

### ***ROS production in rat aortic VSMCs in the presence of SSAO and LOX amines***

Mitochondrial ROS production was determined with the cellular ROS detection assay kit (ab186027) from Abcam, UK. In the initial experiment performed to establish the optimal time for measuring ROS, primary rat aortic vascular smooth muscle cells from late passage number (7 & 8) were plated at  $3 \times 10^4$  cells/ 100 $\mu$ l well in a black 96-well plate and allowed to grow for 24-48 hours to reach confluence. ROS red staining solution was prepared by adding 15 $\mu$ l of ROS red dye to 10ml assay buffer. Cells were washed once with 1XPBS and 80 $\mu$ l of ROS red staining solution was added to each well. Cells were then incubated at 37 $^{\circ}$ C/5% CO $_2$  incubator for one hour. After the incubation cells were treated with 20 $\mu$ l/well benzylamine (500 $\mu$ M), cadaverine (500 $\mu$ M), methylamine (500 $\mu$ M), and aminoacetone (45 $\mu$ M), previously diluted in 1XPBS. 1X PBS (10 $\mu$ l/well) was used for untreated cells and 5 $\mu$ M (20 $\mu$ l/well) 2,3 – dimethoxy – 1,4 naphthquinone (DMNQ) was used like a positive control. DMNQ was selected due to being a redox-cycling agent that induces intracellular superoxide anion formation. To induce ROS production the cell plate was incubated at 37 $^{\circ}$ C, and the reading was taken after 15, 30, 60 and 120 minutes using ClarioStar<sup>®</sup> Microplate Reader (BMG Labtech) with Ex/Em = 520/605 nm. The plate was kept in incubator at 37 $^{\circ}$ C/5% CO $_2$  between readings.

## **ROS production in rat aortic VSMCs in the presence of SSAO and LOX inhibitors**

In the subsequent set of experiments, confluent cells (after previously been incubated for 1h at 37°C/5%CO<sub>2</sub> with ROS red dye) were treated with 20µl/well benzylamine (500µM), methylamine (500µM), and aminoacetone (45µM), or benzylamine (500µM), methylamine (500µM), and aminoacetone (45µM) with 20µl/well 200µM βAPN, or benzylamine (500µM), methylamine (500µM), and aminoacetone (45µM) with 20µl/well 100µM MDL72527. 1XPBS (10µl/well) was used once again for untreated cells and 5µM (20µl/well) 2,3 – dimethoxy – 1,4 naphthquinone (DMNQ) was used like a positive control. The cells were incubated for 30 minutes at 37°C/5%CO<sub>2</sub> and the readings were taken using Clario Star<sup>®</sup> Microplate Reader (BMG Labtech) with Ex/Em = 520/605 nm.

### **Measurement of total GSH**

Total GSH was assessed with a colorimetric recycling assay based on the glutathione recycling system by DTNB (Ellman's reagent) and glutathione reductase (Rahman *et al.*, 2006). Glutathione reductase (an enzyme inducible upon oxidative stress) reduces GSSG to GSH, which then reacts with DTNB to produce a yellow coloured 5-thio-2-nitrobenzoic acid (TNB), which absorbs at 412nm (Figure 80). In this method, any GSSG, present in the samples or formed during the reaction, is also reduced to GSH by glutathione reductase (Katerji *et al.*, 2019). Therefore, the glutathione concentration of the sample measured at absorbance of 412 nm would be the sum of a reduced and oxidized glutathione in a sample ([GSH]<sub>total</sub> = [GSH] + 2 × [GSSG]).

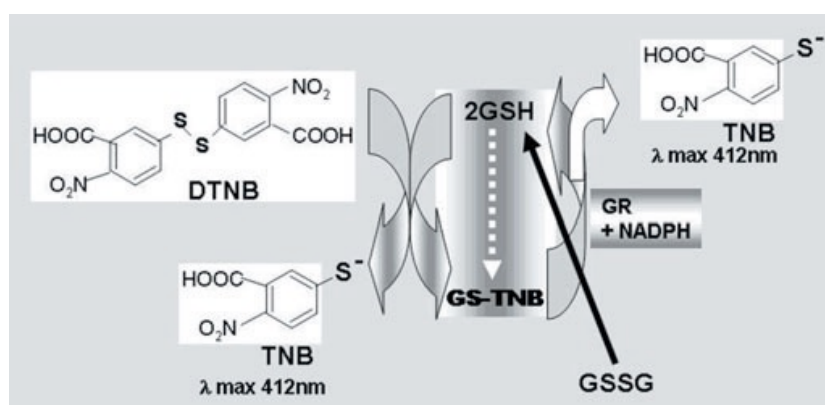


**Figure 80.** The enzymatic recycling of glutathione (GSH) from glutathione disulphide (GSSG) by glutathione reductase (GR) in the presence of NADPH. GSH reacts with DTNB [5,5'-dithio-bis (2-nitrobenzoic acid)] to form TNB (5-thio-2-nitrobenzoic acid) and GS-TNB (glutathione adduct of GSH). GS-TNB is then reduced to GSH akin to GSSG by GR and NADPH (recycling). (Rahman *et al.*, 2006).

### ***Sample preparation***

Primary rat aortic vascular smooth muscle cells from late passage number (7 & 8) were plated at  $5 \times 10^5$  cells/ 1ml/well in a 24-well plate and allowed to grow for 24-48 hours to reach confluence. Confluent cells were treated with 40 $\mu$ l/well benzylamine (500 $\mu$ M), methylamine (500 $\mu$ M), and aminoacetone (45 $\mu$ M), or benzylamine (500 $\mu$ M), methylamine (500 $\mu$ M), and aminoacetone (45 $\mu$ M) with 40 $\mu$ l/well 200 $\mu$ M  $\beta$ APN, or benzylamine (500 $\mu$ M), methylamine (500 $\mu$ M), and aminoacetone (45 $\mu$ M) with 40 $\mu$ l/well 100 $\mu$ M MDL72527. Control culture was incubated without treatment. Treated cells were incubated for 30 minutes at 37 $^{\circ}$ C/5%CO $_2$ . Cells were then washed twice with sterile 1XPBS, scrapped, and collected in a centrifuge tube. Cells were centrifuged at 700 x g for 5 min at 4 $^{\circ}$ C, after which the pellet was washed with 0.5ml 1XPBS and centrifuged again at 700 x g for 5 min at 4 $^{\circ}$ C. The pellet was then lysed with 80 $\mu$ l ice-cold glutathione buffer and incubated on ice for 10 min, after which 20 $\mu$ l of 5% sulfosalicylic acid (SSA) was added, mixed well, and centrifuged again at 8000 x g for 10 minutes. The supernatant was then transferred to a fresh centrifuge tube and kept on ice ready to be used for the glutathione assay.

### ***Glutathione assay***

96-well plate was used to assay both, samples, and standards. Reaction mixture was prepared with the following:

- NADPH generating mix 20 $\mu$ l/well
- Glutathione reductase 20 $\mu$ l/well
- Glutathione reaction buffer 120 $\mu$ l/well

Furthermore, 1ml of 1% SSA was added to GSH standard to generate 1 $\mu$ g/ $\mu$ l glutathione solution, which was then further diluted with 1% SSA to generate 10ng/ $\mu$ l stock. 10ng/ $\mu$ l GSH stock was then used to prepare standards as shown in Table 13.

**Table 13. Standards for GSH assay**

| No | 10 ng/ $\mu$ l GSH standard ( $\mu$ l) | 1 % SSA ( $\mu$ l) |
|----|--|--------------------|
| 1  | 50                                     | 50                 |
| 2  | 40                                     | 60                 |
| 3  | 30                                     | 70                 |
| 4  | 20                                     | 80                 |
| 5  | 10                                     | 90                 |
| 6  | 0                                      | 100                |

160 $\mu$ l of the reaction mixture was added to each well and the plate was incubated at room temperature for 10 minutes to generate NADPH. After 10 minutes incubation 20 $\mu$ l of either GSH standards or samples was added to each well containing reaction mixture and the plate was incubated at room temperature for another 10 minutes. Glutathione substrate (DTNB) was prepared by adding 1ml glutathione reaction buffer to 1 vial substrate. 20 $\mu$ l of DTNB was then added to each well containing GSH standards and samples and the plate was incubated at room temperature for another 10 min. The absorbance was read on Clario Star<sup>®</sup> plate reader (BMG Labtech) set at 412nm. The data was transferred to an Excel spreadsheet and analysed before plotting the absorbance ratio (412nm) versus concentration of GSH standards (ng/ $\mu$ l) (Figure 81). Prepared samples were also used to perform the BCA assay, as explained in methods section 2.2.10. Total GSH was calculated as follows: Total GSH = (Abs sample – Abs blank) / slope STD curve. These values were then corrected for total protein concentration by subtracting them with the protein values obtained from the BCA assay and the total GSH content was expressed as nmol of GSH per mg of total cellular protein.

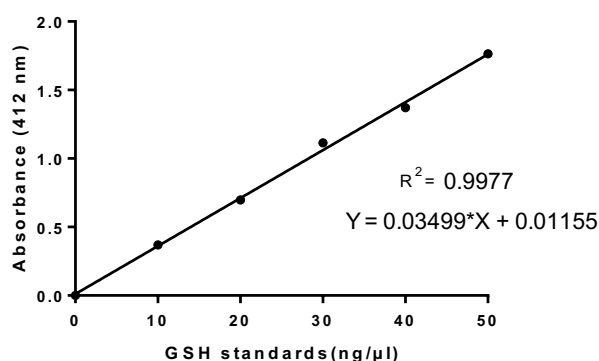


**Figure 81. A linear regression of glutathione standard curve. The plate was incubated at room temperature, for 10 minutes, and absorbance readings were taken at 412nm, on a Clario Star<sup>®</sup> Microplate Reader (BMG Labtech).**

### SECTION 3.5.3 RESULTS

#### *ROS production in rat aortic VSMCs in the presence of SSAO and LOX amines*

ROS production was observed in late passage (7 & 8) cells after pre-incubation with ROS red staining solution and treatment with SSAO (benzylamine, methylamine, aminoacetone) and LOX (benzylamine and cadaverine) substrate amines. 5 $\mu$ M (20 $\mu$ l/well) 2,3 – dimethoxy – 1,4 naphthquinone (DMNQ) was used like a positive control. ROS measurements were taken after 15, 30, 60- and 120-minutes incubation with the amines. Figure 82A presents the detected ROS production versus time (\*) and versus all amine treatments (#). Significant difference in ROS production was detected over time (\*\*p < 0.01 for 15 min vs 120 min and \*\*p < 0.01 for 30 min vs 120 min). Significant difference in ROS production was also detected between treatments. At 15 minutes incubation (####p < 0.0001 for benzylamine vs cadaverine and methylamine; #p < 0.05 for cadaverine vs methylamine & ####p < 0.0001 for cadaverine and methylamine vs aminoacetone). At 30-, 60-, and 120-minutes incubation (####p < 0.0001 for benzylamine vs cadaverine and methylamine & ####p < 0.0001 for cadaverine and methylamine vs aminoacetone). Figure 82B shows a raw data of ROS production detected with DMNQ over different time intervals. As per Figure 82B there is a gradual increase in ROS production over time.

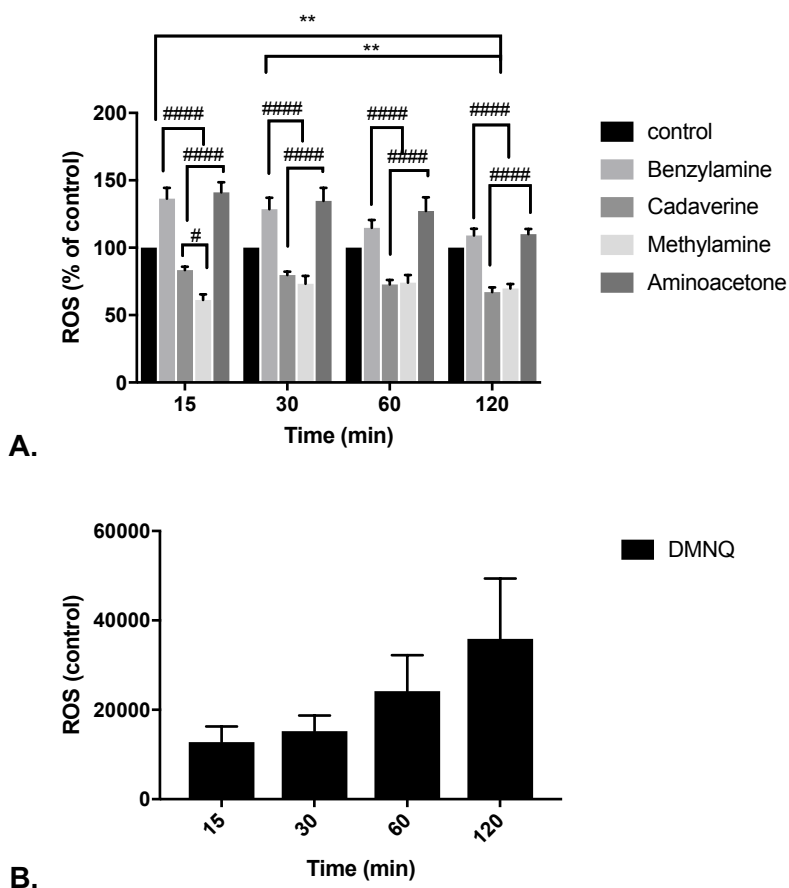


Figure 82. ROS production (percentage relative to DMNQ treated – control) after treatment with 20µl/well benzylamine (500µM), cadaverine (500µM), methylamine (500µM), and aminoacetone (45µM). 1XPBS (10µl/well) was used for untreated cells and 5µM DMNQ (20µl/well) was used like a positive control. Readings were taken after 15, 30, 60- and 120-minutes incubation on a using Clario Star<sup>®</sup> Microplate Reader (BMG Labtech) with Ex/Em = 520/605 nm. The plate was incubated at 37<sup>o</sup>C/5% CO<sub>2</sub> between readings. The data was analyzed by two-way ANOVA (\*\*\*p < 0.001), followed by Tukeys' multiple comparison test. Significant difference in ROS production was detected over time (\*\*p < 0.01 for 15 min vs 120 min and \*\*p < 0.01 for 30 min vs 120 min). Significant difference in ROS production was also detected between treatments. At 15 minutes incubation (####p < 0.0001 for benzylamine vs cadaverine and methylamine; #p < 0.05 for cadaverine vs methylamine & ####p < 0.0001 for cadaverine and methylamine vs aminoacetone). At 30-, 60-, and 120-minutes incubation (####p < 0.0001 for benzylamine vs cadaverine and methylamine & ####p < 0.0001 for cadaverine and methylamine vs aminoacetone). The data is presented as means ± S.E.M. of five independent experiments with three replicates in each. The asterisk (\*) indicates statistical significance in ROS production detected over time. The hash (#) indicates statistical difference in ROS production detected between treatments at each time point.

### ***ROS production in rat aortic VSMCs in the presence of SSAO and LOX inhibitors***

ROS production was observed once again in late passage (7 & 8) cells after pre-incubation with ROS red staining solution and treatment with SSAO (benzylamine, methylamine, aminoacetone) and LOX (benzylamine) substrate amines (without inhibitor), and in the presence of their respective inhibitors, MDL72527 (with MDL72527) and βAPN (with βAPN). 5µM (20µl/well) 2,3 – dimethoxy – 1,4 naphthquinone (DMNQ) was used like a positive control. Treated cells were incubated for 30 minutes at 37<sup>o</sup>C/5%CO<sub>2</sub> and the readings were taken using ClarioStar<sup>®</sup> Microplate Reader (BMG Labtech) with Ex/Em = 520/605 nm. In benzylamine treated cells there was a significant difference in ROS production in cells without inhibitor and in the presence of MDL72527 and βAPN (\*\*\*\*p < 0.0001 for without inhibitor vs MDL72527 & \*p < 0.05 for without inhibitor vs βAPN). In methylamine treated cells there was a significant difference in ROS production in cells without inhibitor and in the presence of MDL72527 (\*\*\*\*p < 0.0001 for without inhibitor vs MDL72527). In aminoacetone treated cells there was a significant difference in ROS production in cells without inhibitor and in the presence of MDL72527 (\*\*\*\*p < 0.001 for without inhibitor vs MDL72527). There was no statistical difference (p > 0.05) in ROS production in methylamine and aminoacetone treated cells without inhibitor and in the presence of βAPN. Additionally, significant difference in ROS production was detected between MDL72527 and βAPN in benzylamine treated cells (####p < 0.0001 for MDL72527 vs βAPN), methylamine treated cells (####p < 0.0001 for MDL72527 vs βAPN), and aminoacetone treated cells (####p < 0.0001 for MDL72527 vs βAPN).

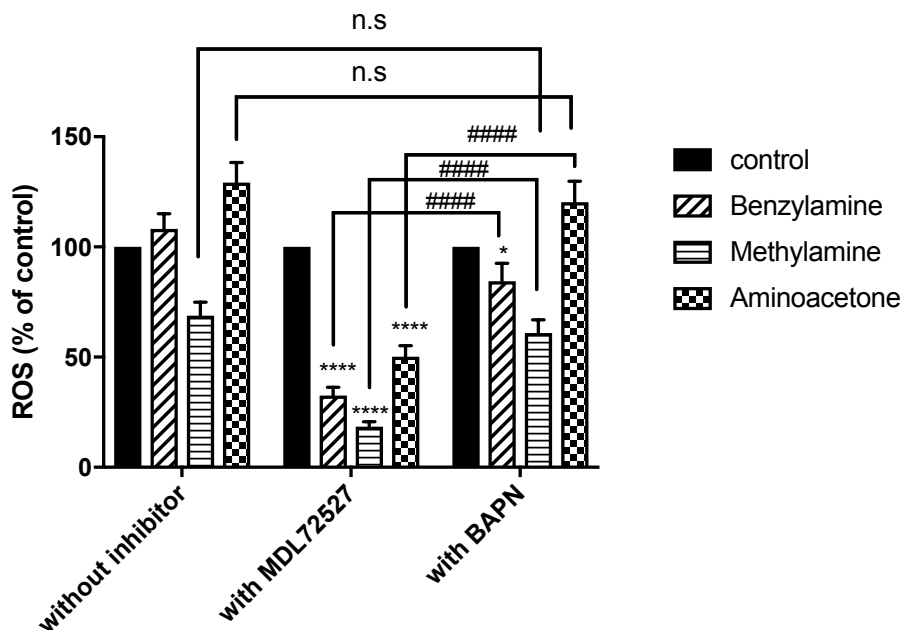
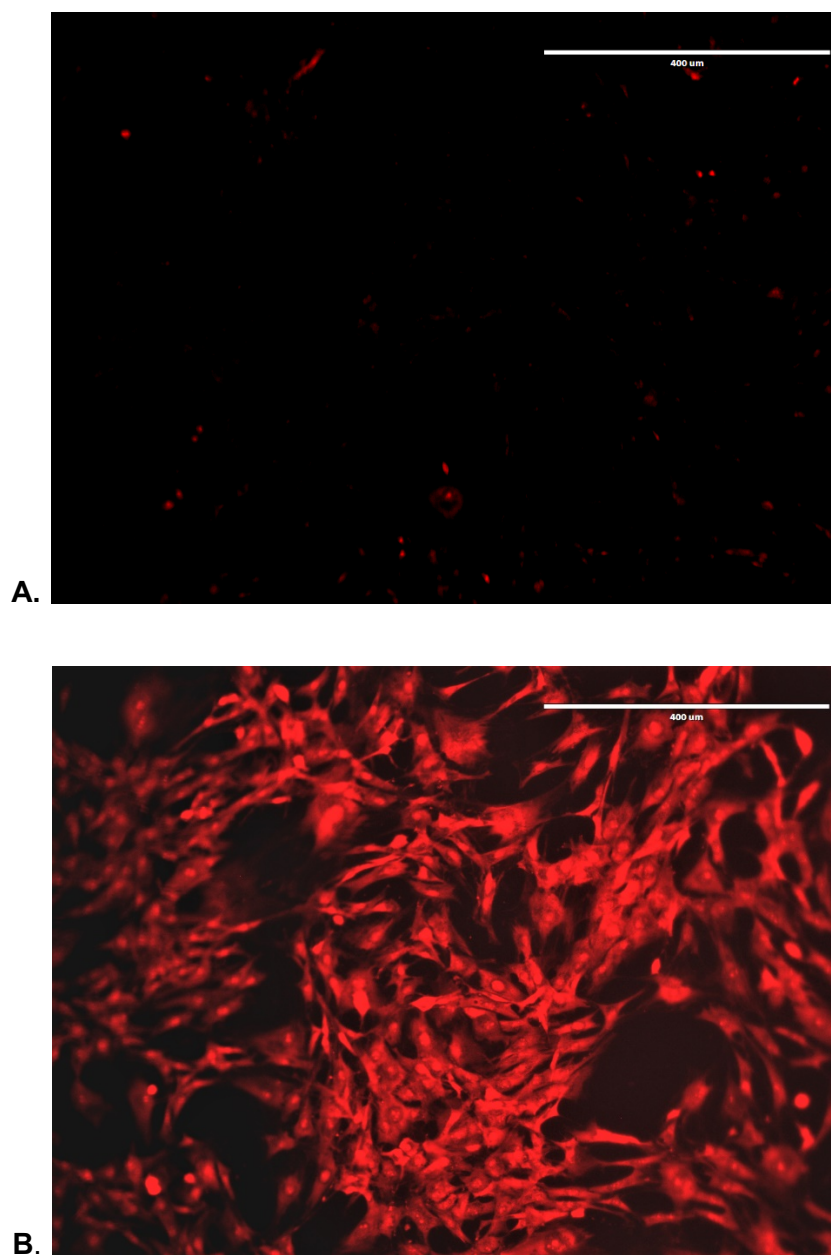
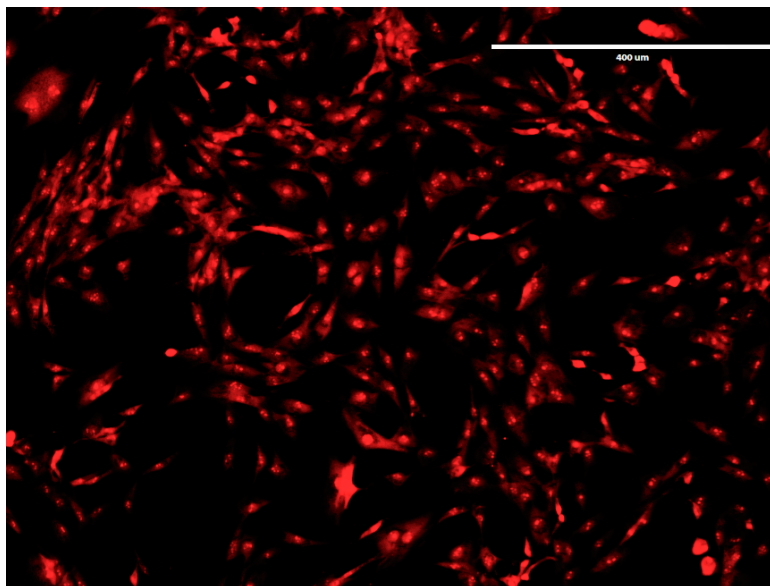
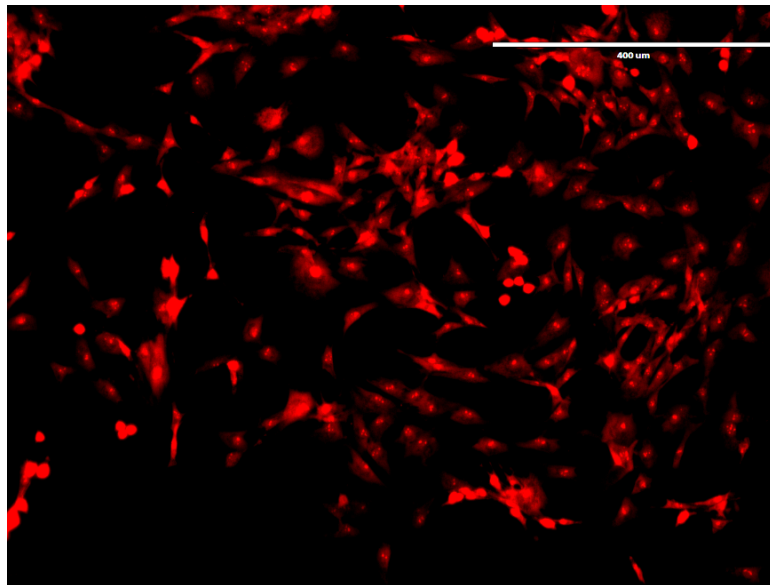
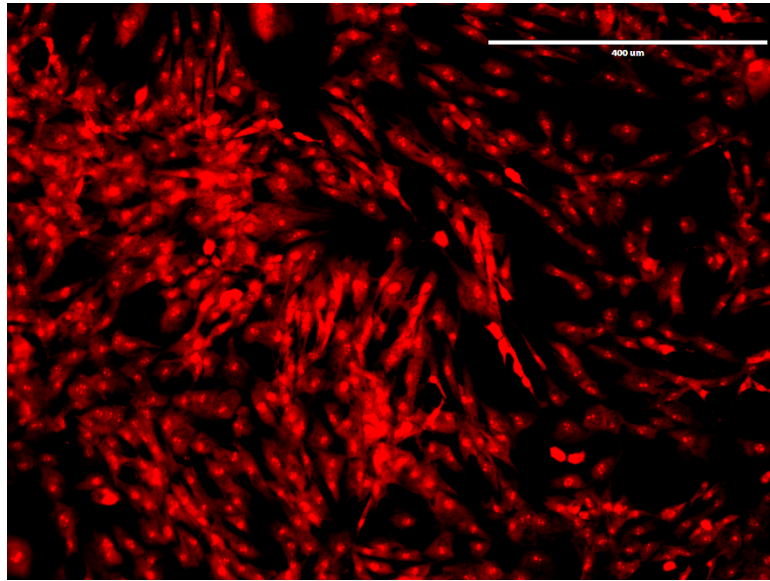
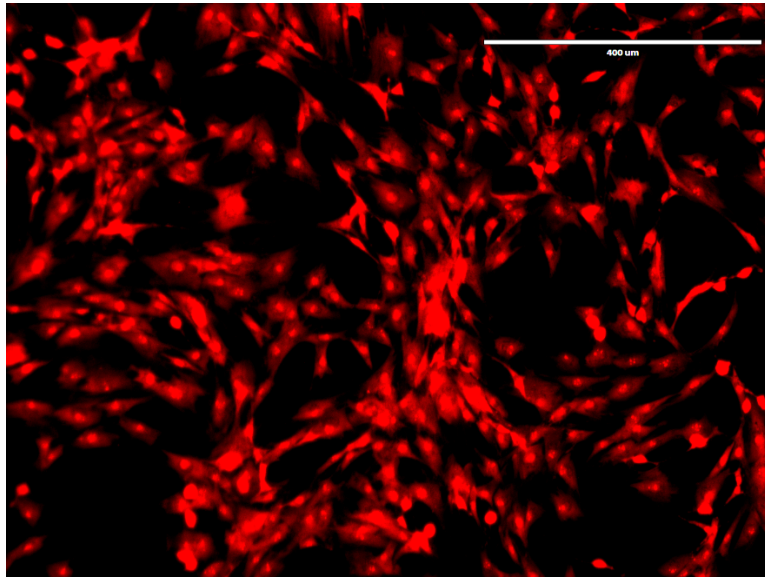


Figure 83. ROS production (percentage relative to DMNQ treated – control) after treatment with benzylamine (500 $\mu$ M), methylamine (500 $\mu$ M), and aminoacetone (45 $\mu$ M) (without inhibitor), benzylamine (500 $\mu$ M), methylamine (500 $\mu$ M), and aminoacetone (45 $\mu$ M) in the presence of 100 $\mu$ M MDL72527 (with MDL72527), and benzylamine (500 $\mu$ M), methylamine (500 $\mu$ M), and aminoacetone (45 $\mu$ M) in the presence of 200 $\mu$ M  $\beta$ APN (with  $\beta$ APN). 1XPBS (10 $\mu$ l/well) was used for untreated cells and 5 $\mu$ M DMNQ (20 $\mu$ l/well) was used like a positive control. Readings were taken after 30 minutes incubation at 37 $^{\circ}$ C/5%CO $_2$  using Clario Star<sup>®</sup> Microplate Reader (BMG Labtech) with Ex/Em = 520/605 nm. The data was analyzed by two-way ANOVA (\* $p$  < 0.0001), followed by Dunnett's and Tukeys' multiple comparison tests. In benzylamine treated cells there was a significant difference in ROS production in cells without inhibitor and in the presence of MDL72527 and  $\beta$ APN (\*\*\*\* $p$  < 0.0001 for without inhibitor vs MDL72527 & \* $p$  < 0.05 for without inhibitor vs  $\beta$ APN). In methylamine treated cells there was a significant difference in ROS production in cells without inhibitor and in the presence of MDL72527 (\*\*\*\* $p$  < 0.0001 for without inhibitor vs MDL72527). In aminoacetone treated cells there was a significant difference in ROS production in cells without inhibitor and in the presence of MDL72527 (\*\*\*\* $p$  < 0.001 for without inhibitor vs MDL72527). There was no statistical difference ( $p$  > 0.05) in ROS production in methylamine and aminoacetone treated cells without inhibitor and in the presence of  $\beta$ APN. Additionally, significant difference in ROS production was detected between MDL72527 and  $\beta$ APN in benzylamine treated cells (#### $p$  < 0.0001 for MDL72527 vs  $\beta$ APN), methylamine treated cells (#### $p$  < 0.0001 for MDL72527 vs  $\beta$ APN), and aminoacetone treated cells (#### $p$  < 0.0001 for MDL72527 vs  $\beta$ APN). The data is presented as means  $\pm$  S.E.M. of five independent experiments with three replicates in each. The asterisk (\*) indicates statistical difference between cells without inhibitor and cells treated with MDL72527 or  $\beta$ APN. The hash (#) indicates statistical difference between MDL72527 and  $\beta$ APN for each substrate.

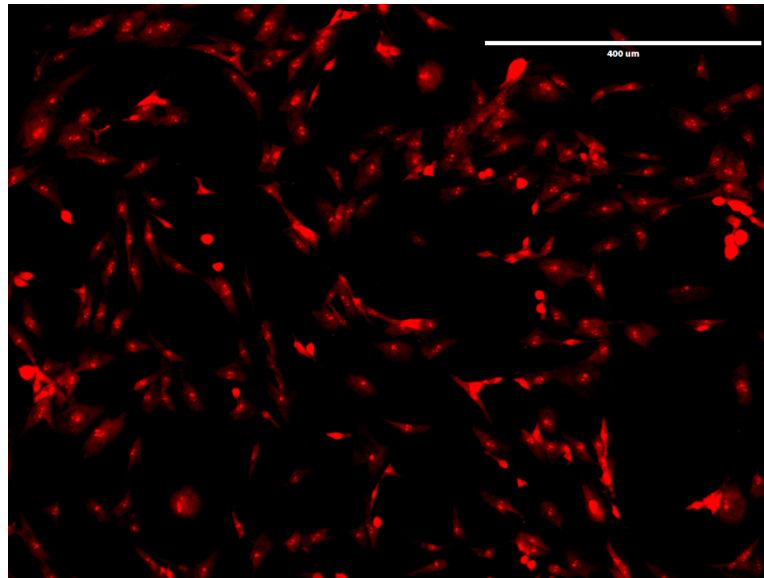
Figure 84 is a visual presentation of the stained rat aortic VSMCs with ROS red dye. The dye is cell permeable and reacts with ROS present in the cell to generate a red fluorescent signal. Cells were treated with 1XPBS (A - negative control), 5 $\mu$ M DMNQ (B – positive control), 500 $\mu$ M benzylamine (C), 500 $\mu$ M benzylamine + 100 $\mu$ M MDL72527 (D), 500 $\mu$ M benzylamine + 200  $\mu$ M  $\beta$ APN (E), 500 $\mu$ M methylamine (F), 500 $\mu$ M methylamine + 100 $\mu$ M MDL72527 (G), 500 $\mu$ M methylamine + 200 $\mu$ M  $\beta$ APN (H), 45 $\mu$ M aminoacetone (I), 45 $\mu$ M aminoacetone + 100 $\mu$ M MDL72527 (J), 45 $\mu$ M aminoacetone + 200 $\mu$ M  $\beta$ APN (K) and incubated for 30 minutes at 37 $^{\circ}$ C/5%CO $_2$ . The images were acquired after 30 minutes incubation.



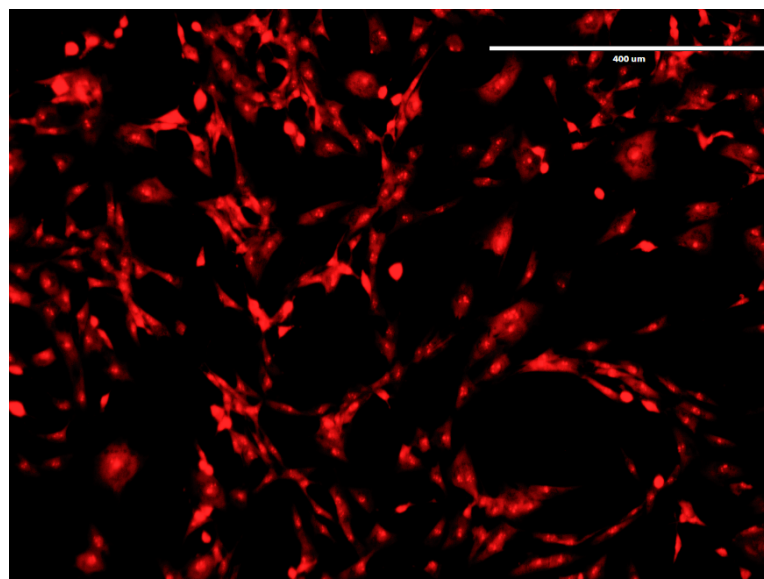




F.



G.



H.

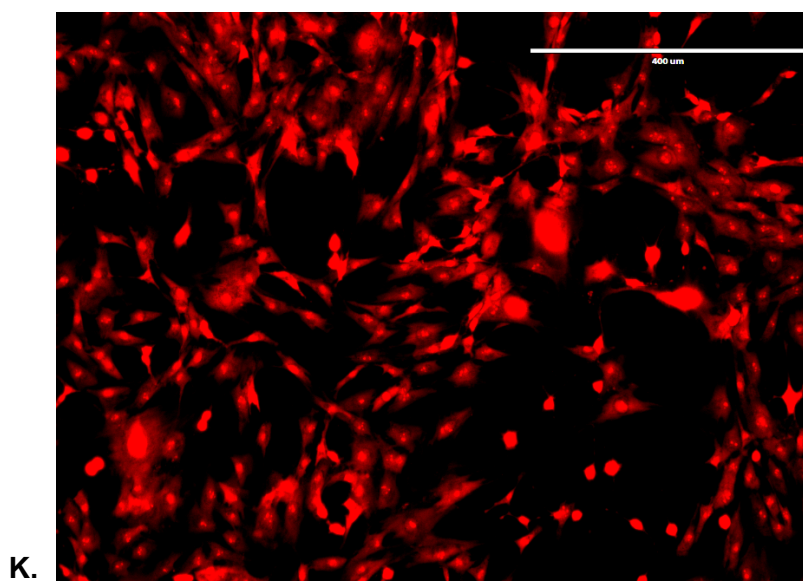
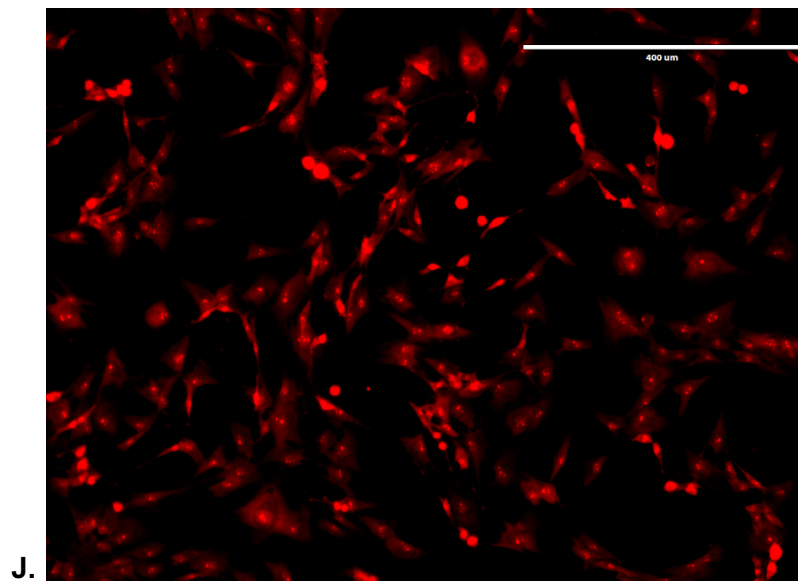
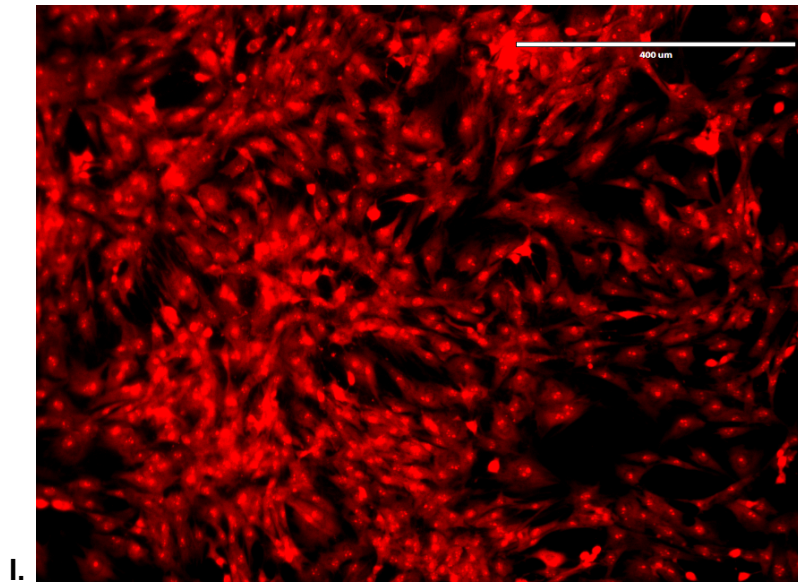


**Figure 84. Fluorescent images depicting ROS production in: cells treated with 1XPBS (A - negative control), 5 $\mu$ M DMNQ (B – positive control), 500 $\mu$ M benzylamine (C), 500 $\mu$ M benzylamine + 100 $\mu$ M MDL72527 (D), 500 $\mu$ M benzylamine + 200  $\mu$ M  $\beta$ APN (E), 500 $\mu$ M methylamine (F), 500 $\mu$ M methylamine + 100 $\mu$ M MDL72527 (G), 500 $\mu$ M methylamine + 200 $\mu$ M  $\beta$ APN (H), 45 $\mu$ M aminoacetone (I), 45 $\mu$ M aminoacetone + 100 $\mu$ M MDL72527 (J), 45 $\mu$ M aminoacetone + 200 $\mu$ M  $\beta$ APN (K). Scale bar 400 $\mu$ m, magnification is X10.**

### **Measurement of total GSH**

Total GSH (nM/mg protein) was detected with a colorimetric recycling assay based on the glutathione recycling system by DTNB (Ellman’s reagent) and glutathione reductase. Late passage (7 & 8) VSMCs were treated with SSAO (benzylamine, methylamine, aminoacetone) and LOX (benzylamine) substrate amines (without inhibitor); and in the presence of their respective inhibitors, MDL72527 (with MDL72527) and  $\beta$ APN (with  $\beta$ APN). Cells in culture medium - without treatment, were used like control. The cells were incubated for 30 minutes at 37<sup>0</sup>C/5%CO<sub>2</sub> and the absorbance was read on 412nm using ClarioStar<sup>®</sup> Microplate Reader (BMG Labtech). Significant reduction in total GSH production was detected in cells without inhibitor (\*\*\*\*p < 0.0001 for benzylamine, methylamine and aminoacetone treated cells vs control); cells treated with MDL72527 (\*\*\*\*p < 0.0001 for benzylamine, methylamine, and aminoacetone vs control); and cells treated with  $\beta$ APN (\*\*\*\*p < 0.0001 for benzylamine, methylamine and aminoacetone treated cells vs control). Furthermore, in benzylamine, methylamine and aminoacetone treated cells there was no statistical difference between cells without inhibitor and cells treated with MDL72527 and  $\beta$ APN (p > 0.05).

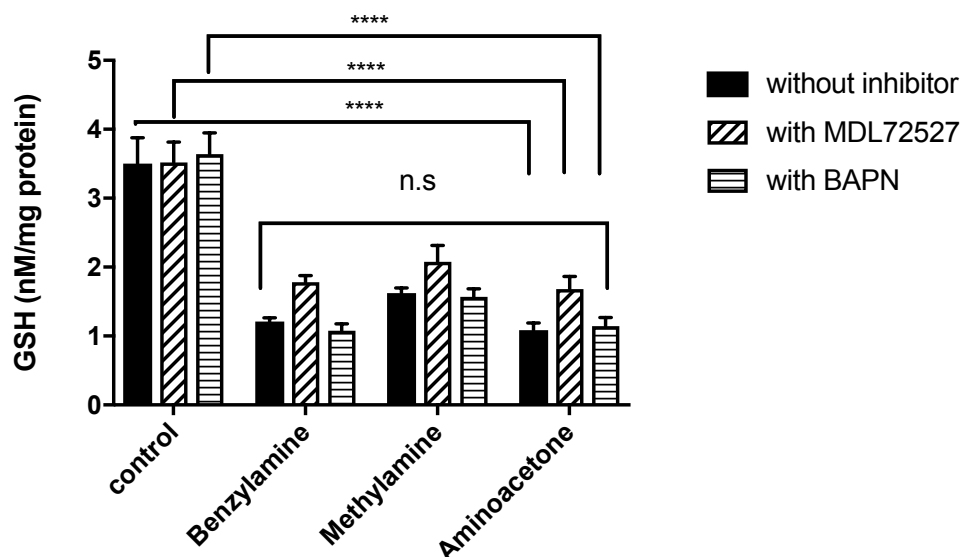


**Figure 85. GSH production (nM/mg protein) in VSMCs after treatment with benzylamine (500 $\mu$ M), methylamine (500 $\mu$ M), and aminoacetone (45 $\mu$ M) (without inhibitor), benzylamine (500 $\mu$ M), methylamine (500 $\mu$ M), and aminoacetone (45 $\mu$ M) in the presence of 100 $\mu$ M MDL72527 (with MDL72527), and benzylamine (500 $\mu$ M), methylamine (500 $\mu$ M), and aminoacetone (45 $\mu$ M) in the presence of 200 $\mu$ M  $\beta$ APN (with  $\beta$ APN). Cells in culture medium - without treatment, were used like a control. The absorbance was taken after 30 minutes incubation at 37<sup>o</sup>C/5%CO<sub>2</sub> using ClarioStar<sup>®</sup> Microplate Reader (BMG Labtech) with 412 nm. The data was analyzed by two-way ANOVA (\*\*\*\*p < 0.0001), followed by Dunnett's multiple comparison test. Significant reduction in total GSH production was detected in cells without inhibitor (\*\*\*\*p < 0.0001 for benzylamine, methylamine and aminoacetone treated cells vs control); cells treated with MDL72527 (\*\*\*\*p < 0.0001 for benzylamine, methylamine, and aminoacetone vs control); and cells treated with  $\beta$ APN (\*\*\*\*p < 0.0001 for benzylamine, methylamine and aminoacetone treated cells vs control). In benzylamine, methylamine and aminoacetone treated cells there was no statistical difference between cells without inhibitor and cells treated with MDL72527 and  $\beta$ APN (p > 0.05). The data is presented as means  $\pm$  S.E.M. of four independent experiments with three replicates in each. The asterisk (\*) indicates statistical significance between benzylamine, methylamine and aminoacetone treated cells vs control.**

#### **SECTION 3.5.4 DISCUSSION**

Reactive oxygen species (ROS) are key mediators of signalling pathways and as such contribute to the development of various pathologies. ROS mediate signalling pathways by acting as secondary messengers and inducing secondary effects such as signal transduction, cell proliferation, chemotaxis, apoptosis, and necrosis (Chao *et al.*, 2014). Furthermore, due to their high chemical reactivity ROS also lead to direct protein oxidation and degradation; and lipid peroxidation (Chao *et al.*, 2014). For example, superoxide anion (O<sub>2</sub><sup>-</sup>), hydroxyl radical ( $\cdot$ OH) and H<sub>2</sub>O<sub>2</sub> are well recognized inducers of mutagenesis by direct chemical reaction with DNA (Maynard *et al.*, 2009).

Regarding vascular pathologies, previous studies have already supported the notion that ROS released from dysfunctional mitochondrial respiratory chain; and enhanced ROS production through nicotinamide adenine dinucleotide phosphate (NADPH) oxidase, myeloperoxidase (MPO), xanthine oxidase (XO), lipoxygenase (LO), and nitric oxide synthase (NOS) have a causative role in the initiation and progression of atherosclerosis (Bonomini *et al.*, 2008). To generate energy (e.g., ATP) and synthesize essential cellular components (e.g., nucleic acids), mammalian cells depend on a series of oxidation and reduction (redox) reactions. The redox reactions are associated with flow of electrons from reducing agents (reductants) to oxidizing agents (oxidants) (Xiao & Loscalzo, 2020).

Healthy vascular cells metabolize oxygen and generate in favour of reductants. Therefore, in the vascular wall reductive stress is intimately linked to oxidative stress. For example, an overproduction of reducing equivalents, such as NAD(P)H, could lead to production of substances that can undergo repetitive rounds of oxidation/reduction, consequently leading to the increased generation of superoxide anion radical and secondary oxidants (Bonomini *et al.*, 2008). In this section ROS production was assessed in VSMCs from passage number 7 & 8. This is because VSMCs with a greater passage number correlate with aged VSMCs. Previous studies have already highlighted that enhanced production of ROS and insufficient removal by scavenging systems are major characteristics in aged VSMCs, and as such contribute to vascular remodelling (Muyao & Fukagawa, 2010). The major forms of ROS found in VSMCs are superoxide anions ( $O_2^{\cdot-}$ ) and  $H_2O_2$ . Since  $O_2^{\cdot-}$  has a short half-life, it does not have a major role in vascular cell signalling.  $H_2O_2$  on the other hand, being a more stable metabolite with a half-life of several minutes is a perfect candidate to mediate signalling pathways and ROS formation in these cells.

As per the data presented in section 3.3, SSAO and LOX are expressed and active in aged VSMCs, with SSAO exhibiting higher activity comparing to LOX in VSMCs with a greater passage number. Highly active SSAO in aged VSMCs would also mean accelerated production of  $H_2O_2$ . In the initial set of experiments ROS production was first assessed over different time intervals (15, 30, 60 and 120 minutes) in aged VSMCs previously treated with benzylamine, cadaverine, methylamine or aminoacetone. DMNQ was used like a positive control to induce ROS formation because it does not conjugate with GSH directly, but it participates in redox reactions, resulting in continuous intracellular generation of ROS, thereby inducing oxidation of GSH to GSSG (Nur *et al.*, 2011).

As per Figure 82A significant difference in ROS production was detected over time (\*\* $p < 0.01$  for 15 min vs 120 min and \*\* $p < 0.01$  for 30 min vs 120 min). The raw data from Figure 82B complements this by showing gradual increase in DMNQ driven ROS production over time. Significant difference in ROS production was also detected between different amine treatments (Figure 82A). At each time point, highest ROS production was detected in aminoacetone and benzylamine treated cells, in comparison with the other amines. After 15 minutes incubation (#### $p < 0.0001$  for benzylamine vs cadaverine and methylamine; # $p < 0.05$  for cadaverine vs methylamine & #### $p < 0.0001$  for cadaverine and methylamine vs aminoacetone). After 30-, 60-, and 120-minutes incubation (#### $p < 0.0001$  for benzylamine vs cadaverine and methylamine & #### $p < 0.0001$  for cadaverine and methylamine vs aminoacetone).

Since benzylamine is a substrate for both, SSAO and LOX, and aminoacetone is a very specific endogenous SSAO amine substrate, this data could indicate predominantly SSAO driven ROS production in aged VSMCs. ROS formation has previously been associated with methylglyoxal in vascular endothelial cells (Kim *et al.*, 2020), and pancreatic beta cells (Liu *et al.*, 2020). Kim *et al.* (2020) demonstrated increase in mitochondrial and total cellular ROS formation in vascular endothelial cells after early stages of methylglyoxal treatment. Furthermore, Liu *et al.* (2020) demonstrated increase in mitochondrial ROS and overproduction of advanced glycation end products (AGEs) in pancreatic beta cells after methylglyoxal treatment. Since methylglyoxal is an aldehyde produced through SSAO catalysed reaction in which aminoacetone is oxidatively deaminated to aldehyde (methylglyoxal), the findings in Figure 82A correlate with these studies and associate SSAO activity with mitochondrial ROS production in VSMCs.

Furthermore, the data in this section also shows high ROS production after benzylamine treatment (Figure 82A), which could be related to both, SSAO and LOX activity in VSMCs. Previous studies have already associated LOX activity with enhanced oxidative stress and the activation of p38MAPK, structural alterations of elastin, and vascular stiffness in VSMCs (Martinez-Revelles *et al.*, 2017). However, as per the findings presented in section 3.1 where an increase in SSAO affinity towards benzylamine was detected in late passage cells, the benzylamine driven ROS production observed here (Figure 82A) could be attributed to a predominant SSAO effect over LOX. This could also be supported with the previous finding from section 3.3 in which higher SSAO activity was detected in VSMCs with a greater passage number in comparison to LOX.

Furthermore, the ROS production observed from benzylamine and aminoacetone treated cells was highest at 15 and 30 minutes and declined over time. Same pattern was observed with cadaverine treated cells; however, in methylamine treated cells the production of ROS was increased with time (Figure 82A). Since ROS are defined as relatively short-lived molecules, in the subsequent set of experiments ROS was measured after 30 minutes incubation with benzylamine, methylamine, or aminoacetone; in the presence of either MDL72527 or  $\beta$ APN, respectively. Moreover, 30 minutes was selected as an optimal time to take forward in the subsequent set of experiments because the ROS production observed after methylamine treatment was higher in comparison to 15 minutes and there was not much difference in benzylamine and aminoacetone driven ROS production between 15 and 30 minutes (Figure 82A).

As per Figure 83, in cells treated without inhibitor, the highest ROS production was detected in aminoacetone comparing to control (DMNQ), followed by benzylamine and methylamine. Furthermore, in benzylamine treated cells there was a significant difference in ROS production in cells without inhibitor and in the presence of MDL72527 and  $\beta$ APN (\*\*\*\* $p < 0.0001$  for without inhibitor vs MDL72527 & \* $p < 0.05$  for without inhibitor vs  $\beta$ APN). In methylamine treated cells there was a significant difference in ROS production in cells without inhibitor and in the presence of MDL72527 (\*\*\*\* $p < 0.0001$  for without inhibitor vs MDL72527). In aminoacetone treated cells there was a significant difference in ROS production in cells without inhibitor and in the presence of MDL72527 (\*\*\*\* $p < 0.001$  for without inhibitor vs MDL72527). There was no statistical difference ( $p > 0.05$ ) in ROS production in methylamine and aminoacetone treated cells without inhibitor and in the presence of  $\beta$ APN (Figure 83).

This data once again confirms the notion that the ROS production observed here is predominantly SSAO driven. This is because in benzylamine treated cells, an 80% reduction in ROS was observed after MDL72527 treatment, and 30% after  $\beta$ APN treatment, comparing to cells treated without inhibitor (Figure 83). Moreover, in methylamine and aminoacetone treated cells no significant reduction in ROS was detected after  $\beta$ APN treatment; 50% reduction in ROS was detected after MDL72527 treatment for methylamine, comparing to cells treated without inhibitor; and 90% reduction after MDL72527 treatment for aminoacetone, comparing to cells treated without inhibitor (Figure 83). Additionally, when comparing significance between the different inhibitor treatments, in benzylamine treated cells ROS reduction was higher after MDL72527 treatment, comparing to  $\beta$ APN (#### $p < 0.0001$  for MDL72527 vs  $\beta$ APN). The same was observed for methylamine (#### $p < 0.0001$  for MDL72527 vs  $\beta$ APN), and aminoacetone treated cells (# $p < 0.0001$  for MDL72527 vs  $\beta$ APN) (Figure 83). Therefore, this data demonstrates higher potency of MDL72527 in reducing ROS comparing to  $\beta$ APN, which once again prioritise SSAO over LOX in ROS production.

Furthermore, Figure 84 complements the data from Figure 83 by depicting ROS-stained cells after benzylamine, methylamine, and aminoacetone treatment, and after amine treatment and addition of MDL72527 or  $\beta$ APN, respectively. As per Figure 84 a higher reduction in the number of stained cells was detected after MDL72527 treatment (D), and less reduction after  $\beta$ APN treatment (E), comparing to benzylamine treated cells without inhibitor (C). The same pattern was observed in methylamine treated cells (Figure 84F, G, H), and aminoacetone treated cells (Figure 84I, J, K). Moreover, the cells treated with DMNQ (positive control) depicted high ROS production in comparison to PBS (negative control) treated cells (Figure 84A & B).

Overall, the ROS data presented here shows significant increase in ROS production over time and significant difference in ROS production between different amine treatments over different time intervals (Figure 82A); significant reduction in ROS in benzylamine, methylamine, and aminoacetone treated cells after MDL72527 treatment, comparing to cells treated without inhibitor (Figure 83; Figure 84), and significant reduction in ROS in benzylamine, but not methylamine or aminoacetone treated cells after  $\beta$ APN treatment, comparing to cells treated without inhibitor (Figure 83; Figure 84).

Since aged VSMCs are associated with higher SSAO activity in comparison to LOX (as per the data in section 3.3); SSAO affinity for its substrate benzylamine increases as the cells age with passage (as per the data in section 3.1); SSAO has higher affinity for aminoacetone in comparison to methylamine (as per the data in section 3.2); MDL72527 strongly inhibits SSAO activity and expression in late passage VSMCs and has no inhibitory potential over LOX (as per the data in section 3.3); and  $\beta$ APN has no strong inhibitory potential over SSAO in late passage cells (as per the data in section 3.3), active SSAO could be associated with ROS production in aged VSMCs.

In addition to measuring ROS total GSH production (nM/mg protein) was also assessed in late passage (7 & 8) VSMCs previously treated with SSAO (benzylamine, methylamine, aminoacetone) and LOX (benzylamine) substrate amines (without inhibitor); and in the presence of their respective inhibitors, MDL72527 and  $\beta$ APN. This is because glutathione is the main antioxidant that reduces hydrogen peroxide through glutathione peroxidase (GPx) catalyzed reactions (Aquilano *et al.*, 2014). As per Figure 85 there was a significant difference in total GSH production in cells without inhibitor ( $****p < 0.0001$  for benzylamine, methylamine and aminoacetone treated cells vs control – non-treated cells); cells treated with MDL72527 ( $****p < 0.0001$  for benzylamine, methylamine, and aminoacetone vs control – non-treated cells); and cells treated with  $\beta$ APN ( $****p < 0.0001$  for benzylamine, methylamine and aminoacetone treated cells vs control – non-treated cells). Furthermore, there was no statistical difference in total GSH between benzylamine, methylamine and aminoacetone treated cells without inhibitor, MDL72527, or  $\beta$ APN (Figure 85). Additionally, as per Figure 85, slight increase (but not statistically significant) in total GSH was seen in benzylamine, methylamine and aminoacetone treated cells after MDL72527 but not  $\beta$ APN treatment.

Exposure to ROS could reduce total GSH through its oxidation during which levels of oxidised GSH (GSSG) are increased (Musaogullari *et al.*, 2020). Moreover, hydroxyl radicals could lead to direct oxidation of GSH and consequently GSSG formation. As per Figure 85 significant reduction in total GSH was observed after benzylamine, methylamine and aminoacetone treatment. These findings complement the previous data where significant increase in ROS was detected after aminoacetone, benzylamine and methylamine (Figure 83). GSH is an important intracellular antioxidant and therefore reduction in its levels are paralleled with the generation of different ROS including hydroxyl radicals, superoxide anions, hydrogen peroxide and lipid peroxide (Franco *et al.*, 2007). As per the data presented here an addition of the above-mentioned amines leads to ROS formation, as seen by the reduction of total GSH (Figure 85). This is because in the presence of ROS total GSH levels drop due to increased conversion to GSSG, which is a defence mechanism of the cells to counteract ROS (Patel *et al.*, 2020). Since these amines are specific SSAO substrates (apart from benzylamine that is also deaminated by LOX), and hydrogen peroxide is a by-product of SSAO catalysed reaction, it would mean that active SSAO contributes to reduced GSH in these cells, because of ROS formation.

However, in contrast to the ROS data presented in Figure 83, where MDL72527 significantly reduced ROS and it was more potent in its inhibitory potential over ROS comparing to  $\beta$ APN, the GSH data does not show significant restoration of total GSH after MDL72527 or  $\beta$ APN treatment (Figure 85). Slight increase in total GSH was observed after MDL72527 treatment, in the presence of all three amines, however, not statistically significant (Figure 85). The reason for this could be that the VSMCs used in this experiment were late passage (aged cells). Previous studies have associated aging with reduced GSH synthesis, due to a corresponding fall in GCL and GS gene expression (Wang *et al.*, 2003; Liu *et al.*, 2004). GSSG produced from the consumption of GSH can be either restored again through NADPH-dependent catalysis of the flavoenzyme GSH reductase, or excreted from the cell (Aquilano *et al.*, 2014). However, since aging affects GSH synthesis, it is reasonable to think that it might also equally affect the restoration of GSH from GSSG. Furthermore, previous studies have also dissociated the relationship between ROS and GSH by demonstrating that reduced GSH was necessary contributing factor for ROS generation; however, inhibition of ROS by antioxidants does not necessarily restore GSH levels, which indicates independence from the generation of ROS (Franco *et al.*, 2007).

### **SECTION 3.5.5 CONCLUSION**

The data presented in this section associates predominantly active SSAO over LOX in ROS formation, in aged VSMCs. VSMCs treated with aminoacetone and benzylamine presented higher ROS production in comparison to cadaverine and methylamine treated cells. Moreover, ROS measured after aminoacetone and benzylamine treatment was highest at early time point (15 and 30 minutes) and then gradually decreased over time. In the presence of MDL72527, ROS levels were significantly abolished in aminoacetone and benzylamine treated cells.  $\beta$ APN treatment did not significantly reduce ROS in aminoacetone treated cells and demonstrated slight reduction in ROS in benzylamine treated cells. The effect of MDL72527 and  $\beta$ APN on ROS production was also confirmed with ROS-stained images of cells pre-treated with benzylamine, aminoacetone and methylamine. Furthermore, total GSH levels were significantly reduced after benzylamine, methylamine and aminoacetone treatment due to increased conversion to GSSG, because of defence mechanism of the cells to counteract ROS; however, failed to be restored after addition of MDL72527 and  $\beta$ APN.

## CHAPTER VI: MAIN DISCUSSION

Cardiovascular disease remains a leading cause of death and morbidity in the western world (WHO, 2019). One of the main features of cardiovascular disease is atherosclerosis which is characterised by the build of fatty deposits (plaques), calcification, inflammation and oxidative stress caused by highly specific cellular and molecular responses. Ruptured unstable atherosclerotic plaques are the major starting point for stroke and myocardial infarction (Bonomini *et al.*, 2007). Cigarette smoking, obesity, hypertension, diabetes, and dyslipidaemias are known atherogenic risk factors that can impair endothelial and smooth muscle cell function (Bennett *et al.*, 2016; Bonomini *et al.*, 2007). The activity of SSAO is implicated in the pathogenesis of atherosclerosis, as the activity of the enzyme measured in plasma is raised in type I and II diabetes, obesity, cerebrovascular disease, and in smokers (Salmi & Jalkanen, 2001; 2017; Conklin *et al.*, 2006; Zorzano *et al.*, 2003).

The endothelial, membrane bound SSAO is known to be involved in leukocyte rolling, adhesion, and transmigration into inflammatory sites, and the hydrogen peroxide and ammonia produced by SSAO are known to be cytotoxic to vascular cells at high concentrations (Salmi & Jalkanen, 2001; 2017; Unzeta *et al.*, 2006). The SSAO mediated production of toxic aldehydes can induce endothelial injury through the production of advanced glycation end-products (AGEs) and the cross-linking of proteins to each other (Wang *et al.*, 2018). However, there is no evidence available regarding the activity of SSAO in vascular smooth muscle cells associated with atherosclerosis. Furthermore, SSAO activity has not been previously compared with other copper rich amine oxidases such as LOX, which is also highly expressed in this cell type. Moreover, the role of SSAO and LOX as modulators of VSMCs function and their contribution in ROS formation, through production of hydrogen peroxide and aldehydes has not been investigated explicitly in this cell type.

This thesis aims to investigate SSAO and LOX catalytic activity in rat aortic VSMCs, and their contributory role in oxidative stress and chemotaxis (important hallmarks in atherosclerosis), through ROS formation and vascular remodelling. To be able to address the mechanism by which SSAO and LOX metabolism of model amines causes vascular damage it was crucial to develop an *in vitro* cell culture model that would effectively characterise SSAO and LOX activity in rat aortic vascular smooth muscle cells. It has been previously established that cultured cells are essential tools to investigate copper-containing enzymes pharmacology, biochemistry, and function (El Hadri *et al.*, 2002).

Moreover, the main advantages of using cultured cells are to allow a better control of experimental conditions with a higher reproducibility, and to provide more reliable and available biological materials (El Hadri *et al.*, 2002). Vascular SMCs were selected due to expressing high activity of SSAO in the vasculature. VSMCs are the main stromal cells in the medial layer of the vascular wall and are involved in many physiological functions and pathological changes that take place in the vasculature (Lacolley *et al.*, 2012). These cells produce the extracellular matrix (ECM) which is important to provide the arterial wall with the capacity to withstand the pressure from the circulating blood (Lacolley *et al.*, 2012). As mentioned earlier, VSMCs are characterised with high plasticity which enables them to re-programme their expression pattern in response to external stimuli. Therefore, based on the signals present in their local environment these cells can change phenotype from quiescent – contractile to proliferative - synthetic phenotype. The acquired synthetic phenotype will enable these cells to migrate and proliferate inwardly from the medial to the intimal layer of the arteries, leading to intimal hyperplasia which is one of the main characteristics in the pathophysiology of atherosclerosis (Gimbrone & Garcia-Cardena, 2016).

The VSMCs were isolated using aortic explants from male Wistar rats and characterised with the smooth muscle cell marker SM22 $\alpha$ , as explained in the methods sections 2.2.4 and 2.2.9. Cells were routinely passaged, as explained in section 2.2.5 and the percentage of viable cells was calculated with each passage, as explained in section 2.2.6. Cell monolayers from passage 3, 5 and 8, and with confluence of ~80 - 90% were used for experimental analysis. Firstly, the Amplex<sup>®</sup> Red monoamine oxidase assay was optimised to detect SSAO activity in rat aortic VSMCs based on H<sub>2</sub>O<sub>2</sub> production. The Amplex<sup>®</sup> Red (10-acetyl-3,7-dihydroxyphenoxazine) is a fluorogenic probe widely used to detect and quantify H<sub>2</sub>O<sub>2</sub> in biological systems (Debski *et al.*, 2016). The detection of H<sub>2</sub>O<sub>2</sub> in this assay is based on peroxidase-catalysed oxidation of Amplex<sup>®</sup> Red to resorufin, as explained in Figure 33, section 2.2.12. While optimising the Amplex<sup>®</sup> Red monoamine oxidase assay (as explained in section 3.1), maximal SSAO activity was detected at 6h from addition of reaction mixture (Section 3.1; Figure 37). Furthermore, a statistically significant (\*\*p < 0.01) passage dependent increase in SSAO affinity for its substrate benzylamine was shown by a 3-fold reduction in the Km as passage increased from 3 (Km = 0.2084) to 8 (Km = 0.07267). (Section 3.1; Figure 40).

These were novel findings that have not been previously documented in the literature. A study done by Hernandez *et al.* (2006) investigated SSAO kinetic parameters in rat aorta A7r5 cells while studying the mechanism behind induced apoptosis because of SSAO catalysed reaction. Hernandez *et al.* (2006) compared SSAO kinetic parameters in the presence of benzylamine, methylamine and tyramine as substrates and demonstrated highest SSAO affinity for benzylamine in rat aortic A7r5 cells with  $V_{max} = 87 \pm 5$  and  $K_m = 0.8 \pm 0.1$ . The kinetic parameters for SSAO in the presence of benzylamine as shown in this thesis (Section 3.1; Figure 40, where  $V_{max} = 20 \pm 4$  and  $K_m = 0.2 \pm 0.07$ ) are within the range demonstrated by Hernandez *et al.* (2006). Moreover, the advantage of this data in comparison to Hernandez *et al.* (2006) is that higher SSAO affinity for benzylamine was detected in rat aortic VSMCs from primary cell line, which was passage dependent as the cells aged with passage (Section 3.1; Figure 40). Furthermore, the SSAO kinetic activity expressed in this thesis was congruent with previous tissue culture models (Wang *et al.*, 2018; Jarnicki *et al.*, 2016). The close pharmacological findings in SSAO activity as shown in the *in vitro* cell culture model optimised here and the previously described *in vitro* tissue models support the idea that the *in vitro* system represents the most appropriate model to study copper rich amine oxidases biochemistry, regulation, and function.

After successfully optimising the model to assess SSAO activity in rat aortic VSMCs, the same was evaluated further by assessing SSAO inhibition with reversible and irreversible inhibitors and observing SSAO kinetic parameters in the presence of its endogenous amines, aminoacetone and methylamine. Furthermore, a set of cytotoxicity studies were performed to explore the consequences of SSAO catalysed reaction on VSMCs viability in culture. It has been documented that SSAO, through aliphatic amine metabolism, could exert cytotoxic effects on smooth muscle cells *in vitro* and cause vascular damage, which sometimes resemble the pathological changes observed in atherosclerosis (El Hadri *et al.*, 2002).

Semicarbazide, methylhydrazine and MDL72527 were demonstrated potent in inhibiting SSAO, with no cytotoxic effect on cell growth (Section 3.2; Figure 42A, B & C). Furthermore, 15 minutes incubation with semicarbazide, methylhydrazine and MDL72527 was demonstrated as most successful to inhibit SSAO activity, as reflected in the  $K_i$  values (Table 8). Methylhydrazine was identified as the most potent reversible inhibitor showing successful SSAO inhibition at 1nM (Section 3.2; Figure 43B), and MDL72527 as the most potent irreversible inhibitor demonstrating successful inhibition at 50 $\mu$ M (Section 3.2; Figure 43C). The inhibition potency of methylhydrazine to inhibit SSAO in reversible manner has been previously reported (Holt & Callingham, 1994; O'Rourke *et al.*, 2007; 2008).

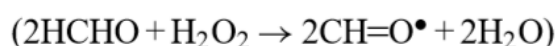
O'Rourke *et al.* (2008) have examined the effectiveness of methylhydrazine in homogenate of aorta rat tissue and identified a significant potency of methylhydrazine to inhibit SSAO within the nanomolar range. Irreversible SSAO inhibition with MDL72527 has also been widely noted in previous studies (Seiler *et al.*, 2000; Duranton *et al.*, 2002; Agostinelli *et al.*, 2006). Duranton *et al.* (2002) have identified MDL72527 as a highly selective and potent PAO and SSAO inhibitor, with no cytotoxic effect on cell growth.

Furthermore, the data presented in this thesis demonstrates VSMCs cytotoxicity because of SSAO catalysed reaction and enhanced cytotoxic effect after simultaneous addition of SSAO derived aldehydes and H<sub>2</sub>O<sub>2</sub> (Section 3.2; Figure 44A & B; Figure 45A & B). Moreover, VSMCs death was detected after addition of aminoacetone and methylamine at concentrations 50 & 1000µM (Section 3.2; Figure 44A & B). To confirm that cell viability loss was mediated through SSAO catalytic activity a specific and irreversible inhibitor MDL72527 was added, which in this thesis was shown potent in inhibiting SSAO with no cytotoxic effect on cell growth (Section 3.2; Figure 42C & Figure 43C). MDL72527 reversed cytotoxicity in VSMCs and completely abolished cell death (Section 3.2; Figure 44A & B). Cytotoxic effects induced by SSAO catalytic activity have been previously reported in other studies (Braun *et al.*, 2018; Hernandez *et al.*, 2006; Duranton *et al.*, 2002). Braun *et al.* (2018) observed rat aortic A7r5 cell death because of SSAO mediated metabolism of aminoacetone and methylamine. In the study by Braun *et al.* (2018) 1mM aminoacetone and 1mM methylamine induced rat aortic A7r5 cell death which was completely inhibited by 1mM semicarbazide. The data presented here (Section 3.2; Figure 44A) supports the finding by Braun *et al.* (2018) regarding methylamine and demonstrates higher potency of aminoacetone in reducing cell viability in VSMCs grown from primary cell line (Section 3.2; Figure 44B).

Furthermore, a cytotoxic effect on VSMCs was also detected after direct exposure to SSAO generated aldehyde (formaldehyde and methylglyoxal) products, H<sub>2</sub>O<sub>2</sub>, or the combination of both (Section 3.2; Figure 45A & B). In these findings, the aldehydes and H<sub>2</sub>O<sub>2</sub> reached between 30 – 40% reduction in cell viability comparing to control (Section 3.2; Figure 45A & B). Cytotoxicity induced by methylglyoxal and formaldehyde has been widely reported in previous studies (Braun *et al.*, 2018; Lin *et al.*, 2005; 2006; Gautam *et al.*, 2006). Formaldehyde has been reported cytotoxic in rat aortic endothelial cells by inducing covalent binding between functional groups in lysine residues of protein, and DNA base (Lin *et al.*, 2005). Gubisne-Haberle *et al.* (2004) have reported that when present at small concentrations (< 0.01mM) formaldehyde mainly induces DNA breakage, whereas at high concentrations (> 0.01mM) it has ability to induce DNA crosslinks.

Methylglyoxal has also been previously shown as inducer of apoptosis in human umbilical vein endothelial cells (HUVECs) by significantly altering gene expression profiles (Braun *et al.*, 2018). Hydrogen peroxide has also been identified as a modulator for inducing apoptosis in various cell types (Lin *et al.*, 2005; Gautam *et al.*, 2006). Gautam *et al.* (2006) have observed a marginal rise (~8%) in Leydig cells apoptosis induced by physiological concentrations of H<sub>2</sub>O<sub>2</sub> (30 to 50µM) and Lin *et al.* (2005) have reported induced rat aortic VSMCs apoptosis caused by high concentrations (1 and 2mM) H<sub>2</sub>O<sub>2</sub>; which in the study by Lin *et al.* (2005) was demonstrated as important modulator in increasing DNA protein crosslinks.

The data presented here shows an additive effect between SSAO derived aldehydes and H<sub>2</sub>O<sub>2</sub> in inducing VSMCs death (Section 3.2; Figure 45A & B). In these findings, methylglyoxal and H<sub>2</sub>O<sub>2</sub> combined caused 70% cell death, and formaldehyde and H<sub>2</sub>O<sub>2</sub> caused 60% cell death above control (Section 3.2; Figure 45A & B). Studies suggesting interactions between SSAO derived aldehydes and H<sub>2</sub>O<sub>2</sub> have been reported in other cell types but not VSMCs (Lin *et al.*, 2005; Conklin *et al.*, 2004; Gubisne-Haberle *et al.*, 2004). Lin *et al.* (2005) have suggested that formaldehyde and H<sub>2</sub>O<sub>2</sub> can injure endothelial cells synergistically through DNA protein crosslinks. Lin *et al.* (2005) have demonstrated this by observing changes in DPC (DNA protein coefficient) which is one of the most important forms of DNA injury. The explanation behind the enhanced cytotoxic effect detected here between SSAO generated aldehydes and H<sub>2</sub>O<sub>2</sub> could be the accelerated formation of oxidative stress. In a study by Yu & Zuo (1996) it was suggested that reactive free radicals can be generated from formaldehyde in the presence of H<sub>2</sub>O<sub>2</sub> as per the following reaction:



According to Lin *et al.* (2005) chronic exposure to oxidative stress caused by reaction between formaldehyde and H<sub>2</sub>O<sub>2</sub> could progressively damage endothelial cells by inducing DNA-protein crosslinks or cross-linkage of structural proteins, which would gradually and cumulatively increase until dysfunction occurs.

Furthermore, the data presented in this thesis demonstrates fast metabolism (~ 4 nmol/min) of aminoacetone and methylamine in rat aortic VSMCs because of SSAO catalysed reaction (Section 3.2; Figure 46A & B). Fast generation of methylglyoxal and formaldehyde could contribute to auto-oxidation of lipids and fatty acids within the cell and consequently lead to cell damage (Dator *et al.*, 2019). The data presented here shows a greater production of methylglyoxal comparing to formaldehyde because of SSAO catalysed reaction (Section 3.2; Figure 46A & B). Cellular concentrations of methylglyoxal are estimated to be between 1 – 5  $\mu$ M and higher concentrations than this can have damaging effect to the cell, mainly due to its highly reactive nature (Dator *et al.*, 2019). Being a highly reactive aldehyde methylglyoxal could affect cell cycle progression by activating apoptotic pathways; also contributing to the formation of AGE and increasing levels of oxidative stress (Braun *et al.*, 2018; Dhar *et al.*, 2008; Kenneth *et al.*, 2002). Dhar *et al.* (2008) have shown that aminoacetone induced methylglyoxal production in the VSMCs leads to AGE formation, oxidized DCF formation (an indicator of peroxynitrite) and increased iNOS levels.

After successful evaluation of the model, the same was applied further to study SSAO and LOX activity *in vitro*; explore their role in VSMCs proliferation, and their potential involvement in vascular remodelling. The data in this thesis shows a higher LOX activity in early passage cells and reduced LOX activity in cells with a greater passage number (Section 3.3; Figure 49A & B). Furthermore, it shows maintained LOX affinity (Section 3.3; Figure 52A, B & C) and Pro-LOX expression (Section 3.3; Figure 53A) in VSMCs from passage 3, 5 & 8; and accelerated loss in activity (more predominantly in late passage cells), but not expression, after addition of  $\beta$ APN (Section 3.3; Figure 50A). The use of  $\beta$ APN as irreversible inhibitor of LOX activity has been an important criterion for the role of LOX in various cell types (Payne *et al.*, 2005; Farjanel *et al.*, 2005; Lucero *et al.*, 2008). In this study,  $\beta$ APN was applied at concentration of 200 $\mu$ M which was previously shown to selectively inhibit LOX among other amine oxidases without exerting cytotoxic effect on cells (Lucero *et al.*, 2008).

As mentioned earlier, in the VSMCs LOX has a significant role in intra - and intermolecular covalent cross-linkage of collagen and elastin, an important physiological process in ECM formation and stability. Previous studies, however, have also highlighted a minor role of SSAO in synthesis, maturation, and organization of ECM proteins (Langford *et al.*, 2002; Gokturk *et al.*, 2007; Mercier, 2009). The detected reduction in LOX activity after  $\beta$ APN treatment, which as per the data presented here was observed at late passage cells, could result with defective cross-linking and consequently ECM disorganization (Ponticos & Smith, 2014).

Dysregulated ECM has been previously associated with the development of atherosclerosis, restenosis, and hypertension (Ponticos & Smith, 2014). In addition, Rodriguez *et al.* (2008) have suggested that altered ECM structure because of downregulated LOX activity could impair endothelial barrier function and lead to collagen accumulation.

Furthermore, the data presented here shows a gradual increase in SSAO activity (Section 3.3; Figure 49B) and affinity (Section 3.3; Figure 51A & B) after  $\beta$ APN treatment; and reduced VAP-1 expression observed at each passage, with the most noticeable reduction at passage 3 (Section 3.3; Figure 53B). Therefore, these findings indicate predominant SSAO activity in late passage VSMCs and predominant LOX activity in early passage cells. They also pose the question of possible interactions between SSAO and LOX in early passage VSMCs. This is because the reduction in SSAO activity and VAP-1 expression observed after  $\beta$ APN treatment could be associated with an indirect inhibitory mechanism caused by  $\beta$ APN driven LOX inhibition. Lucero *et al.* (2008) have demonstrated an ability of LOX to oxidise VSMCs cell surface proteins, further suggesting that VAP-1 might be one of the cell surface proteins oxidised by LOX. Oxidation of proteins could lead to activation of the same (Davies, 2016). Therefore, it could be that active LOX in early passage VSMCs contribute to the activation of SSAO in these cells by oxidising its membrane bound VAP-1, which would also mean that inhibited LOX would consequently result with inhibition of VAP-1 expression and SSAO activity in early passage VSMCs.

Dysregulated LOX activity and increased SSAO activity have been previously associated with cell differentiation (Bennett *et al.*, 2016; Filip *et al.*, 2016; El Hadri *et al.*, 2002). In normal physiological condition regulated ECM, due to physiologically active LOX, suppresses phenotypic switching by keeping VSMCs in a contractile state that is less responsive to mitogens (Bennett *et al.*, 2016). Conversely, breakdown of ECM, collagen, or elastin, by downregulated LOX activity could promote phenotypic switching and facilitate both cell proliferation and migration (Bennett *et al.*, 2016). On the other hand, Filip *et al.* (2016) have suggested that SSAO expression and activity is also closely associated with cell differentiation Filip *et al.* (2016) have demonstrated increased SSAO enzymatic activity and expression in primary rat chondrocytes by observing 3-fold increase in transcript levels and a 4-fold change in enzyme activity after 21 days in culture. In another study El Hadri *et al.* (2002) have used a serum-free medium permissive for *in vitro* VSMC differentiation, and observed a differentiation dependent increase in SSAO activity, mRNA, and protein levels. Interestingly, in a study by Sung *et al.* (2005), SSAO driven enhanced H<sub>2</sub>O<sub>2</sub> production has also been associated with VSMCs switch from contractile to synthetic.

The data presented here shows suppressed SSAO activity (Section 3.3; Figure 49B) and VAP-1 expression (Section 3.3; Figure 59B; Figure 60A) after 1h MDL72527 treatment. This data complements previous finding by Langford *et al.* (2002) which has demonstrated downregulated SSAO activity in both lung and aortic tissues after MDL-72274 and MDL72145 treatment. Langford *et al.* (2002) have demonstrated significant depression of SSAO activity with MDL72274 (high and low doses) and MDL72145, at which SSAO activity was lowered by approximately 70% in aortic tissue and 65% in lung. In this study MDL72527 was proven equally effective as MDL-72274 and MDL72145 in reducing SSAO activity. Therefore, the data presented here enhances the finding by Langford *et al.* (2002) and demonstrates successful MDL mediated downregulation of not only SSAO activity but also VAP-1 expression in primary rat aortic VSMCs with a greater passage number. Additionally, Langford *et al.* (2002) have also detected a reduction in LOX activity with MDL-72274 and MDL-72145 in lung tissue; however, they have not observed significant reduction of LOX activity in aorta. The data presented here confirms the same by showing no significant reduction of LOX activity in primary rat aortic VSMCs after 1h MDL72527 treatment (Section 3.3; Figure 50B).

Furthermore, despite the loss of contractile markers observed in non-treated, control cells (Section 3.3; Figure 55A), additional loss of contractile markers was detected at passage 3 after treatment with MDL72527 (Section 3.3; Figure 61B & 62B), benzylamine (Section 3.3; Figure 68B & C; Figure 69A; Figure 70A) and cadaverine (Section 3.3; Figure 68 B & C; Figure 70B). Since benzylamine is also a substrate for LOX this data correlates high LOX activity with a reduction in contractile markers in early passage primary rat aortic VSMCs. LOX has already been established as a potent chemokine with ability to induce migration of various cell types (Li *et al.*, 2000; Lucero *et al.*, 2008; Rodrigez *et al.*, 2008). As per Li *et al.* (2000), the chemotactic response initiated by LOX requires direct access between LOX and a substrate molecule tightly associated with the VSMCs. This finding was confirmed later by Rodrigez *et al.* (2008) who emphasized the importance of interaction between LOX and a tightly bound cell surface substrate or, an intrinsic membrane protein as a crucial event for LOX induced cell chemotaxis. Moreover, Lucero *et al.* (2008) have demonstrated that the expression of LOX in VSMCs results in optimal binding affinity and maximal binding capacity of PDGFR $\beta$ . Lucero *et al.* (2008) have also shown that the longevity of phosphorylated intermediates in the PDGFR $\beta$  signal-transduction pathway, as well as that of the activated receptor at the cell surface, are both diminished by inhibition of LOX activity in cell culture.

In accordance with the finding by Lucero *et al.* (2008) the data in this thesis also correlates LOX and PDGFR $\beta$  expression in primary rat aortic VSMCs by demonstrating reduced PDGFR $\beta$  expression in cells at passage 8, after inhibition of LOX with  $\beta$ APN (Section 3.3; Figure 57A & B; Figure 58). However, the data presented here also correlates SSAO activity and PDGFR $\beta$  expression and demonstrates reduced PDGFR $\beta$  expression in VSMCs at passage 3, 5 and 8 after SSAO inhibition with MDL72527 (Section 3.3; Figure 63A & B; Figure 64). Li *et al.* (2000) have identified LOX produced H<sub>2</sub>O<sub>2</sub> as important inducer in chemotactic activity in VSMCs. Since LOX's produced H<sub>2</sub>O<sub>2</sub> is critical for the chemotactic response initiated by LOX, it is wise to think that the SSAO driven H<sub>2</sub>O<sub>2</sub> production would also have the same effect on the cell. This has already been mentioned previously by Lucero *et al.* (2008) who has suggested that the H<sub>2</sub>O<sub>2</sub> by-product produced by SSAO catalyzed reaction could also be involved in the LOX-mediated modulation of chemotactic response. Furthermore, Lucero *et al.* (2008) have demonstrated that the H<sub>2</sub>O<sub>2</sub> by itself is insufficient to trigger chemotactic response by observing no elicited chemotaxis after glucose oxidase produced hydrogen peroxide, which once again strongly associates endogenously active LOX and SSAO, and no other amine oxidases, with VSMCs chemotaxis.

Since both, SSAO and LOX are abundantly present in VSMCs additional molecular studies were performed to investigate possible interactions between these two enzymes and observe changes in AOC3 and LOX mRNA levels in the presence of their respective suicide inhibitors. In VSMCs from passage 3, 5 and 8  $\beta$ APN and MDL72527 resulted with no significant difference in LOX mRNA expression levels (Section 3.4; Figure 73B); however, changes in AOC3 mRNA levels were detected at passage 3 after  $\beta$ APN treatment (\*p < 0.05 for non-treated vs  $\beta$ APN treated cells), and passage 8 (\*p < 0.05 for non-treated vs MDL72527 treated cells) after MDL72527 treatment (Section 3.4; Figure 73A). This data is consistent with the previous findings presented here which demonstrate significant reduction in SSAO activity (seen as H<sub>2</sub>O<sub>2</sub> production) in early passage VSMCs previously treated with  $\beta$ APN (Section 3.3; Figure 49B). Furthermore, it complements the western blot data which shows reduced VAP-1 expression in VSMCs from passage 3 previously treated with  $\beta$ APN (Section 3.3; Figure 53A & B). The  $\beta$ APN inhibitory potential over AOC3 mRNA expression levels was diminished in cells with a greater passage number (Section 3.4; Figure 73A); and this effect was consistent with  $\beta$ APN's effect on SSAO activity and VAP-1 protein expression previously observed (Section 3.3; Figure 49B; Figure 53A & B).

Since  $\beta$ APN has been previously demonstrated effective in exhibiting inhibitory potential over both, SSAO and LOX, additional qPCR experiments were performed to silence LOX gene and observe what changes would this bring on AOC3 mRNA expression levels. This study demonstrates successful silencing of LOX gene 72h post transfection with SiRNA6 (\*\*\*\*p < 0.0001 for Sictrl vs Si6 treated cells), and SiRNA8 (\*\*\*\*p < 0.001 for Sictrl vs Si8 treated cells), comparing to control (Section 3.4; Figure 75). Significant reduction in AOC3 gene expression was also detected with SiRNA6 (####p < 0.0001 for Sictrl vs Si6 treated cells), and SiRNA8 (####p < 0.001 for Sictrl vs Si8 treated cells), comparing to control (Section 3.4; Figure 75). 72h post transfection an approximate 60% decrease in LOX mRNA levels was observed with SiRNA6 and 30% decrease in LOX mRNA levels was detected with SiRNA8 (Section 3.4; Figure 75). Additionally, 72h post transfection an approximate 80% decrease in AOC3 mRNA levels was observed with SiRNA6 and 40% decrease in AOC3 mRNA levels was detected with SiRNA8 (Section 3.4; Figure 75). The protein expression from LOX was also significantly abolished 72h post transfection with SiRNA6 and SiRNA8, and VAP-1 protein expression was only significantly reduced with SiRNA8 comparing to control (Section 3.4; Figure 76). Moreover, the protein quantification data showed significant reduction in LOX protein expression with both, SiRNA6 and SiRNA8 (\*\*p < 0.01 for Sictrl vs Si6 treated cells and Sictrl vs Si8 treated cells); additionally, significant reduction in VAP-1 protein expression was only detected with SiRNA8 (#p < 0.05 for Sictrl vs Si8 treated cells) (Section 3.4; Figure 77).

This data answers the previously posed question of potential interaction between SSAO and LOX in early passage VSMCs and suggests that the previously seen reduction in SSAO activity and VAP-1 expression after  $\beta$ APN treatment is an indirect mechanism of inhibition due to irreversibly inhibited LOX. A synergistic relationship between SSAO and LOX in VSMCs has previously been highlighted (Mercier, 2009). Mercier (2009) demonstrated a minor contributory role of SSAO in ECM formation and related this to SSAO's synergistic relationship with LOX. The synergistic relationship between SSAO and LOX in the normal physiological development of elastin was also mentioned in a study by Langford *et al.* (2002) which demonstrated disorganisation of elastin fibres within tunica media because of inhibited SSAO and LOX. Furthermore, Lucero *et al* (2008) have shown an ability of LOX to oxidise, hence activate membrane bound cell surface proteins such as VAP-1, which associates VAP-1 dependence with LOX. The data presented here complements these findings and confirms synergistic interaction between these two enzymes in young (early passage) primary rat aortic VSMCs, while also highlighting a predominant LOX activity in young primary VSMCs and predominant SSAO activity in aged (late passage) primary VSMCs.

Since LOX is the main enzyme which contributes to the maintenance and assembly of the ECM, it is expected to demonstrate predominant activity over SSAO in primary early passage VSMCs. This is because ECM components are of vital importance in regulating physiological cell processes such as cell proliferation, survival, differentiation, and migration (Yue, 2015). Moreover, since this data shows reduced AOC3 mRNA expression and VAP-1 protein because of silencing LOX (Section 3.4; Figure 75; Figure 76), it complements the finding by Lucero *et al* (2008) which suggests VAP-1 activation dependence on LOX. Furthermore, it also enhances the findings by Mercier (2009) and Langford *et al* (2002) by suggesting that SSAO's contributory role in ECM formation in young (early passage VSMCs) might be a result of an indirect mechanism, due to active LOX.

Predominant SSAO activity has been previously associated with aging. Hernandez *et al.* (2005) have reported that membrane bound SSAO is overexpressed in the cerebrovascular tissue of Alzheimer's disease (AD). Since ageing is the primary risk factor for AD, which is characterised with significant microvascular degeneration affecting smooth muscle cells and endothelial cells, it could be associated with overactive SSAO. In another study, Unzeta *et al.* (2007) demonstrated that under physiological conditions, the expression of SSAO in human cerebrovascular tissue could contribute, by its own catalytic action, to the oxidative stress and vascular damage associated with AD. Aging is also a prominent risk factor for atherosclerosis by contributing to VSMCs proliferation, migration, and inflammation. Since inflammation induces the expression of the membrane bound VAP-1, it would also increase the activity of soluble SSAO. This is because the soluble SSAO is a result of a proteolytic cleavage of the membrane bound VAP-1. Increased number of soluble SSAO molecules would result with higher production of H<sub>2</sub>O<sub>2</sub> and reactive aldehydes. In this study SSAO activity was predominantly higher in VSMCs with a greater passage number in comparison to LOX, as reflected in the H<sub>2</sub>O<sub>2</sub> production (SSAO produced 150nmol/h/mg protein H<sub>2</sub>O<sub>2</sub> vs LOX produced 100nmol/h/mg protein H<sub>2</sub>O<sub>2</sub> at VSMCs passage 8) (Section 3.3; Figure 49A & B; Figure 50A & B).

Enhanced H<sub>2</sub>O<sub>2</sub> production would consequently lead to accelerated generation of reactive oxygen species (ROS) in aged cells. Elevated ROS and insufficient removal of the same by scavenging systems have been defined as hallmarks of vascular aging (Li & Fukagawa, 2010). The major forms of ROS found in the VSMC are superoxide anions which target heme groups, Fe-S clusters, cysteine residues, or other electron transfer units, and H<sub>2</sub>O<sub>2</sub> (Li & Fukagawa, 2010). Superoxide anions have a very short half-life in comparison to H<sub>2</sub>O<sub>2</sub> which is more stable metabolite with ability to diffuse freely across the vascular wall; therefore, it poses a higher risk for ROS formation and consequently oxidative stress.

The data presented in this thesis associates active SSAO with ROS production in aged VSMCs. In the first instance, to elucidate which copper-containing vascular enzyme (SSAO or LOX) generates more ROS, ROS was measured over different time intervals after treatment with benzylamine, cadaverine, methylamine and aminoacetone. The data presented here shows significant difference in ROS production over time (\*\*p < 0.01 for 15 min vs 120 min and \*\*p < 0.01 for 30 min vs 120 min) and significant difference in ROS production between the different amine treatments (Section 3.5; Figure 82). Furthermore, at each time point the highest ROS production was detected in aminoacetone and benzylamine treated cells, in comparison with the other amines (at 15 minutes incubation #p < 0.0001 for benzylamine vs cadaverine and methylamine; #p < 0.05 for cadaverine vs methylamine & #p < 0.0001 for cadaverine and methylamine vs aminoacetone; at 30-, 60-, and 120-minutes incubation #p < 0.0001 for benzylamine vs cadaverine and methylamine & #p < 0.0001 for cadaverine and methylamine vs aminoacetone).

Additionally, in benzylamine treated cells, this data shows 80% reduction in ROS after MDL72527 treatment, and 30% after  $\beta$ APN treatment, comparing to cells treated without inhibitor (Section 3.5; Figure 83). Moreover, in methylamine and aminoacetone treated cells no significant reduction in ROS was detected after  $\beta$ APN treatment; 50% reduction in ROS was detected after MDL72527 treatment for methylamine, comparing to cells treated without inhibitor; and 90% reduction in ROS was detected after MDL72527 treatment for aminoacetone, comparing to cells treated without inhibitor (Section 3.5; Figure 83). Since benzylamine is a substrate for both enzymes and aminoacetone is a very specific endogenous SSAO amine substrate our data associates predominantly SSAO driven ROS production in aged VSMCs.

This data is in accordance with the previous finding where predominantly higher SSAO activity was detected in VSMCs with a greater passage number in comparison to LOX (Section 3.3; Figure 49A & B; Figure 50A & B). Therefore, these findings suggest that in aged VSMCs SSAO activity is higher in comparison to LOX, and this copper-containing enzyme is the main contributor for ROS formation in these cells. SSAO has previously been suggested as a mediator of oxidative stress in the early stages of atherosclerosis and a contributor to atherosclerotic plaque development (Wang *et al.*, 2018; Bonomini *et al.*, 2008; Exner *et al.*, 2001). In the vascular cells, SSAO driven production of ROS (through induced generation of hydroxyl radicals because of largely produced H<sub>2</sub>O<sub>2</sub>) can directly injure cell membranes and nuclei (Bonomini *et al.*, 2008). In the endothelial cells, SSAO driven ROS interacts with endogenous vasoactive mediators and modulates vasomotion and the atherogenic process (Wang *et al.*, 2018).

In the vascular smooth muscle cells, SSAO driven ROS peroxidases lipid components, leading to the formation of oxidized lipoproteins (LDL), one of the key mediators of atherosclerosis. Interestingly, a study by Sung *et al.* (2005) demonstrated that an increase in ROS contributes to accelerated VSMCs switch from contractile to synthetic, and as such initiates VSMCs proliferation and migration, leading to intimal hyperplasia.

Active SSAO has been previously highlighted as a contributor of ROS in other pathologies. Unzeta *et al.* (2007) have associated increased SSAO expression and activity as a major source of oxidative stress in the blood vessel wall in AD. Calcific aortic valve stenosis (CAVS) is another pathology in which SSAO was associated with elevated oxidative stress. Moreover, in this pathology SSAO derived ROS was highlighted as contributory factor in increasing valve calcification and CAVS disease burden (Doroszko *et al.*, 2020). Furthermore, Doroszko *et al.* (2020) have reported high SSAO serum levels in patients with severe CAVS comparing to patients with moderate CAVS and have assessed this by echocardiography. In another study Mercier *et al.* (2020) have shown a gradual and significant increase in SSAO mRNA, protein, and activity in calcified and intermediate human aortic valves when compared to healthy aortic valves. Furthermore, Mercier *et al.* (2020) have also highlighted that SSAO upregulation with valve calcification was independent of the cardiovascular and CAVS risk factors obesity, diabetes, and smoking.

Exposure to ROS could reduce total GSH through its oxidation during which levels of oxidised GSH (GSSG) are increased (Musaogullari *et al.*, 2020). Moreover, hydroxyl radicals can lead to direct oxidation of GSH and consequently GSSG formation (Musaogullari *et al.*, 2020). Therefore, in addition to measuring ROS total GSH production (nM/mg protein) was also assessed in late passage (7 & 8) VSMCs previously treated with SSAO (benzylamine, methylamine, aminoacetone) and LOX (benzylamine) substrate amines (without inhibitor); and in the presence of their respective inhibitors, MDL72527 and  $\beta$ APN. This is because glutathione is the main antioxidant that reduces hydrogen peroxide through glutathione peroxidase (GPx) catalyzed reactions (Aquilano *et al.*, 2014).

As per the data presented here significant reduction in total GSH was observed after benzylamine, methylamine and aminoacetone treatment (Section 3.5; Figure 85). As per Figure 85 there was a significant difference in total GSH production in cells without inhibitor (\*\*\*\*p < 0.0001 for benzylamine, methylamine and aminoacetone treated cells vs control – non-treated cells); cells treated with MDL72527 (\*\*\*\*p < 0.0001 for benzylamine, methylamine, and aminoacetone vs control – non-treated cells); and cells treated with  $\beta$ APN (\*\*\*\*p < 0.0001 for benzylamine, methylamine and aminoacetone treated cells vs control – non-treated cells).

Furthermore, there was no statistical difference in total GSH between benzylamine, methylamine and aminoacetone treated cells without inhibitor, and cells treated with MDL72527 or  $\beta$ APN (Section 3.5; Figure 85). Additionally, as per Figure 85, slight increase (but not statistically significant) in total GSH was seen in benzylamine, methylamine and aminoacetone treated cells after MDL72527 but not  $\beta$ APN treatment.

These findings complement the previous data where significant increase in ROS was detected after aminoacetone, benzylamine and methylamine (Section 3.5; Figure 83). GSH is an important intracellular antioxidant and therefore reduction in its levels are paralleled with the generation of different ROS including hydroxyl radicals, superoxide anions, hydrogen peroxide and lipid peroxide (Franco *et al.*, 2007). As per this data, addition of the above-mentioned amines leads to ROS formation, as seen by the reduction of total GSH (Section 3.5; Figure 85). This is because in the presence of ROS total GSH levels drop due to increased conversion to GSSG, which is a defence mechanism of the cells to counteract ROS (Patel *et al.*, 2020). Since these amines are specific SSAO substrates (apart from benzylamine which is also deaminated by LOX), and hydrogen peroxide is a by-product of SSAO catalysed reaction, it would mean that active SSAO contributes to reduced GSH in these cells, because of ROS formation.

High SSAO activity has been previously associated with reduced GSH because of elevated ROS. A study by Ucar *et al.* (2005), in which SSAO's contribution was investigated in excessive ROS generation during ischemia–reperfusion (I/R) injury, indicated that the SSAO driven H<sub>2</sub>O<sub>2</sub> release in IR lung tissue was the main contributor for ROS. Furthermore, Ucar *et al.* (2005) have associated high ROS levels with reduced GSH, and further demonstrated elevated GSH levels after SSAO inhibition with semicarbazide. In this study MDL72527 did not completely restore GSH levels in rat aortic VSMCs (Section 3.5; Figure 85). However, the findings presented here are incomparable with the findings by Ucar *et al.* (2005), mainly because Ucar *et al.* (2005) have used lung tissues of previously dosed rats with 1ml/kg semicarbazide hydrochloride, whilst in our experiment we used primary VSMCs previously treated with 100 $\mu$ M MDL72527. In another study done in humans Ucar *et al.* (2003), have suggested that enhanced plasma SSAO activity might contribute to the production of ROS detected in the liver of alcoholics. Ucar *et al.* (2003) have suggested this by demonstrating correlation between increased plasma SSAO activity with elevated plasma, lipid peroxidation levels, and reduced GSH in alcoholics.

## SECTION 4.1 CONCLUSION

In this thesis, an *in vitro* cell culture model that can effectively measure SSAO and LOX activity in rat aortic VSMCs was optimised and validated. The model was validated by characterising SSAO inhibition with reversible and irreversible inhibitors potent in inhibiting SSAO with no cytotoxic effect on cell growth. Methylhydrazine was identified as the most potent reversible, and MDL72527 as the most potent irreversible inhibitor. Furthermore, cellular toxicity was identified because of SSAO catalysed reaction and enhanced cytotoxic effect was observed due to simultaneous addition of SSAO derived products, aldehydes and H<sub>2</sub>O<sub>2</sub>. In this thesis, fast generation of methylglyoxal and formaldehyde was demonstrated in rat aortic VSMCs because of SSAO catalysed reaction; and higher SSAO affinity for aminoacetone comparing to methylamine, which indicates a greater production of methylglyoxal comparing to formaldehyde in these cells.

The optimised model was applied further to study SSAO and LOX activity in VSMCs, as cells were being passaged from lower to higher passage number. At basal level and in the presence of its substrate cadaverine Pro-LOX expression and LOX's affinity were maintained between passages, while LOX activity was reduced as the cells aged with passage. In the presence of cadaverine, LOX's respective suicide inhibitor  $\beta$ APN resulted with a significant reduction in LOX activity, which was more predominant in late passage cells; and no changes in Pro-LOX expression and LOX mRNA levels were detected in cells from passage 3, 5 and 8. In the presence of cadaverine, SSAO's respective suicide inhibitor MDL72527 had no effect on LOX's activity, Pro-LOX expression, and LOX mRNA levels. At basal level and in the presence of its substrate benzylamine SSAO activity was firstly seen to reduce as the cells aged with passage, while VAP-1 expression was maintained in cells between passage 3, 5 and 8. Furthermore, a gradual increase in SSAO affinity for its substrate benzylamine was observed as the cells passage number increased. In the presence of benzylamine, SSAO's respective suicide inhibitor MDL72527 resulted with a significant reduction in SSAO activity, which was more predominant in late passage cells; and demonstrated reduced VAP-1 expression and AOC3 mRNA levels in cells from passage 8. In the presence of benzylamine LOX's respective suicide inhibitor  $\beta$ APN demonstrated inhibitory potential over SSAO activity, VAP-1 expression, and AOC3 mRNA levels in early passage cells; however, its inhibitory potential was diminished as the cells aged with passage.

Since benzylamine is a common substrate and  $\beta$ APN has inhibitory potential for both enzymes, the observed reduction in SSAO activity, protein, and mRNA expression after  $\beta$ APN treatment was investigated further by silencing LOX mRNA in early passage VSMCs. This thesis demonstrates a successful silencing of LOX gene, as seen by the reduction in LOX mRNA and protein expression levels, which also resulted with reduced AOC3 mRNA expression and VAP-1 protein levels. Therefore, indicating a synergistic relationship between these two enzymes in early passage VSMCs, while also suggesting that the previously seen reduction in SSAO activity and VAP-1 expression after  $\beta$ APN treatment could be a result of an indirect mechanism of inhibition due to irreversibly inhibited LOX. Treatment with benzylamine had no effect on LOX and VAP-1 expression and treatment with cadaverine resulted with a significant reduction in VAP-1 expression, with the most noticeable reduction observed at passage 3. Furthermore, a noticeable loss of contractile markers was observed in non-treated cells. In early passage cells there was additional reduction in contractile markers after treatment with MDL72527, cadaverine and benzylamine. Additionally, a reduction in PDGFR $\beta$  expression was observed after LOX (passage 8) and SSAO (passage 3, 5 & 8) inhibition. Reduced PDGFR $\beta$  levels were also detected at passage 3 after cadaverine and benzylamine treatment. In this thesis SSAO and LOX contribution in ROS formation was assessed in aged VSMCs and a highest ROS production was detected in aminoacetone and benzylamine treated cells in comparison to cadaverine and methylamine treated cells. In the presence of MDL72527, ROS levels were significantly abolished in aminoacetone and benzylamine treated cells, which suggests SSAO driven ROS production.  $\beta$ APN treatment did not significantly reduce ROS in aminoacetone treated cells and demonstrated slight reduction in ROS in benzylamine treated cells, which once again suggests that the ROS production detected in benzylamine treated cells is predominantly SSAO driven. ROS formation was also reflected in the reduction of total GSH. Total GSH levels were significantly reduced after benzylamine, methylamine and aminoacetone treatment due to increased conversion to GSSG, because of defense mechanism of the cells to counteract ROS; however, failed to be restored after addition of MDL72527 and  $\beta$ APN.

Overall, SSAO and LOX activity and expression were detected in primary rat aortic VSMCs. A synergistic relationship between both enzymes was confirmed in early passage cells in which LOX was demonstrated as the predominant copper-containing enzyme. Additionally, SSAO activity was shown to predominate in aged (late passage) VSMCs in which SSAO was identified as the main contributor in ROS formation. Furthermore, inhibition of both enzymes and treatment with benzylamine and cadaverine resulted with reduced PDGFR $\beta$  expression, which could associate active LOX and SSAO with VSMCs phenotyping modulation, and consequently vascular remodeling.

## 4.2 FUTURE DIRECTION

Since this study established that LOX is the predominant enzyme in young (early passage) cells it would be good to attempt to delete AOC3 gene in aged (late passage) VSMCs and observe what changes, if any, would this bring on LOX mRNA and protein levels. This would explain whether the reduced LOX activity detected at passage 8 is a consequence of an overactive SSAO or is a physiological phenomenon.

Future studies could also be performed to investigate the mechanism which leads to high SSAO activity in cells with a greater passage number. Moreover, to investigate whether integrin binding (surface adhesion receptors involved in cell–cell binding and interactions between cells and ECM proteins) regulates SSAO activity, by blocking the SSAO's RGD motif with a peptide and measuring hydrogen peroxide production.

Additional cytotoxicity assays such as LDH and presto blue could be done to differentiate between additive and synergistic relationship between SSAO derived products (aldehydes and hydrogen peroxide) in inducing cell death. Furthermore, additional cytotoxicity studies could also be done with different concentrations and ratios of the aldehydes and hydrogen peroxide to confirm this.

The role of SSAO in oxidative stress formation could be evaluated in more detail by using transition metals such as DTPA, which acts as chelating agent. Furthermore, the ability of SSAO's model compounds (aminoacetone and methylamine) to oxidise lipids can be assessed by measuring the production of lipid oxidation products malondialdehyde and 4-hydroxynonenal, in addition to changes in electrophoretic mobility of LDL.

# LITERATURE CITED

- Aalto K., Maksimow M., Juonala M., Viikari J. *et al.* (2012). Soluble vascular adhesion protein-1 correlates with cardiovascular risk factors and early atherosclerotic manifestations. *Arterioscler Thromb Vasc Biol.* 32(12), 523–532.
- Abella, A., Garcia-Vicente, S. *et al.* (2004). *Diabetologia.* 47(4), 429– 438.
- Abella, A., Malti, L., Camps, M. (2003). Semicarbazide-Sensitive Amine Oxidase/Vascular Adhesion Protein-1 Activity Exerts an Antidiabetic Action in Goto-Kakizaki Rats. *Diabetes.* 52(4), 1004-1013.
- Agostinelli, E., Palmigiani, P. *et al.* (2006). Interaction of bovine serum amine oxidase with the polyamine oxidase inactivator MDL72527. *Biochemical and biophysical research communications.* 340(3), 840-844.
- Al-Wabel, N.A. (2008). Comparative activities of semicarbazide-sensitive amine oxidase (SSAO) in five domestic species. *Polish Journal of Veterinary Sciences.* 11(1), 63-66.
- Aleman, L.M., Doench, J., Sharp, P.A. (2007). Comparison of siRNA-induced off-target RNA and protein effects. *RNA.* 13(3), 385–395.
- Alexander, M.R., Owens, G.K. (2012). Epigenetic control of smooth muscle cell differentiation and phenotypic switching in vascular development and disease. *Annual Review of Physiology.* 74, 1–28.
- Almarghalani, D.A. and Shah, Z.A. (2021). Progress on siRNA-based gene therapy targeting secondary injury after intracerebral haemorrhage. *Gene therapy.* 12(7), 1-7.
- Andrae, J., Gallini, R. *et al.* (2008). Role of platelet-derived growth factors in physiology and medicine. *Genes and Development.* 22(8), 1276-1331.
- Aquilano, K., Baldelli, S., Ciriolo, M. (2014). Glutathione: new roles in redox signalling for an old antioxidant. *Frontiers in Pharmacology.* 14(5), 196-202.
- Arya, M., Shergill, I.S. *et al.* (2005). Basic principles of real-time quantitative PCR. *Expert Rev. Mol. Diagn.* 5(2), 209-219.
- S. Awasthi, P.J. Boor. (1993). Semicarbazide protection from in vivo oxidant injury of vascular tissue by allylamine. *Toxicology Letters.* 66(2), 157-163.
- Bennett, M.R., Sinha, S., Owens, G.K. (2016). Vascular smooth muscle cells in atherosclerosis. *Circulatory research.* 118(4), 692–702.
- Bey, P., Bolkenius, F.N. (1985). N-2,3-Butadienyl-1,4-butanediamine derivatives: potent irreversible inhibitors of mammalian polyamine oxidase. *Journal of medical chemistry.* 28(5), 1-2.
- Bisswanger, H. (2014). Enzyme assays. *Perspectives in Science.* 14(1), 41-55.

- Bligt-Lindeń, E., Pihlavisto, M., Szatmańri, I. *et al.* (2013). Novel pyridazinone inhibitors for vascular adhesion protein-1 (VAP-1): old target-new inhibition mode. *Journal of Medical Chemistry*. 13(56), 9837–9848.
- Bode, M.K., Mosorin, M., Satta J. *et al.* (1999). Complete processing of type III collagen in atherosclerotic plaques. *Arterioscler Thromb Vasc Biol* 29(19). 1506–1511.
- Boomsma, F., Hut, H., Bhaggoe, U. (2005). Semicarbazide-sensitive amine oxidase: from cell to circulation. *Med Sci Monit*. 11(4), 122-126.
- Boomsma, F., Bhaggoe, U. (2000). Variation in semicarbazide-sensitive amine oxidase activity in plasma and tissues of mammals. *Pharmacology, Toxicology and Endocrinology*. 126(1), 69-78.
- Bonomini, F., Tnegattini, S. *et al.* (2008). Atherosclerosis and oxidative stress. *Histology and Histopathology*. 8(33), 381-390.
- Bour, S., Prévot, D., Guigne, C. *et al.* (2007). Semicarbazide-sensitive amine oxidase substrates fail to induce insulin-like effects in fat cells from AOC3 knockout mice. *J Neural Transm*. 11(4), 829-833.
- Boveris, A., Chance, B. (2013). The mitochondrial generation of hydrogen peroxide. General properties and effect of hyperbaric oxygen. *Biochem. J*. 23(134), 707–716.
- Braun, J.D., Pastene, D.O. *et al.* (2018). Methylglyoxal down-regulates the expression of cell cycle associated genes and activates the p53 pathway in human umbilical vein endothelial cells. *Scientific reports*. 2(18), 23-65.
- Brazeau, B.J., Jonhson, B.J. *et al.* (2004). Copper-containing amine oxidases. Biogenesis and catalysis; a structural perspective. *Archives of Biochemistry and Biophysics*. 428(1). 22-31.
- Brown, M.R., Miller, J. *et al.* (1999). Overexpression of human catalase inhibits proliferation and promotes apoptosis in vascular smooth muscle cells. *Circulatory Research*. 85(6), 524-533.
- Bucala R, Makita Z, Vega G, *et al.* (1994). Modification of low-density lipoprotein by advanced glycation end products contributes to the dyslipidaemia of diabetes and renal insufficiency. *Proc Natl Acad Sci USA*. 91(20), 9441–9445.
- Byon, C.H., Javed, A. *et al.* (2008). Oxidative stress induces vascular calcification through modulation of the osteogenic transcription factor Runx2 by Act signalling. *Journal of biological chemistry*. 283(22), 15219-15327.
- Chacko, B.K., Zhi, D. *et al.* (2016). The Bioenergetic Health Index is a sensitive measure of oxidative stress in human monocytes. *Redox Biology*. 8(16), 43-50.
- Chang, H.B., Heath, J.M., Chen, Y. (2016). Redox signalling in cardiovascular pathophysiology: A focus on hydrogen peroxide and vascular smooth muscle cells. *Redox biology*. 9(16), 244-253.
- Chang, S., Song, S. *et al.* (2014). Phenotypic Modulation of Primary Vascular Smooth Muscle Cells by Short-Term Culture on Micropatterned Substrate. *PLoS One*. 9(2), 88-89.
- Chanoki, M., Ishii, M., Kobayashi, H., *et al.* (1995). Increased expression of lysyl oxidase in skin with scleroderma. *Br. J. Dermatol*. 133(5), 710–715.

Chao, M.W., Erkekoglu, P. *et al.* (2014). Intracellular Generation of ROS by 3,5-Dimethylaminophenol: Persistence, Cellular Response, and Impact of Molecular Toxicity. *Toxicological sciences*. 141(1), 300–311.

Chatterjee, S., Feinstein, S.I. *et al.* (2011). Peroxiredoxin 6 phosphorylation and subsequent phospholipase A2 activity are required for agonist mediated activation of NADPH oxidase in mouse pulmonary vascular endothelium and alveolar macrophages. *Journal of biological chemistry*. 286(13), 1696-1706.

Cheng, T., Liu, Q. *et al.* (2014). Lysyl oxidase promotes bleomycin-induced lung fibrosis through modulating inflammation. *Journal of Molecular Cell Biology*. 6(6), 506–515.

Chi, J., Meng, L. *et al.* (2017). Primary Culture of Rat Aortic Vascular Smooth Muscle Cells: A New Method. *Med Sci Monit*. 22(23), 4014–4020.

Conklin, D., Boyce, C., Trent, M. *et al.* (2001). Amine metabolism: a novel path to coronary artery vasospasm. *Toxicology and applied pharmacology*. 175(2), 149-159.

Conklin, D.J., Cowley, H.R. *et al.* (2004). Vasoactive effects of methylamine in isolated human blood vessels: role of semicarbazide-sensitive amine oxidase, FA, and hydrogen peroxide. *Am. J. Physiol. Heart Circ. Physiol*. 286 (2), 667–676.

Conklin, D., Bhatnagar, A. *et al.* (2006). Acrolein generation stimulates hypercontraction in isolated human blood vessels. *Toxicology and applied pharmacology*. 217(3), 277–288.

Dana, H., Chalbatani, G.M., Karimloo, R. *et al.* (2017). Molecular Mechanisms and Biological Functions of siRNA. *Int J Biomed Sci*. 13(2), 48–57.

Dator, R.P., Morwena, J.S. *et al.* (2019). Bioanalytical and Mass Spectrometric Methods for Aldehyde Profiling in Biological Fluids. *Toxics*. 22(19), 32-45.

Davies, M.J. (2016). Protein oxidation and peroxidation. *Biochemical Journal*. 473(7), 805–825.

Debski, D., Smulik, R. *et al.* (2016). Mechanism of oxidative conversion of Amplex<sup>®</sup> Red to resorufin: pulse radiolysis and enzymatic studies. *Free Radic Biol Med*. 16(95), 323–332.

Deng, Y., Yu, P.H. (1999). Assessment of the Deamination of Aminoacetone, an Endogenous Substrate for Semicarbazide-Sensitive Amine Oxidase. *Analytical Biochemistry*. 2(17), 97-102.

Desai, K.M., Chang, T. *et al.* (2010). Oxidative stress and aging: Is methylglyoxal the hidden enemy? *Canadian Journal of Physiology and Pharmacology*. 88(3), 10-21.

Dhar, A., Desai, K. *et al.* (2008). Methylglyoxal production in vascular smooth muscle cells from different metabolic precursors. *Metabolism*. 57(9), 1211-1220.

Doench, J.G., Petersen, C.P., Sharp, P.A. (2003). siRNAs can function as miRNAs. *Genes Dev*. 17(4), 438-442.

Dogan, A., Rao, A.M. *et al.* (1999). Effects of MDL72572, a specific inhibitor of PO, on brain oedema, ischemic injury volume and tissue polyamine levels in rats after temporary middle cerebral artery occlusion. *Journal of Neurochemistry*. 92(9), 765-770.

- Doroszkowski, A., Radziwon-Balicka, A., Skomro, R. (2020). Novel Approaches for Diagnosing and Management of Cardiovascular Disorders Mediated by Oxidative Stress. *Oxidative Medicine and Cellular Longevity*. 20(3), 10-15.
- Duranton, B., Holl, V. *et al.* (2002). Cytotoxicity effects of the polyamine oxidase inactivator MDL72527 to two human colon carcinoma cell lines SW480 and SW620. *Cell biology and toxicology*. 18(2), 381-396.
- Elbashir, S.M., Harborth, J., Lendeckel, W. *et al.* (2001). Duplexes of 21-nucleotide RNAs mediate RNA interference in cultured mammalian cells. *Nature*. 20(411), 494–498.
- El Hadri, K., Moldes, M., Mercier, N. *et al.* (2002). Semicarbazide-Sensitive Amine Oxidase in Vascular Smooth Muscle Cells. Differentiation-Dependent Expression and Role in Glucose Uptake. *Arteriosclerosis, Thrombosis, and Vascular Biology*. 22(1), 89-94.
- Enrique-Tarancon, G., Castan, I., Morin, N. *et al.* (2000). Substrates of semicarbazide-sensitive amine oxidase co-operates with vanadate to stimulate tyrosine phosphorylation of insulin-receptor-substrate proteins, phosphoinositide 3-kinase activity and GLUT4 translocation in adipose cells. *Journal of Biochemistry*. 350(1), 171-180.
- Ernst, O., Zor, T. (2010). Linearization of the Bradford Protein Assay. *Journal of Visualized Experiments*. 10(38), 19-28.
- Esteban, G., Bolea, I., Sun, P. *et al.* (2013). A therapeutic approach to cerebrovascular diseases based on indole substituted hydrazides and hydrazines able to interact with human vascular adhesion protein-1, monoamine oxidases (A and B), AChE and BuChE. *Journal of Neural Transmission*. 23(120), 911–918.
- Exner, M., Hermann, M., Kapiotis, S. *et al.* (2001). Semicarbazide-sensitive amine oxidase catalyzes endothelial cell-mediated low-density lipoprotein oxidation. *Cardiovascular Research*. 21(50), 583–588.
- Farjanel, J., Borel, A., Sommer, P., and Hulmes, D. J. S. (2005). Inhibition of lysyl oxidase activity can delay phenotypic modulation of chondrocytes in two-dimensional culture. *Osteoarthritis and Cartilage*. 13(25), 120–128.
- Fernandez de Arriba, A., Tipton, K.F. *et al.* (1996). Inhibition of bovine lung SSAO by some hydrazine derivatives. *Biochemical pharmacology*. 52(16), 187-195.
- Filip, A., Pinzano, A., Bianchi, A. *et al.* (2016). Expression of the semicarbazide-sensitive amine oxidase in articular cartilage: its role in terminal differentiation of chondrocytes in rat and human. *Osteoarthritis and cartilage*. 24(16), 1223-1234.
- Finkel, T., Holbrook, N.J. (2000) Oxidants, oxidative stress and the biology of ageing. *Nature*. 20(408), 239–247.
- Fire, A., Xu, S., Montgomery, M.K. *et al.* (1998). Potent and specific genetic interference by double-stranded RNA in *Caenorhabditis elegans*. *Nature*. 98(391), 806–811.
- Floris, G., Mondovi, B. (2009). Copper amine oxidases: structure, catalytic mechanisms, and role in pathophysiology. (3<sup>rd</sup> Ed). *Taylor & Francis. London*.

- Fogelgren, B., Polgar, N., Szauter, K.M. *et al.* (2005). Cellular fibronectin binds to lysyl oxidase with high affinity and is critical for its proteolytic activation. *J Biol Chem.* 25(280), 24690–24697.
- Foot, J.S., Yow, T.T., Schilter, H. *et al.* (2013). PXS-4681A, a potent and selective mechanism-based inhibitor of SSAO/VAP-1 with anti-inflammatory effects in vivo. *Journal of Pharmacology.* 23(347), 365–374.
- Fowler, J.S., Logan, J. *et al.* (2009). Reversible Inhibitors of Monoamine Oxidase-A (RIMAs): Robust, Reversible Inhibition of Human Brain MAO-A by CX157. *Neuropsychopharmacology.* 35(2), 623-631.
- Franco, R., Panayiotidis, M.I. *et al.* (2007). Glutathione Depletion Is Necessary for Apoptosis in Lymphoid Cells Independent of Reactive Oxygen Species Formation. *The journal of biological chemistry.* 282(42), 30452–30465.
- Gacheru, S.N., Thomas, K.M., Murray, S.A. *et al.* (1997). Transcriptional and post-transcriptional control of lysyl oxidase expression in vascular smooth muscle cells: effects of TGF- $\beta$ 1 and serum deprivation. *J Cell Biochem.* 97(65), 395–407.
- Gella, A., Sole, M. *et al.* (2013). A comparison between radiometric and fluorimetric methods for measuring SSAO activity. *Journal of Neural Transmission.* 13(120), 1015-1018.
- Gharanei, S., Fishwick, K. *et al.* (2020). Vascular Adhesion Protein-1 Determines the Cellular Properties of Endometrial Pericytes. *Front Cell Dev Biol.* 20(8), 621-626.
- Gimbrone, M.A., Garcia-Cardena, G. (2016). Endothelial cell dysfunction and the pathobiology of atherosclerosis. *Circulation Research.* 16(18), 620-636.
- Gokturk, C., Sugimoto, H., Blomgren, B. *et al.* (2007). Macrovascular changes in mice overexpressing human semicarbazide-sensitive amine oxidase in smooth muscle cells. *American Journal of Hypertension.* 20(7), 743-750.
- Gonzalez-Santamaria, J., Villalba, M. *et al.* (2016). Matrix cross-linking lysyl oxidases are induced in response to myocardial infarction and promote cardiac dysfunction. *Cardiovascular research.* 109(1), 67–78.
- Green, R.S, Lieb, M.E, Weintraub, A.S. *et al.* (1995), Identification of lysyl oxidase and other platelet-derived growth factor-inducible genes in vascular smooth muscle cells by differential screening. *Lab Invest.* 95(73), 476–482.
- Grimsrud, P.A., Hongwei, X. *et al.* (2008). Oxidative Stress and Covalent Modification of Protein with Bioactive Aldehydes. *Journal of Biological Chemistry.* 8(32), 283-300.
- Gubisne-Haberle, D., Hill, W., Kazachkov, M. *et al.* (2004) Protein cross-linkage induced by formaldehyde derived from semicarbazide-sensitive amine oxidase-mediated deamination of methylamine. *J Pharmacol Exp Ther.* 310(4), 1125–1132.
- Hajdu, I., Kardos, J. *et al.* (2018). Inhibition of the LOX enzyme family members with old and new ligands. Selectivity analysis revisited. *Bioorganic & Medicinal Chemistry Letters.* 28(18), 3113-3118.

Halline, A.G., Dudeja, P.K. *et al.* (1990). Effect of polyamine oxidase inhibition on the colonic malignant transformation process induced by 1,2-dimethylhydrazine. *Carcinogenesis*. 9(11), 2127-2129.

Hao-Liang, X., Luisa, S.D. *et al.* (2006). Vascular Adhesion Protein-1 Plays an Important Role in Postischemic Inflammation and Neuropathology in Diabetic, Oestrogen-Treated Ovariectomized Female Rats Subjected to Transient Forebrain Ischemia. *Journal of Pharmacology and Experimental Therapeutics*. 317(1), 19-29.

Hecht, S.S. (2003). Tobacco carcinogens, their biomarkers and tobacco induced cancer. *Natural Reviews Cancer*. 2(3), 733-744.

Hernandez, M.M., Esteban, M. *et al.* (2005). Human plasma semicarbazide sensitive amine oxidase (SSAO),  $\beta$ -amyloid protein and aging. *Neuroscience Letters*. 384(2), 183-187.

Hernández-Guillamón, M., Garcia Bonilla, M. *et al.* (2010). Plasma VAP-1/SSAO Activity Predicts Intracranial Hemorrhages and Adverse Neurological Outcome After Tissue Plasminogen Activator Treatment in Stroke. *Stroke*. 41(7), 1528-1535.

Hernandez-Guillamon, M., Solé, M., Delgado, P., García-Bonilla, L., Giralte, D., Boada, C., *et al.* (2012). VAP-1/SSAO Plasma Activity and Brain Expression in Human Hemorrhagic Stroke. *Cerebrovasc. Dis.* 33(12), 55–63.

Hernandez, M., Sole, M. *et al.* (2006). Soluble Semicarbazide Sensitive Amine Oxidase (SSAO) catalysis induces apoptosis in vascular smooth muscle cells. *Biochemistry*. 6(63), 165-173.

Higgins, D.F., Kimura, K. *et al.* (2007). Hypoxia promotes fibrogenesis in vivo via HIF-1 stimulation of epithelial-to-mesenchymal transition. *J Clin Invest*. 7(117), 3810–3820.

Hill, B.G. & Bhatnagar, A. (2009). Beyond Reactive Oxygen Species. Aldehydes as Arbitrators of Alarm and Adaptation. *Circulatory Research*. 105(11), 1044–1046.

Holt, A., Callingham, B.A. (1992). Effects In-vitro of Procarbazine Metabolites on Some Amine Oxidase Activities in the Rat. *Journal of Pharmacy and Pharmacology*. 44(6), 494–499.

Holt, A., Callingham, B.A. (1994). The *ex vivo* effects of procarbazine and methylhydrazine on some rat amine oxidase activities. *Journal of neural transmission*. 43(4), 439-450.

Hu, C., Cong, X.D., Dai, D.Z. *et al.* (2011). Argirein alleviates diabetic nephropathy through attenuating NADPH oxidase, Cx43, and PERK in renal tissue. *Naunyn Schmiedebergs Arch Pharmacol*. 383(3), 309–319.

Huang, T., Long, M., Huo, B. (2010). Competitive Binding to Cuprous Ions of Protein and BCA in the Bicinchoninic Acid Protein Assay. *The Open Biomedical Engineering Journal*. 10 (4), 271-278.

Huffman, M.D., Curci, J.A., Moore, G. *et al.* (2000). Functional importance of connective tissue repair during the development of experimental abdominal aortic aneurysms. *Surgery*. 20(128), 429–438.

Hutchinson, J.H., Rowbottom, M.W. *et al.* (2017). Small Molecule Lysyl Oxidase-like 2 (LOXL2) Inhibitors: The Identification of an Inhibitor Selective for LOXL2 over LOX. *Med. Chem. Lett*. 17(8), 423–427.

- Iglesias-Osma, M.C., Bour, S. *et al.* (2005). Methylamine but not mafenide mimics insulin-like activity of the semicarbazide-sensitive amine oxidase-substrate benzylamine on glucose tolerance and on human adipocyte metabolism. *Pharmacological Research*. 52(6), 475-484.
- Iffíú-Soltész, Z., Wanecq, E., Lomba, A. *et al.* (2010). Chronic benzylamine administration in the drinking water improves glucose tolerance, reduces body weight gain and circulating cholesterol in high-fat diet-fed mice. *Pharmacology Resolution*. (10)61, 355–363.
- Ikenaga, N., Peng, Z.W. *et al.* (2017). Selective targeting of lysyl oxidase-like 2 (LOXL2) suppresses hepatic fibrosis progression and accelerates its reversal. *Gut*. 66(17),1697-1708.
- Iturbide, A., García de Herreros, A., Peiró, S. (2014). A new role for LOX and LOXL2 proteins in transcription regulation. *The FEBS Journal*. 282(215), 1768–1773.
- Iwasaki, A., Sakai, K. *et al.* (2016). Molecular mechanism responsible for fibronectin-controlled alterations in tissue stiffness in advanced chronic liver fibrogenesis. *The Journal of biological chemistry*. 291(1), 72–88.
- Jackson, A.L., Linsley, P.S (2004). Noise amidst the silence: off-target effects of siRNAs? *TRENDS in Genetics*. 20(11), 521-534.
- Jacobsson, E., Nilsson, J. *et al.* (2005). Structure of human semicarbazide-sensitive amine oxidase/vascular adhesion protein-1. *Biological Crystallography*. 5(61), 1500-1562.
- Jarolimek, W., Charlton, B. (2015). Phase 1 results from PXS-4728A, a selective SSAO/VAP-1 inhibitor, for the treatment of non-alcoholic steatohepatitis. *Journal of hepatology*. 62(15), 274-275.
- Jalkanen, S., Salmi, M. (2001). Cell surface monoamine oxidases: enzymes in search of a function. *EMBO J*. 20(1), 3893–3901.
- Jalkanen, S., Karikoski, M., Mercier, N. *et al.* (2007). The oxidase activity of vascular adhesion protein-1 (VAP-1) induces endothelial E- and P-selectins and leukocyte binding. *Blood*. 110(6), 1864-1870.
- Jalkanen, S., Salmi, M. (2017). Vascular Adhesion Protein-1: A Cell Surface Amine Oxidase in Translation. *Antioxidants and Redox signalling*. 20(7), 544-632.
- Jarnicki, A.J., Schilter, H., Liu, G. *et al.* (2016). The inhibitor of semicarbazide-sensitive amine oxidase, PXS-4728A, ameliorates key features of chronic obstructive pulmonary disease in a mouse model. *British Journal of Pharmacology*. 16(173), 3161-3175.
- Johnston, B., Kanwar, S. *et al.* (1996). Hydrogen peroxide induces leukocyte rolling modulation by endogenous antioxidant mechanisms including NO. *American Journal of Physiology*. 271(2), 614-621.
- Jufang, C., Liping, M., Sunlei, P. (2017). Primary Culture of Rat Aortic Vascular Smooth Muscle Cells: A New Method. *Medical Science Monitor*. 23(17), 4014-4020.
- Kagan, H.M., Raghavan, J., Hollander, W. (1991). Changes in aortic lysyl oxidase activity in diet-induced atherosclerosis in the rabbit. *Arteriosclerosis* 19(1), 287–291.
- Kagan, H.M. (2000). Intra- and extracellular enzymes of collagen biosynthesis as biological and chemical targets in the control of fibrosis. *Acta Trop*. 20(77),147–152.

Kagan, H. M. and Li, W. (2003). Lysyl oxidase: properties, specificity, and biological roles inside and outside of the cell. *J. Cell. Biochem.* 88, 660–672.

Katerji, M., Filippova, M. *et al.* (2019). Approaches and Methods to Measure Oxidative Stress in Clinical Samples: Research Applications in the Cancer Field. *Oxidative Medicine and Cellular Longevity.* 21(29), 19-25.

Kazachkov, M., Chen, K, *et al.* (2007). Evidence for in Vivo Scavenging by Aminoguanidine of Formaldehyde Produced via Semicarbazide-Sensitive Amine Oxidase-Mediated Deamination. *Journal of Pharmacology and Experimental Therapeutics.* 322(3), 1201-1207.

Kenneth, C.M., Ponnampalam, S.N. *et al.* (2002). Semicarbazide-sensitive amine oxidase in aortic smooth muscle cells mediates synthesis of a methylglyoxal-AGE: Implications for vascular complications in diabetes. *Biochemical and Biophysical Research Communications* 297(2), 863–869.

Kim, D., Kim, K.A. *et al.* (2020). Methylglyoxal-Induced Dysfunction in Brain Endothelial Cells via the Suppression of Akt/HIF-1 $\alpha$  Pathway and Activation of Mitophagy Associated with Increased Reactive Oxygen Species. *Antioxidants.* 9(20), 311-323.

Kim, K., Eberwine, J.H. (2010) Mammalian cell transfection: the present and the future. *Anal Bioanal Chem.* 10(397), 3173–3178.

Kinemuchi, H., Sugimoto, H. *et al.* (2004). Selective Inhibitors of Membrane-Bound Semicarbazide-Sensitive Amine Oxidase (SSAO) Activity in Mammalian Tissues. *Neurotoxicology.* 25(2), 325-335.

Kirton, C.M., Laukkanen, M.L., Nieminen, A. *et al.* (2005). Function-blocking antibodies to human vascular adhesion protein-1: a potential anti-inflammatory therapy. *European Journal of Immunology.* 5(35), 3119–3130.

Koskinen, K., Vainio, P.J. *et al.* (2004). Granulocyte transmigration through the endothelium is regulated by the oxidase activity of vascular adhesion protein-1 (VAP-1). *Blood.* 103(9), 3388-3395.

Kubota, R., Reid, M.J. *et al.* (2020). Comparison of Inhibitor and Substrate Selectivity between Rodent and Human Vascular Adhesion Protein-1. *Mediators of inflammation.* 20(9), 112-115.

Kuykendall, J.R. (2010). *Comprehensive Toxicology.* 2<sup>nd</sup> Ed. *Elsevier Science.*

Lacolley, P., Regnault, V., *et al.* (2012). The vascular smooth muscle cell in arterial pathology: a cell that can take on multiple roles. *Cardiovascular research.* 12(95), 194-204.

Lamensdorf, I., Moussa, B.H. *et al.* (1996). Effect of Long-Term Treatment with Selective Monoamine Oxidase A and B Inhibitors on Dopamine Release from Rat Striatum In Vivo. *Journal of Neurochemistry.* 3(5), 12-23.

Langford SD, Trent MB, Boor PJ. (2002). Semicarbazide-sensitive amine oxidase and extracellular matrix deposition by smooth-muscle cells. *Cardiovascular Toxicology.* 2(2), 141-150.

Lazarus, H.M., Cruikshank, W.W. *et al.* (1995). Induction of human monocyte motility by lysyl oxidase. *Matrix Biol.* 95(14), 727–731.

- Lee, Q.T., Harris, J., Magliocco, A.M. *et al.* (2009). Validation of lysyl oxidase as a prognostic marker for metastasis and survival in head and neck squamous cell carcinoma. *Journal of clinical oncology*. 27(26), 4281–4286.
- Leung, L., Smithen, D., Lopez, S. *et al.* (2019). Anti-metastatic Inhibitors of Lysyl Oxidase (LOX): Design and Structure–Activity Relationships. *Journal of Medicinal Chemistry*. 62(12), 5863–5884.
- Levental, K.R., Yu, H., Kass, L. *et al.* (2009). Matrix crosslinking forces tumour progression by enhancing integrin signalling. *Cell*. 139(5), 891–906.
- Li, W., Liu, G., Chou, I.N. *et al.* (2000). Hydrogen peroxide-mediated, lysyl oxidase-dependent chemotaxis of vascular smooth muscle cells. *J Cell Biochem*. 20(78), 550–557.
- Li, H.-Y., Lin, M.-S., Wei, J.-N., Hung, C. S., Chiang, F.-T., Lin, C.-H., *et al.* (2009). Change of Serum Vascular Adhesion Protein-1 after Glucose Loading Correlates to Carotid Intima-Medial Thickness in Non-diabetic Subjects. *Clinica Chim. Acta*. 403(9), 97–101.
- Li, W., Nellaiappan, K., Strassmaier, T. *et al.* (1997) Localization and activity of lysyl oxidase within nuclei of vascular smooth muscle cells. *Proc Natl Acad Sci*. 94(97), 12817–12822.
- Li, M., & Fukagawa, N.K. (2010). Age-Related Changes in Redox Signalling and VSMC Function. *Antioxidants & redox signalling*. 12(5), 641-655.
- Lin, M.T., Beal, M.F. (2006). Mitochondrial dysfunction and oxidative stress in neurodegenerative diseases. *Nature*. 6(443), 787–795.
- Lin, Z., Luo, W. (2005). The effect of endogenous formaldehyde on rat aorta endothelial cells. *Toxicology letters*. 159(25), 134-143.
- Liu, C., Cao, B., Zhang, Q. (2020). Inhibition of thioredoxin 2 by intracellular methylglyoxal accumulation leads to mitochondrial dysfunction and apoptosis in INS-1 cells. *Endocrine*. (20) 68, 103–115.
- Liu, H., Wang, H. *et al.* (2004). Glutathione metabolism during aging and in Alzheimer disease. *Ann N Y Acad Sci*. 24(1019), 346–349.
- Liu, G., Cao, H. *et al.* (2016). Effect of Lysosomotropic Polyamine oxidase Inhibitor MDL-72527 on Platelet Activation. *Cellular Physiology and Biochemistry*. 16(38), 1695-1702.
- Lucero, H.A., Ravid, K. *et al.* (2008). Lysyl Oxidase Oxidizes Cell Membrane Proteins and Enhances the Chemotactic Response of Vascular Smooth Muscle Cells. *The Journal of Biological Chemistry*. 28(35), 2413-2417.
- Lucero, H.A., Kagan, H.M. (2006). Lysyl oxidase: an oxidative enzyme and effector of cell function. *Cell. Mol. Life Sci*. 63(26), 2304–2316.
- Luisa, M., Wang, E. *et al.* (2005). Anti-Inflammatory Effects of Inhibiting the Amine Oxidase Activity of Semicarbazide-Sensitive Amine Oxidase. *Journal of Pharmacology and Experimental Therapeutics*. 315(2), 553-562.
- Lyles, G.A. (1996). Mammalian plasma and tissue bound semicarbazide sensitive amine oxidases: biochemical, pharmacological and toxicological aspects. *Journal of Biochemistry and Cell Biology*. 6(28), 259-274.

- Lyles, G.A., Pino, R. (1998). Properties and functions of tissue-bound semicarbazide-sensitive amine oxidases in isolated cell preparations and cell cultures. *J Neural Transm Suppl.* 8(52), 239–250.
- Lyles, G.A., Singh, I. (1995). Vascular smooth muscle cells: a major source of the semicarbazide-sensitive amine oxidase of the rat aorta. *Journal of Pharmacy and Pharmacology.* 37(9), 637- 643.
- Ma, W., Chen, K., Li, Y. *et al.* (2017). Advances in Cadaverine Bacterial Production and Its Applications. *Green Chemical Engineering.* 3(17), 308–317.
- Ma, Q., Manaenko, A., Khatibi, N. H., Chen, W. *et al.* (2011). Vascular Adhesion Protein-1 Inhibition Provides Anti-inflammatory protection after an Intracerebral Haemorrhagic Stroke in Mice. *J. Cereb. Blood Flow Metab.* 31(11), 881–893.
- Mahmood, T., Yang, P.C. (2012). Western Blot: Technique, Theory, and Trouble Shooting. *North American Journal of Medical Sciences.* 4(9), 429-434.
- Maki, J.M., Rasanen, J. *et al.* (2002). Inactivation of the lysyl oxidase gene *Lox* leads to aortic aneurysms, cardiovascular dysfunction, and perinatal death in mice. *Circulation.* 106(19), 2503–2509.
- Mäki J.M., Sormunen R., Lippo S. *et al.* (2005). Lysyl oxidase is essential for normal development and function of the respiratory system and for the integrity of elastic and collagen fibres in various tissues. *Am. J. Pathol.* 167(205), 927-936.
- Martinez-Revelles, S., Garcia-Redondo, A.B. *et al.* (2017). Lysyl Oxidase Induces Vascular Oxidative Stress and Contributes to Arterial Stiffness and Abnormal Elastin Structure in Hypertension: Role of p38MAPK. *Antioxidants & redox signalling.* 27(7), 379-397.
- Marttila-Ichihara, F., Castermans, K., Auvinen, K., *et al.* (2010). Small- molecule inhibitors of vascular adhesion protein-1 reduce the accumulation of myeloid cells into tumours and attenuate tumour growth in mice. *Journal of Immunology.* 10(184), 3164–3173.
- Mathys, K.C., Ponnampalam, S.N., Padival, S. (2002). Semicarbazide-sensitive amine oxidase in aortic smooth muscle cells mediates synthesis of a methylglyoxal-AGE: implications for vascular complications in diabetes. *Biochemical and Biophysical Research Communications.* 297(4), 863-869.
- Matveychuk, D., Dursun, S.M., Wood, P.L., Baker, G.B. (2011). Reactive aldehydes and neurodegenerative disorders. *Clinical Psychopharmacology.* 11(21), 277–288.
- Maynard, S., Schurman, S. H. *et al.* (2009). Base excision repair of oxidative DNA damage and association with cancer and aging. *Carcinogenesis.* 30(9), 2–10.
- Maynard, S., Fang, E.F. *et al.* (2015). DNA damage, DNA repair, aging, and neurodegeneration. *Cold Spring Harb. Perspect. Med.* 15(5), 25-30.
- Mercier, N. (2009). The role of “semicarbazide-sensitive amine oxidase” in the arterial wall. *Artery Research.* 9(3), 141-147.
- Mercier, N., Pirault, J. *et al.* (2020). Semicarbazide-Sensitive Amine Oxidase Increases in Calcific Aortic Valve Stenosis and Contributes to Valvular Interstitial Cell Calcification. *Oxid Med Cell Longev.* 20(20), 519-567.

- Merinen M, Irjala H, Salmi M, Jaakkola I, Hañninen A, and Jalkanen S. (2005). Vascular adhesion protein-1 is involved in both acute and chronic inflammation in the mouse. *Am J Pathol.* 166(5), 793–800.
- Min, H.-K., Kapoor, A., Fuchs, M., Mirshahi, F. *et al.* (2012). Increased Hepatic Synthesis and Dysregulation of Cholesterol Metabolism Is Associated with the Severity of Non-alcoholic Fatty Liver Disease. *Cel Metab.* 15(12), 665–674.
- Mishin, V., Gray, J.P., Heck, D.E. *et al.* (2010). Application of the Amplex Red/Horseradish Peroxidase Assay to Measure Hydrogen Peroxide Generation by Recombinant Microsomal Enzymes. *Free Radical Biology Medicine.* 48(11), 1485-1491.
- Mody, N., Parhami, F. *et al.* (2001). Oxidative stress modulates osteoblastic differentiation of vascular and bone cells. *Free Radical Biological Medicine.* 31(4), 509-519.
- Moldes, M., Fève, B., Pairault, J. (1999). Molecular cloning of a major mRNA species in murine 3T3 adipocyte lineage. differentiation-dependent expression, regulation, and identification as semicarbazide-sensitive amine oxidase. *Journal of Biology and Chemistry.* 2(74), 9515-9523.
- Morin, N., Lizcano, J.M., Fontana, E. *et al.* (2001). Semicarbazide-sensitive amine oxidase substrates stimulate glucose transport and inhibit lipolysis in human adipocytes. *J Pharmacol Exp Ther.* 29(7), 563-72.
- Muyao, L., Fukagawa, N.K. (2010). Age-Related Changes in Redox Signaling and VSMC Function. *Antioxidants & redox signalling.* 12(5), 641-657.
- Nakashima, Y., Sueishi, K. (1992). Alteration of elastic architecture in the lathyrus rat aorta implies the pathogenesis of aortic dissecting aneurysm. *Am J Pathol.* 92(140), 959–969.
- Nave, A.H., Mizikova, I. *et al.* (2014). Lysyl oxidases play a causal role in vascular remodelling in clinical and experimental pulmonary arterial hypertension. *Arterioscler Thromb Vasc Biol.* 34(7), 1446–14458.
- Nellaiappan, K., Risitano, A., Liu, G. *et al.* (2000). Fully processed lysyl oxidase catalyst translocates from the extracellular space into nuclei of aortic smooth-muscle cells. *J Cell Biochem* 20(79), 576–582.
- Nemcsik, J., Szoko, E. *et al.* (2007). Alteration of serum semicarbazide-sensitive amine oxidase activity in chronic renal failure. *J Neural Transm.* (27)14, 841–843.
- Noda, K., Miyahara, S., Nakazawa, T. *et al.* (2008). Inhibition of vascular adhesion protein-1 suppresses endotoxin-induced uveitis. *FASEB J.* 22(18), 1094–1103.
- Noda, K., Nakao, S., Zandi, S. *et al.* (2009). Vascular adhesion protein-1 regulates leukocyte transmigration rate in the retina during diabetes. *Experimental Eye Research.* 89 (29), 774–781.
- Nur, E., Verwijs, M., Waart, D.R. *et al.* (2011). Increased efflux of oxidized glutathione (GSSG) causes glutathione depletion and potentially diminishes antioxidant defence in sickle erythrocytes. *Biochimica et Biophysica Acta.* 1812(211), 1412-1417.
- Obata, T. (2006). Diabetes and semicarbazide-sensitive amine oxidase (SSAO) activity: A review. *Life Sciences.* 79(5), 417-422.

- O'Brien, P.J., Siraki, A.G., Shangari, N. (2005). Aldehyde sources, metabolism, molecular toxicity mechanisms, and possible effects on human health. *Crit. Rev. Toxicol.* 5(35), 609–662.
- Ochiai, Y., Itoh, K., Sakurai, E. *et al.* (2006). Substrate selectivity of monoamine oxidase A, monoamine oxidase B, diamine oxidase, and semicarbazide-sensitive amine oxidase in COS-1 expression systems. *Biological and Pharmaceutical Bulletin.* 29(12), 2362-2366.
- Ogrodnik, M. (2021). Cellular aging beyond cellular senescence: Markers of senescence prior to cell cycle arrest *in vitro* and *in vivo*. *Aging Cell.* 20(4), 133 -138.
- Okin, D., and Medzhitov, R. (2016). The Effect of Sustained Inflammation on Hepatic Mevalonate Pathway Results in Hyperglycemia. *Cell.* 165(16), 343–356.
- O'Rourke, A. M., Wang, L. *et al.* (2007). Benefit of inhibiting SSAO in relapsing experimental autoimmune encephalomyelitis. *Journal of Neural Transmission.* 114(7), 845–849.
- O'Rourke, A. M., Wang, L. *et al.* (2008). Anti-inflammatory effects of LJP 1586 [Z-3-fluoro-2-(4-methoxybenzyl) allylamine hydrochloride], an amine-based inhibitor of semicarbazide-sensitive amine oxidase activity. *Journal of Pharmacology.* 324(18), 867–875.
- O'Sullivan, J.O., Unzetta, M. *et al.* (2004). Semicarbazide-Sensitive Amine Oxidases: Enzymes with Quite a Lot to Do. *NeuroToxicology.* 25(4), 303–315.
- O'Sullivan M., Tipton, K.F., McDevitt, W.E. (2002). Immunolocalization of semicarbazide-sensitive amine oxidase in human dental pulp and its activity towards serotonin. *Arch Oral Biol.* 2(47), 399–406.
- Owens, G.K. (1995). Regulation of differentiation of vascular smooth muscle cells. *Physiol Rev.* 95(75), 487–517.
- Owens, G.K., Kumar, M.S., Wamhoff, B.R. (2004). Molecular regulation of vascular smooth muscle cell differentiation in development and disease. *Physiology Reviews.* 24(84), 767–801.
- Palamakumbura, A. H., Sommer, P. and Trackman, P. C. (2003) Autocrine growth factor regulation of lysyl oxidase expression in transformed fibroblasts. *J. Biol. Chem.* 278(23), 30781–30787.
- Pan, P., Fu, H. *et al.* (2010). Angiotensin II upregulates the expression of placenta growth factor in human vascular endothelial and smooth muscle cells. *Cell biology.* 11(10), 24-36.
- Pannecoeck, R., Serruys, D. *et al.* (2015). Vascular adhesion protein 1: Role in human pathology and application as a biomarker. *Critical Reviews in Clinical Laboratory Sciences.* 52(6), 284-300.
- Patel, J., Thakur, S. *et al.* (2020). 2-Oxothiazolidine-4-carboxylic acid inhibits vascular calcification via induction of glutathione synthesis. *Journal of Cellular Physiology.* 221(236), 2696–2705.
- Parastatidis, L., Weiss, D. *et al.* (2013). Overexpression of catalase in VSMCs prevents the formation of abdominal aortic aneurism. *Arteriosclerosis, Thrombosis, and Vascular Biology.* 33(10), 2389-2396.

- Payne, S.L., Hendrix, M.J. *et al.* (2006). Lysyl oxidase regulates actin filament formation through the p130(Cas)/Crk/DOCK180 signalling complex. *Journal of cellular biochemistry*. 98(4), 827–837.
- Payne, S. L., Fogelgren, B., Hess, A. R. *et al.* (2005). Lysyl oxidase enzymatic function increases stiffness to drive colorectal cancer progression through FAK. *Cancer Research*. 65(25), 11429–11436.
- Peet, G.W., Lukas, S. *et al.* (2011). Bioluminescent method for assaying multiple semicarbazide-sensitive amine oxidase (SSAO) family members in both 96- and 384-well formats. *Journal of Biomolecular Screening*. 16(9), 1106–1111.
- Pestov, N.B. Okkelman, I.A *et al.* (2011). Control of lysyl oxidase activity through site-specific deuteration of lysine. *Bioorganic & Medicinal Chemistry Letters*. 21(11), 255-258.
- Peng, Y., Wang, J. *et al.* (2016). Inactivation of Semicarbazide-Sensitive Amine Oxidase Stabilizes the Established Atherosclerotic Lesions via Inducing the Phenotypic Switch of Smooth Muscle Cells. *Plos One*. 4(16), 13-23.
- Pizzimenti, S.; Ciamporcerro, E. *et al.* (2013). Interaction of aldehydes derived from lipid peroxidation and membrane proteins. *Front. Physiol*. 13(4), 242 – 255.
- Pizzorno, J. (2014). Glutathione. *Integrative Medicine*. 13(8), 5-12.
- Ponticos, M., Smith, B.D. (2014). Extracellular matrix synthesis in vascular disease: hypertension, and atherosclerosis. *Journal of Biomedical Research*. 28(1), 25–39.
- Presnell, C.E., Bhati, G. *et al.* (2013). Computational insights into the role of glutathione in oxidative stress. *Curr Neurovasc Res*. 10(2), 185-194.
- Pyla, R., Poulouse, N., Jun, J.Y. *et al.* (2013). Expression of conventional and novel glucose transporters, GLUT1, -9, -10, and -12, in vascular smooth muscle cells. *American Journal of Cell Physiology*. 304(6), 574–589.
- Quelhas-Santos, J., Sampaio-Maia, B. *et al.* (2015). Assessment of Renalase Activity on Catecholamines Degradation. *The Open Hypertension Journal*. 15(7), 14-18.
- Quemener, V., Moulinoux, J. P. (1992). Polyamine deprivation enhances anti-tumoral efficacy of chemotherapy. *Anticancer Res*. 12(12), 1447–1453.
- Rahman, I., Kode, A., Biswas, S.K. (2006). Assay for quantitative determination of glutathione and glutathione disulphide levels using enzymatic recycling method. *Nature protocols*. 6(27), 3150-3165.
- Ramos, K., Grossman, S.L. *et al.* (1998). Allylamine-induced vascular toxicity *in vitro*: Prevention by semicarbazide-sensitive amine oxidase inhibitors. *Toxicology and Applied Pharmacology*. 95(1), 61-71.
- Rao, X., Huang, X. *et al.* (2013). An improvement of the  $2^{-\Delta\Delta CT}$  method for quantitative real-time polymerase chain reaction data analysis. *Biostat Bioinforma Biomath*. 3(3), 71–85.
- Raposo, B., Rodriguez, C., Martinez-Gonzalez, J. *et al.* (2004). High levels of homocysteine inhibit lysyl oxidase (LOX) and down-regulates LOX expression in vascular endothelial cells. *Atherosclerosis*. 24(177), 1–8.

Rcheulishvili, N., Papukashvili, D. *et al.* (2021). Simulated microgravity alters the expression of plasma SSAO and its enzymatic activity in healthy rats and increases the mortality in high-fat diet/streptozotocin-induced diabetes. *Life Sciences in Space Research*. 30(21), 24-28.

Rezende, F.F., Martins Lima, A. *et al.* (2012). Integrin is a redox regulated target of hydrogen peroxide in vascular smooth muscle cell adhesion. *Free radicals*. 53(3), 521-531.

Riss, T.L., Moravec, R.A. *et al.* (2016). Cell viability assays. *Assay guidance manual*. 3(16), 2-7.

Rodriguez, C., Raposo, B., Martinez-Gonzalez, J. *et al.* (2002). Low density lipoproteins down-regulates lysyl oxidase in vascular endothelial cells and the arterial wall. *Arterioscler Thromb Vasc Biol*. 22(22), 1409–1414.

Rodriguez, C., Alcudia, J.F. *et al.* (2004). Lysyl oxidase (LOX) down-regulation by TNF $\alpha$ : a new mechanism underlying TNF $\alpha$ -induced endothelial dysfunction. *Atherosclerosis*. 28(196), 558–564.

Rodriguez, C., Raposo, B., Martinez-Gonzalez, J. *et al.* (2008). Regulation of lysyl oxidase in vascular cells: Lysyl oxidase as a new player in cardiovascular diseases. *Cardiovascular Research*. 28(79), 1-7.

Rodriguez, C., Martinez-Martinez, E. *et al.* (2016). The lysyl oxidase inhibitor ( $\beta$ -aminopropionitrile) reduces leptin profibrotic effects and ameliorates cardiovascular remodelling in diet-induced obesity in rats. *Journal of Molecular and Cellular Cardiology*. 92(16), 96-104.

Roy, S., Ha, J., Trudeau, K. *et al.* (2010). Vascular basement membrane thickening in diabetic retinopathy. *Current eye research*. 35(12), 1045–1056.

Saito, Y., Nishio, K. *et al.* (2005). Cytotoxic effect of formaldehyde with free radicals via increment of cellular reactive oxygen species. *Toxicology*. 31(5), 211-243.

Salmi, M., Jalkanen, S. (2000). Human vascular adhesion protein-1 (VAP-1) plays a critical role in lymphocyte-endothelial cell adhesion cascade under shear stress. *Circ. Res*. 86(20), 1245-1251.

Salmi, M., Jalkanen, S. (2001). A Cell Surface Amine Oxidase Directly Controls Lymphocyte Migration. *Immunity*. 14(3), 265-276.

Salmi, M., Jalkanen, S. (2017). Vascular Adhesion Protein-1: A Cell Surface Amine Oxidase in Translation. *Antioxidants & Redox Signalling*. 12(1), 34-52.

Salter-Cid, L.M., Wang, E., O'Rourke, A.M *et al.* (2005). Anti-inflammatory effects of inhibiting the amine oxidase activity of semicarbazide- sensitive amine oxidase. *Journal of Pharmacology*. 25(315), 553–562.

Sartori, A., Humberto, M. *et al.* (2008). Aminoacetone, a putative endogenous source of methylglyoxal, causes oxidative stress and death to insulin-producing  $\beta$  cells. *Chem. Res. Toxicol*. 8(21), 1841-1850.

Sartori, A., Mano, C. *et al.* (2010). Oxidative Damage to Cytochrome C Induced by Aminoacetone. *Free Radical Biology and Medicine*. 49(10), 171-177.

- Scacheri, P.C., Caplen, N.J. *et al.* (2004). Short interfering RNAs can induce unexpected and divergent changes in the levels of untargeted proteins in mammalian cells. *PNAS*. 17(101), 1892-1897.
- Schulz, J.B., Lindenau, J., *et al.* (2000). Glutathione, oxidative stress and neurodegeneration. *Eur. J. Biochem.* 267(20), 4904-4911.
- Seiler, N., Badolo, N. *et al.* (2000). Effect of the polyamine oxidase inactivator MDL 72527 on N1-(n-octanesulfonyl) spermine toxicity. *The international journal of biochemistry and cell biology*. 32(2), 1055-1068.
- Sharma-Bhandari, A., Park, S.H. *et al.* (2015). Lysyl oxidase modulates the osteoblast differentiation of primary mouse calvaria cells. *International journal of molecular medicine*. 36(6), 1664 –1670.
- Shaw, J.H., Lloyd, P.G. *et al.* (2012). Post-transcriptional regulation of placenta growth factor mRNA by hydrogen peroxide. *Microvascular research*. 84(2), 155-160.
- Singh, B., Tschernig, T. *et al.* (2003). Expression of vascular adhesion protein-1 in normal and inflamed mice lungs and normal human lungs. *Virchows Arch*. 23(442), 491–495.
- Smith, D.J., Vainio, P.J. (2007). Targeting vascular adhesion protein-1 to treat autoimmune and inflammatory diseases. *Ann. N.Y. Acad. Sci.* 1110(7), 382–388.
- Smith, D.J., Salmi, M., Bono, P. *et al.* (1998). Cloning of vascular adhesion protein 1 reveals a novel multifunctional adhesion molecule. *The Journal of experimental medicine*. 188(1), 17-27.
- Smithen, D.A., Leung, H. *et al.* (2019). 2-Aminomethylene-5-sulfonylthiazole Inhibitors of Lysyl Oxidase (LOX) and LOXL2 Show Significant Efficacy in Delaying Tumour Growth. *Journal of Medicinal Chemistry*. 20(63), 2308-2324.
- Smolock, E., Berk, B.C (2012). Vascular Smooth Muscle Cell Remodelling in Atherosclerosis and Restenosis. *Fundamental Biology and Mechanisms of Disease*. 2(12), 1301-1309.
- Stolen, C. M., Yegutkin, G. G. *et al.* (2004). Origins of Serum Semicarbazide-Sensitive Amine Oxidase. *Circulatory Research*. 95(4), 50–57.
- Sun, P., Esteban, G., Inokuchi, T. *et al.* (2015). Protective effect of the multitarget compound DPH-4 on human SSAO/VAP-1-expressing hCMEC/D3 cells under oxygen-glucose deprivation conditions: an in vitro experimental model of cerebral ischaemia. *Br. J. Pharmacol.* 172(15) 5390–5402.
- Sun, P., Hernandez-Guillamón, M. *et al.* (2018). Simvastatin blocks soluble SSAO/VAP-1 release in experimental models of cerebral ischemia: Possible benefits for stroke-induced inflammation control. *Molecular Basis of Disease*. 1864(2), 542-553.
- Sun, Y., Byon, C.H. *et al.* (2012). Smooth muscle cell specific runx2 deficiency inhibits vascular calcification. *Circulatory research*. 111(5), 543-552.
- Sung, H.J. *et al.* (2005). Oxidative stress produced with cell migration increases synthetic phenotype of vascular smooth muscle cells. *Ann. Biomed. Eng.* 33 (11), 1546–1554.

Suowen, X., Jiajia, F. *et al.* (2009). Development of an optimized protocol for primary culture of smooth muscle cells from rat thoracic aortas. *Cytotechnology*. 9(61), 65-72.

Tang, Y., Yang, X. *et al.* (2011). Mechanisms of TGF-beta-induced differentiation in human vascular smooth muscle cells. *Journal of Vascular Research*. 11(48), 485 – 494.

Tang, C., Klinman, J.P. (2001). The catalytic function of bovine lysyl oxidase in the absence of copper. *The Journal of biological chemistry*. 276(33), 30575–30580.

Tallquist, M.D., Klinghoffer, R.A. *et al.* (2000). Retention of PDGFR- $\beta$  function in mice in the absence of phosphatidylinositol 3'-kinase and phospholipase C $\gamma$  signalling pathways. *Genes Development*. 14(24), 3179-3190.

Tchivilev, I., Vendrov, A.E. *et al.* (2008). Identification of a protective role for protein phosphatase 1c $\gamma$ 1 against oxidative stress-induced vascular smooth muscle cell apoptosis. *J Biol Chem*. 283(32), 22193-22205.

Thornalley, P.J. (1996). Pharmacology of methylglyoxal: Formation, modification of proteins and nucleic acids, and enzymatic detoxification. *Gen. Pharmacol*. 16(27), 565–573.

Tipnis, UR., He, G.Y. (1998). Mechanism of Polyamine Toxicity in Cultured Cardiac Myocytes. *Toxicology in vitro*. 12(3), 233-240.

Toma, A., McCaffrey, T.A. (2012). Transforming growth factor- $\beta$  and atherosclerosis: interwoven atherogenic and atheroprotective aspects. *Cell tissue research*. 347(1), 155-175.

Toraason, M., Luken, M.E. *et al.* (2009). Comparative toxicity of allylamine and acrolein in cultured myocytes and fibroblasts from neonatal rat heart. *Toxicology*. 56(1), 107-117.

Trackman, P.C. (2016). Lysyl Oxidase Isoforms and Potential Therapeutic Opportunities for Fibrosis and Cancer. *Expert Opin Ther Targets*. 20(8), 935–945

Trent, M., Conklin, D., Boor, P. (2002). Culture medium enhances semicarbazide-sensitive amine oxidase activity. *In Vitro Cellular and Developmental Biology*. 38(9), 523-528.

Ucal, S., Häkkinen, M.R., Alanne, A.L., Alhonen, L. *et al.* (2018). Controlling of N-alkylpolyamine analogue metabolism by selective deuteration. *Biochemical Journal*. 475(3), 663-676.

Ucar, G., Topaloglu, E. *et al.* (2005). Elevated semicarbazide-sensitive amine oxidase (SSAO) activity in lung with ischemia–reperfusion injury: Protective effect of ischemic preconditioning plus SSAO inhibition. *Life Sciences*. 78(25), 421 – 427.

Ucar, G., Basaran, D. (2003). Plasma Semicarbazide-Sensitive Amine Oxidase Activity in Type I and II Alcoholics. *Life Sciences*. 13(15), 345 – 367.

Uchida, K. (2000). Role of reactive aldehyde in cardiovascular diseases. *Free Radical Biology and Medicine*. 28 (2), 1685–1696.

Unzeta, M., Sole, M. *et al.* (2006). Semicarbazide-sensitive amine oxidase (SSAO) and its contribution to vascular damage in Alzheimer's disease. *Journal of neural transmission*. 7(114), 857-862.

- Uzel, M.I., Scott, I.C. *et al.* (2001). Multiple bone morphogenetic protein 1-related mammalian metalloproteinases process pro-lysyl oxidase at the correct physiological site and control lysyl oxidase activation in mouse embryo fibroblast cultures. *The Journal of biological chemistry*. 276(25), 22537–22643.
- Vidrio, H., Medina, M., Gonza´lez-Romo, P. *et al.* (2003). Semicarbazide-sensitive amine oxidase substrates potentiate hydralazine hypotension: Possible role of hydrogen peroxide. *Journal of Pharmacology and Experimental Therapeutics*. 307(2), 497–504.
- Wang, S.H., Yu, T.Y. *et al.* (2018a). Inhibition of Semicarbazide- sensitive Amine Oxidase Reduces Atherosclerosis in Cholesterol-fed New Zealand White Rabbits. *Scientific Reports*. 18(8), 24-38.
- Wang, S.-H., Yu, T.-Y., Tsai, F.-C., Weston, C. J. *et al.* (2018b). Inhibition of Semicarbazide-Sensitive Amine Oxidase Reduces Atherosclerosis in Apolipoprotein E-Deficient Mice. *Translational Res*. 197(8), 12–31.
- Wang, G., Karamariti, E. *et al.* (2015). Origin and differentiation of vascular smooth muscle cells. *The Journal of Physiology*. 15(14), 1313-1330.
- Wang, E.Y., Gao, H., Salter-Cid, L. *et al.* (2006). Design, synthesis, and biological evaluation of semicarbazide-sensitive amine oxidase (SSAO) inhibitors with anti-inflammatory activity. *Journal of Medical Chemistry*. 26(49), 2166–2173.
- Wang, J., Zhu, Y. *et al.* (2016). Lysyl oxidase promotes epithelial-to mesenchymal transition during paraquat-induced pulmonary fibrosis. *Molecular bio Systems*. 12(2), 499–507.
- Wang, H., Liu, H., Liu, R.M. (2003). Gender difference in glutathione metabolism during aging in mice. *Exp Gerontology*. 23(38), 507–517.
- Watanabe, T., Pakala, R. *et al.* (2001). Low density lipoprotein acts synergistically with angiotensin II in inducing vascular smooth muscle cells hypertension. *Journal of hypertension*. 19(6), 1065-1073.
- Weissen-Plenz, G., Eschert, H., Volker, W. *et al.* (2008). Granulocyte macrophage colony-stimulating factor deficiency affects vascular elastin production and integrity of elastic lamellae. *J Vasc Res*. 28(45), 103–110.
- WHO (2020) [https://www.who.int/health-topics/cardiovascular-diseases/#tab=tab\\_1](https://www.who.int/health-topics/cardiovascular-diseases/#tab=tab_1). Assessed on 17/06/2020.
- Wong, M., Saad, S. *et al.* (2014). Semicarbazide-sensitive amine oxidase (SSAO) inhibition ameliorates kidney fibrosis in a unilateral ureteral obstruction murine model. *American journal of renal physiology*. 13(5), 23-25.
- Wong MY, Saad S, Wong MG, Stangenberg S, Jarolimek W, Schilter H, *et al.* (2020) Semicarbazide-sensitive amine oxidase inhibition ameliorates albuminuria and glomerulosclerosis but does not improve tubulointerstitial fibrosis in diabetic nephropathy. *PLoS ONE*. 15(6), 34-53.
- Xiao, Q., Liu, Z. *et al.* (2009). Embryonic stem cell differentiation into vascular smooth muscle cells is mediated by NOX4 produced hydrogen peroxide. *Cell physiology*. 296(4), 711-722.

Xiao, W., Loscalzo, J. (2020). Metabolic Responses to Reductive Stress. *Antioxidants & redox signalling*. 32(18), 1332-1345.

Xu, H.L., Salter-Cid, L., Linnik, M.D. *et al.* (2006). Vascular adhesion protein- 1 plays an important role in inflammation and neuropathology in diabetic, oestrogen-treated ovariectomized female rats subjected to transient forebrain ischemia. *Journal of Pharmacology*. 6(317), 19–29.

Yang, W., Li, H., Luo, H., and Luo, W. (2011). Inhibition of Semicarbazide- Sensitive Amine Oxidase Attenuates Myocardial Ischemia-Reperfusion Injury in an In Vivo Rat Model. *Life Sci*. 88(11), 302–306.

Yoshida, T., Kaestner, K.H., Owens, G.K. (2008). Conditional deletion of Kruppel-like factor 4 delays downregulation of smooth muscle cell differentiation markers but accelerates neointimal formation following vascular injury. *Circulatory Research*. 28(102), 1548–1557.

Yraola, F., Garcia-Vicente, S. *et al.* (2006). New efficient substrates for semicarbazide-sensitive amine oxidase/vap-1 enzyme: analysis computational docking. *Journal of Medicinal Chemistry*. 49(6), 6197–6208.

Yu, P.H. (1998). Increase of formation of methylamine and formaldehyde in vivo after administration of nicotine and the potential cytotoxicity. *Neurochemistry Research*. 23(9), 1205-1210.

Yu, P., Wang, M., Deng, Y., Fan, H., and Shira-Bock, L. (2002). Involvement of Semicarbazide-Sensitive Amine Oxidase-Mediated Deamination in Atherogenesis in KKAY Diabetic Mice Fed with High Cholesterol Diet. *Diabetes*. 45(20), 1255–1262.

Yu, P.H., Wang, M. *et al.* (2004). Involvement of SSAO-mediated deamination in adipose glucose transport and weight gain in obese diabetic KKAY mice. *American Journal of Physiology and Endocrinology Metabolism*. 286(4), 34-41.

Yu, P.H., Davis, B.A., Deng, Y. *et al.* (2001). 2-Bromoethylamine as a potent selective suicide inhibitor for semicarbazide-sensitive amine oxidase. *Biochemistry and Pharmacology*. 21(61), 741–748.

Yu, P. H., and Deng, Y. L. (1998). Endogenous Formaldehyde as a Potential Factor of Vulnerability of Atherosclerosis: Involvement of Semicarbazide-Sensitive Amine Oxidase-Mediated Methylamine Turnover. *Atherosclerosis*. 140(9), 357–363.

Yu, P.H., Zuo, D.M. *et al.* (1996). Formaldehyde produced endogenously via deamination of methylamine. A potential risk factor for initiation of endothelial injury. *Atherosclerosis*. 120(12), 189-197.

Yu, P.H., Zuo, D.M. *et al.* (1997). Aminoguanidine inhibits semicarbazide-sensitive amine oxidase activity: implications for advanced glycation and diabetic complications. *Diabetes*. 97(40), 1243-1250.

Yu, P.H., Lu, L.X. *et al.* (2006). Involvement of Semicarbazide-Sensitive Amine Oxidase-Mediated Deamination in Lipopolysaccharide-Induced Pulmonary Inflammation. *American Journal of Pathology*. 26(168), 718–726.

Yue, B. (2015). Biology of the Extracellular Matrix: An Overview. *J Glaucoma*. 14(15), 23-25.

Zorzano, A., Abella, A., Marti, L. *et al.* (2003). Semicarbazide-sensitive amine oxidase activity exerts insulin-like effects on glucose metabolism and insulin-signalling pathways in adipose cells. *Biochim Biophys Acta*. 16(47), 3-9.

Zhao, B., Summers, F.A., Mason, R.P. (2012). Photooxidation of Amplex Red to resorufin: implications of exposing the Amplex Red assay to light. *Free Radical Biology Medicine*. 53(5), 1080-1087.

Zhexuan, Lin., Hui, Li., Hongjun, Luo. *et al.* (2011). Benzylamine and methylamine, substrates of semicarbazide-sensitive amine oxidase, attenuate inflammatory response induced by lipopolysaccharide. *International Immunopharmacology*. 11(2), 1079–1089.

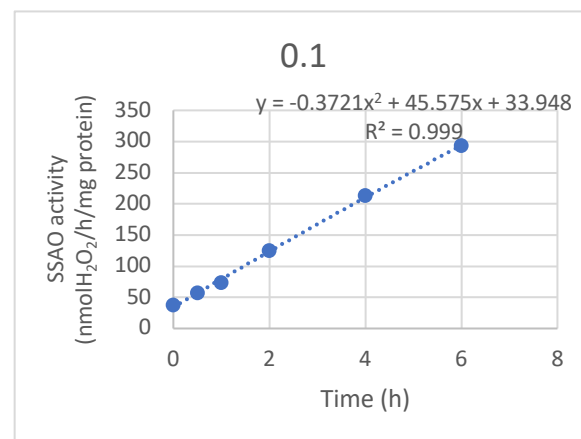
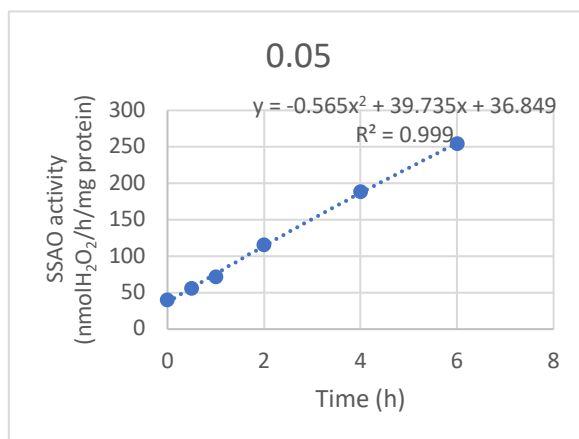
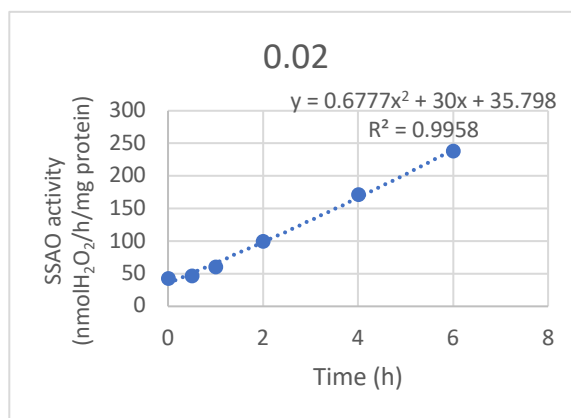
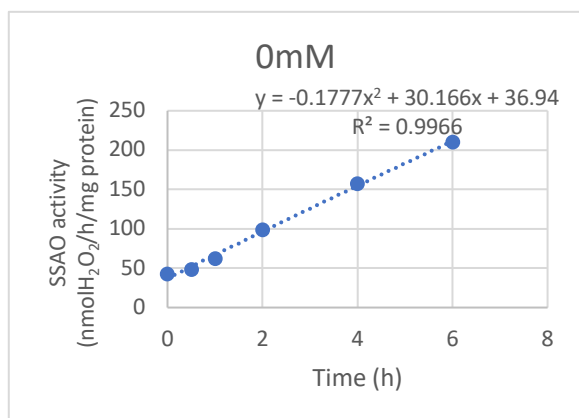
Zhang, M., Liu, L., Zhi, F., Niu, P., Yang, M., Zhu, X., *et al.* (2016). Inactivation of Semicarbazide-Sensitive Amine Oxidase Induces the Phenotypic Switch of Smooth Muscle Cells and Aggravates the Development of Atherosclerotic Lesions. *Atherosclerosis*. 249(16), 76–82.

# APPENDIX

## APPENDIX 1

**Table 14. SSAO activity (nmolH<sub>2</sub>O<sub>2</sub>/h/mg protein) in rat aortic VSMCs from passage 3, over different times and in the presence of different substrate concentrations**

| Time | 0mM      | 0.02mM   | 0.05mM   | 0.1mM    | 0.5mM    | 1mM      | 5mM      |
|------|----------|----------|----------|----------|----------|----------|----------|
| 0    | 42.26654 | 42.80218 | 39.87229 | 36.9632  | 34.64099 | 37.04725 | 39.83255 |
| 0.5  | 48.62217 | 46.86657 | 55.58773 | 56.85934 | 60.26441 | 66.18997 | 70.19701 |
| 1    | 61.65654 | 59.89643 | 71.60078 | 73.64063 | 78.12974 | 84.94278 | 91.35076 |
| 2    | 98.54325 | 99.70541 | 115.6455 | 124.3685 | 132.1766 | 141.7665 | 160.0452 |
| 4    | 157.2289 | 170.9697 | 188.2602 | 212.9003 | 223.7868 | 241.0057 | 264.8743 |
| 6    | 210.3932 | 238.3525 | 254.1976 | 292.9063 | 311.2539 | 333.138  | 369.8757 |



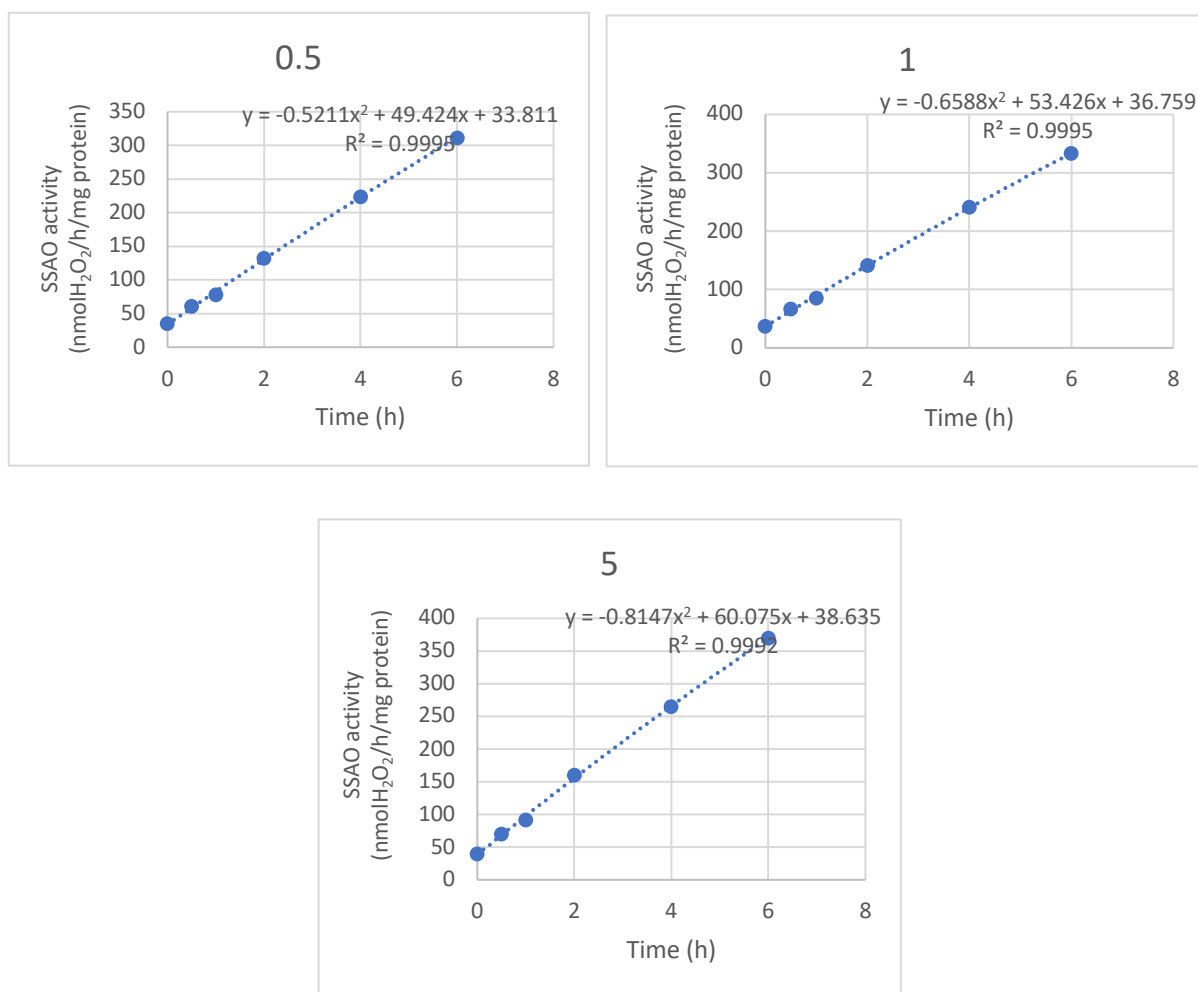
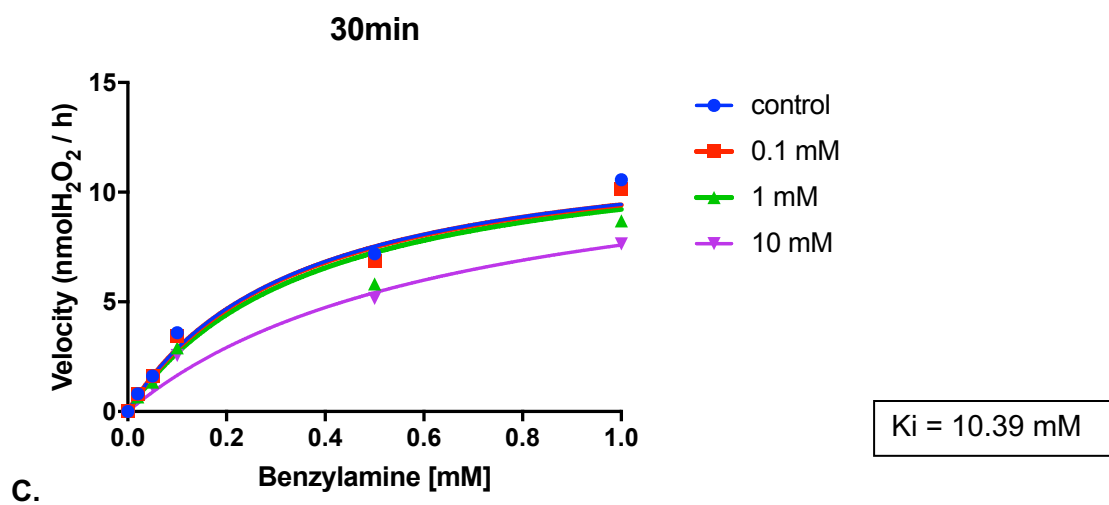
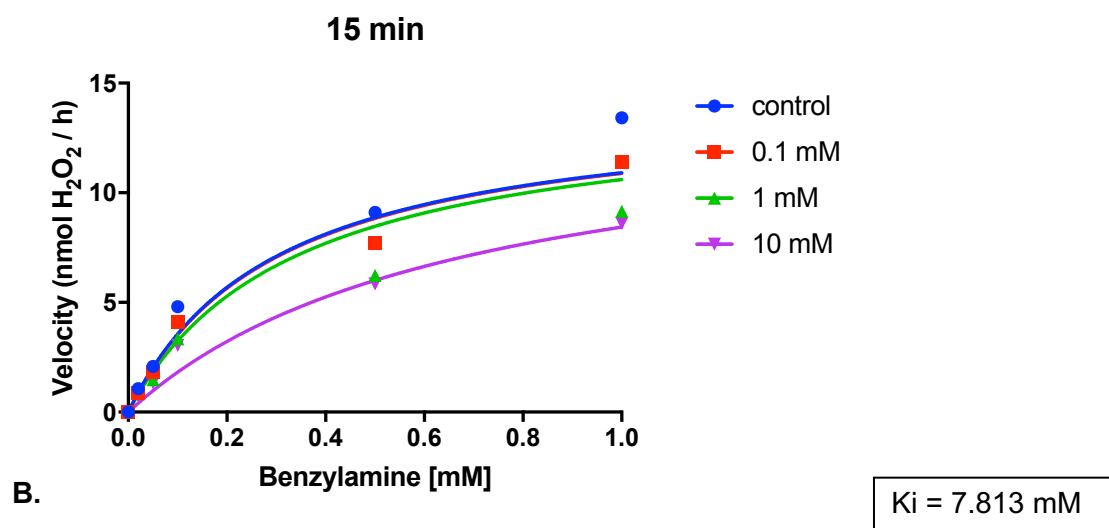
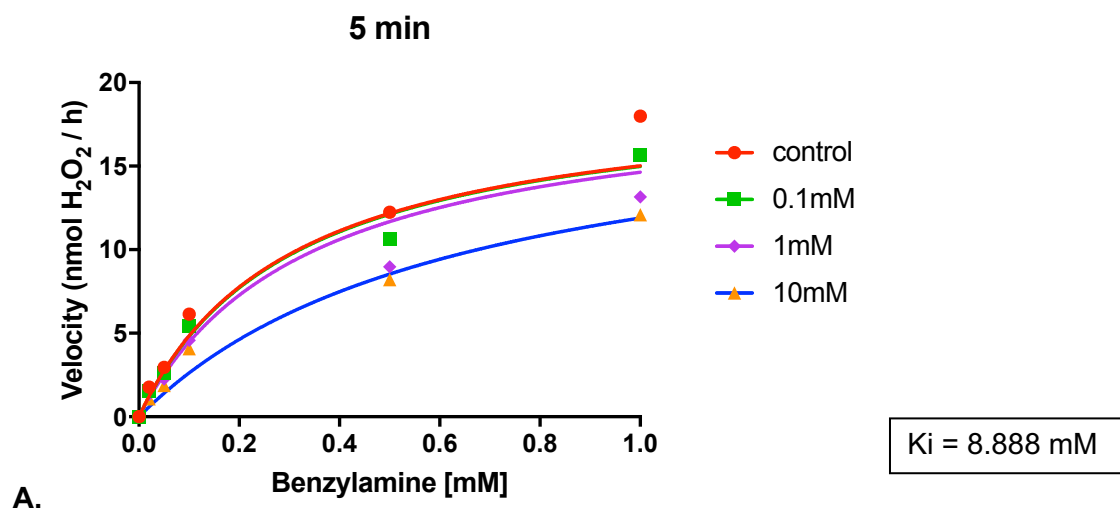


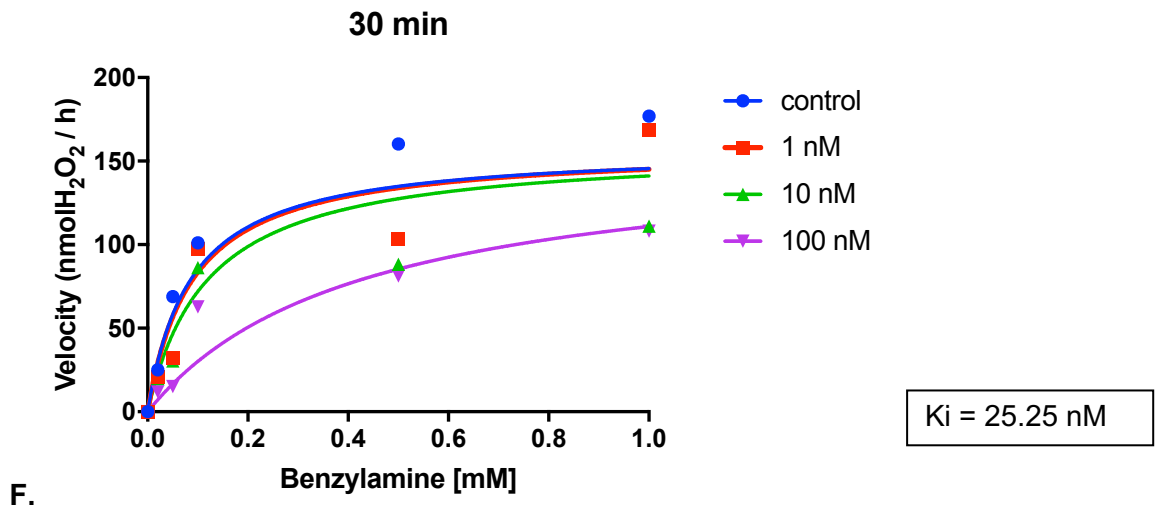
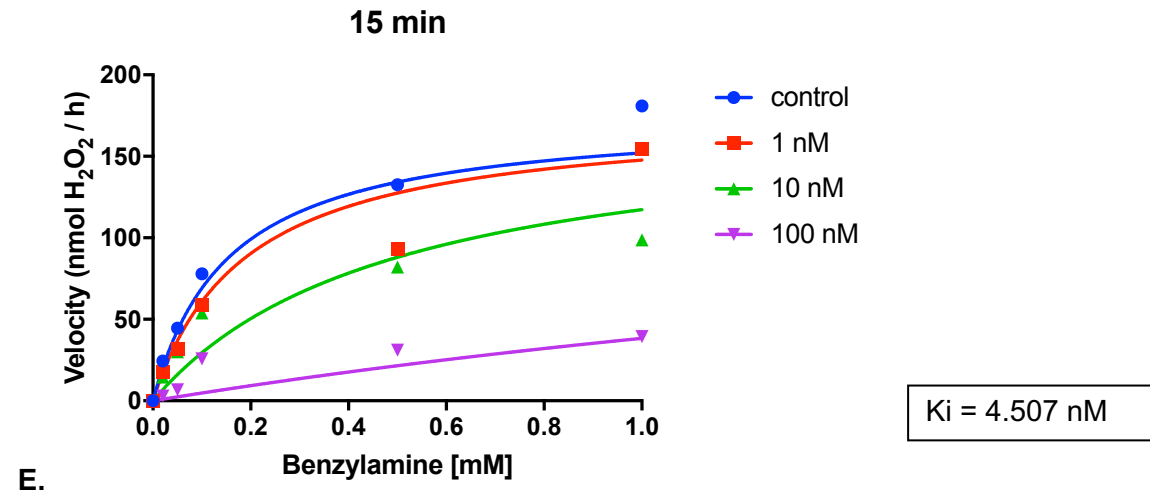
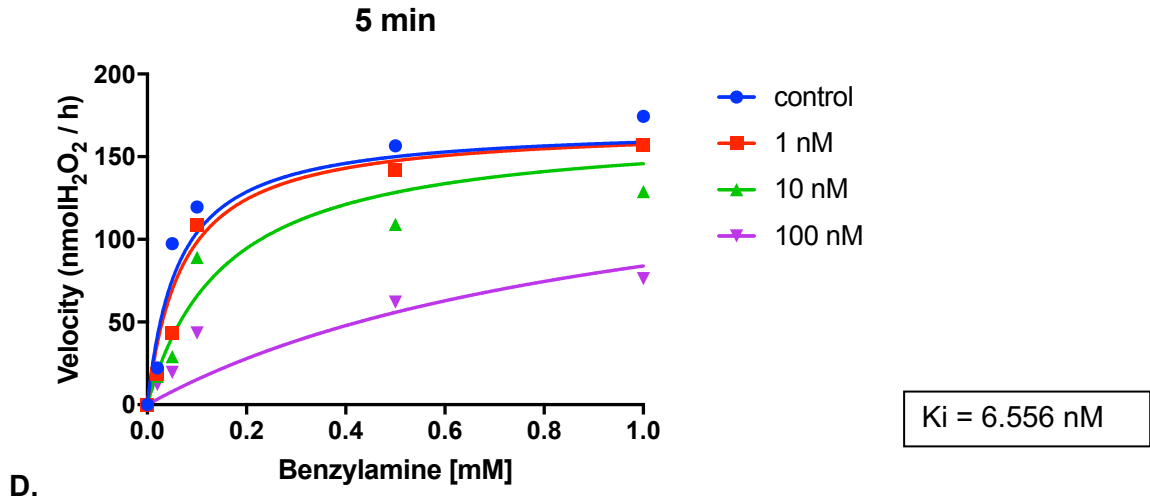
**Figure 86. Progress curves of SSAO activity (nmolH<sub>2</sub>O<sub>2</sub>/h/mg protein vs time) in the presence of different substrate concentrations.**

**Table 15. SSAO reaction velocity (V) in rat aortic VSMCs from passage 3 (n = 5). The velocity expressed as (nmol H<sub>2</sub>O<sub>2</sub> / h) in the presence of different substrate concentrations was derived from the slope of the linear part of the progress curve from the SSAO activity vs time graph (Figure 86) for each substrate concentration.**

| Conc | RV 1     | RV 2     | RV 3     | RV 4     | RV5      | MEAN     | MEAN-bl  | SD       | SEM      |
|------|----------|----------|----------|----------|----------|----------|----------|----------|----------|
| 0    | 29.10624 | 23.77636 | 36.48588 | 34.29575 | 34.96663 | 31.72617 | 0        | 4.686612 | 2.092238 |
| 0.02 | 34.0428  | 27.99907 | 37.29923 | 34.92348 | 35.59086 | 33.97109 | 2.244914 | 3.171036 | 1.415641 |
| 0.05 | 36.36438 | 29.35585 | 37.50064 | 36.03569 | 38.0083  | 35.45297 | 3.726801 | 3.132658 | 1.398508 |
| 0.1  | 43.3548  | 32.05067 | 43.37881 | 36.23472 | 44.57782 | 39.91936 | 8.193189 | 4.918621 | 2.195813 |
| 0.5  | 46.31509 | 37.14322 | 45.85754 | 44.01345 | 46.89473 | 44.0448  | 12.31863 | 3.58316  | 1.599625 |
| 1    | 49.49651 | 42.45272 | 49.61601 | 48.72246 | 47.04399 | 47.46634 | 15.74017 | 2.669657 | 1.191811 |
| 5    | 55.21475 | 48.29204 | 56.2795  | 50.48445 | 49.93313 | 52.04077 | 20.3146  | 3.129161 | 1.396947 |

## APPENDIX 2





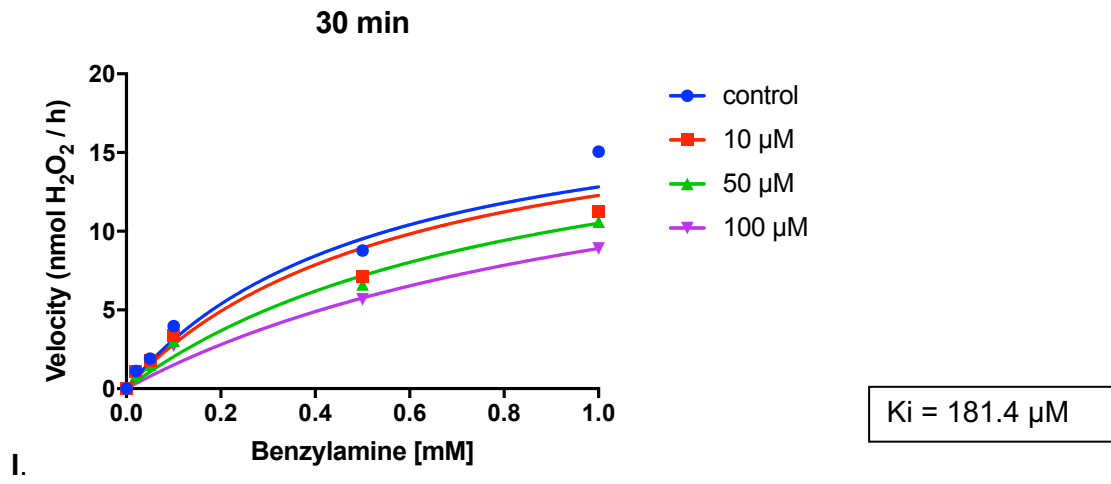
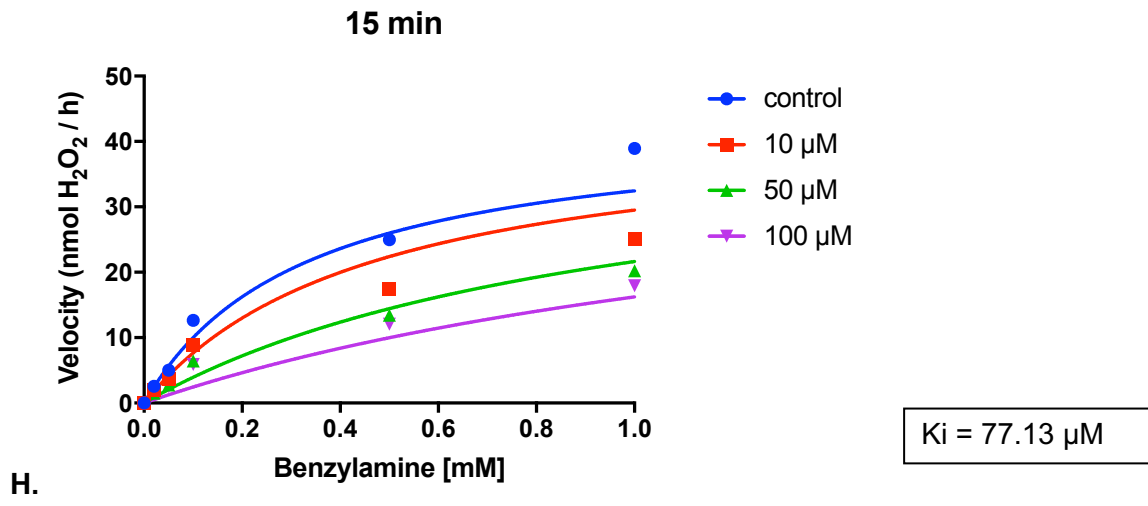
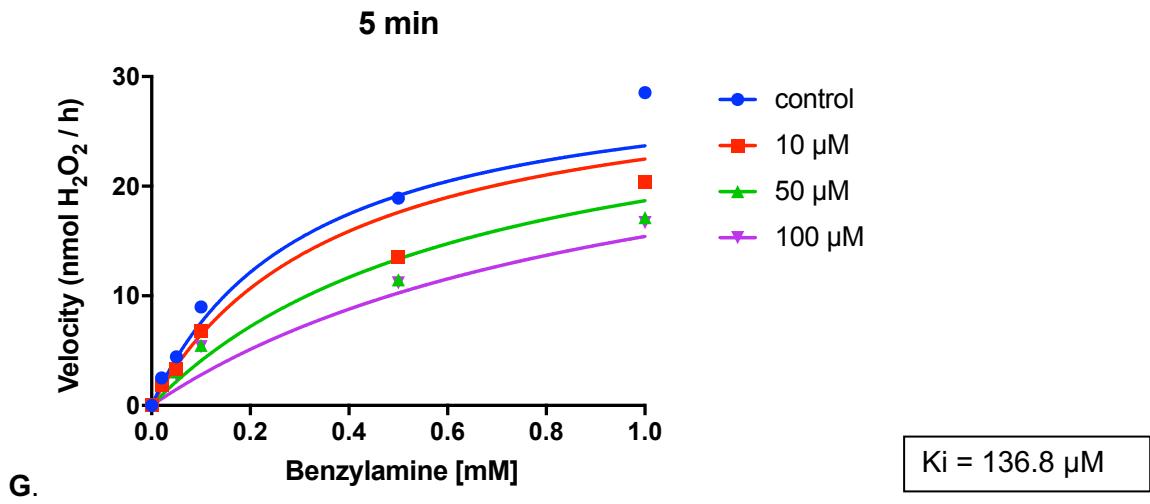
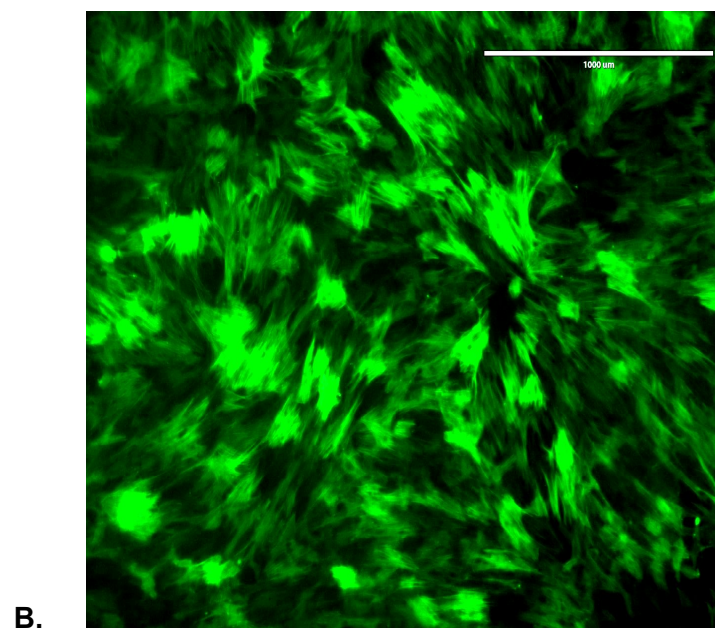
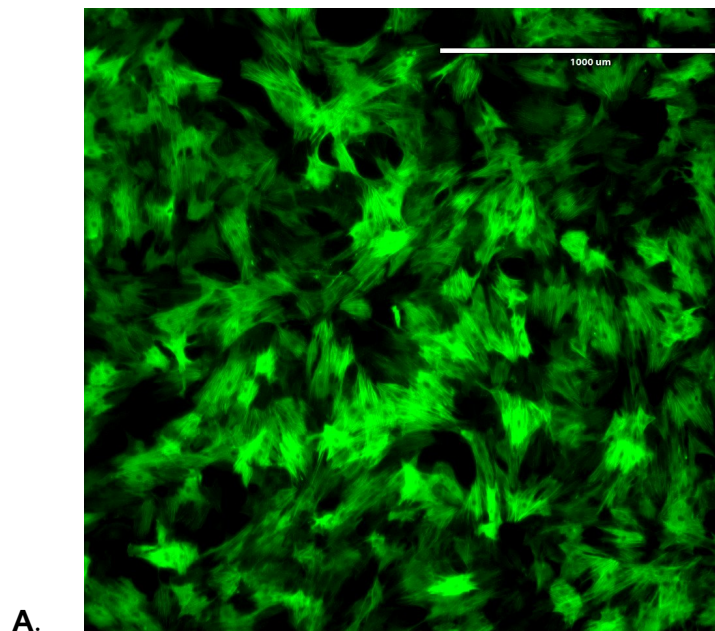


Figure 87. The inhibition time for each inhibitor was optimised by comparing the inhibition constant ( $K_i$ ) values derived by GraphPad Prism 7, which were obtained by measuring the substrate-velocity curves at 5, 15 and 30 minutes, in the presence of different inhibitor concentrations. Semicarbazide (A, B and C), methylhydrazine (D, E and F) and MDL72527 (G, H and I). For semicarbazide and methylhydrazine, the data was analysed with GraphPad Prism 7 using the competitive enzyme inhibition equation:  $K_{mObs} = K_m \cdot (1 + [I]/K_i)$   $Y = V_{max} \cdot X / (K_{mObs} + X)$ . For MDL72527, the data was analysed with GraphPad Prism 7 using the non-competitive enzyme equation:  $V_{maxinh} = V_{max} / (1 + I/K_i)$   $Y = V_{maxinh} \cdot X / (K_m + X)$ .

## APPENDIX 3



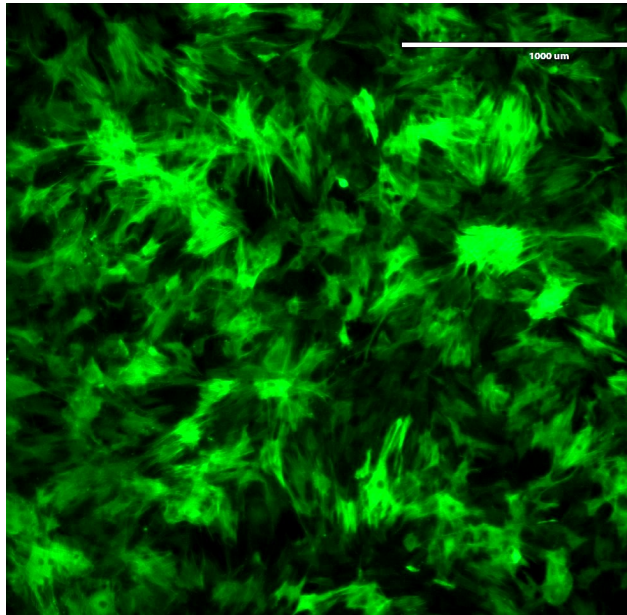
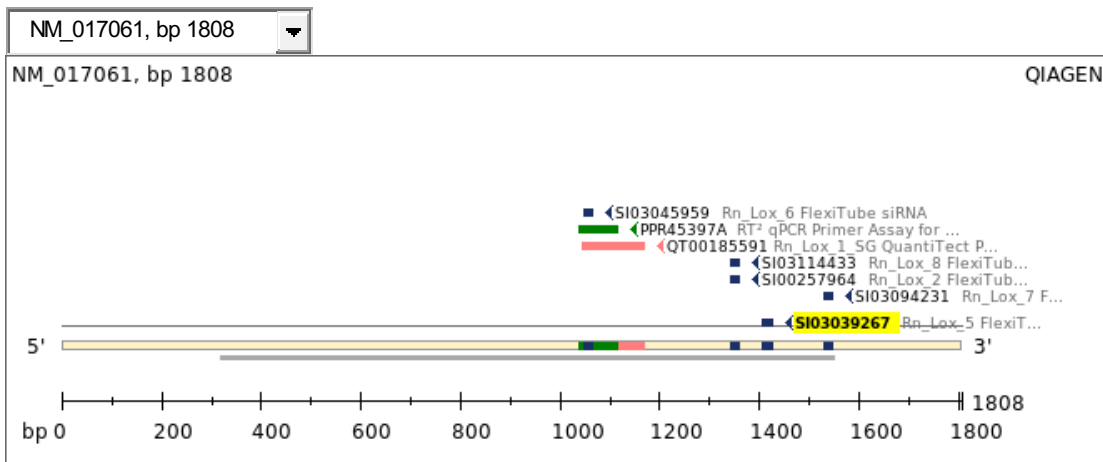


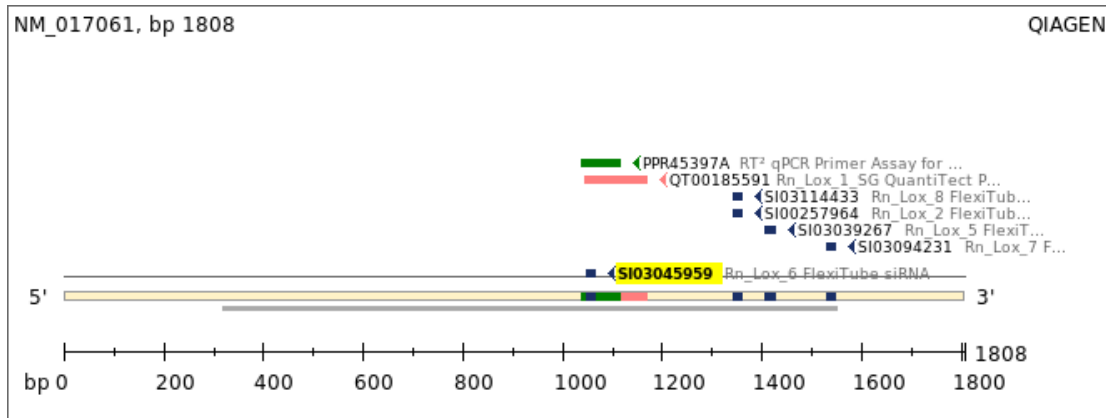
Figure 88. Immuno-stained microscopic image of rat aortic VSMCs depicting the presence of clustered SM22alpha actin fibres. Passage 3 (A), passage 5 (B), passage 8 (C) (scale bar: 1000 μm).

## APPENDIX 4

SiRNA\_LOX\_5 (highlighted in yellow)



**SiRNA\_LOX\_6 (highlighted in yellow)**



**SiRNA\_LOX\_8 (highlighted in yellow)**

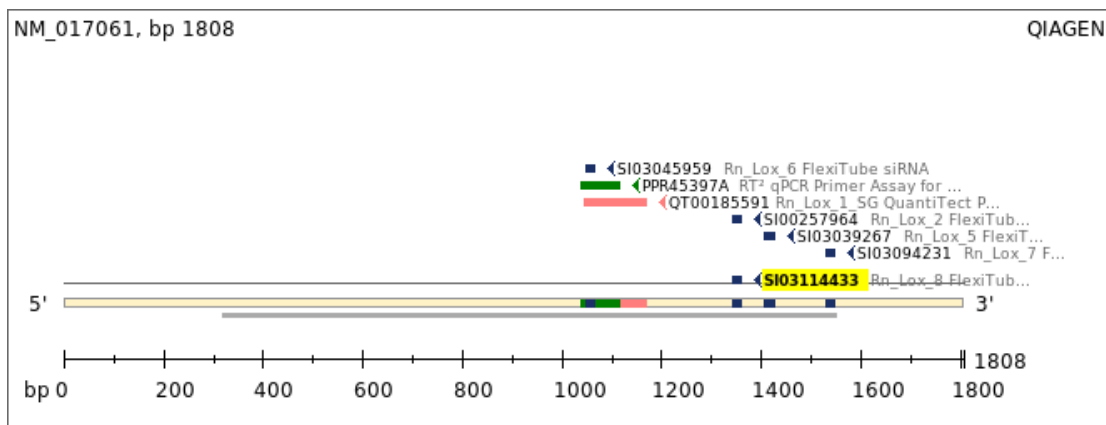


**Figure 89: SiRNA5, SiRNA6 and SiRNA8 targeted to LOX gene**